Alma Mater Studiorum – Università di Bologna

DOTTORATO DI RICERCA

Science for Conservation

Ciclo **XXII**

Settore/i scientifico disciplinari di afferenza: **CHIM/12**

TITOLO TESI

ON THE DEGRADATION MECHANISMS UNDER THE INFLUENCE OF PEDOLOGICAL FACTORS THROUGH THE STUDY OF ARCHAEOLOGICAL BRONZE PATINA

Presentata da: **Marta QUARANTA**

Coordinatore Dottorato   **Relatore**

Prof. Rocco MAZZEO   **Prof. Ion SANDU**

Esame finale anno 2009

Alma Mater Studiorum – Università di Bologna

DOTTORATO DI RICERCA

Science for Conservation

Ciclo **XXII**

Settore/i scientifico disciplinari di afferenza: **CHIM/12**

TITOLO TESI

ON THE DEGRADATION MECHANISMS UNDER THE INFLUENCE OF PEDOLOGICAL FACTORS THROUGH THE STUDY OF ARCHAEOLOGICAL BRONZE PATINA

Presentata da: **Marta QUARANTA**

Coordinatore Dottorato   **Relatore**

Prof. Rocco MAZZEO   **Prof.Ion SANDU**

Esame finale anno 2009

<u>Tutori</u>

Dr. Harry LEFAKIS

Dr. Bill WEI

Prof. Rocco MAZZEO

Content

III - Material and methods

IV -Results and discussion

Introduction

The conservation of a metallic artifact is a study in itself [*Plenderleith 1956*]. This sentence encloses the important aspect of the scientific understanding behind any conservation practice which involves metal museum objects.

The present work is carried out to deepen the study of degradation processes occurring in burial environment involving copper and its alloys.

Copper has played an important role in the history of human beings. The use of native copper is at least 10.000 years old and the use of bronze became universal during the Bronze Age. Copper-based alloys have been used, since then, throughout the history for the realization of various art objects, from jewellery to statuary [*Leyssens 2007*].

Copper is not a noble metal, and its exposure to the atmosphere change the aspect of its surface, due to oxidation phenomena. The same is true for its alloys.

Bronze *patina* may be aesthetically pleasant, preserving the original shape of the object, and thereby conferring an added value to an artifact. Bronze artifacts, recovered from archaeological excavation sites, seldom present such a desirable degradation structure: more often they are covered with a thick and incoherent multilayered patina, more reasonably called corrosion.

In general, the degradation of metal artefacts in soil occurs through processes which are different in nature: they can occur through chemical, electrochemical and microbiological reactions. As a result, metal tend to return to its mineral's state, as thermodynamically more stable than the metallic one. The way this processes occur is a function of multiple factors that can be classified as endogenous (nature of alloy, technology of manufacture, microstructure) and exogenous (soil texture, aeration, pH, conductivity, depth of burial and many others).

Those mentioned above are the main causes of degradation of bronze artefacts discovered during archaeological excavation, and a better knowledge of forms of alteration phenomena observed in certain soil environments will certainly help conservator and restorers to better preserve the excavated material.

This research project is carried on with the collaboration of archaeologists working at the sites of Dobrudja, the region of Romania. This region is home to Danube's Delta into the Black Sea and bears a long history as strategic location, which was exploited during Roman, Byzantine and Ottoman times.

Archeological objects offer a great opportunity to investigate long-term corrosion behaviors of bronze and copper-based alloys providing precious information, which are unlikely to be obtained by laboratory experiments. Nevertheless, if the aim is to establish the mechanisms of corrosion, simulation experiments can be a complementary tool, which allow investigation of the effect of different parameters (related both to alloy or burial environment) on electrochemical corrosion processes occurring in soil. This approach is considered in the second part of this thesis: the attention is focused on commercially available bronzes, similar in composition and microstructure to the ancient ones.

Scope of the thesis

The objective of the present research project is to acquire a better knowledge on the determining factors that cause the decay of archaeological bronzes in soil. The main issues explored are the archaeological context, climate and geographical location, the metal composition, the identification of corrosion products and the physical-chemical characterization of burial soils.

Once a general picture of the conservation state and a profound knowledge of corrosion patterns of archaeological bronze is gathered, the scientific efforts move to laboratory experiments of simulation aimed to assess corrosiveness of natural media acting as electrolytes, such as the soil and the seawater (of archaeological interest taking into consideration the location of sites). These experiments are aimed to estimate reactions' mechanisms and kinetics, and to characterize anodic layers formed in electrolytes simulating burial conditions.

As a conservation outcome of the research, the author feels the need to recommend some general guidelines for the *in situ* conservation practice of archaeological bronze artefacts excavated in this region of Romania where they were excavated.

Chapter I

Background

This chapter contains the background information needed for the understanding of corrosion processes of bronze artifacts taking place in burial environments. A reminding of the basic principles involved is presented, followed by a review of the parameters playing a role in the underground corrosion. A major role in the history of metals has been occupied by copper and its alloys. This is the main reason why the present research deals with the study of degradation and deterioration processes which involves bronzes.

I.1 Underground corrosion of archaeological bronzes

Metal atoms are present in nature as stable chemical compounds (minerals). The same amount of energy needed to extracts metals from their combined state is emitted during the chemical reactions that produce corrosion. The figure below (Figure I.1) illustrates the "life cycle" of a metallic object. Starting from the top, through extractive metallurgy, metal are obtained from their ores by reduction processes and, afterwards, metalworking procedures allow producing metallic objects or crafting works of art. After their period of use [*Mourey 1987*], the objects live a period of abandon during which they are subjected to degradation and deterioration processes ($\Delta G<0$), whose nature depends on the aggressiveness of environmental conditions.
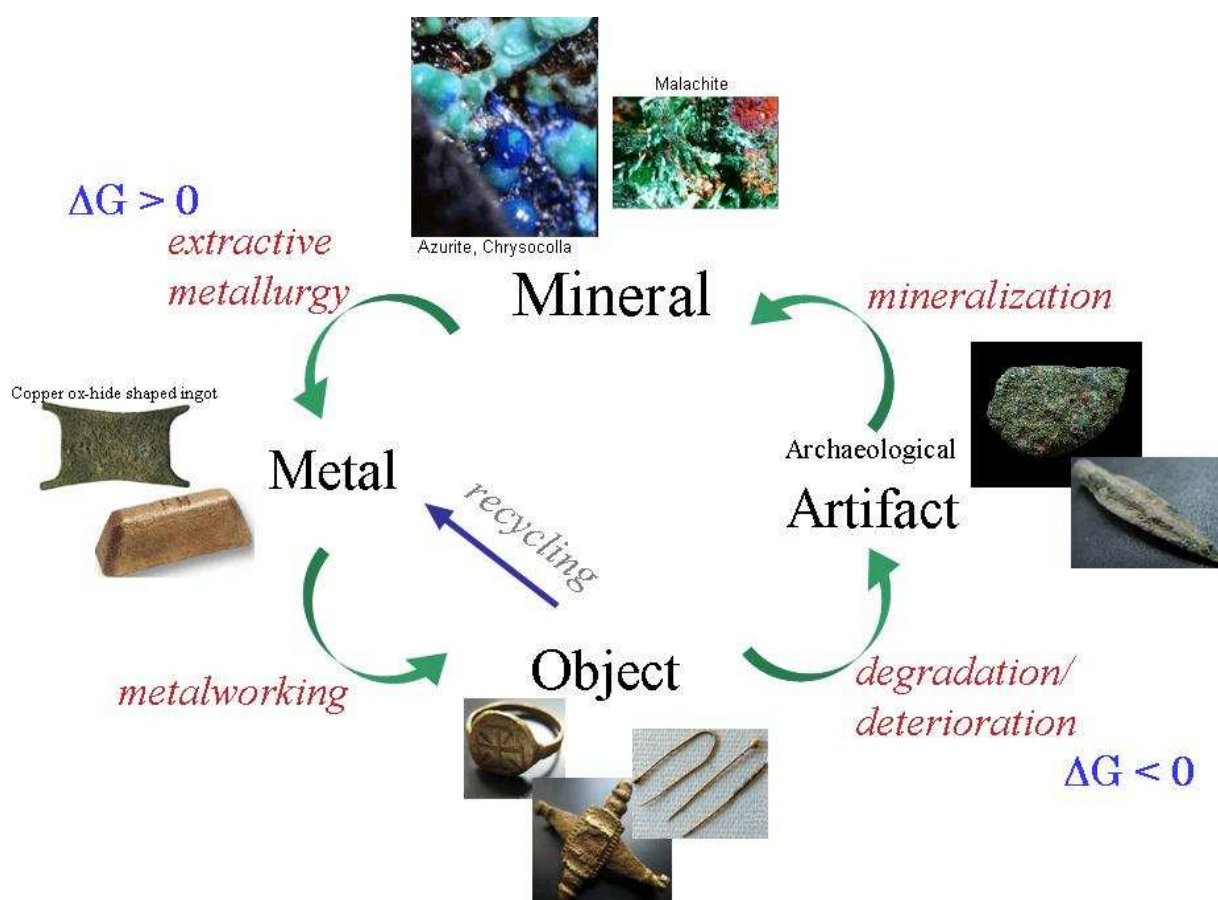
Figure I.1. Life cycle of a metal artifact.

At a certain point, after few centuries or even millennia, archaeological excavation procedures brings them back to light, and the interest (and duty) of conservators and restorers is preserving them from further degradation processes, which could revert metals to their original mineral form [*Gettens 1963*].

The study of underground corrosion had mainly industrial aims, as it started when the big pipeline for the oil and gas transport took place. An ample literature [*Romanoff 1957; Uhlig 2000; Brown 1989*] do exist about the research in this field, which was especially driven by the increasing cost of the corrosion as it was written in the Circular for the National Bureau of Standards issued in 1945 [*Romanoff 1957*].

This background chapter serves as an introduction for the topic of this research. The scientific interest of corrosion scientists is nowadays dedicated to the development of new and performing alloys for various industrial applications. On the contrary, the concern of conservation scientists is addressed towards a better understanding of corrosion phenomena, which has affected ancient metal objects, for conservation purposes. Ancient alloys often show a big variability in their composition and microstructure, and this is why this field of research is widely explored and still raises up the interest of scientists.

It is important also to be well aware of the variety of factors and parameters which play a role in the corrosion behavior of a bronze alloy. Different corrosion features are observed for example on bronze exposed to different atmospheric environments and namely, rural, urban or marine. In all these media, bronzes develop a different kind of patina, according to the nature of the predominant corrosive agent.

I.1.1   General principles of corrosion

Corrosion in aqueous media is of electrochemical nature. [*Stambolov 1985; Selwyn 200); Jones 1996 and others*]. This is the most aggressive and the one involved in underground corrosion medium.

Dry or chemical corrosion occurs by direct reaction of metals with a corrosive agent: the most important is the direct oxidation due to the direct reaction with oxygen. Anyway, this reaction occurs at significant rates only at high temperatures.

The electrochemical process implies two or more electrode reactions: the oxidation of a metal (anode) and the reduction of an oxidizing agent (cathode). Furthermore, the corrosion process also requires an ionic connection (an electrolyte) between the anode and the cathode to allow the flow of ionic species. In most corrosion processes, this ionic connection is provided by

water, e.g. condensation from humid air, rain, seawater. Whenever the relative humidity is higher than 65%, there is enough adsorbed water on most clean metals surfaces to approach the behavior of bulk water and promote electrochemical reactions [*Stambolov 1985*].

The anodic half reactions can be written as:

$$M_{(s)} \rightarrow M^{z+}{}_{(aq)} + ze^- \qquad\qquad (I.1)$$

which take place in acidic media; in basic media the predominant reaction is:

$$M_{(s)} + zH_2O \rightarrow M(OH)_z + zH^+ + ze^- \qquad (I.2)$$
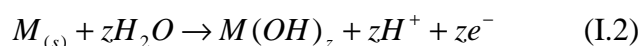
or the formation of the corresponding oxide, whose chemical formula depends on the metal and the pH.

The corresponding cathodic reaction is the hydrogen evolution, in absence of enough air to produce the oxygen reduction:

$$zH^+ + ze^- \rightarrow \frac{z}{2}H_2 \qquad\qquad (I.3)$$

$$\frac{z}{4}O_2 + zH^+ + ze^- \rightarrow \frac{z}{2}H_2O \qquad\qquad (I.4)$$
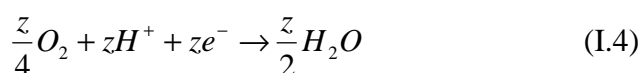
or the reduction of other depolarizing species.

The properties and behavior of the film of oxidation products, on the metal's surface, are of primary importance for the subsequent corrosion reactions, especially in what regards the nature and kinetics of reaction involved.

In practice, during corrosion, hydrogen ions are consumed when the cathodic reactions take place and an increase in pH allows the precipitation of slightly soluble salts, oxides or hydroxides. Sometimes, these compounds don't offer a protective action to the metal, but for some metals, these processes are slow enough to allow a passive layer to form, thus protecting the metal's surface.

Corrosion process is ruled by both kinetic and thermodynamic laws. The main interest in research in corrosion is certainly whether or not a reaction can take place, but of utmost importance is the knowledge of the speeds of oxidation and dissolution processes.

The current flowing in an electrochemical cell is a measure of corrosion rate, and it is called corrosion current. Electrochemical corrosion reactions, as electrode processes, occur at the interface metal-electrolyte and imply several steps: oxygen transportation towards the reaction surface, reaction at the interface and the transport of corrosion products to the solution. The overall speed of reaction is determined by those of the slower process (limit speed of reaction) in comparison with the others.

From the thermodynamic point of view, a reaction is possible when the condition ΔG < 0. If ΔG > 0, a metal is stable in the corrosion medium under given conditions. Whether corrosion can take place and, if so, which corrosion products will eventually be formed, can conveniently be surveyed in a type of stability diagram, called potential-pH or Pourbaix diagrams *[Mattson, 1989]*.

Before exploring the significance of these tools in predicting the nature of corrosion products, the factors influencing underground corrosion will be touched upon.

The principles mentioned here are valid in general. When dealing with underground corrosion, multiple factors shall be considered. Those related to the nature of the alloy, but also those related to the environment. The following paragraphs explore them.

I.1.2   Factors influencing corrosion

I.1.2.1   Endogenous factors

Endogenous factors are those related to the object and its structural characteristics as well as thermal and mechanical treatments to which it has been subjected.

I.1.2.1.1   Manufacturing technology

Copper is the first metal used by humans (VIII B.C., native copper [*Selwyn 2004*]; VI B.C. copper extraction in Anatolia [*Scott 2002*] and II B.C. Balkans and Spain [*Selwyn 2004*]). It is ductile (can be drawn in wire) and malleable (can be hammered into sheets) and possess a very high thermal and electrical conductivity. Anyway, it lacks mechanical strength, that is why it is often used alloyed with other elements such as arsenic (As), antimony (Sb), tin (Sn), zinc (Zn).

Bronze, an alloy of copper and tin, appeared about 3200-3100 B.C., probably by chance. Before the era of copper-tin bronzes, a common practice has consisted in the addition of arsenic to the copper ore during roasting, as it appeared to be the only way to harden the copper metal. This practice was relatively soon abandoned as during roasting the arsenic formed toxic arsenic trioxide, which caused a loss of arsenic and consequently a less quality alloy [*Stambolov 1985*].

The use of bronze, as true alloy of copper and tin, became pervasive and universal during the Bronze Age. Since tin source was the mineral cassiterite (SnO_2), however, the advent of tin bronze is still mysterious, such as are its sources and development of knowledge for its mining [*Scott, 2002*]. In the full Bronze Age, the attention of detail increased, with the production of finer objects and more accurate castings. An addition of lead was often made to

increase the fluidity of the metal. However, the leading of bronzes was rather local and by no means universal [*Tylecote, 1992*]. Brass, an alloy of copper and zinc, became important during the Roman period by co-smelting zinc and copper ores (as for smelting zinc the temperature needed exceeds its boiling point). For example, Romans produced brass coinage from 45 B.C. [*Scott, 2002*].

The knowledge of metallurgical technologies and their evolution has a fundamental manifestation in the alloy microstructures of bronze artifacts.

Phase diagrams are the tool which allows examining which are the stable phases of a precise metal system varying the temperature and composition [*Garagnani 2004*]. Their analysis allows studying which are the stable phases of an alloy during heating or cooling processes in equilibrium condition. Indeed, there exist different versions of phase diagrams, where stability regions are reported for realistic working circumstances, for which non-equilibrium conditions are likely to occur. These are reported in the Figure I.2.
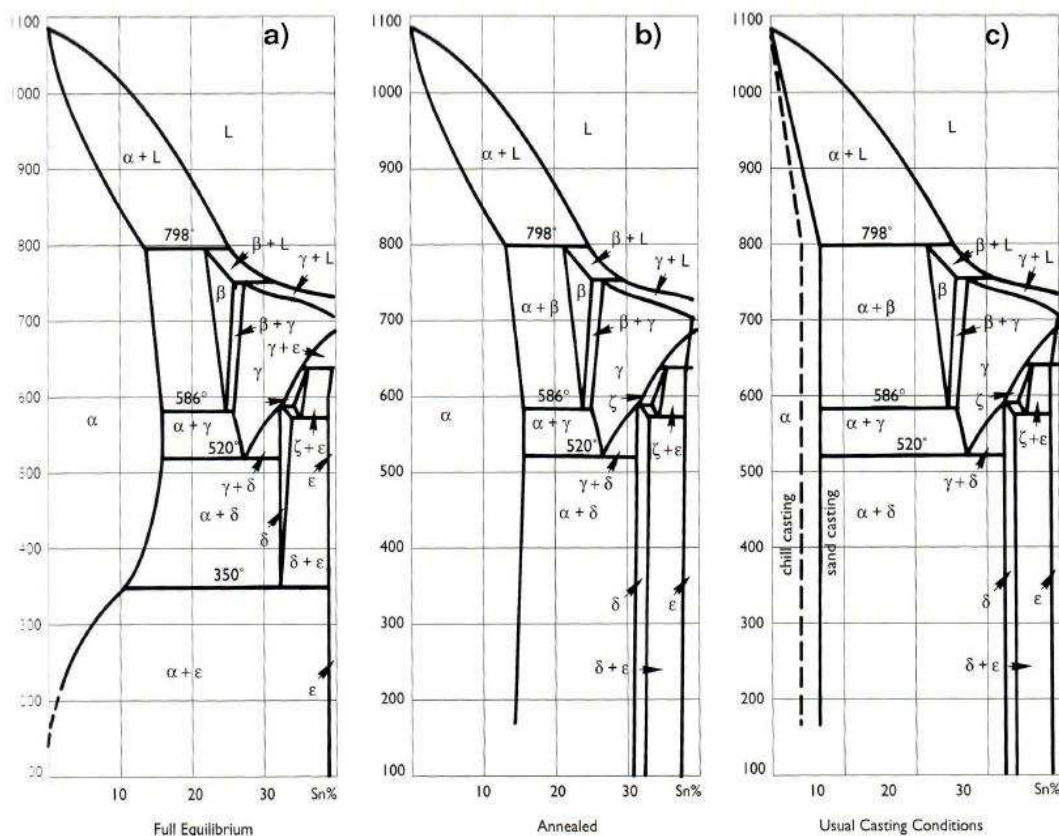
Figure I.2. Phase diagram for Cu-Sn system in different conditions: a) full equilibrium; b) annealing conditions and c) under usual casting condition. [Scott, 1991]

Annealing refer to a slow cooling down in the oven, while under casting condition the alloy is let cooling down in the mould.

The analysis of the diagrams allow inferring that for bronzes with tin content < 30% (which

represents the most common situation because for higher Sn content the alloy becomes more brittle), the stable phases are:

- **α** for Sn < 8-15%
- **(α+δ)** for 8-15 < Sn < 30 %.

It can be deduced that copper is able to dissolve an amount of tin which diminishes as the cooling rate increases. A bronze can therefore present a mono-phased rather than a bi-phased structure according to the rate of cooling. If this is faster, then two-phased structure is formed [*Garagnani2004*]. When a melt is allowed to cool slowly, the phases stable at high temperatures give way to those stable at low temperatures. By rapid cooling, however, this transition does not occur. Instead, the phases stable at high temperatures remain unchanged also at lower temperatures, but in a metastable state.

Many bronzes are leaded. With low-tin bronzes, typically casting, the lead does not alloy with the copper and occurs as small globules throughout the structure [*Scott, 2002*].

I.1.2.1.2 Alloy microstructure

Metallography is the scientific discipline of examining and determining the constitution and the structure of the constituents in metals and alloys [*Wayman 2004*]. The metallographic procedures allow studying the crystalline grains (morphology and dimensions), the identification of stable phases present (kind and morphology) and the presence of defects such as porosity and failures or non-metallic inclusions, witnesses of the thermal and mechanical history of the alloy [*Garagnani 2004*].

In general, there are two ways to manipulate metals, by casting or by working [*Scott 1991*]. As a result, metals and alloys present typical microstructures according to the manufacturing or crafting technology and the amount and nature of alloying elements.

The great majority of ancient castings show a dendritic microstructure (see Figure I.3), which follows a tree-like growing path (the term comes from the Greek word for tree). Sometimes outlines of grains form between them, and the rate to which they grow influence their size: the faster the rate of cooling the smaller the dendrites *[Scott 1991*]. Dendritic growth is a segregation phenomenon occurring during casting, which arises in alloys because one of the constituent of the alloy has a lower melting point (such as it happens in bronzes: melting points for Cu= 1083˚C and Sn= 232˚C). The dendrites usually form by coring, which is a common feature in ancient alloys and involves the occurrence of a compositional gradient from the inner region to the outer surface due to the different rate of cooling of the two constituents of the alloy. In the case of bronzes, the inner part is therefore richer in copper, which solidifies first and the outer part is richer in tin. The remaining fluid in the

interdendritic areas is likely to form a different phase, which is defined as a homogeneous state of a substance with a well-defined composition [*Scott, 1991*].

It is worth underlining that dimension of dendrites and their spacing, which depend on cooling rate, have an influence on mechanical properties (the best performances owing for a smaller secondary dendrites arm spacing, SDAS) [*Garagnani 2004*].
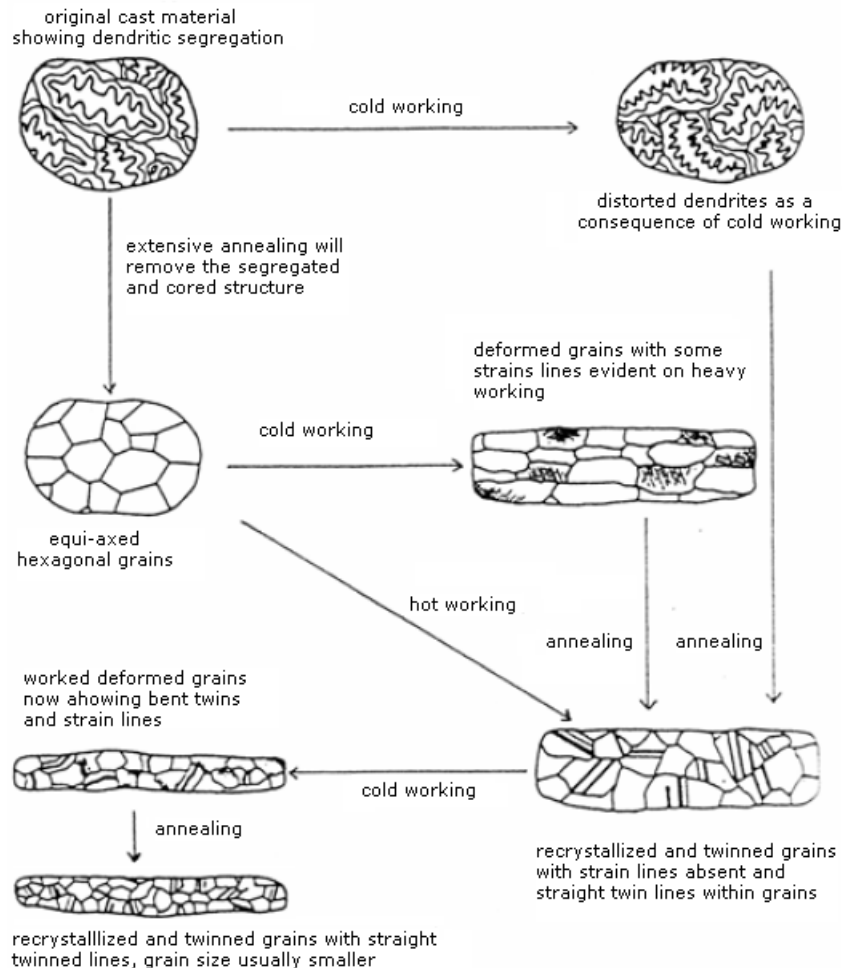
Figure I.4. Scheme representing the micro-structural transformation induced by mechanical and thermal treatments in a f.c.c metal or its alloys [Scott 2002]

Figure I.4 illustrates the simplified scheme, reported by *D.A. Scott* [*1991*], where he evidences the structural modification induces on the microstructure of a pure *fcc* metal or its alloy by working cycles. Working refers to a method or combination of methods for changing the shape of a metal or an alloy by techniques such as hammering, turning, raising, drawing...etc. which can be performed either at room temperature or by annealing, when the material becomes too brittle to be further worked.

As an example, Figure I. 5 and I.6 report two examples of microstructure for a bronze alloy, respectively, a dendritic structure and a recrystallized one.
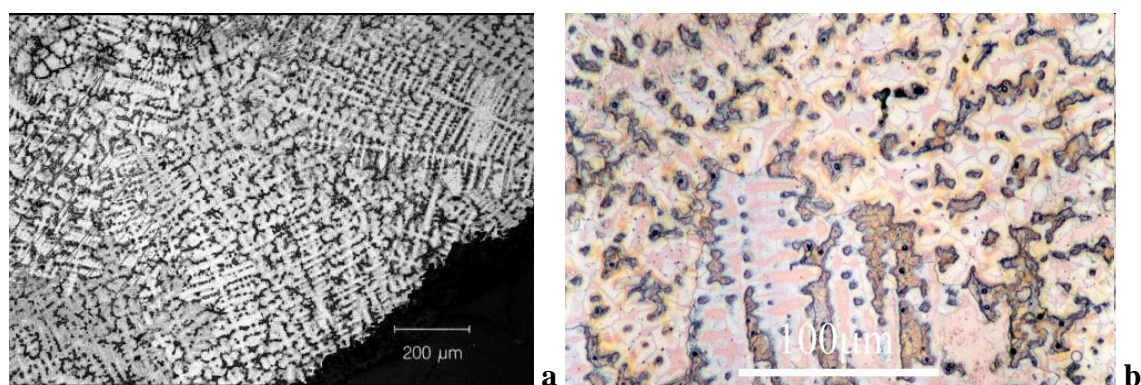
Figure I.5. Two examples of dendritic segregation for Cu-Sn alloys (a. from Garagnani 1996; b. from http://www.doitpoms.ac.uk)
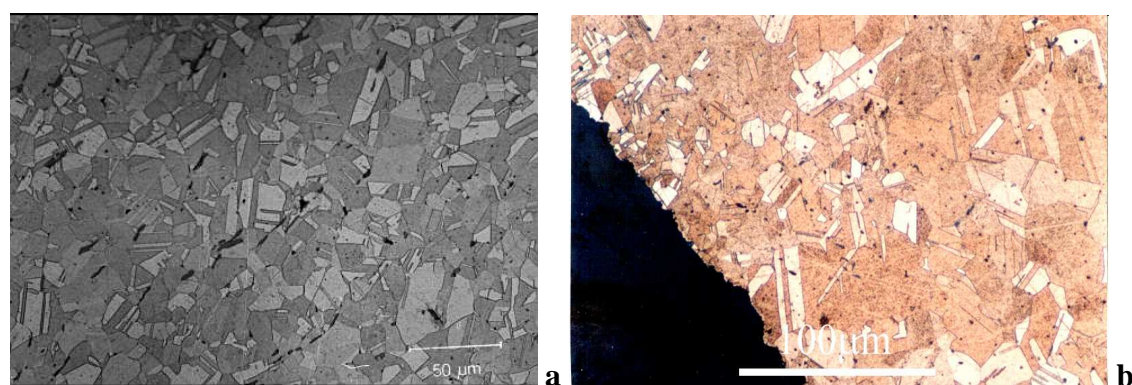
Figure I.6. Two examples of recrystallized grain structure obtained by working techniques (a. from Garagnani 1996; b. from http://www.doitpoms.ac.uk).

Microstructure and therefore the manufacturing technology used to obtain an object, has a great influence on corrosion behavior.

Crystallographic orientation of grains has an effect on corrosion resistance *[Jones, 1996]*. By definition, metal atoms situated along grain boundaries are not located in a regular crystal array (i.e. a grain). Their increased strain energy translates into an electrode potential that is anodic to the metal in the grains proper. Thus, corrosion can selectively occur along grain boundaries. Regions within a metal subjected to cold-work contain a higher concentration of dislocations, and as a result will be anodic to non-cold-worked regions. Thus, cold-worked sections of a metal will corrode faster *[nace.org]*.

I.1.2.1.3   Nature and amount of alloy elements

As formerly introduced, copper is alloyed with different metals to increase its mechanical strength. The nature and amount of these elements has an influence both in the alloy microstructure and therefore in the corrosion behavior of the alloy. Bronze refers to a pure alloy Cu-Sn, but the term is used to indicate a wide variety of alloys comprising copper alloyed with Sn, Zn and Pb as minor elements and several other trace elements (Fe, As,

Sb…).

Individual phases possess different electrode potentials, resulting in one phase acting as an anode and selectively subject to corrosion.

I.1.2.1.4   Effective redox potential

Each metal when exposed to a certain environment, assumes a certain potential, the corrosion potential, E_{cor}, that is the result of possible oxidation and reduction reactions, which could take place [*Jones, 1996*].

I.1.2.1.5   Ability of the alloy to form a protective (passive) film

Passivation is defined as the process of formation of a very thin oxide layer exhibiting protective properties (or s a kinetic barrier) towards further oxidation or dissolution of the alloy [*Silvestroni, 1996*]. When metal dissolves, its ions are produced at the interface metal-electrolyte. For high corrosion rates (high value of corrosion current) the concentration of M^{z+} on the metal surface easily exceeds the solubility equilibrium constant of the hydroxide (or any other reaction product in a specific electrolyte), thus leading to its precipitation. The formation of a compact layer of oxide on the metal surface causes a high over-potential to be reached, which hinder further alloy dissolution.

In order to form a protective layer, several conditions must be satisfied, namely: the metal should be easily corrodible and the value of the solubility equilibrium constant for the oxide must be very small. Moreover, it shall be taken into account the relative volumes of the oxide formed in respect with the volume of the metal consumed to produce it. Pilling and Bedworth has defined a relationship (Eq. I.4) between these two values and they call it Q-value [*Stambolov 1985*]:

$$Q = \frac{V_0}{nV_m} \qquad (I.4)$$

where V and V_0 are, respectively, the atomic and molecular volumes of the oxide and the metal, while n gives the number of metal atoms in the oxide. Metals with Q-values greater than unity form films which impede the diffusion, thus exhibiting protective properties, and avoiding further dissolution of the alloy [*Stambolov 1985*].

I.1.2.2   Exogenous factors

Exogenous factors are represented by the environmental condition in which the artefacts have been laying during the burial time. In the next paragraphs the main parameters playing a role in underground corrosion will be considered.

I.1.2.2.1   Soil texture

Soil is the corrosion medium for archaeological bronzes. Its name is comprehensive for a mixture of various materials which usually contains mineral matter, organic matter, water and air [*Stambolov, 1985*]. Their nature, and the way how these factors interrelate, will determine the aggressiveness of a given soil in respect with metal artefacts corrosion.

Mineral matter is a conglomerate of sand, silt and clay and their relative amount determine the soil texture (see Figure I.6).
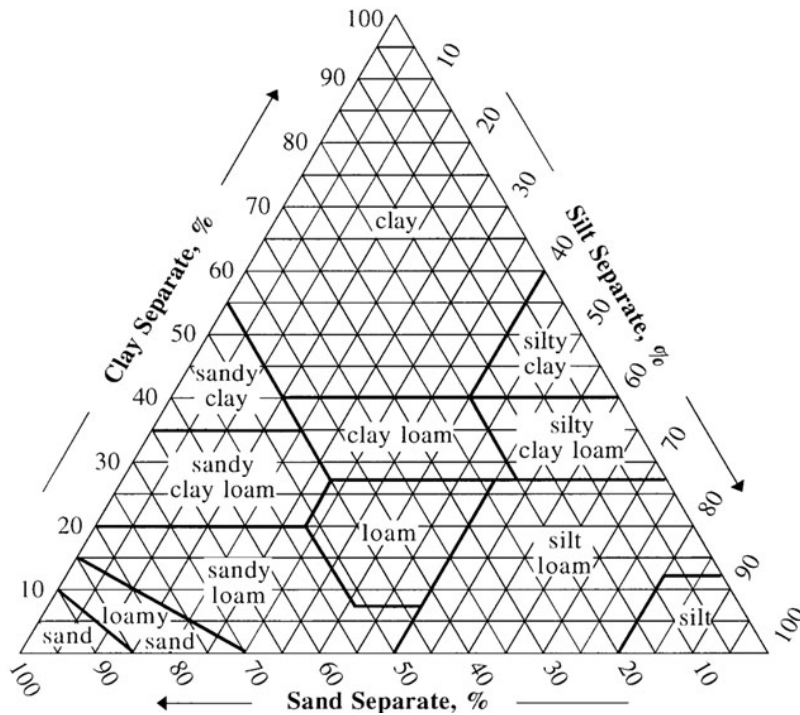
Figure I.6. Soil texture triangle defined by the USDA (www.wikipedia.it)

Sand consists of large particles with negligible specific surface (Surface/Volume). Compact sand grains give rise to a structure of wide pores through which water and air may percolate at random. Moreover, its stable chemical composition determines inertness as regards physical-chemical reactions and serve but as a framework to which active soil may be fastened [*Stambolov 1985*].

Silt consists of almost un-decomposed mineral matter even if smaller of sand particles, silt particles do not have a specific surface large enough to be influential in a chemical or physical sense. Their particles, having small and variable size allow a dense packing: silt pores are narrow and therefore movement of water is obstructed. They have water holding capacity [*Stambolov 1985*].

Clay is the product left after decomposition of various igneous rocks and consists of hydrated aluminum silicates often contaminated with Fe, Mg and other impurities. Particles have a

large specific surface and small dimensions providing water holding capacity. Water is absorbed as a film on each clay particle which coated in its turn and may hold debris of dissolve salts and keep them attached to its surface. Water causes the clay to swell, its wetting leads to a quite compact mass which is practically inaccessible to air.

For this reason, clay soils are non-corrosive. But this is true for entirely clay-containing soil as the tightness responsible for this impermeability is due to the enormous specific surface of clay matter (million times more than those of coarse sand).

Organic matter (or humus) has a complex chemical composition, combining in an inhomogeneous mass such diverse materials as tannins, fats, waxes, gums, resins, lignin, cellulosic remains and protein. It seems that the complex structure of humus consists of ordered aggregates of amphiphiles (molecules with separate polar and non polar parts) composed mainly of relatively unaltered plant polymer segments attached to carboxylic groups. These reacts with soil mineral grains to form membrane-like coatings of amphiphiles with highly charged exterior surfaces which act as separate ion-exchange phases [*Wagner 1997*].

As illustrate in the Figure I.5 real soils are not purely sandy silt or clayish but they are made up of different proportion of the mineral particles, having different sizes and this will determine the soil texture.

I.1.2.2.2   Position of water table

Water plays a major role in corrosion. The position of the water table influences the nature of corrosion process as it can determine the rates of oxygen transport (the aeration) in the soil. Its position can vary seasonally and this may influence the nature of corrosion process occurring on the buried structure. There exist three sources of water (Figure I.7): gravitational water (rainfall, snow), capillary water (held within capillary in soil particles) and groundwater (result of the accumulation of water at the water table).
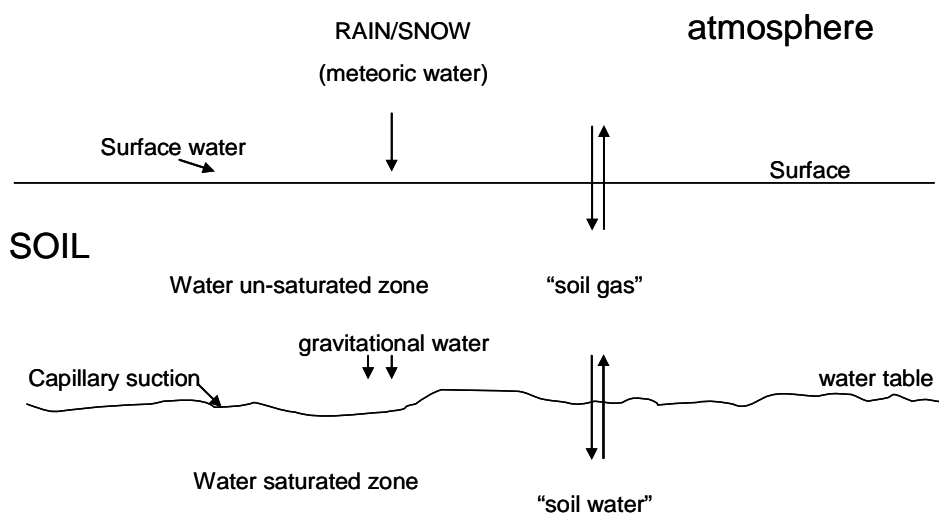
Figure I.7. Illustration of water dynamics in soil: corrosiveness of soil is strictly dependant on occurrence of water un-saturated zones [after Brown 1977].

Subterranean water dynamics determine the occurrence of water unsaturated and saturated zones in soil and this can directly affect the oxygen availability and therefore the oxidation rate of a metal buried in it.

In water-saturated deep soils, oxygen is transported by diffusion, which is a slow process and therefore the corrosion rate in these conditions is very low. In the zones next to the ground surface, the soil pores are open and the aeration is usually good. In spite of this, the corrosion rate may be low due to the lack of electrolyte. In the zones just above the water table, where the soil pores are partly filled with water, the condition are most favorable to corrosion; both oxygen supply and electric conductivity are sufficient for the corrosion cells to be active [*Mattson, 1996*].

In natural soils, the degree of water saturation is variable. It is the frequency of the reversible transition from unsaturated to saturated condition which is damaging for buried metals as the change from unsaturated to saturated condition increases the corrosion current density [*Romanoff 1985*].

As a consequence, in autumn, when rainfall increases and saturation condition are likely to occur, the rate of underground corrosion tends to slow down (if compared with summer). On the contrary, in the late spring, when temperatures starts to rise up, and water evaporation increases, underground corrosion is at its highest level.

Soil aeration is also affected by the land use: *Escalante* [*1989*] has defined *disturbed* soil those in which digging or backfilling has taken place. Soils used for agricultural purposes, and therefore subjected to ploughing, cultivation and harrowing, can be assimilated to this category as well. Soil compacted by heavy vehicles, on the contrary, decrease aeration [*Mattson 1996*].

Differential aeration corrosion, or oxygen concentration cells, has been since long time investigated [*Evans 1924*]. It implies region where oxygen concentration is different and therefore the reaction $\frac{z}{4}O_2 + zH^+ + ze^- \rightarrow \frac{z}{2}H_2O$ occurs at different rates on different regions on a metal surface in contact, for example, with a drop of water. The O_2-rich area is positive in comparison with other regions, which act as negative and therefore corrode at a higher rate.

The mechanism can be explained as follows: when the metal surface is in contact with water it dissolves producing an excess of electrons which reduces the oxygen in air by the well known reaction II.4 causing the precipitation of metal oxides. The oxygen consumed in this reaction is not reintegrated at the same speed in oxygen rich (at the edge of a water drop) and oxygen poor areas (in the middle of a water drop). That is why the corrosion occurs faster in the edges of a water droplet.

I.1.2.2.3   Nature and concentration of ions in solution

The soil solution represents the electrolyte in electrochemical cells which set up in underground conditions. The nature and concentration of soluble salts dissolved in it determine the electrical conductivity, which is a measure of the ability of a medium to conduct an electrical current.

Conductivity, represented by the Greek letter σ, is the reciprocal of the electrical resistivity, ρ, and it is expressed as units of Siemens per meter (S·m^{-1}), Eq. I.6:

$$\sigma = \frac{1}{\rho} \hspace{3cm} \text{(I.6)}$$

As soil resistivity become lower (groundwater saltier and more conductive) the soil corrosion becomes faster. The electrical conductivity of the medium is determined by the amount of soluble species dissolved in it. We are mainly interested in the following anions: Cl^-, SO_4^{2-}, CO_3^{2-}, HCO_3^-, PO_4^{3-} not only for their contribution to conduct electric current, but also for their specific interaction with the metal or alloy. For example, as we will see later in the discussion, chlorine anions have a detrimental effect on corrosion of buried metal as may cause the breakdown of protective passive layers [*Mattson 1996*].

Sulphates have a main role in atmospheric corrosion of metal exposed to polluted areas; in soil its occurrence is not significant, even though, especially in estuarine environments, when anaerobic condition occur, the action of sulfate-reducing bacteria (See paragraph II.1.2.2.6) can reduce sulfate specie to sulfidric acid, more harmful for metals.

Even if soluble ion content has a direct impact upon the resistivity, certain ions will have

opposite effect: for example Ca^{2+} and Mg^{2+} tend to form insoluble carbonate deposits at the metals surface, thus slowing the corrosion rate. Calcium hydrogen carbonate produces protective effects through two mechanisms, which are considered here in the specific case of copper-based alloys [*Stambolov 1985*]. HCO_3^-, being a salt of a weak acid, its watery solution reacts alkaline and by binding active carbon dioxide it prevents dissolution of oxide layers such as copper (I) oxide. Furthermore, at pH greater than 8, it precipitates as carbonate (also on the bronzes surface, thus protecting it) and by subsequent acid condition it dissolves, instead of the copper (II) compounds.

It is believed that phosphates have a benefic effect being used as a corrosion inhibitor for iron objects [*Mattson 1996*]. Phosphates occur in soils as mineral apatite, but it often has an anthropological origin as it is used like additive in fertilizers. Natural sources of phosphates are bones and ivory which are believed to be able to absorb copper (II) salts producing the basic copper (II) phosphate, libethinite $Cu_4(OH)_2(PO_4)_2$ [*Romanoff 1985*].

I.1.2.2.4   Soil pH

The development of acidity is the results of the natural processes of weathering under humid conditions [*Romanoff, 1965*]. Commonly, soil pH varies in the range 5-8. Soil containing well humified organic matter tends to be acidic. Mineral soil may become acidic due to the leaching of basic cations (Ca^{2+}, Mg^{2+}, K^+) by rainwater and because of dissolved CO_2 into the groundwater. According to Pourbaix diagrams, pH values influence the stability of corrosion compounds formed. However, soil pH is generally considered not to be the dominant variable affecting corrosion rates [*www.nace.org*]. Most soils and all loams are fairly well buffered, resulting in a soil pH that is not affected by rainfall. Sand, because of its high moisture diffusivity, can have its soluble salts leached out or diluted to the point that its pH will change during heavy rain [*Escalante, 1989*].

I.1.2.2.5   Soil temperature

The temperature of soil is certainly a factor in the corrosion processes as it influences the reaction speed. Some interesting effects have been pointed out. The resistivity of soils is inversely proportional to temperature, and an increase in soil temperature would be expected to increase the rate of reaction. However, an increase in temperature also reduces the solubility of oxygen, which tends to reduce the reaction rate at the cathode [*Escalante, 1989*]. The net result is that temperature doesn't have a large effect on underground corrosion. Also it shall be considered that a changing of temperature is of significance only at very superficial depths.

I.1.2.2.6 Presence of microorganisms

The microfauna present in soil feeds on the humus and therefore, by decomposing organic matter, hydrogen sulphide is formed. Copper sulphides are therefore expected corrosion products within the patina. After subsequent oxidation they will be transformed to soluble sulphates [*Tylecote 1979*].

Microorganisms, naturally occurring in soil, colonize the metals surface and produce biofilms (see Figure II.8), where they are able to maintain different condition from the bulk environment [*McNeil and Little 1992*]. If anaerobic condition occurs, an important class of bacteria that could play an important role in corrosion is constituted by sulphate-reducing bacteria (SRB). They require oxygen-free environments and pH values in the range 4-8. These bacteria utilize hydrogen in reducing SO_4^{2-} to S^{2-} and H_2S, in this way they promote the formation of sulphide films.
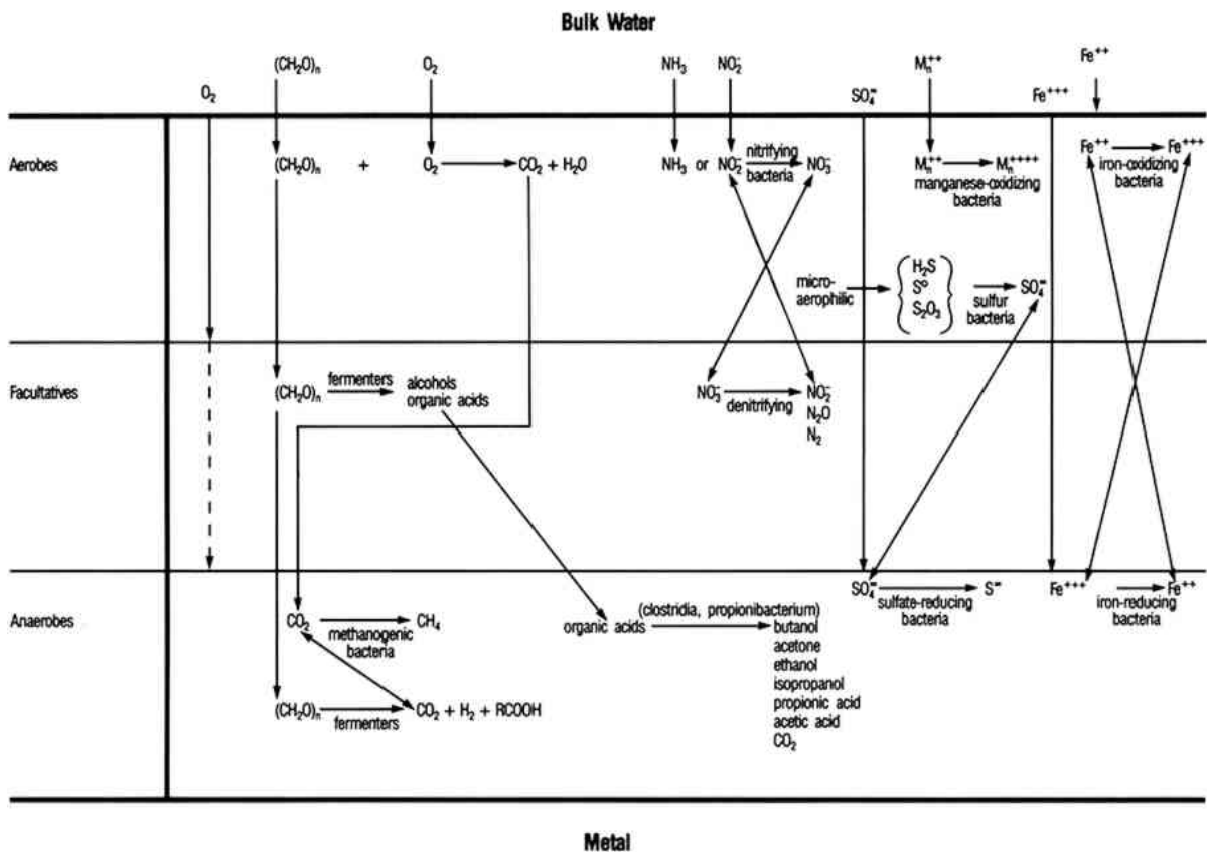
Figure I.8. Possible reactions within a natural occurring biofilm [McNeil and Little, 1992].

I.1.3 The use of Pourbaix diagrams for prediction of corrosion products

The study of bronze corrosion has a very long history [*Chase 2007; Scott 2002*] and the E_h-pH (or Pourbaix) diagrams are often used in explaining corrosion of archaeological artifacts [*Schweizer 1994; Lins 1994; Scott 2002; Little 1999*].

Pourbaix diagrams are graphical representations of thermodynamic and electrochemical equilibria between metal and water, indicating stable phases as a function of electrode potential and pH. They can be used for the prediction and interpretation of long term corrosion products. In these graphs there are usually reported the regions of stability for water as it is itself sensible to variations in potential and pH. Two lines in the graph define the upper and lower limits of water stability against the oxidation to oxygen and reduction to hydrogen. The figure below (Figure I.9) reports the overlapping between the Pourbaix diagram for water and the values for E_h and pH recorded in many different natural environments.
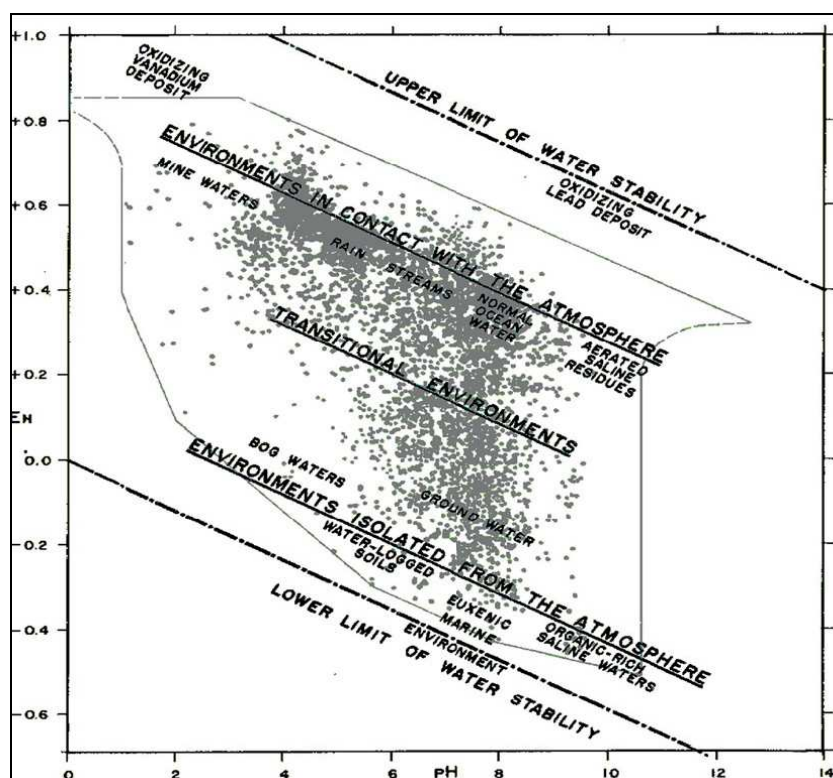
Figure I.9. Environments represented on a E_h-pH diagram: the cloud indicates points measured for thousands of natural environments [Garrels and Christ, 1965].

The thin line which separates the points indicates the limit of possible environments at atmospheric pressure. The interesting thing is that any local condition can be specified on the graph simply by measuring potential and pH in situ.

Figure I.10 provides the Pourbaix diagram for copper-water system. It can be drawn also to indicate regions where copper is immune or inert (meaning that the corrosion is impossible),

passive or active, rather than the exact copper species [*Pourbaix 1963*].

It must, however, be remembered that Pourbaix diagrams do have their limitations. They can be drawn only for equilibrium conditions and specific environments (temperature, pressure and concentration of reactants). Moreover, the construction of these diagrams doesn't take into account of kinetic of reactions [*Pourbaix 1963*]. Even if a compound is thermodynamically stable in defined conditions, kinetic factors do not allow its formation and empirically is not encountered.

It is worth mentioning here the case of tenorite, as we are mainly interested in the use of this tool for the interpretation and prediction of corrosion products for copper and bronzes.
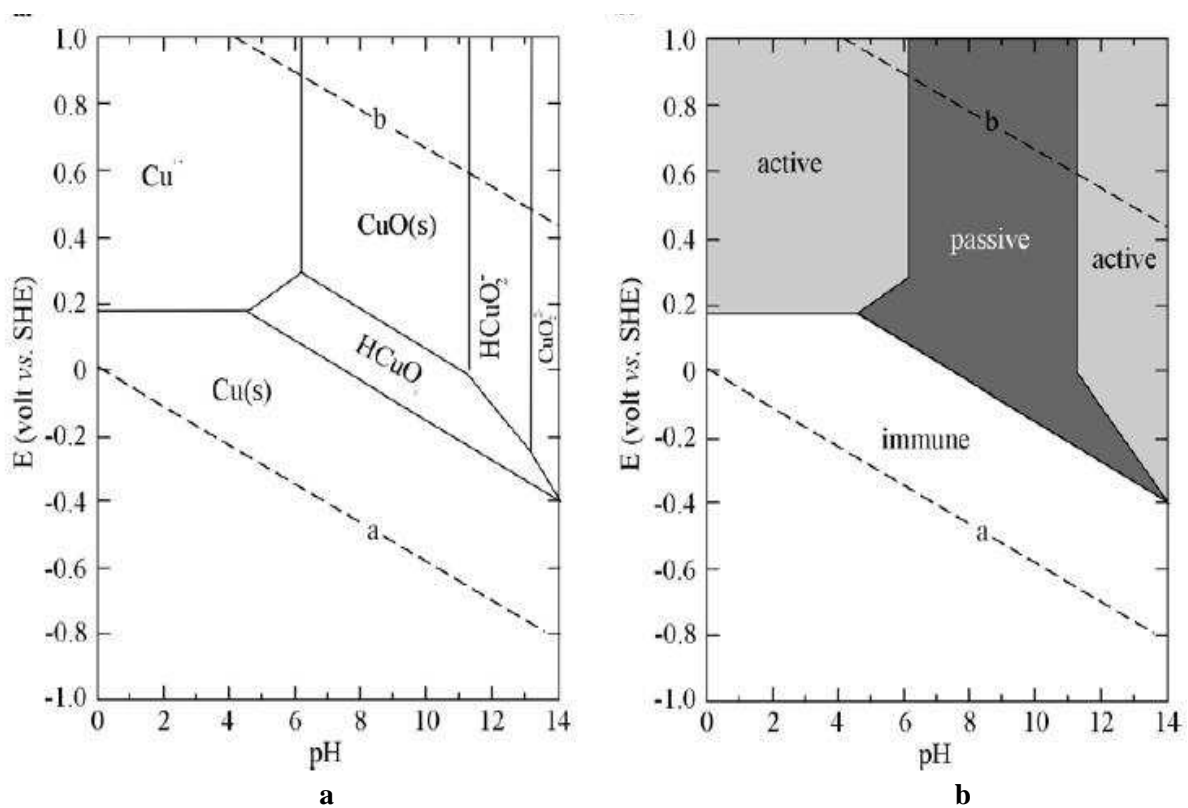
Figure I.10. Pourbaix diagram for a copper-water system (25˚C, 1 atm, $10^{-6}M$ Cu^{2+}).
a) Regions are labelled with the species that is most thermodynamically stable in that area. Water is stable within the boundaries set by the dashed lines a and b; it can be oxidized to oxygen gas above the line b and it can be reduced to hydrogen below the line b.
b) the same potential-pH diagram, but this time the regions are labeled as immune, active or passive.[Selwyn 2004].

The graphs for Cu-H_2O system (Figure I.10) show a wide areas of stability for the copper (II) oxide, the mineral tenorite, which is in practice rarely encountered. The product usually found on copper surfaces in the copper (I) oxide, cuprite. Tenorite is not kinetically favored and is usually found only in burned burial environments; corrosion appears to be strongly influenced by the presence of cuprite and by the growth of minerals that can occur from subsequent reactions with cuprite or with copper ions [*Scott 2002*].

Stability diagrams can be created for whichever system and it is useful to determine the stable corrosion products forming in each condition. Figure I.10 reports as an example the stability diagram of copper in seawater. The main corrosion products encountered in this medium are cuprite [Cu_2O], trihydroxyl-chlorides [general formula $Cu_2(OH)_3Cl$] and spertiinite [$Cu(OH)_2$].
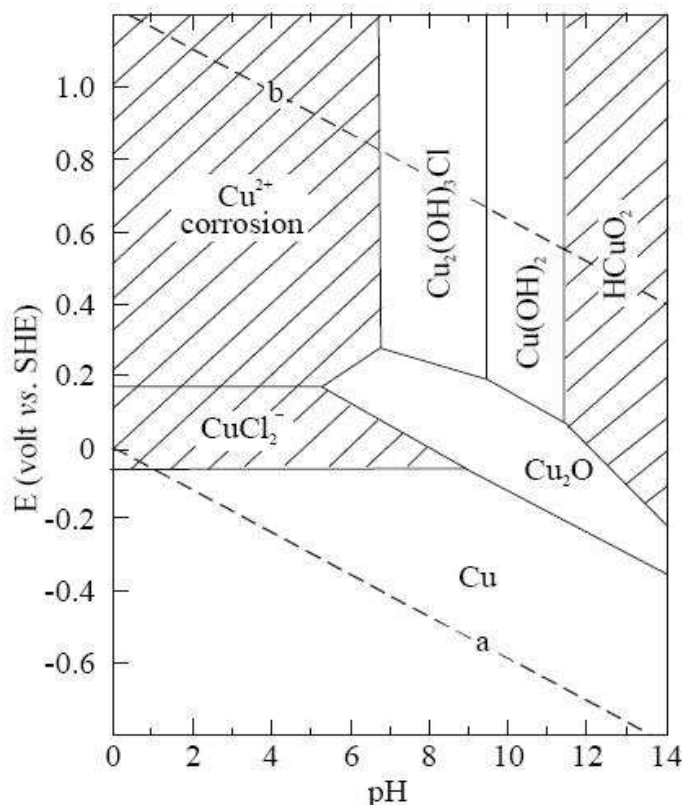
Figure I.11. Pourbaix diagram for copper in seawater [after Taylor and Macleod, 1985].

A recent work by Chase *et al.*[*2007*] proposes new Eh-pH diagrams incorporating copper and tin together as well as intermetallic phases, a very useful tool for an enhanced understanding of corrosion processes regarding archaeological bronzes.

It is reported here (Figure I.12) the diagram for the system $Cu-Sn-CO_2-H_2O$ at various concentration of CO_2. It can be noticed that increasing the concentration of CO_2, the right-hand limit of the field of stability of malachite, $Cu_2(OH)_2CO_3$ (in the figure indicated as $CH_2O_5Cu_2$), a copper basic carbonate, is displaced toward higher pH, and the field of stability of tenorite (CuO), becomes smaller. It is also pointed out here the question of stability of malachite and azurite: it seems that these solids have similar stabilities and one, the other or both could be stable.
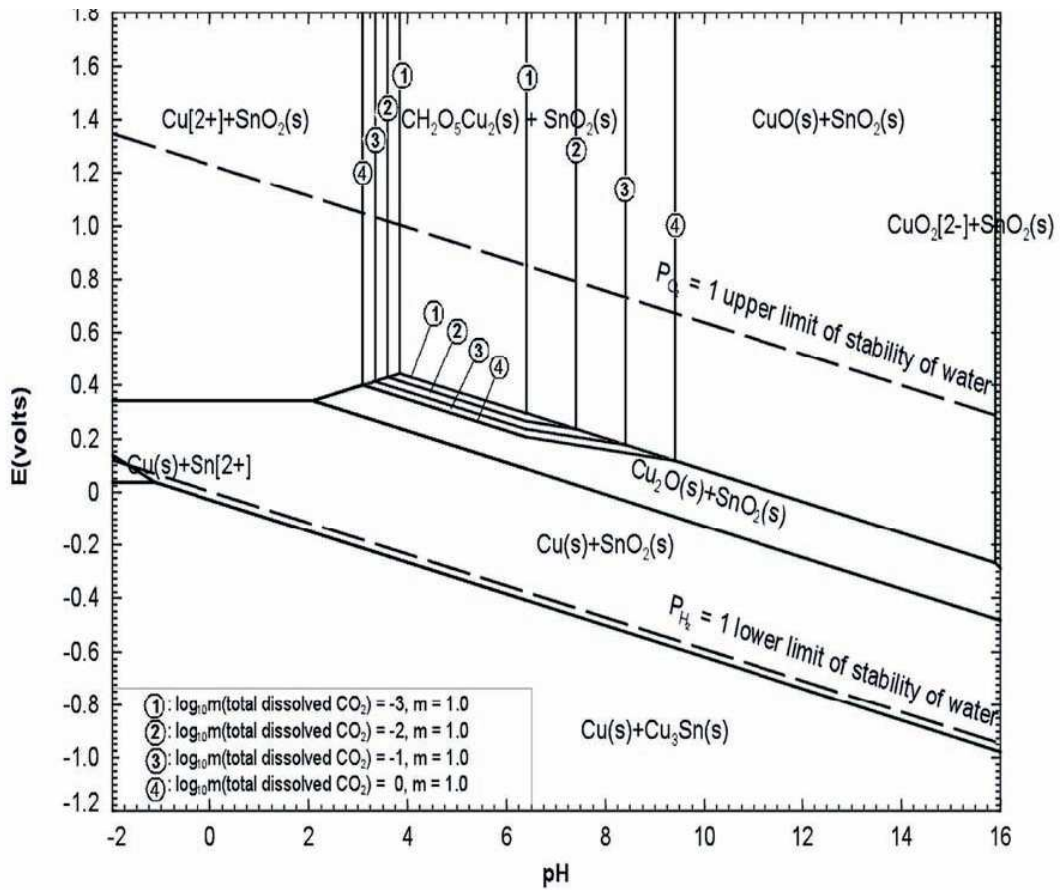
Figure I.11. Eh-pH diagram for the system Cu-Sn-CO$_2$-H$_2$O at 298.15˚C.
Log$_{10}$ m(CO$_2$)=-3 to 0 (44 ppm to 4.4%); log$_{10}$ for other aqueous species=1. Different concentration
for CO$_2$ are marked by circled numbers [Chase 2007].

A major result, worth underlining here, is the diffuse presence of solid tin oxide (SnO$_2$) as stable phase for tin. Moreover, when the diagram was built including the intermetallic phase Cu$_3$Sn$_{(s)}$ (corresponding to δ), this phase has resulted more stable. Even though it is known that tin oxide is very insoluble, its role in the corrosion of bronze is still not completely clear.

I.2   Critical review of published literature

The interest in the research field of long term corrosion behavior of bronze artifacts is demonstrated by the great number of works published in Conservation Journals [*Tylecote 1979; Scott 1985; Gettens 1975; Schweizer 1998; Mazzeo 2004; Robbiola 2006; and others*]. Recently, a conspicuous number of publications concerned the study of bronze behavior in different electrolytes [*Sidot 2006; Wang 2007; Souissi 2007; Robbiola 2008*].

It is worth remembering here that already in 1977 [*Brown 1977*] the National Bureau of Standard (nowadays NIST) organized an international meeting which was an opportunity to bring together material science people, such as engineers and corrosion scientists, with conservators and archaeologists. It has been a dialogue useful on both fields, as the restoration practices could have a scientific approach, but also the study of corrosion products that have taken centuries to form on metal artifacts can reveal needed kinetic information that usually are not accessible with the short test periods commonly employed.

The ICOM-CC Metal Working Group Congress held in 1995 saw the participation of authors who proposed a classification of soils in terms of impact of **conservability** for archaeological heritage [*Wagner 1995 and Kars 1998*]. The definition of **soil archives** has arisen as it indicates the nearly stable burial condition, which induces a slow but steady corrosive decay.

As early as in 1976, a Polish chemist, Hanna Jedrzejewska [*Jedrzejewska 1976*], suggested to consider ancient bronzes as "document of the past" and proposed to preserve materials of little or no artistic value for scientific investigations. Since that time, several authors [*Scott 1985, Robbiola 1992, 1993, 1998; Nord 2005; McNeil 1992, 1999; and others*] dedicate their scientific interest to the elucidation of the long-term corrosion mechanisms occurring for artifact made of bronze or copper alloys. An early publication by *Tylecote* [*1979*] investigated the effects of soil parameters on the long-term corrosion of buried tin-bronzes and copper.

It has been emphasized the specific effects of soil characteristics which are variable among archaeological sites: sandy, silt or clay soil can have either a protective or detrimental effect on metal corrosion buried in them [*Stambolov 1985*].

A project, developed along such research direction, was undertaken by the Sweden Central Board of National Antiquities [*Mattson 1996*]. The interest was to investigate the causes of deterioration of archaeological material, as archaeologists have reported an increase in their degradation as a consequence of the acidification of rain.

Recently [*Ingo 2007*] the ISMN-CNR Institute in Roma has published the results obtained

over a five year project, EFESTUS, aimed to propose tailored strategies for conservation, restoration and valorization of historical and archaeological copper-based artifacts from Mediterranean Countries. The result was the examination of a wide variety of archaeological metallic artifacts which provided a good insight into the nature of corrosion layers grown on archaeological artifacts, pointing out the main causes of degradation phenomena. It was found that all over the Mediterranean archaeological contexts (Italy, Turkey, Jordan, Spain and Tunisia) the main and most harmful corrosive agent is chlorine, as demonstrated by the occurrence, in some cases, of bronze disease.

Robbiola [*2006*] has recently proposed a global approach based on the alloy-patina-environment system with the purpose of authentication of ancient bronzes as the bronze patina shall be regarded as the result of the interaction between the alloy and a specific environment. *Mazzeo* [*2004*] reminded the pathways of *patina*'s genesis in different media of interaction, such as urban, marine and underground. As already introduced, typical corrosion products found on bronze coincide with the mineral ore from which copper was extracted and the most common are reported in Table IV.2 in chapter IV, Material and Methods. For example, basic copper chlorides characterize patinas recovered from marine environments, while basic copper carbonates are commonly encountered on archaeological bronzes. Sulphates and nitrates are considered relatively „new" corrosion products as are commonly found in urban environments as a result of alloy interaction with pollutants [*Lins 1995*].

The morphologies and mechanisms of formation of natural patinas formed on bronze alloys have been widely investigated by Robbiola and colleagues, who published an ample work [*Robbiola 1998*] where a phenomenological model is proposed. There were evidenced the occurrence of two kinds of structures as a result of higher or lower dissolution rates. After this step, one phase controlled by ionic species diffusion through the oxides layers takes place followed by the ageing of corrosion products with oxidation of cuprous to cupric species. The steady state is rapidly reached with respect to the burying time, the duration of the two first steps being much shorter than that of the last one.

Type I structure is effectively a passive layer and can be ascribed to internal tin oxidation, accompanied by copper selective dissolution [*Robbiola 1998*]. It can be described as a two-layered structure, the outer one characterized by low copper content and presence of elements from the corrosive environment (O, Si, Al, P, Fe, Ca and Cl). In contact with the alloy, there is an internal layer, irregular in shape and thickness characterized by copper content lower than in the alloy (decuprification) and higher tin content, probably present as oxide.

Type II structure are characterized by a three layered structure (and the presence of a cuprous oxide) and the corrosion process is assumed to be controlled by mass transportation of aggressive anions from the soil (such as oxygen and chlorine).

In the last decade, the scientific interest of researchers involved in this field has moved to the basic understanding of bronze corrosion in different media [*Ammeloot 1999; Debiemme-Chouvy 2001; Sidot 2006; Souissi 2007; Chiavari 2007; Satovic 2009; Bernardi 2009*] using standard electrochemical methods.

Even though laboratory simulation timescale is not comparable with the hundreds or thousand year of exposure to burial condition, it is useful to perform these experiments in order to understand the earlier phenomena occurring in different more or less aggressive environments.

It shall be reminded here that bronze corrosion has been commonly explained using the copper model [*North 1987; Hamilton 1998*] as the main components of bronze corrosion products are copper-based compounds [*Scott 2002; Mazzeo 2004*].

The role of tin has been recently pointed out by some authors, who evidenced the different electrochemical behavior of bronze as compared to that of copper [*Souissi 2007*]. New versions of conventional Pourbaix diagrams have been proposed, as they provide understanding of corrosion under diverse conditions and emphasized the role of tin oxide [*Chase 2007*].

Cyclic Voltammetry proved to be a powerful technique for mechanistic and kintetic studies of metals and alloys [*dos Santos 2008*], while Electrochemical Impedance Spectroscopy is nowadays a widely used technique for the investigation of protective properties on bronze artifacts [*Cano 2008; Letardi 1998*] as it is a powerful technique to characterize the surfaces' structure and electrochemical properties.

Chapter II

Archaeological Context

II.1   The region of Dobrogea and its archaeological sites

The research has been carried out in close relationship with archaeologists from the Research Institute Eco-Museal in Tulcea, ICEM, which is in Dobrudja, a region located in the South-East of Romania (Figure II.1). This area, which is extended both in Romania and Bulgaria, presents a very interesting history, especially during the Roman and Byzantine times. It has been of noticeable strategic importance, due to its location next to the Danube Delta. In the following paragraphs, we will discover a taste of its long history.

*Figure II.1: Map of the region of Dobrudja (**http://www.restromania.ro**).*

The period of the Roman domination in Dobrudja (I B.C. – beginning of VII A.D.) is well-known due to the investigations made at the fortresses Orgame-Argamum (Jurilovca - Capul Dolojman), Dinogetia (Garvan), Halmyris (Murighiol), Troesmis (Iglita,Turcoaia)

Noviodunum (Isaccea), Ibida (Slava Rusa), Aegyssus (Tulcea), at the burghs (fortifications) at the *villas rusticate* from the zone Horia, Niculitel and Telita, at the necropolis from Noviodunum, Beroe and Enisala.

The antiquity of Christianity on the territory of Dobrudja is proved by the discovery of basilicas with martyrs' crypts at Halmirys, Niculițel, Beroe, the Palaeo-Christian Complex from Ibida/Slava Rusa and by the organization of 15 bishoprics, subordinated to the bishop of Tomis, the capital of the province.

In VII – IX A.D., the Slave invasion determined the abandonment of the towns and, implicitly, of the urbane life in Dobrudja. A new culture (Dridu culture), specific for the Balkan-Danubian space appeared, fact proved by the archaeological discoveries made at Enisala (settlement), Nalbant and Valea Nucarilor (necropolis).

At the end of X A.D., the territory between Danube and Black Sea enters in the Byzantine Empire, fact which will lead to a flourishing of the economic life, demonstrated by the investigations from the sites of Preiaslaveț (Nufaru), Isaccea, Dinogetia-Garvan, Beroe.

After a period of peace and relative prosperity, beginning with the second half of XVIII A.D., Dobrudja becomes war theatre in the Russian - Turkish or Austrian–Russian – Turkish confrontations, fact which will lead to the destruction of the fortifications from Babadag, Isaccea, Tulcea, Macin.

The war for the Romanian state independence brought back Dobrudja inside the Romanian state borders. A period of administrative, social and cultural integration of the new province followed up. After this moment, Dobrudja will have a natural evolution inside Romania, with the particularities given by the presence of more than 15 nationalities on its territory.

II.2   (L)Ibida: a case study

Among the archaeological sites visited during these years, we had the chance to study deeper in detail the one of (L)Ibida (nowadays, Slava Rusa). The possibility arose from an interdisciplinary research project, which has involved the University "Al. I. Cuza" from Iasi, as well as other institution in Romania. Thanks to this project I had the possibility to work together with other chemists and geologists who sampled the soil in the area in order to carry out archaeo-zoological studies [*Stanc 2009*].

II.2.1 History

The gradual integration of the Dobrudja region, comprised between the Danube River, the Black Sea and the Balkans, to the Roman Empire during the I century AD, did change the shape and aspect of the inhabited region in the valley of the Slava River. Coins and roman material, such as ceramics and glasses, suggested the trades, which took place in the region.

The Romanian historian and archaeologist, Prof. Vasile Parvan, identified the city as *polis Ibida*, in a writing of Procopius from Caesarea, who mentions it as one of the cities rebuilt by Justinian.

(L)Ibida was described as the biggest city of Dobrogea, having a total area of 24 ha, fortified walls built over an area of 2000 m, 24 towers and three gates, in the shape preserved since the Tetrarchy period (284-305 AD), with reconstructions dated back to the Giustinian time. The city has showed up to the archaeologists of the XIX century as "a city with enormous walls and towers" (P.Polonic), "exceptionally big-the most significant of the whole region of Dobrogea and, surely, the crossroad of all the northern ways of the Province" (V. Parvan).

The defensive system of the city was ultimate with a fortress, built on the hill Harada ("The city of the lady" in Turkish), whom Northern side coincides with the city's one.

Archaeological investigations, carried on, non-continuously, since the beginning of the XIX Century, has revealed – in the city center – a *basilica* with three naves and three apses, with marble columns and capitals and mosaic decorated floors, a unique monument in the region of Roman-Byzantine Dobrogea. The stratigraphy of the city (I-VII Century AD) was established by subsequent studies.

Since 2001 'til today important vestiges from the Roman times were brought back to light: the city-wall in the areas of **Curtina G**, Curtina D, and the West Gate, the *pillae* of the old bridge crossing the River Slava, a few houses, small oven for glass, the sewer network. The inhabited *extramuros* centres, either in the North and South –West part of the city, were identified and investigated. In the necropolis of the Roman-Byzantine city over 100 tombs were investigated

and also a family grave. The latter, having big dimensions (8x3,5 m), built up in bricks and stones, is constituted of a *dromos* and a funeral room, painted in the interior part, with the brick floor, was used by 39 persons of an important family of the city.

II.2.2 Geography and general geological information

General information regarding climate, geography and geology were gathered at the National Geological Institute, Bucharest, before any soil sampling has been carried out.

Generally, the climate of the region is temperate-continental and therefore characterized by dry and hot summers and cold and rainy autumn-winter, with temperatures mitigated by the vicinity of the Black Sea. Precipitations results to be generally scarce, generally not exceeding the value of 600 mm/year (see Table II.1).

Table II.1. Data relative to the mean temperatures and average rainfall recorded
in Tulcea, for the period 1961-2007

Meteo station: Tulcea					
Year	Annual Mean Temperature	mm rain (sum over an year)	Year	Annual Mean Temperature	mm rain (sum over an year)
1961	11.4	389.6	**1985**	9.6	389.2
1962	11.2	508.5	**1986**	11.0	363.4
1963	10.6	501.7	**1987**	9.7	415.5
1964	10.8	413.3	**1988**	10.8	627.7
1965	10.2	524.9	**1989**	12.0	439.8
1966	12.2	666.4	**1990**	12.3	353.5
1967	11.1	328.3	**1991**	10.8	420.9
1968	11.2	445.7	**1992**	11.3	436.6
1969	10.3	567.3	**1993**	10.7	432.3
1970	11.6	392.8	**1994**	12.4	298.1
1971	11.2	490.9	**1995**	11.3	454.3
1972	11.0	501.9	**1996**	10.6	522.5
1973	10.3	342	**1997**	10.5	732
1974	10.6	466.3	**1998**	11.5	527.2
1975	12.0	394.9	**1999**	12.2	640.9
1976	10.5	423.3	**2000**	12.3	357.7
1977	11.2	383.1	**2001**	11.8	419.9
1978	10.5	457.3	**2002**	12.3	460.4
1979	11.4	486.8	**2003**	10.8	397.5
1980	10.2	625.2	**2004**	11.6	619
1981	11.4	442.7	**2005**	11.4	651.9
1982	11.1	285.9	**2006**	11.3	421.4
1983	11.5	273.7	**2007**	12.9	508.3
1984	10.9	476.1			

The depression area in the plateau of Badabag (see Figure I=II.), at the junction of the rivers Slava and Basprinar present land with reduced slope 5%, altitude 50 m ca., Nordic exposure, and a good drainage.

Superficial deposit consists of material loess argillaceous, limestone (< 20% $CaCO_3$) with the

addition of calstic[1] calcareous material (5–10%). In the lower areas of the site there appears also argillaceous fluvial deposits, calcareous and with rock fragments.

The Actual soil cover is Chernozem[2] and calcareous Chernozem, with– 4 % of humus, weak alkaline-alkaline reaction (pH = 7.5 – 8.0). The reaction becomes alkaline with depth (pH = 8.0 – 8.5). Apart from $CaCO_3$ (5 – 15%) it doesn't seem to be present other salts. An area of the site, a location, it is occupied by soil of Rendzinic type (Rendzinas Leptosols) that is the subsoil is constituted by a high porous limestone, with a humus content until 4-5% and a weak alkaline-alkaline reaction (pH = 7.5 – 8.0).
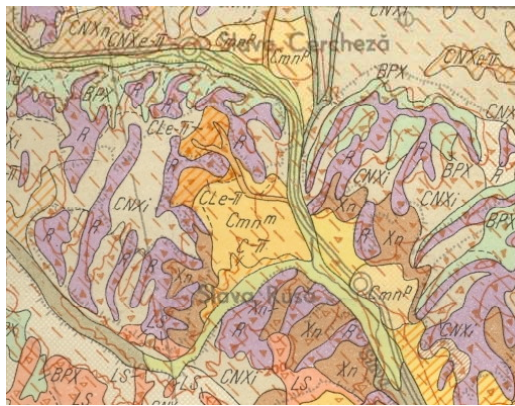
Simbol on the map	Name (terminology WRB-SR-2006)
SAdl	Calcic Haplic Fluvisols
LS	Lithic-Eutric Leptosol
R	Rendzinic-Lithic Leptosol
Cmn^m	Calcic-Voronic Chernozems
Cmn^P	
CLe-π	Calcic Chernozems (eroded phase)
Xn	Calcic Chernozems Greyic
CNXi	
BPx	Calcic Luvisols

Figure II.2: Geological chart of the region of Slava Rusa (Ibida) with its legend.

---

[1] of or belonging to or being a rock composed of fragments of older rocks (e.g., conglomerates or sandstone).

[2] **Chernozem**, or **Black Earth** (from Russian: *black soil*) is a black-coloured soil containing a very high percentage of humus — 3% to 15%, and high percentages of phosphoric acids, phosphorus and ammonia. Chernozem is very fertile and produces a high agricultural yield.
Source: Wikipedia, The free encyclopedia, www.wikipedia.com.

II.2.3 Physical and chemical characterization of soil

II.2.3.1   Material and methods

Soil sampling was carried out in three locations at Slava Rusa. They were aimed to characterize reference soil profiles (Area Curtina G, Area "Vasilis"), and the soil where the examined bronze objects were discovered (Area Building 1, Area Curtina G).

Laboratory analyses were conducted using a common pH-meter provided with electrodes to measure both pH and conductivity. *Anions* (Cl^-, NO_2^-, NO_3^-, PO_4^{3-} and SO_4^{2-}) were determined by ion chromatography using a Dionex ICS 3000 instrument equipped with ICS-3000 SP isocratic pump with degas, ICS-3000-TC thermal compartment with Rheodyne injector, Dionex Ion Pac AG22- guard column (4 x 50 mm) and AS22 column(4 x 250 mm), ASRS 3000 4-mm conductivity suppression unit and ICS-3000-CD conductivity detector. Isocratic eluent (1.2 mL min^{-1} flow rate) was a mixture of 4.5 mM Na_2CO_3 and 1.4 mM $NaHCO_3$. Applied current was 31 mA and injection volume was 25 µl. All chemicals were reagent grade and used as purchased from DIONEX without any further purification. Details of analytical operations are reported elsewhere *[Vione 2006]*. For the present anions analysis soil samples have been treated as following. About 10 g of each solid sample has been weighted into clean dry beaker. After that, 100 ml of bidistilled water has been added and the new mixture undergoes sonification for 45 minutes. After few hours, time enough to allow residue to settle, aliquots of 10 mL was vacuum filtered on cellulose acetate filters (0.45 µm pore diameter) before injection on IC apparatus. Filtration was motivated to avoid damage to the analytical apparatus.

The samples were previously characterized [*Pirnau 2009*] to determine their texture (Kackinski method), calcium, magnesium carbonate (Scheibler method) and humus (Walkley-Black, Gogosarea modified) content. Mineralogical composition by FTIR and micro-FTIR spectroscopy was performed in our laboratory.

II.2.3.2   Results

Analyses of two soil profiles were aimed to characterize the soil in two different area of the archaeological site: one (Proprietatea Vasilis) located in the village of Slava Rusa (actual name of the former city of Ibida) and the other (Curtina G) situated close to the external wall of the city (see Figure II.3, the map of the site).

Another sample was taken during excavation procedures where few bronze artifacts were

discovered. This sample has been used to perform the simulation experiments.

In general, data obtained from reference earth samples (soil profile studied in undisturbed areas) suggest the stability of climate condition over a long time. Soils are weakly developed (Calcareous Chernozem, A-C profile type) their texture being not well differentiated and calcium carbonate being present from the soil surface until a depth of 3-4 m. All these characteristics confirm that actual climatic condition (high temperatures, low precipitation) were unchanged over a long timescale, showing only small oscillations [*Pirnau 2009*].
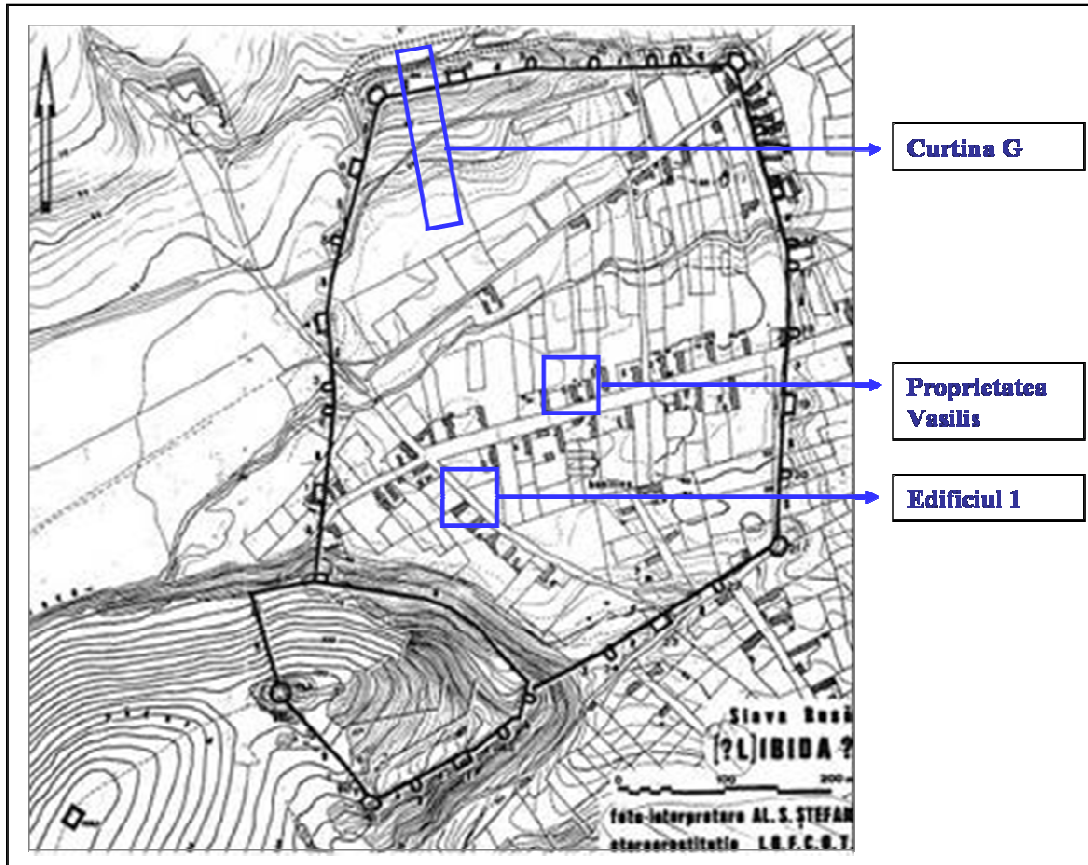
Figure II.3.Map of the archaeological site of (L)Ibida

Area "Curtina G"

0-30cm: pH-8,5; CaCO$_3$-10,43%; humus-1,76%; clay-25,8%; loam, silt

30-48cm: pH-8,5; CaCO$_3$-12,23%; humus2,13%; clay -22,6%; loam, silt

48-69cm: pH - 8,5; CaCO$_3$ - 38,91%; clay - 15,1%; sandy loam

69-90cm: pH - 8,4; CaCO$_3$ - 29,22%; clay - 17,3%; sandy loam

110-137cm: pH-8,2; CaCO$_3$-6,46%; humus-0,86%; clay -20,6%; loam, silt

137-150cm: pH-8,2; CaCO$_3$-2,88%; humus-0,38%; P-328ppm; K-1332ppm; clay -24,8%; loam, silt

150-190cm: pH - 8,4; CaCO$_3$ - 6,46%; clay - 36,8%; clay

190-250cm: pH - 8,4; CaCO$_3$ - 16,31%; clay - 34,8%; clay
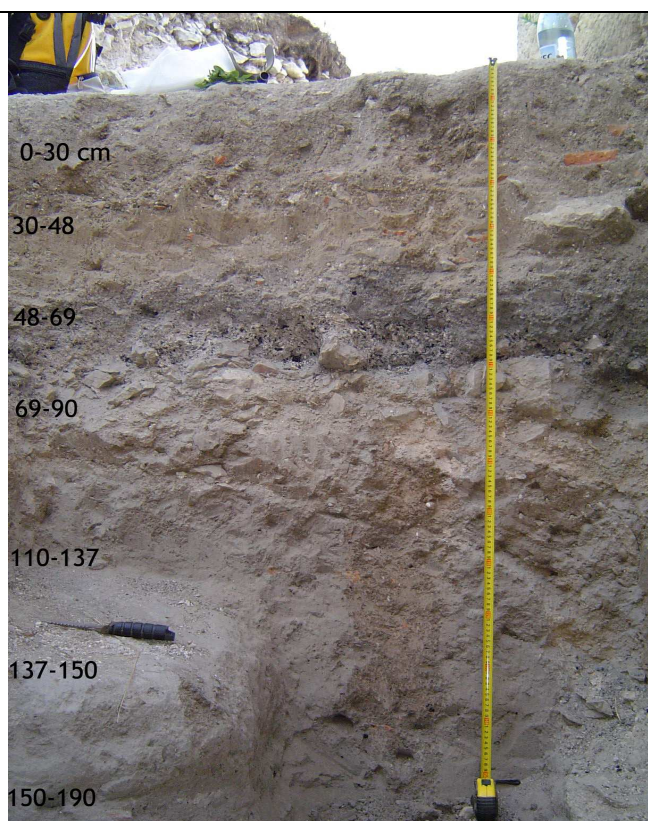
Figure II.4. Soil profile
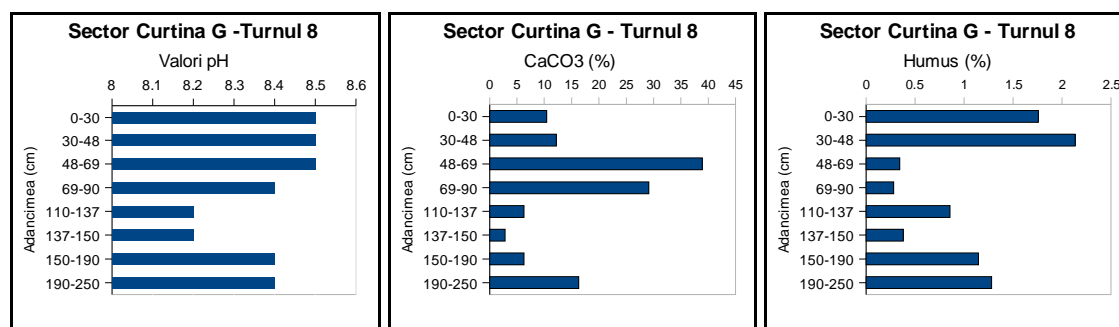
Figure III.5: pH values, CaCO$_3$ content and humus content in the

A critical examination of results allow to say that pH values are higher in the upper part, until 1 m, where also content in calcium carbonate is higher (10.43-38.91 %, the interval 50-70 cm corresponds to a level of mortar with traces of burning). From a depth of 1 m, chemical parameters present usual values for the area, pH, calcium carbonate content and clay, increasing with depth.

Morphological aspect and physical-chemical parameters of this profile indicate a layer heavily disturbed and mixed until the depth of 1 m. Below this level, soil is more homogeneous, but it presents as well features influenced by men.

Area "Vasilis"

0-30cm: pH - 8,4; $CaCO_3$ - 3,7%; humus - 4,22%; clay-24,0%; loam silt

30-70cm: pH - 8,4; $CaCO_3$ - 4,2%; humus - 3,65%; clay - 25,8%; loam silt

70-80cm: pH-9,0; $CaCO_3$ -49,79%; humus-2,56%; argila-24,9%; loam silt

90-136cm: pH - 8,8; $CaCO_3$ - 3,03%; humus - 2,08%;; clay - 27,6%; loam silt

136-165cm: pH-8,8; $CaCO_3$-7,06%; humus- 1,71%;; clay - 28,8%; loam silt

165-200cm: pH - 8,8; $CaCO_3$ - 7,57%; clay - 30,9%; loam silt

200-265cm: pH-8,7;$CaCO_3$-8,75%; clay -27,3%; loam silt

280-310cm:pH-8,7;$CaCO_3$-2,19%;clay-29,8%; loam silt
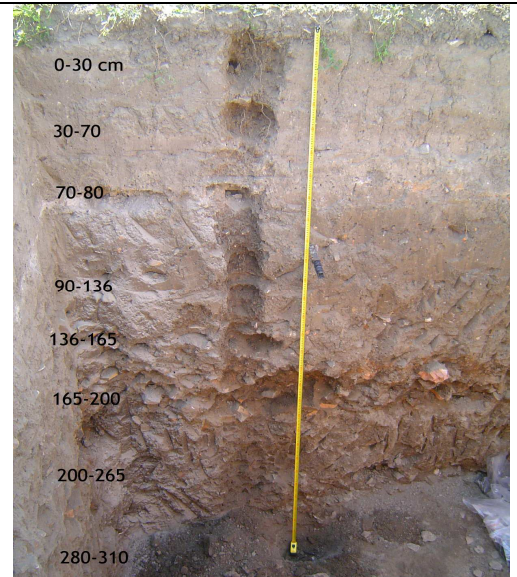
Fig. II.6. Soil profile.
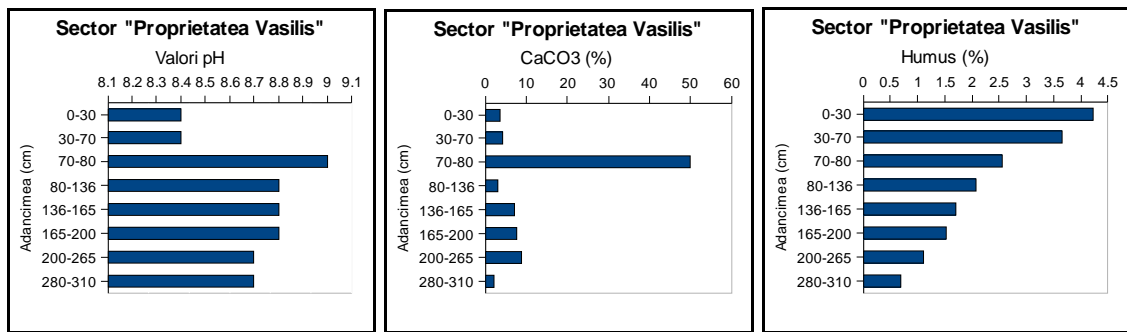
Figure II.7: pH values, $CaCO_3$ content and humus content in the

This site is located in the village Slava Rusa, close to the actual river Slava. Values of pH and calcium carbonate content until a depth of 310 cm are in accordance with characteristic values for this region. The layer 70-80 cm present a lighter color and the high value of pH and calcium carbonate content confirm the presence of a layer of bricks and mortar with traces of burning.

Soil samples from this site were available to perform further chemical investigation by ion chromatography and flame atomic absorption spectroscopy in order to measure anions and heavy metal content.
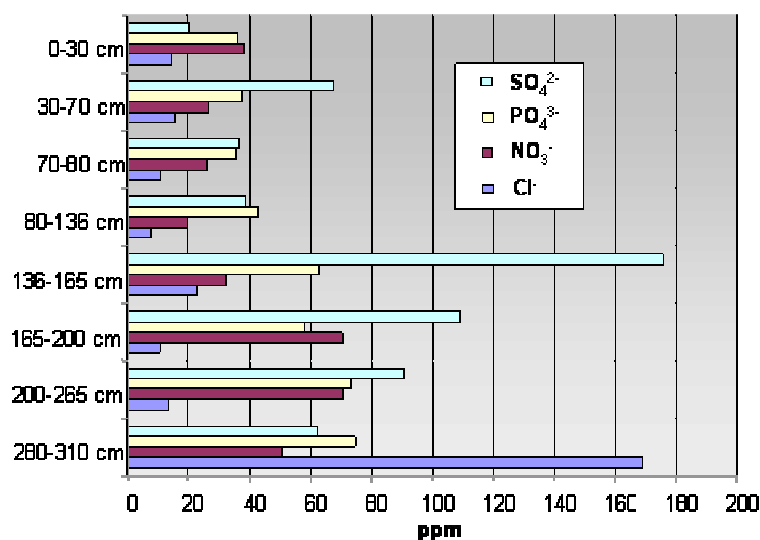
Figure II.8: IC results for the profile Vasilis Property.

Particularly interesting to notice is the increasing concentration of chlorine with depth (Figure II.8), fact which could be explained to the influence of the vicinity of the Black Sea. Furthermore, chlorides are leached easily by percolating water and thus present higher concentrations in depth.

This result is confirmed also by conductivity measurements which register the higher values (around 300 (μS/cm)) for the samples collected at depths > 2 m (see Table II.2). Anyway, it shall be reminded that these values are very low, as they are comparable with the conductivity of still water.

Table II.2. Values of conductivity for the samples according to the depth of sampling

Sample	Conductivity (μS/cm)	T ($^{\bullet}$C)
0-30 cm	133.5	20.4
30-70 cm	181.3	20.5
70-80 cm	209	19.9
80-136 cm	168.5	19.7
136-165 cm	269	20.1
165-200 cm	273	20.3
200-265 cm	300	20.4
280-310 cm	304	20.7

Area "Building E1" (Edificiul I)

Another soil sample was taken during excavation procedure, when few artifacts were discovered. The location is illustrated in the Figure II.9.

Figure II.9: Location of sampling during excavation procedures.

230-240cm:pH-8,7;CaCO$_3$- 0,76%;clay-17,7%; sandy

Clay content is particularly low for this sample, and it can be classified as sandy soil.

Results provided information useful for the realization of simulating solution to be used as electrolytes in the electrochemical experiments.

Taking into consideration the depth where the samples were taken, the value of conductivity (Table II.3) is expected and comparable to the one registered for soil samples at **Proprietatea Vasilis**.

Table II.3. Conductivity value for the withdrawn sample

Sample	Conductivity (µS/cm)	T (˙C)
230-240 cm	316	21.2

Chapter III

Material and methods

III.1   The excavated bronze artefacts

III.1.1   Selection of archaeological bronzes

As introduced in the previous chapter, archaeological finds were kindly provided by the archaeologists working on the excavation site located in the region of Dobrogea, Romania. Archaeological samples have been chosen according to the following criteria:

- Object similar in shapes and dimension, dating approximately from the same historical period: the choice was addressed to small artefacts for their easier availability and suitability to be sampled. They are mostly bronze coins, fibulae, rings, earrings, hairpins, bars, etc.;

- The materials should not have been subjected to restoration nor to cleaning procedures since the interest was to study the object in its integrity, preserving information stored in the corrosion layers and external deposit. Highly corroded material were preferred in order to investigate the development of corrosion layers during burial;

- Samples for which the knowledge about the location of the excavation and soil's physical-chemical characterization is available are of great importance because they allow establishing some correlation between those parameters and the conservation state of the objects.

Table III.1 displays, as relates the selected objects chosen for scientific investigations, a description of the conservation state and, for some of them, the approximate dating. Among these, the significant case studies, as regards the degradation typology, were selected and a detailed description is provided. They have been all excavated in the archaeological sites located in Dobrogea, Romania, whose description is reported in Chapter II.

The artefacts were indexed after the archaeological site (Arg - Argamum, Ib - Ibida and Nuf - Nufarul) and the year of excavation (e.g. .06. stands for 2006).

Table III..1.List of the examined archaeological bronzes.

Name	Date discovery	Depth of finding	Description	Observations	Dating
Arg.00.1	2000	-	Pre-coin	Compact and uniform light brown-grey patina	VI-V Sec BC
Arg.00.2	2000	-	unidentified		
Arg.00.4	2000	-	blade arrow		
Arg.00.6	2000	-	fibula (part)	Compact and uniform light brown-grey patina	IV-V Sec. AD
Nuf.00	2000	-	Hoard of copper coins (six)	Mineralized, thick black external corrosion	
Ib.05.2	2005	-2.70	Banded bronze sheet	Dark patina, light and dark green spots on the surface (active corrosion)	
Ib.05.3	2005	-2.70	Fibula	Soil incrustation, dark and light green spots all over the surface (active corrosion). Bad condition due to the wrong conservation after excavation.	
Ib.05.5	2005	-2.90	Earing?	Localized light green compounds at the edge where it is broken	
Ib.05.6	2005	-2.70	Bronze sheet	Homogeneous dark corrosion, with localized soil incrustation and light green compounds on the edges where it is broken.	
Ib.05.8	2005	-2.60	Earing or ring	Corrosion which seems to have deformed the original shape of the object. Soil dark corrosion product with a green spot and soil incrustation	
Ib.05.10	2005	-2.60	Bronze plaque	Homogeneous corrosion except for some light green spots and area close to the edge where it is broken. Interesting "buboes" (cfr. Robbiola)	

Ib.05.12	2005	-2.60	Nail?	Dark corrosion with soil incrustation, some green area.
Ib.05.15	2005	-2.70	bronze pin	highly corroded, deformation of original shape, light green compounds and soil incrustation
Ib.06.1	2006	-2.50	probably blade fragments	mineralized stage, present localized corrosion (light green)
Ib.06.9	2006	-3.30	pin or hairstick	almost mineralized stage, present localized corrosion (light green)
Ib.08.1	2008	-2.65	fragment from a buckle	compact and uniform black patina, with some green red concretions (cuprite, malachite) on the surface
Ib.08.3	2008	-2.75	bronze sheets, bended	banded bronze sheets, soils incrustated on the surface.
Ib.08.4	2008	-2.30	fragment from a bronze bracelet	3-4 cm long rod, probably part of a bracelet. It present a dark patina covered by soil remains.
Ib.08.5	2008	-2.75	bronze fragment, defined shape	Two area corroded differently, green red compounds are present on one side
Ib.08.7	2008	-2.60	coin fragment	Coin fragment, black patina, uniform, some remains of soil.
Ib.08.12	2008	-2.50	pin with round shaped head	Highly corroded, sol incrustation.
Ib.08.16	2008	-1.60	bronze fragment sampled from a vase with iron handle	sample taken from the vase (iron handle). Light patina, with green and white compounds.
Ib.08.17	2008	-3.40	ring fragment and bronze flat bar	Dark area, on which green compounds are present.

Case studies

A selection of objects were subjected to more detailed study, which consisted, besides the analysis of external corrosion products, in the sampling of a fragment and the realization of a cross section. The following list is realized basing on the archaeological sites where they were excavated and furnishes some more details regarding the conservation state.

(L)Ibida, Slava Rusa, Dobrogea

Ib.05.08

Figure III.1.

Place	Ibida
Year of findings	**2005**
Depth of finding	**- 2.60 m**
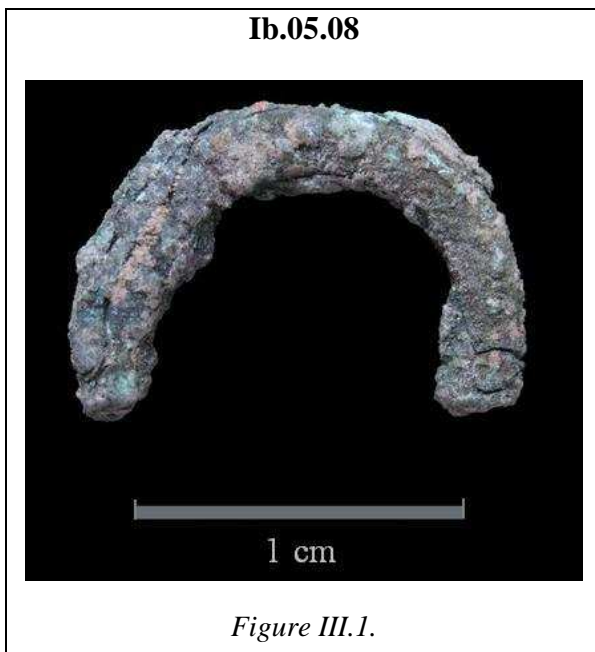
Earring or ring.

The object presents a rough surface characterized by red and green corrosion products and soil concretions.

Fractures are observed along the corrosion layers.

Ib.06.09	
Figure III.2.	
Year of findings	**2006**
Place	**Ibida**
Depth of finding	**- 3.30 m**

Hair-stick or pin

The fragments are almost completely mineralized. The most external corrosion layers contain also soil incrustation, but they mainly consist in green corrosion products. Some lighter green spots are present on the surface, probably made of copper hydroxochlorides.

Ib.08.04	
Figure III.3.	
Year of findings	**2008**
Place	**Ibida**
Depth of finding	**- 2.30 m**

Bracelet

The object presents a uniform dark surface and doesn't show evidences of active corrosion.

- 41 -

Argamum, Jurilovca, Dobrogea

Arg.00.1	
Figure III.4.	
Year of findings	**2000**
Place	**Argamum**
Depth of finding	**-**

Coin (pre-coin)

The object has been identified by the archaeologists Mihaela Iacob (ICEM-Tulcea) as a greek "pre-coin", dating back in the VI-V century BC.

It presents a uniform brown surface, without apprent signs of active corrosion.

The object seems stable from the conservation point of view.

Arg.00.2	
Figure III.5.	
Year of findings	**2000**
Place	**Argamum**
Depth of finding	**-**

Unidentified object

This object could not be identified. The high weight suggests the presence of lead in the alloy.

It presents a rough surface, characterized by the presence of brown, green compounds.

However, the conservation state seems stable.

Arg.00.4	
Figure III.6.	
Year of findings	**2000**
Place	**Argamum**
Depth of finding	**-**
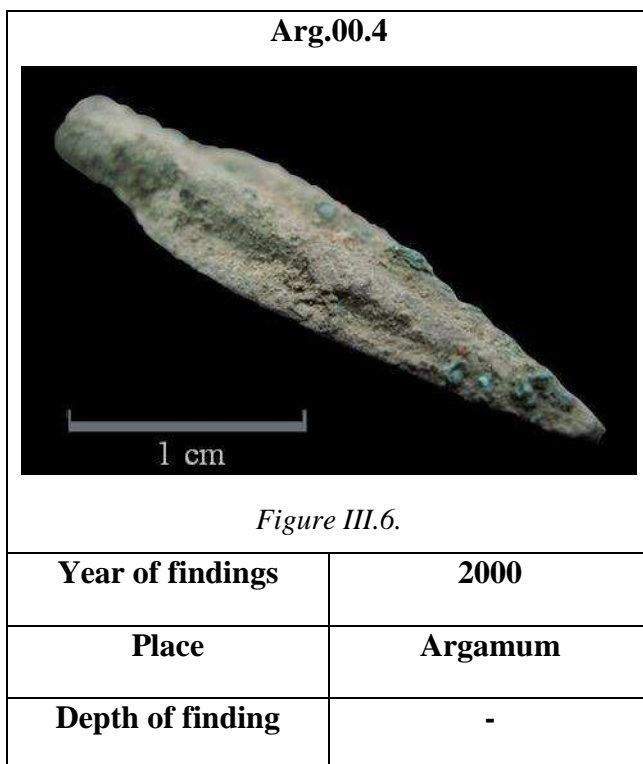
Arrow head

The object is described as an arrow-head, probably Greek.

It presents a rough brown surface, and some green spots probably sign of active corrosion due to copper hydroxochlorides.

Nufarul, Dobrogea

Nuf.00	
Figure III.7.	
Year of findings	**2000**
Place	**Nufarul**
Depth of finding	**-**
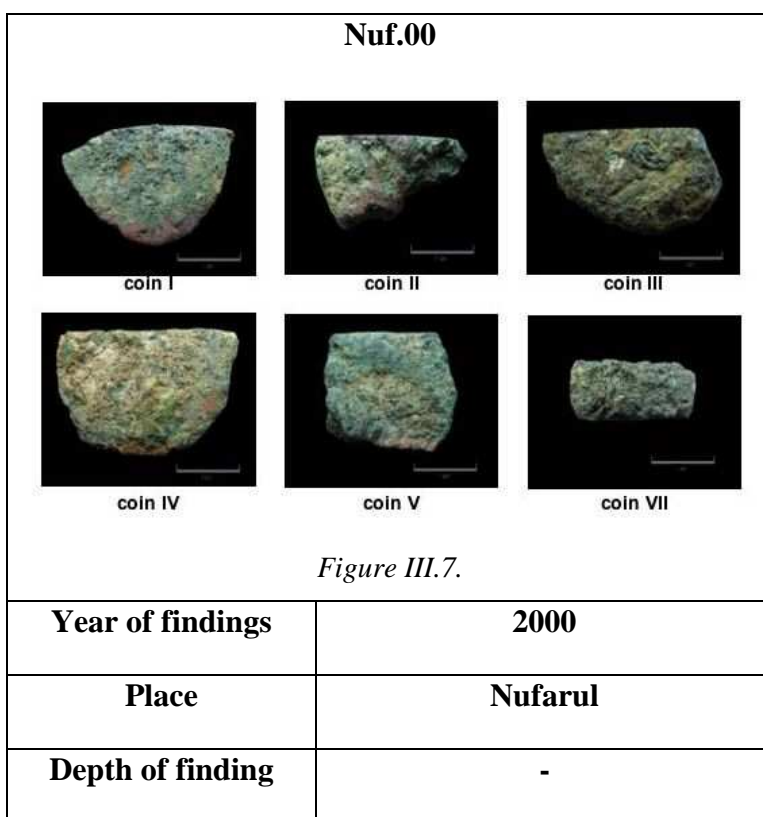
Hoard of copper coins

The coins present similar corrosion patterns. The external layer is made up of green to blue compounds, probably copper corrosion products, and soil incrustation. Evidence of wooden inclusion is also reported. As they were found as fragments, it was possible to identify a thick black layer underneath.

III.1.1   Techniques and procedures

The following paragraphs illustrate the techniques and procedures employed for the characterization of the metal artefacts. The experimental protocol has been developed and implemented according to the instrumentation available in the laboratory and in the partner institution with which a scientific collaboration is activated. These are the Microchemistry and Microscopy Art Diagnostic Laboratory (M2ADL), UNIBO, Ravenna Campus, Italy; the Instituute Collectie Nederlands (ICN), Amsterdam, The Netherlands; the Aristotle University of Thessaloniki (AUTH), Greece.

III.1.2.1   Visual examination

Careful observation, carried out by naked eye but also with the use of the stereomicroscope, and an exhaustive photo-documentation are the immediate approach for a scientific investigation. These operations have the scope to classify the objects and determine the *conservation state* and the degree of deterioration. In addition, when sampling is allowed, this examination has the aim to choose a suitable fragment to be withdrawn and subjected to further investigations.

III.1.2.2   Preparation of cross sections

Representative micro-samples (approximately 50x50 mm) are withdrawn from the object, mounted in a polyester resin, grinded and polished to realize a cross-section (CS).

The methodology used to realize the CS employs the following materials, all provided by Struers, Copenhagen:

- Styrene (Serifix Resin);
- Hardener (methyl ethyl ketone peroxide, Serifix Hardener);
- Mounting cups (SeriForm, Struers)

The procedure consists in the preparation of a mixture by adding a small amount of hardener to the liquid resin (using the proportion 5 to 20 ml), stirring well, but very slowly. The sample is placed on the mounting cups and fixed with glue or wax and the previously obtained mixture is poured on it until its complete immersion.

After one night (twelve hours), the resin is hardened and it is thus possible to remove it from the holder, and proceed to the grinding procedures using Silicon carbide (SiC Paper, grit 320, 500, 800, 1000, 1200, 4000) papers on an automatic polishing machine (LaboPol-5, Struers, Copenhagen). When chemical etching needs to be performed, the sample is polished using diamond (DP-Spray, P; 6-3-1 μm) or alumina (3-1 μm) pastes until a perfect mirror-like surface is obtained.

The cross section thus obtained is ready for the observation at the optical microscope. In order to be analyzed by SEM-EDX the section's surface needs to be conductive and, therefore, it is covered with a very thin layer of graphite. For the present study, a carbon coater EMITECH, K250, coupled to the sputter coater, K575X, provided by QuorumTech, was employed. It works with a Rotary Vacuum pump and it utilizes a variety of fibres types (Carbon Fibre Hi-Purity, Quorum, EmiTech) to cover a wide range of deposition thickness

III.1.2.3   Optical microscopy (OM)

Optical microscope observation, utilizing different magnifications, provides alone much information about the morphology and nature of corrosion compounds [*Scott 1991; Wadsak 2000*]. Their colour allows already getting an idea of their chemical nature as these are all characterized by a specific colour (Table III.2). For example, cuprous oxide (Cuprite, Cu_2O) presents orange to red hues, while hydroxyl-chlorides and hydroxyl-carbonates are characterized by a green-blue tone.

Table III.2. List of the most common corrosion products detected on archaeological bronze [after Scott, 2002, Mazzeo 2004].

Class of compounds	Mineral Name	Chemical Formula	Crystal system	Colour
Oxides	Cuprite	Cu_2O	cubic	submetallic red, orange
	Tenorite	CuO	monoclinic	black
Carbonates	Malachite	$Cu_2 (OH)_2CO_3$	monoclinic	pale green
	Azurite	$Cu_3 (OH)_2(CO_3)_2$	monoclinic	vitreous blue
Chlorides	Nantokite	$CuCl$	cubic	pale green
	Atacamite	$Cu_2(OH)_3Cl$	orthorombic	vitreous green
	Clinoatacamite	$Cu_2(OH)_3Cl$	monoclinic	pale gren
	Paratacamite	$Cu_3(Cu, Zn)[(OH)_3|Cl]$*	rhombohedral	pale green
Sulphides	Covellite	CuS	hexagonal	submetallic blue
	Chalcocite	Cu_2S	hexagonal	metallic blackish gray
	Spionkopite	$Cu_{1.32}S$	rhombohedral	metallic blue gray
Phospates	Libethenite	$Cu_2 (OH)(PO_4)$	orthorombic	light to dark olive green
Silicates	Crhrysocolla	$(Cu,Al)_2H_2(OH)_4Si_2O_5·xH_2O$	monoclinic	vitreous/earthy green

* according to *Scott [2002], Martens [2003]*

While for identification of colours, the dark field method is used, metallographic observations are carried out using the bright field modality. These methods differ because while working in DF modality, a so-called Dark-Field slider is inserted in the optical path and doesn't allow the specular reflected light to reach the eye. This allows a reliable observation of natural colours, which are normally obscured in the bright field mode, appearing greyish.

For this study, two microscopes were mainly used according to the typology of observations made:

- A Zeiss Axio Imager A1m, provided with a high resolution digital camera (AxioCam, MRc), and interfaced to the personal computer with the AxioVisionRel 4.7 sofware;
- A XJP-6A metallurgical microscope, with inversed geometry, and coupled with a Canon PowerShot digital camera[1].

III.1.2.4   Scanning electron microscopy coupled with Energy Dispersive Spectrometer (SEM-EDX)

Scanning electron microscopy is a popular and widely spread technique, nowadays present in almost every laboratory of materials' science. Its success is due to the easiness of employment and the extraordinary results that could be achieved. The "illumination" of the samples occurs with an electron beam and, having a much lower wavelength if compared to normal light, allows a much higher magnification of the object. Not only a much higher magnification can be achieved if compared to classical optical microscopes, but, more important and useful, a much higher depth of field which is responsible of the capability to obtain a three-dimensional-like pictures.

Due to charging phenomena, only conductive samples can be analyzed. The maximum resolution, which is of 3 nm, achieved at 30 kV accelerating voltage, is far from being reached during analyses of archaeological samples, which are often analyzed without any surface preparation. Nevertheless, the power of the technique for this application is surely the higher magnification, but also the possibility of simultaneous imaging (topography and morphology of surfaces) and chemical analyses (elements identification).

As concerns imaging techniques, a scanning electron microscope "builds" the image through different signals (see Figure III.8):

- Secondary electrons (SE) are low energy electrons, which are ejected from the specimen's surface because of the interaction with the primary beam. They create a

---

[1]   Analysis with this microscope were kindly carried out with the help of Prof. Romeo Chelariu at the Material Science Department (SIM) of the "Gh. Asachi" Technical University, Iasi, Romania.

image rich in surface information.

- Backscattered electrons (BSE) are those that suffer multiple collisions with atomic nuclei making up the specimen, without loosing much of their initial energy. This produces images with a higher atomic number (Z) contrast, which arises because the backscattering coefficient rises monotonically with atomic number of the scattering atoms [*Blake, 1990*].
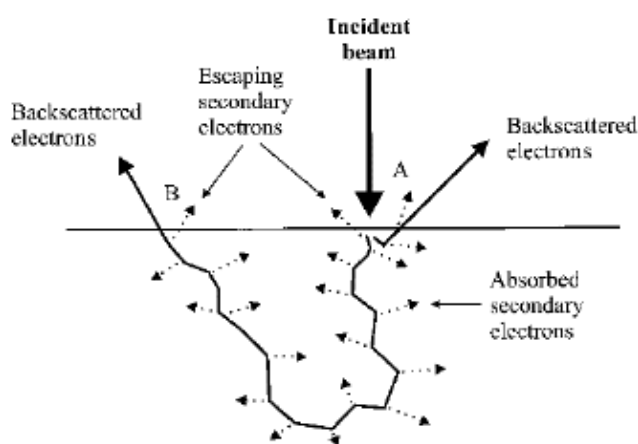
Figure III.8. Schematic drawing of the possible phenomena of the interaction between the incident electron beam and the matter.

Semi-quantitative analyses are performed using the ZAF method without standard. A high number of point analyses are preformed for each object, and quantification is done using the software Esprit. For each analysis, the sum of concentration for elements with $Z > 11$ is equal to 100. Therefore, the concentration obtained are not absolute values but interdependent. In order to get rid of this analytical constrain, concentrations are normalized to that of an element which can be considered a neutral variable of an analysis.

The present research has been carried out using a SEM VEGA II LSH manufactured by Tescan Co., Czech Republic, coupled with an EDX QUANTAX QX2 detector manufactured by Bruker/Roentec Co., Germany. The following instrumental settings were used: 20kV accelerating voltage, 120 nm beam spot size, 16.6 mm working distance. The working pressure is less than 10^{-3} Pa. Quantification was performed using the standard ZAF method [*Goldstein 1992*]. The image acquisition is obtained using the software VEGA TC, while the microanalysis is controlled through the Esprit software. The latter allows a variety of methods to be used, such as point or area analysis, elemental scan over a line or mapping of selected elements over an area freely selected.

SEM-EDX makes up the major part of the present work as the information provided, coupled and compared to the ones obtained by optical microscope, allows an accurate characterization

of the specimen's surface, concerning its morphology, colour and elemental composition.

III.1.2.5 Metallography

Crystalline structure of metals and alloys is revealed through the chemical attack of a polished cross section by means of etchings (i.e. reagents able to dissolve selectively the grain boundaries thus revealing the microstructure) [*ASM Metal Handbooks, 2004*].

In archaeometallurgy, metallography is used to reveal and interpret the microstructures of ancient metal artefacts and, in conjunction with the results of other chemical analysis and microanalysis, information about the history of the material and metallurgical technologies employed to obtain them are gathered.

A major limitation to this kind of studies for archaeological samples is the possibility to perform a sampling, as often there are restrictions to this practice due to its invasiveness. Moreover, even though sampling could be permitted, the fragment obtained could be far from optimum metallographic conditions, especially as regards its being representative of the whole object (e.g. sampling of a knife in his sharp edge or at the basement of the blade). When sampling is restricted, it could be permissible to perform metallography on the external surface, without cutting the object, for example by polishing the rim of a coin. Whichever the methodology employed, it is important to obtain a flat surface in order to observe it at the optical microscope. However, if it is not so, the scanning electron microscope provides a good alternative, with its significantly higher depth of field.

Another inconvenient, when dealing with archaeological samples, is their poor condition, meaning their advanced state of degradation and deterioration. The burial for long time causes the conversion of metal into corrosion products, even deeply in the object. It is common the preferential attack of one phase, which provides the reveal of the original microstructure without the need of metallographic etching.

The present work concerns mainly the study of copper and copper-based alloys: the following table (Table III.3) reports the main composition and procedures of etching solutions.

Table III.3. Chemical composition and employment procedures commonly utilized for copper-based alloys [Scott, 2002; ASM Metal Handbooks2004]

Composition			Procedure
$FeCl_3$, g	HCl, mL	H_2O, mL	Immersion or swabbing, etch
5	50	100	lightly or by successive light
20	5	100	etches to required results
25	25	100	
1	20	100	

8	25	100	
5	10	100	
5 g FeCl$_3$, 100 mL ethanol, 5-30 mL HCl			Immersion or swabbing from 1 to several minutes
25 mL NH$_4$OH, 5-25 mL H$_2$O$_2$, 25 mL H$_2$O			Immersion or swabbing
diluted HNO$_3$			Immersion or swabbing

The alcoholic ferric chloride solution represents the main choice for the results presented in this work. Nevertheless, each case study needs to be considered individually and often several trials are done in order to obtain the best result.

III.1.2.6 FTIR spectroscopy

Fourier-transformed infrared spectroscopy is a commonly used technique for the analysis of organic and inorganic compounds characterized by specific molecular vibrations. We based on published literature as regards basic principles of this technique [*Atkins 1997; Derrick 1999*]. The following table (Table III.4) present the characteristic absorption frequencies for the typical compounds encountered on archaeological bronzes and provide a tool for the interpretation of the spectra collected in the Appendix I.

Table III.4. *Characteristics absorption frequencies identifying the minerals detected on the excavated bronzes.*

Calcite	Quartz	Aluminosilicates (montmorillonite)	Malachite	Paratacamite*	Atacamite	Cuprite	Cassiterite
$CaCO_3$	SiO_2	$(Na,Ca)_{033}(Al,Mg)_2(OH)_2Si_4O_{10}$	$Cu_2(OH)_2(CO_3)$	$Cu_2(OH)_3Cl$	$Cu_2(OH)_3Cl$	Cu_2O	SnO_2
ν (cm⁻¹)	ν (cm⁻¹)	ν (cm⁻¹)	ν (cm⁻¹)	ν (cm⁻¹)	ν (cm⁻¹)	ν (cm⁻¹)	
		3598w		3443s	3444s		
		3378m	3405m	3359s	3337s		
			3311m	3338m			
2510w							
2073w							
					1944vw		
1790w		1612w	1508vs, b	1647	1646		
1424vs			1389vs, b				
	1166		1096m, sh				
	1081vs	1036vs	1047s, sh				
				988m	985m		
				950w	949m		
		916w		917m	915m		
				897m	894m		
873m			871s, sh				
				848m	849m		
			820s, sh		819w		
	796w						
	776w						
			749m				
			712m				
704w							
	691w						
		618w				620vs	627vs
				598	596		
			571m				
							533s
			523m				
		521m					
				517	513		
	512w						
			504m				
					480		
				454	445		
			429m				
(1)	(1)	(1)	(2)	(2)	(2)	(3)	(1)

Legend: vs=very strong, s=strong, m=medium, w=weak,vw=very weak; b=broad, sh=sharp

References:
(1) OPUS Library
(2) Reference: Omnic Library (M2ADL Laboratory)
(3) Reference: Bentley, Smithson, Rozek, Infrared Spectra and Characteristic Frequencies ~700-300 cm⁻¹. Interscience.
*Or, more correctly, **clinoatacamite**, the monoclinic polymorph of the compound $Cu_2(OH)_3Cl$.

III.1.2.6.1 Diffuse and specular micro-FTIR

Micro-FTIR spectroscopy allows realizing spectra in a completely non-destructive (not-touching) way or directly on the cross section, by focusing the IR radiation on a selected area of the sample and by registering the spectrum in reflection mode. It is worth mentioning that the result spectrum may be complicated because two components of the reflected radiation are registered simultaneously: diffused and specular. In the following paragraphs, theoretical considerations are briefly touched upon, being necessary to better interpret and extract information from the spectrum obtained.

Specular reflection

In the presentation of this technique, we'll consider only the specular reflection mode under small angles of incidence (10-30°) due to configuration of the objective of the microscope we used. Pure reflectance spectrum is obtained for samples having a reflecting surface, flat, homogeneous and opaque (meaning that no radiation should come from the rare surface of the sample) *[Bruker]*.

Taking into account this aspect as the main phenomenon, which could happen during one measurement, the reflection spectrum could have a derivative-like shape, which is caused by the frequency dependence of the dispersion of the sample refractive index. The Kramer-Kroening transformation (KKT) command from OPUS software, extract from a sample reflectance spectrum either the complex refractive index, complex dielectric constant, an absorption spectrum or the phase change of the IR beam due to reflection. In principle, KKT enables to determine all important optical parameters on the basis of its reflectance spectrum of the sample.

The sample reflectance is defined by the refractive indices of the sample and the air. In the case of Fresnel reflection, the reflectivity can be calculated as a function of the frequency by:

$$R(\nu) = r^2(\nu) = \left[n(\nu)-1\right]^2 / \left[n(\nu)+1\right]^2 \qquad\qquad \text{(III.1)}$$

where: ν = wave number; $r(\nu)$ = amplitude of the reflected light; $n(\nu)$ = refractive index

For absorbing samples, $r(\nu)$ and $n(\nu)$ are complex:

$$n^*(\nu) = n(\nu) - ik(\nu); \ \ r^*(\nu) = r(\nu)e^{i\Phi(\nu)} = \left[n^*(\nu)-1\right]/\left[n^*(\nu)+1\right] \qquad \text{(III.2)}$$

where: $r^*(\nu)$ - Fresnel coefficient for reflected light; $\eta(\nu)$ - phase difference between reflected and incident beam; $k(\nu)$ - absorption index.

From the imaginary part of the refractive index, the so-called absorption coefficient $k(\nu)$, the

absorbivity A(ν) of a layer with a thickness d can be calculated by:

$$A(\nu) = \log(e) 2\pi \nu d k(\nu)$$

(III.3)

Equation (3) is implemented such that OPUS does not calculate A(ν) from a given thickness d but selected, with a maximum of A(ν) being 1.0. This results in comparable intensities similar to absorption spectra measured in transmission. Therefore, the intensities of A(ν) are only defined up to a freely selectable scaling factor.

Diffuse reflection

Diffuse reflectance occurs for heterogeneous samples or powders and solids having a rough surface. The diffusely scattered radiation from the sample is collected over a wide range of angles. Different measurement accessories can be applied in MIR and NIR spectral range rather usually for pure diffuse reflection spectrum.

The diffuse reflection spectrum is defined by the absorption and scattering behaviour of the sample. Only the part of the beam that is scattered within a sample and returned to the surface is considered to be diffuse reflection. The mathematical transformation given by Kubelka and Munk expresses the relation between the diffused reflection and the absorption spectrum, which can be described by the equation (III.4):

$$F(R_\infty) = \frac{(1 - R_\infty)^2}{2R_\infty} = \frac{2.303\alpha c}{s}$$

(III.4)

where: R_∞ – reflectivity of an "infinitely" thick sample layer; s - scattering coefficient; α - absorbtivity; c - concentration.

Experimental set-up

The instrument consists of a TENSOR 27 spectrometer for mid-infrared range coupled with a HYPERION 1000 microscope from Bruker Optics–Germany. The spectrometer is an advanced flexible benchtop instrument suitable for routine applications as well as laboratory research. The standard detector is a DLaTGS type, which covers a spectral range from 12000 to $370 cm^{-1}$ and operates at room temperature. The resolution is normally $4 cm^{-1}$. TENSOR is completely software controlled, by OPUS software.

The detector is a MCT cooled with nitrogen liquid. The spectral range is $7500\text{-}600 cm^{-1}$ and the measured area is optimized for a diameter of 250μm with the possibility of reaching a minimum diameter of 20 μm and an IR optical objective of 15x.

III.1.2.7. X-ray diffraction (XRD and micro-XRD)

X-ray diffraction is a versatile technique that reveals information about the crystallographic structure and chemical composition of materials.

This technique is based on constructive interference of monochromatic X-rays and a crystalline sample. These X-rays are generated by a cathode ray tube, filtered to produce monochromatic radiation, collimated to concentrate, and directed toward the sample. The interaction of the incident rays with the sample produces constructive interference (and a diffracted ray) when conditions satisfy the Bragg's law (Eq. III.5):

$$n\lambda = 2d \sin \vartheta \qquad\qquad\qquad (III.5)$$

This law relates the wavelength of electromagnetic radiation to the diffraction angle and the lattice spacing in a crystalline sample. These diffracted X-rays are then detected, processed and counted. By scanning the sample through a range of 2θangles, all possible diffraction directions of the lattice should be attained due to the random orientation of the powdered material. Conversion of the diffraction peaks to d-spacings allows identification of the mineral because each mineral has a set of unique d-spacings: the diffraction pattern is the fingerprint of a crystalline compound. Identification of compounds is achieved by comparison of d-spacings with standard reference patterns.

For the present work a diffractometer: Bruker D8 ADVANCE (Germany, 2006) was employed[2], using the following experimental conditions:

- Technique: Wide Angle X Ray Diffraction (WAXD)
- Bragg-Bretano geometry
- Ni-filtered Cu-K$_\alpha$ radiation ($\lambda = 0.1541$ nm)
- 40 kV; 30 mA;

All the diffractograms were investigated in the range of 2-80 degrees, 2-theta degrees, at room temperature. The analyzed material was finely ground, homogenized and bulk composition was determined.

In the field of cultural heritage, a great limitation of the method is the analysis of bulk samples which causes the lost of spatial information. On a selection of case studies, XRD measurements were carried out at the ICN, Amsterdam. The laboratory is equipped with a Bruker Platform Microdiffractometer which allows a non–destructive analysis, preserving the

---

[2] The analysis were carried out at the Institute of Macromolecular Chemistry "Petru Poni" by Prof. Daniel Timpu.

spatial resolution. The instrument is equipped with a HiStar detector and GADDS software. The diffractograms were aquired using CuK$_\alpha$ radiation at 40 kV and 30 mA and evaluated using the Bruker Eva software package.

The specimen is placed in the chamber and the radiation focused on an area of 2x2 mm, as shown in the picture (Figure III.9). Figure III.10 reports the X-rays pattern obtained.

Figure III.9. Area selection using the micro-Diffractometer.
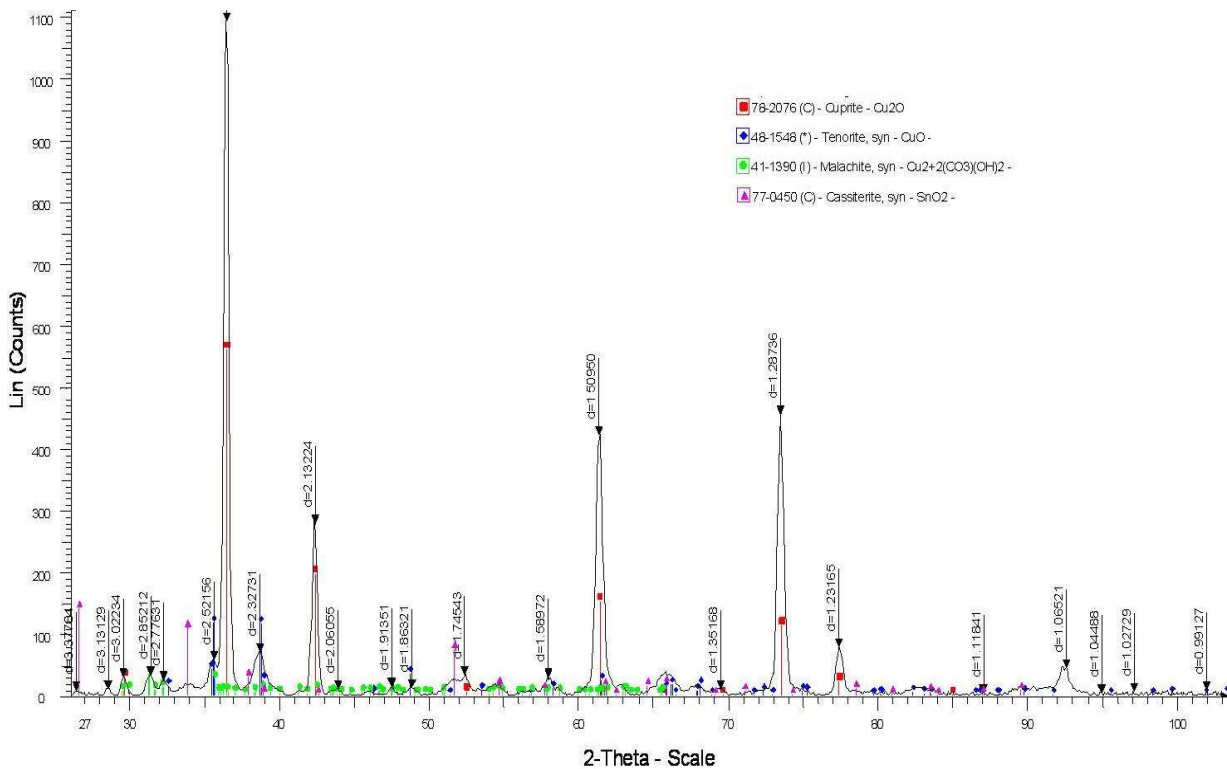
Figure III.10. XRD pattern recorded on the selected area. This particular case reports the analysis of corrosion layers of the sample Ib.06.9 where cuprite is the mainly present.

III.2   Experiments of corrosion simulation

This paragraph furnishes the details regarding materials, techniques and methodologies employed for the experiments of corrosion simulation and which have been conducted at the Department of Chemical Engineering (UTI) and the Department of Analytical Chemistry (UAIC), Iasi.

III.2.1   Material

III.2.1.1   Description of "new" bronze samples

Two commercial bronzes were employed for this study. Both of them present an analogous composition, CuSn11 (wt.%), but they were manufactured using different procedure. The materials were chosen also for their commercial availability, since it is more complicated to manufacture a piece with similar characteristics as the ancient bronzes. Both of them present cast, uniform dendritic structure, which is in good accordance with microstructures observed for ancient cast artefacts.
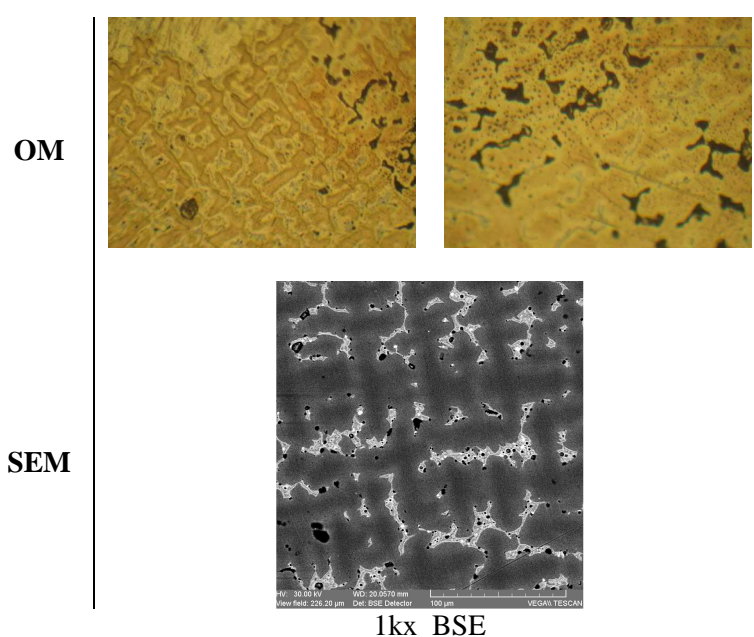
Figure III.11. Bronze 1: optical and scanning electron microscopy evidencing the microstructure of the alloy.

Bronze 1 was produced and kindly provided by the company RANCON S.R.L.., Iasi, Romania: it is a cast bronze; the alloy has been manufactured starting from pure elements Cu and Sn in an electromagnetic inductive furnace, in air. A protection flux (CUPROM, a mixture of salts) has been used in order to clean the alloy from the impurities. Before melting at 1100°C, nitrogen has been gurgled for 7 minutes in order to remove air bubbles. The material was furnished as bars (⌀15 mm). Elemental analysis has been realized with a

spectrometer MetalScan2500.

In order to characterize the microstructure, a disk was cut out and prepared using the metallographic procedure: chemical etching has been performed using in an alcoholic solution of $FeCl_3$ in HCl. As evidenced in the Figure III.11 , the specimen present a dendritic structure and two phases are present. They are particularly evident from the back-scattered electron micrographs, which shows lighter areas in the interdendritic spaces: the eutectoid α+δ is richer in Sn and therefore appears lighter in the figure. Moreover, again the BSE image allows appreciating the high porosity characterizing this material.

Bronze 2 is an industrial product furnished by MetalParm, Parma, Italy. The alloy has been characterized in the same way as for Bronze 1 (Figure III.12) and the results show a similar microstructure, two-phased material with a dendritic structure, but, in this case, the dendrites have a smaller *Secondary Dendrites' Arm Spacing* (SDAS). In this case, porosity is present but is lower then for Bronze 1.

1kx_BSE
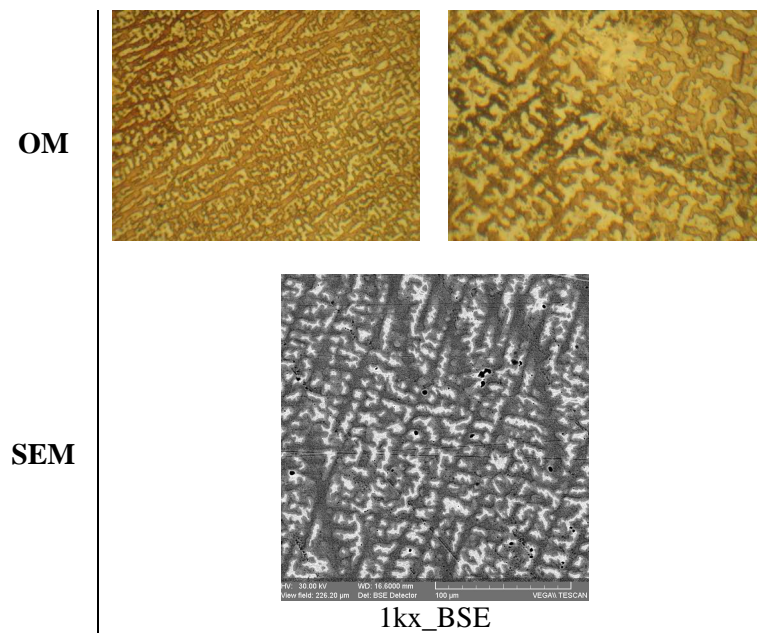
Figure III.12. Bronze 2: optical and scanning electron microscopy evidencing the microstructure of the alloy

The composition of both alloys is provided in the following table (Table III.13):

Table III.5. Elemental composition of the two alloys (values given in wt. %)

		Cu	Sn	Pb	Zn	Fe	Al	Ni	Si	Mn	P
BRONZE 1	**AAS**	rest	11.20	**1.05**	**1.39**	0.40	0.02	0.29	0.02	0.01	-
	EDX*	82.55	12.89	**1.61**	**1.20**	0.40	0.23	0.67	-	-	-
BRONZE 2	**AAS**	rest	11.1	**0.005**	**0.09**	0.09	-	-	0.012	-	-
	EDX*	85.47	13.26	**-**	**0.54**	0.26	0.29	-	-	-	0.17

*mean of three points of analysis on an area of 250μm^2

Manufacture of bronze electrodes

The electrodes (Figure III.13) were manufactured from the bronze bars using a lathe and by embedding the obtained cylinder in Teflon in order to obtain a one-dimensional surface with a diameter of ~ 8 mm. An internal thread (groove) was realized in the interior part of the top side in order to connect it with the support of the instrumentation employed and to use it as a rotating electrode. Before each experiments, the specimens have been polished using SiC paper, from 250 grit up to 4000, in order to obtained a mirror-like surface.
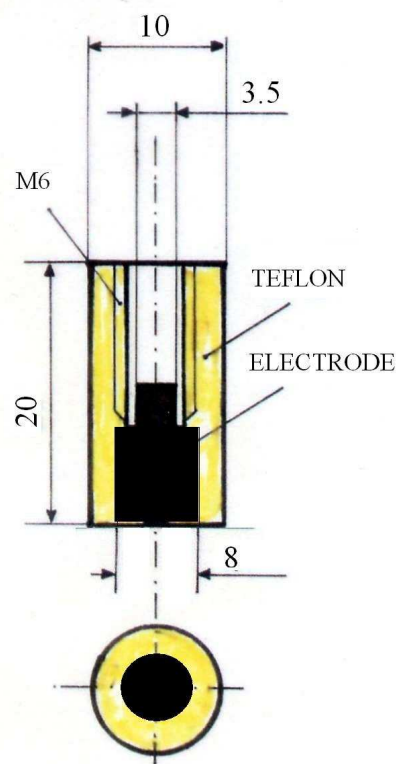
Figure III.134. Scheme of the electrode used for the electrochemical experiments.

III.2.1.3   Corrosion media

As the aim of the study is to simulate the corrosion of bronze samples in the archaeological sites, the electrolytes were chosen in order to reproduce the environment that they could have experienced when objects were buried in these soils. During a field campaign in the region of Dobrudja (Romania), where the archaeological sites are located, samples from a soil profile has been collected (Chapter II). Moreover, since these sites are situated very close to the Black Sea, an amount of seawater was sampled as well. We considered of scientific interest also comparing the electrochemical behavior of bronze in the Black Sea and in Mediterranean Sea, because we could appreciate a sensible difference in their composition as concerns chlorine and sulfate concentration.

The soil extract was prepared by diluting 10 g of soil sampled at the area Building E1 to 100 ml of distilled water. Two artificial solutions, "A" and "B", obtained respectively by doubling, and ten times increasing, the concentration of chlorine, nitrate, phosphate and sulfate (compared to those of the soil extract), were prepared in order to study the electrode's surface after electrochemical experiments and also to simulate accidental local concentration of salts as could happen in soil by evaporation of water.

Table III.6 reports the composition of the corrosion media used for the electrochemical experiments. The artificial solutions were prepared using the following A.R grade chemical

reagents: KCl, NaNO$_3$, K$_3$PO$_4$, Na$_2$SO$_4$·10H$_2$O. The system Na$_2$CO$_3$ / NaHCO$_3$. has been used to adjust the pH to an alkaline value of ~ 8.5.

Seawaters were sampled from Constanta in Romania and in Croatia during 2008.

Table III.6. Composition of electrolytes used for the experiments

	Cl$^-$	NO$_3^-$	PO$_4^{3-}$	SO$_4^{2-}$	pH	Conductivity
	mmol	mmol	mmol	mmol		mS
Soil Extract	1.128	0.726	1.053	1.145	8.86	0.32
Solution "A" (x 2)*	2.323	1.544	2.107	2.292	8.56	8.9
Solution "B" (x 10)*	11.273	7.256	10.529	11.581	8.95	13.03
Black Seawater	244.534	_	_	14.454	7.10	27.45
Mediterranean Seawater	694.209	_	_	37.931	8.22	56.70

III.2.2   Techniques

In this paragraph, the basic principles of the electrochemical measurements performed are touched upon. They include Open Circuit Potential (OCP), potentiodynamic polarization methods (Linear, LV and Cyclic Voltammetry, CV) and Electrochemical Impedance Spectroscopy (EIS).

III.2.2.1   Open Circuit Potential (OCP) measurements

The open circuit potential is the potential of the working electrode relative to a reference electrode when no potential or current is being applied to the working electrode [*Jones 1996*]. Measurement of electrode potential is necessary to determine the driving force or free energy (ΔG) in an electrochemical cell. A characteristic of corrosion phenomena is the occurrence of two different, simultaneous reactions which take place on the electrode surface. The cell potential measured is therefore the so-called corrosion potential, E$_{corr}$, and falls between the standard half-cell potential (E^0) of the reactions of oxidation and reduction involved.

OCP measurements are performed by measuring the voltage difference between a material immersed in a corrosion medium and an appropriate reference electrode. In this study, it was used a Standard Calomel Electrode (SCE), whose potential is 0.241 V versus the Standard Hydrogen Electrode (SHE).

III.2.2.2   Polarization methods

Polarization methods, such as potentiodynamic linear and cyclic polarization and cyclic voltammetry are often used for laboratory corrosion testing because they can provide important information regarding corrosion mechanism, corrosion rate and susceptibility of specific material to corrosion in designed media . They involve varying the working electrode

potential and monitoring the current which is produced as a function of time or potential.

Cyclic polarization (cyclic Voltammetry)

Cyclic polarization consists in the registration of polarization curves by increasing and then decreasing values of the working electrode's potential and registering the current in the circuit. There are several ways to report the results, according to the aim of the work and the process which need to be studied. The most used way to represent the data is by plotting values of current density or current as a function of potential, $J = f(E)$ or $I = f(E)$. Semi-logarithmic scale is also employed to evidence better some processes.

The analysis of cyclic polarization curves (cyclic voltammograms) allows obtaining information regarding the type of electrochemical process occurring at the electrode/medium interface. These could be generalized corrosion, localized corrosion, surface passivation and redox reaction of species in solution. The mathematical or graphical elaboration of these curves allows evaluating the corrosion potential, the breakdown potential and the re-passivation potential (see Figure III.14).
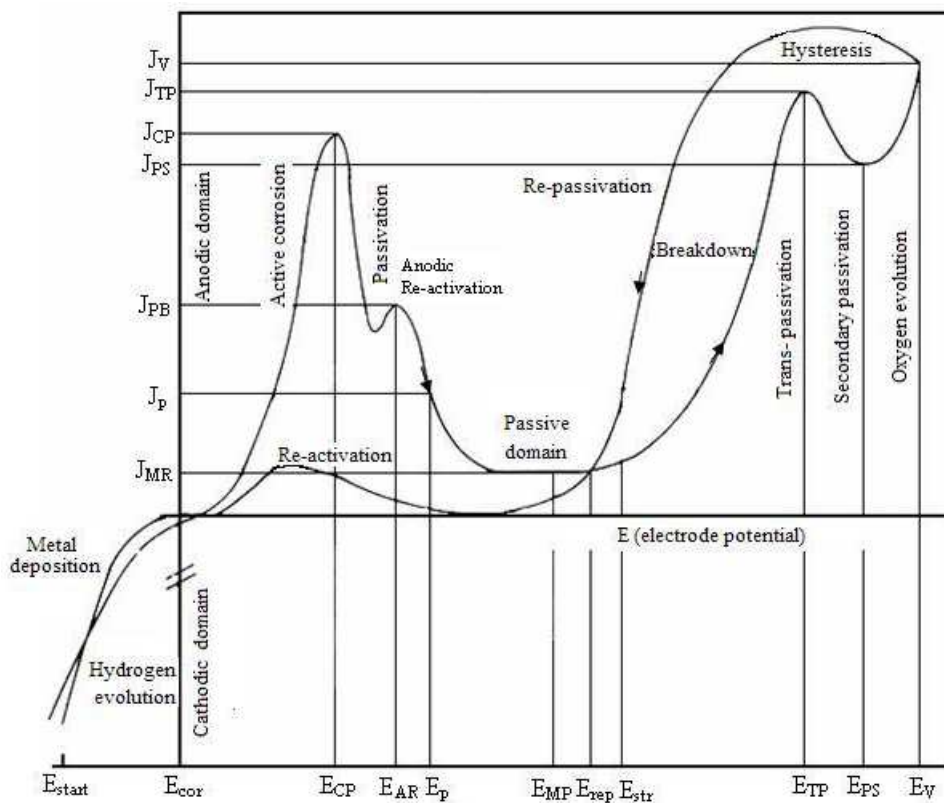
Figure III.14. General aspect of a cyclic voltammogram.

Where:

E_{start} – starting potential, corresponding to the metal's potential when the circuit is closed, without applying an overpotential;

E_{cor} – corrosion potential;

E_{CP} – critic potential of passivation, which corresponds to the begin of the process of primary passivation; the correspondence in the ordinate is the current density, J_{CP} which is the highest value of the current density on the passivation curve;

E_{AR} – anodic re-activation potential: it is present only if the metal shows an accidental activation, after the critic passivation potential;

E_p – passivation potential;

E_{MP} – maximum passivation potential which corresponds to the minimum value of current density, J_{MP};

E_{BD} – breakdown potential, which corresponds to the end of the passive domain;

E_{TP} – trans-passivation potential, corresponding to the current density, J_{TP}, the maximum value of current density in the trans-passivation domain;

E_{SP} – secondary passivation potential – it appears only for polarization curves of metals which show a second passive domain; it corresponds to the current density J_{SP};

E_V – vertex potential – it is the potential corresponding to the inversion of the polarization; it can coincide with the hydrogen evolution potential; it corresponds with the value of current density, J_V;

E_{rp} – re-passivation or protection potential, when a passive layer is produced again.

Cyclic voltammetry involves sweeping the potential in a positive direction until a pre-determined value of current or potential is reached, then the scan is immediately reversed toward more negative values until the original value or potential is reached. In some cases, ths scan is done repeatedly, to determine changes in the current-potential curve produces with scanning. Cyclic polarization test are often used to evaluate pitting susceptibility. The potential is swept in a single cycle (or slightly less than one cycle) and the size of the hysteresis loop is examined along with the differences between the value of the starting open circuit potential and the return to passivation potential. The existence of the hysteresis is usually indicative of pitting corrosion, while the size of the loop is often related to the amount of pitting.

Linear polarization (linear voltammetry)

The method involves the sweeping of working electrode potential towards more positive ot more negative values. Linear polarization curves allow the calculation of the polarization resistance *[Rocchini 1993]*, which is defined as the slope of the potential-current density curve at the free corrosion potential.
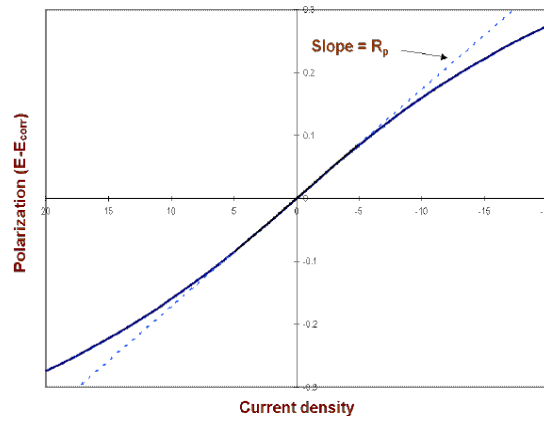
Figure III.15. Ideal linear polarization plot.

The polarization resistance, R_p, can be related to the corrosion current by the Stern-Geary equation [*Roberge 2004*]:

$$R_p = \frac{B}{I_{corr}} = \left(\frac{dE}{di}\right)_{\Delta E \to 0} \qquad B = \frac{b_a b_c}{2.3 \cdot (b_a + b_c)}$$

where:

R_p is the polarization resistance; **i_{corr}** is the corrosion current; **B** is a proportionality constant, which can be calculated from **b_a** and **b_c**, the anodic and cathodic Tafel slopes.

The Tafel slopes themselves can be evaluated experimentally by using real polarization plots. The corrosion currents estimated using these techniques can be converted into penetration (or corrosion) rate using Faraday's Law.

The present study were performed, in aerated solution, at potentials near the E_{cor}, in the potential range ± 150 mV against the open circuit potential and a scan rate of 1 mV/sec. The polarization resistance was calculated as tangent slope at the *electrode potential* vs. *current density* curve, at the E_{cor}. The cathodic Tafel slope (b_c) was calculated as the potential change over one decade (one order of magnitude) decrease in the current density at potential near the E_{cor}. The anodic Tafel slope (a_c) was determined in a similar way using the anodic branch of the polarization curve.

III.2.2.3 Electrochemical Impedance Spectroscopy

Electrochemical impedance spectrometry is an experimental method for characterizing the surface structure of an electrode in an electrochemical system. It has been recently used for the evaluation of the protective properties of coatings for metallic cultural heritage [Cano *et al.*, 2009].

Impedance is the opposition to the flow of alternating current (AC) in a complex system. A passive complex electrical system comprises both energy dissipator (resistors) and energy

storage (capacitors) elements. If the system is purely resistive, then the opposition to AC or direct current (DC) is simply resistance.

An important advantage of EIS, in comparison with other laboratory techniques, is the possibility of using very small amplitude signals without disturbing the properties being measured and also the possibility of studying corrosion reactions and measuring corrosion rates in low conductivity media where traditional DC methods fail [*Letardi, 1998*].

The technique is based on the application of a small-amplitude alternating electric signal (current or voltage) to the corroding metal and the subsequent analysis of response function, which depends on the reactions taking place in the electrochemical system. The response is usually described by the complex impedance Z.

The time-dependent current response I(t) of an electrode surface to a sinusoidal alternated potential signal V(t) has been expressed *[Bard 1980]* as an angular frequency (Ω) dependent impedance Z(Ω), where:

$Z(\Omega) = V(t)/I(t)$

$t =$ time

$V(t) = V0 \sin \Omega.t$

$I(t) = I0\sin(\Omega.t + \tau)$

$\tau =$ phase angle between V(t) and I(t)
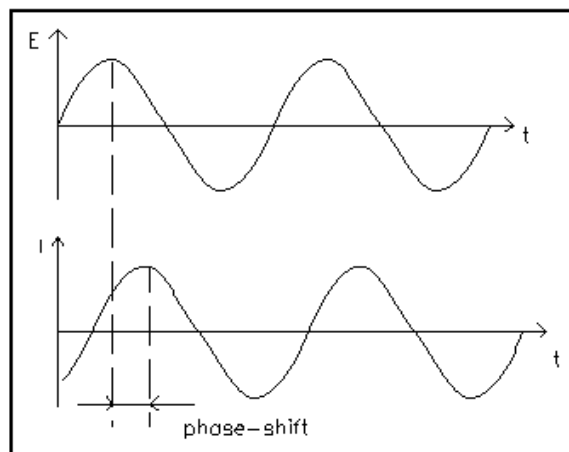
Figure III.16. Sinusoidal responses in a linear system.

Various processes at the surface absorb electrical energy at discrete frequencies, causing a time lag and a measurable phase angle Ω, between the time-dependent excitation and the response signals. These processes have been simulated by resistive-capacitive electrical circuits (e.g. Figure IV.17) and they are usually employed for the interpretation of EIS results.
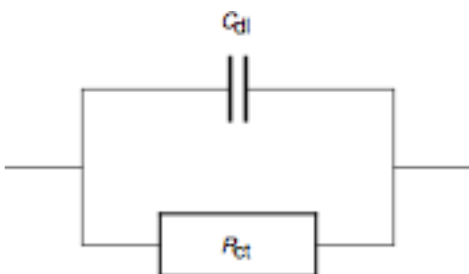
Figure III.17. Equivalent circuit for redox reaction without mass-transfer limitation

These circuits are often an adequate representation of a simple corroding surface under activation control. The different elements of the equivalent electrical circuits are assigned to different physical elements of the system under study, but there is no one-to-one correspondence between EIS data and the equivalent

circuit, and different circuits can be employed to model the same results.

EIS data are often presented using Nyquist plots: they show a semicircle, with increasing frequency in a counter-clockwise direction. At very high frequency, the imaginary component, Z", disappears, leaving only the solution resistance, R_Ω. At very low frequencies, Z" again disappears, leaving a sum of R_Ω. and the faradic reaction resistance or polarization resistance, Rp.
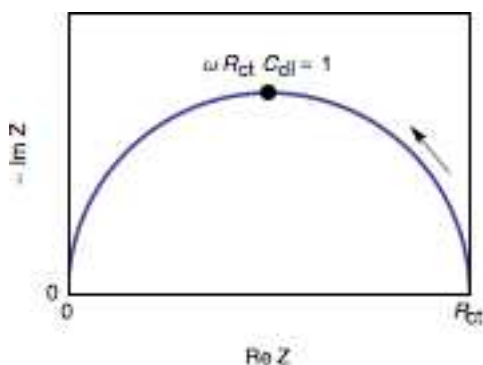
Figure III.18. Nyquist diagram of a RC parallel circuit. The arrow indicates increasing angular frequencies.

The faradic reaction resistance, or polarization resistance, Rp, is inversely proportional to corrosion rate. The impedance. $Z(\Omega)$, may be expressed in terms of real, $Z'(\Omega)$, and imaginary $Z''(\Omega)$, components. $Z(\Omega)=Z'(\Omega)+Z''(\Omega)$. The impedance of an electrode may be expressed in Nyquist plots of Z" (Ω) as a function of $Z'(\Omega)$ or in a Bode plots, which display the logarithm of the impedance modulus (log|Z|), and phase angles, τ. versus the logarithm of the frequency f (in cycles

per second, hertz), where $\Omega=2\pi.f$.

The EIS spectra were registered with The PGZ 301 potentiostat (Radelkis, Copenhaga), using the same three-electrode cell as in the potentiodinamic measurements.

For analysis of the impedance data, a software program "ZSimWin" was used, after a priori data conversion, with a special software. The program used a variety of electrical circuits to numerically fit the measured impedance data. The program is capable of conducting analysis of heavily convoluted frequency dispersion data by deconvoluting the complex response into those of simple subcomponents. This approach combined with the general nonlinear least squares fit procedure allowed us to construct equivalent circuit (EC), whose simulated responses fit actually measured data well. After each experiment, the AC impedance data were displayed as Bode plots (|Z| vs. Frequency and Phase angle vs. Frequency, where |Z| is the absolute value of the impedance). The advantage of the Bode plot is that the data for all measured frequencies are shown and that a wide range of impedance values can be displayed. The frequency dependence of the phase angle indicates whether one or more time constants occur and can be used to determine the values of the parameters in the equivalent circuit (EC).

III.2.2.4 Surface characterization by optical and chemical methods

The corroded electrodes' surfaces were documented using a normal digital camera in order to have a first criterion for their examination. Further, more detailed, analyses were performed

using an optical microscope (Zeiss, AXIO) equipped with dark and bright field filters and a digital camera, and a scanning electron microscope (Tescan).

Attempts, successful in few cases, to characterize the corrosion products formed on their surfaces were realized by using micro-FTIR spectrometry, previously described (paragraph III.1.2.).

III.2.3   Methods

The experiments of potentiodynamic polarizazion and electrochemical impedance spectroscopy were performed with a VoltaLab 21 Electrochemical System (PGP201 – Radiometer Copenhagen) equipped with the acquisition and processing data software VoltaMaster4. A three electrode electrochemical cell was used.

The evolution of the OCP was measured using an electronic millivoltmeter ALDA, type 890C, with entrance impedance of 10 MOhm. At the positive pole, was placed the bronze specimen, while at the negative one, the standard calomel electrode (SCE) was positioned.

III.2.3.1   Evolution of Open Circuit Potential in simulated and natural soil

The evolution of the open circuit potential (OCP) was investigated using the electrochemical system illustrated schematically in the Figure III.19.
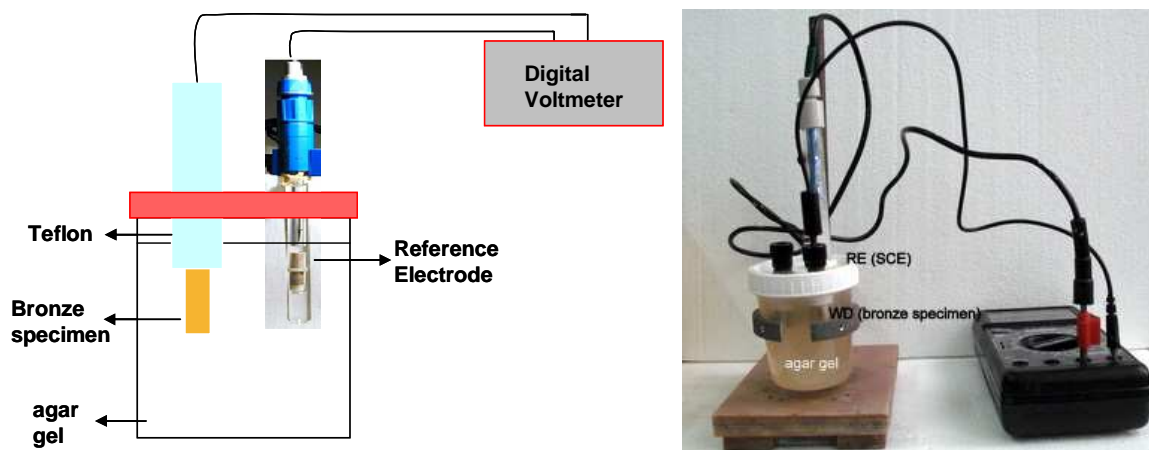
Figure III.19. Electrochemical cell for the OCP measurements in agar gel; the same installation was employed also for the study in soil.on the right-hand side, the photo of the experimental set-up.

Soil simulation was obtained by using an agar gel solution (20g/L) soaked with a mixture of anions (Cl$^-$, PO$_4^{3-}$, SO$_4^{2-}$, NO$_3^-$) at pH 8.5 and concentration which provides the soil environment of the selected archaeological site. The reference electrode is a saturated calomel electrode (SCE). OCP measurements were recorded approximately every day for a month. The same installation was used also to measure the OCP in natural soil, which have been sampled in the archaeological site of Ibida, in the Area Building E1.

Details are given in the chapter III.

III.2.3.2 Corrosion simulation in natural soil

Three working electrodes for each Bronze type were kept in a closed PET container filled up with natural soil (E1), humidified with distillate water, pressed and kept in a dark environment. At the beginning the electrodes' surface was polished with SiC up to 4000 grit. The specimens/working electrodes were characterized after 30, 60, 90 days by means of different electrochemical methods: EIS, OCP, LV, CV. Since EIS does not modify the surface composition, after these measurements the electrode's surface was investigated by means of OM and SEM-EDX. Linear and cyclic voltammetries induce an oxidation of the surface and therefore were performed after optical methods.

III.2.3.3 Corrosion simulation in natural soil solution, seawater and soil-simulated solution

The aggressiveness of different solutions on the corrosion of bronze was investigated by immersing the working electrodes into different corrosive media as described in section III.2.1.3. The electrodes' surface was investigated by OM, SEM-EDX and micro-FTIR.

III.2.3.4 Electrochemical behaviour of bronze in soil, soil simulated solutions and seawater

The study of bronze behaviour in different solutions has been performed using the following sequence of electrochemical techniques:

1. OCP (5')	
2. LV (-300…+500) vs last; $v = 0.5$ mV/s	
(-300…+500) vs last; $v = 1.0$ mV/s	
3. EIS Max frequency 100 kHz	
Min frequency 10 mHz	
Frequency per decade 10	
4. CV $E_0 = 1500$ mV (start)	
E=free	
$E_1 = -500$ mV (end)	
$E_2 = +1500$ mV (max)	
$v = 10$ mV/s	

All the measurements were performed in aerated conditions.

Electrodes surface was characterized by optical and chemical methods after the measurements in order to investigate the morphology and composition of the corrosion layers.

Chapter IV

Results and discussion

IV.1 Examination of excavated bronze artifacts

The research took into consideration twenty-two objects (introduced in Chapter III), recently excavated archaeological bronzes, originating from three Romanian archaeological sites (described in Chapter II) and presenting different degradation patterns.

The approaches for this study aimed to careful characterize both, the alteration layers and the metal core in order to investigate the long-term corrosion behavior of copper-based alloys. It can be summarized in the following points:

A. Visual examination of the artifacts: general observation regarding the aspect of degradation layers, photographic documentation → aesthetics and morphology of natural patina;

B. Physical-chemical characterization of corrosion layers (FTIR and micro-FTIR, XRD, Raman);

C. Selection of few objects which could suffer sampling in order to perform metallography and study the transversal section of corrosion layers by OM and SEM-EDX to evidence their stratigraphy;

D. Discussion of the results of this work and comparison with literature;

E. Plan of corrosion simulation experiments based on experimental observation on real case studies, in order to simulate specific conditions.

This chapter aims to present the results obtained for the case studies which were selected among the archaeological artifacts excavated. We would like to mention here that a large amount of material was studied and classified, but only a selection of these was subjected to further investigations for the purpose of this thesis. A large amount of material was found completely mineralized, and no metal core was left. Since we were interested in studying the dissolution of copper and the other alloying elements and their nature as corrosion products, only the objects for which the metal core was still present was taken into consideration.

IV.1.1 Morphology of corrosion products and aesthetics of ancient bronzes

Metal objects recovered from excavation sites don't show anymore their lustrous and shiny surface, but are often covered by a succession of corrosion layers.

Even though the term *patina* recall a smooth and protective layer made up of stable corrosion compounds, implying a positive or desirable aspect, it is widely used since Gettens as early as in introduced it 1975, [*Gettens, 1975*]. Nowadays, the term has a broad meaning and refers to the effects of time, weathering, accumulation of particulate matter, corrosion on different kind

of materials.

Gettens distinguishes between patina *nobile* when the protective and desirable layers occur, but refer to patina *vile* (weak, poor) when the growths of corrosion products lead to the disruption of the *original surface* [*Bertholon, 2001*].

Robbiola [*1998*] classifies these structures in Type I (or "even" surfaces) or Type II (or "coarse" or "burgeoning" surfaces) for which is not possible anymore to extract information about the original surface from the external layers.

The visual examination of the objects has allowed to make some observation about the morphology of the corroded structures and, in order to classify them, the nomenclature proposed by Robbiola and co-Authors [*Robbiola, 1998*] to describe archaeological patinas, have been used. Information regarding the colour, aesthetical appearance, hardness of external layers is reported (Table IV.1). The general corrosion type and the preservation or not of the original shape and surface of the object is also mentioned.

Table IV.1. A description of the external corrosion layers of the archaeological artifacts.

Sample	Colour	Appearance	Hardness	Limit of the original surface	Corrosion type
Arg.00.1	Grey, brown	Smooth, compact	Dense, very hard	Preserved	Uniform
Arg.00.2	Grey, brown, red	Rough	Hard	Preserved by corrosion products	Uniform (intergranular), presence of spots
Arg.00.4	Green, grey, brown	Smooth, locally rough	Hard to powdery	Preserved	Uniform (interdendritic) + localized
Arg.00.6	Grey, brown	Smooth	Dense	Preserved	Uniform
Ib.05.2	Brown, green	Rough	Hard to powdery	Destroyed	Uneven, localized
Ib.05.3	Brown, light-dark green	Rough	Hard to powdery	Destroyed	Uneven, localized
Ib.05.5	Brown, green	Rough	Hard to powdery	Deformed	Uniform+localized
Ib.05.6	Brown, green locally	Uniform	Hard to powdery	Deformed (?)	Uniform+localized
Ib.05.8	Brown, red green	Rough	Hard (concretions)	Destroyed	Uneven, advanced craks

Ib.05.10	Brown, green	Rough (presence of "buboes")	Hard to powdery	Deformed	Uniform +localized
Ib.05.12	Green, red	Rough	Hard	Seems preserved	Uniform
Ib.05.13	Red to green (presence of wood)	Rough	Hard	-	Uniform+localized
Ib.05.15	Brown to light green	Rough	Hard to powdery	-	Uneven, ,mineralized
Ib.06.01	Brown, dark/light green	Rough	Hard	Mineralized	Uniform + local attack
Ib.06.09	Green, red, brown	Rough	Hard	Mineralized	Uniformly advanced corrosion, cracks
Ib.08.1	Brown	Smooth, compact	Hard	Preserved	Uniform
Ib.08.3	Brown, green	Rough	Hard to powdery	-	Uniform
Ib.08.4	Brown	Smooth, soil incrustation	Hard	-	Preserved as corrosion
Ib.08.5	Brown, green	Smooth – Rough	Hard to powdery – Hard	Lost	Localized
Ib.08.7	Dark brown	Smooth	Hard	Preserved	Uniform
Ib.08.12	Brown	Rough	Hard to powdery	Lost	Uneven
Ib.08.16	Brown	Smooth	Hard	-	Uniform
Ib.08.17	Brown	Rough	Hard	Preserved by corrosion products	Uniform+local attack
Nuf.00.1	Brown, black	Rough	Very hard	Mineralized	Uniform

Mainly, two different corroded structures are observed.

One is characterized by a uniform smooth appearance, hard and compact patina, which preservs the original shape of the object [and its original surface; *Bertholon, 2001*]. This structure has been observed for few case studies, as they are illustrated in the figure (Figure IV.1).
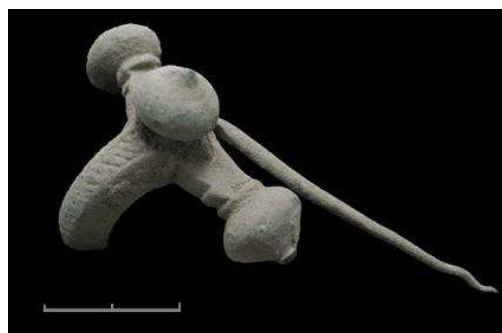
Ib.08.7   **Arg.00.6**

Ib.08.1   **Arg.00.1**

Figure IV.1. Examples of archaeological bronze showing a "noble" patina (according to Gettens) or Type I corrosion pattern (according to Robbiola).

These objects represent a good example to shows how the noble *patina* [*Getterns 1975*] could look like: a homogeneous and compact layer which protects the underneath metal. A deeper elemental investigation reveals the composition and stratigraphical subsequence of corrosion layers.

A second type of corrosion structure is observed for most of the objects. This is characterized by rough incrustation made up of light and dark green minerals mixed together with red/orange compounds and soil particles. In this case, the original shape of the object is not preserved and the original surface is hidden or disfigured. In Figure V.2. some examples are reported.
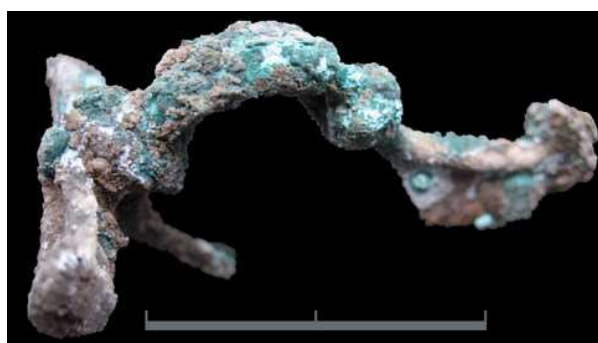
a. Ib.05.3

b. Ib.05.8

c. Ib.08.5.particular

d. Ib.05.6

e. Ib.05.15

Figure IV.2 Examples of archaeological bronzes showing a patina "vile" (Gettens) or Type II corrosion patterns (Robbiola).

In some extreme case, as shown in Figure V.2.e, the ultimate effect of corrosion (bronze disease, as we'll see later on) is to reduce the metal to a heap of light green powdery material. These kinds of structures have been classified by *Gettens* [*1975*], as presenting the so called *patina vile* and more recently, by *Robbiola* [*1998*] Type II structures (see Chapter II).

IV.1.2 Relationship between patina and burial environment

Soil can be described as a mixture of various materials such as mineral matter, organic matter, water, air. Each of these items will have an influence on corrosion of metallic structures [*Stambolov 1985*] in such a way that peculiar soil characteristics will correspond to specific aggressiveness on buried metals. This is the reason why physical-chemical characterization of the burial soil has been carried out at the archaeological site of (L)Ibida.

Details of the results obtained for the analysis of soil profile in the archaeological site of Ibida have been reported in detail in Chapter II.

In this region, soils are weakly developed (Calcareous Chernozem, A-C profile type) their texture being not well differentiated and calcium carbonate being present from the soil surface until a depth of 3-4 m. All these characteristics confirm that actual climatic condition (high temperatures, low precipitation) were unchanged over a long timescale, showing only small oscillations.

In this paragraph we attempt a correlation between the corroded structures observed on archaeological objects and the characteristics of burial environment.

As presented earlier, the most of samples recovered from the archaeological site of (L)Ibida present uneven surfaces with incoherent and heterogeneous corrosion products (examples are reported in Figure IV.3).

Figure IV.3. Examples of artefacts showing uneven and incoherent corroded surface.

This observation is in accordance with the results obtained for soil analysis. From the granulometry point of view, they are classified as <u>loam silt</u> soils, because of the low amount of clay. This is also the reason why they present a relevant porosity, which induces a good aeration until a significant depth.

Also, the moderate amount of gravel or stone within the archaeological stratigraphy (building materials due to human activity) will contribute to the formation of spaces among the soil particles, thus providing a good aeration. This is also further confirmed by the presence of

high quantity of $CaCO_3$, which means that air and water are easily transferred along the soil profile.

However, chemical analysis has shown an alkaline pH and a low content in aggressive anions, such as Cl^-, NO_2^-, NO_3^-, PO_4^{3-} and SO_4^{2-}, indicating a definitely non-aggressive environment from the chemical point of view. Values of conductivity are very low, about 320 μS, a value comparable with still water.

In these conditions, the tool of stability of Pourbaix diagram previously introduced allows to make some consideration about the occurrence of stable corrosion products. Malachite and azurite, two basic copper carbonates, respectively $Cu_2(OH)_2CO_3$ and $Cu_3(OH)_2(CO_3)_2$, are stable corrosion products in well aerated soils, as well as the cupric oxide, CuO, tenorite.

Nevertheless, IC analysis carried out for a soil profile, revealed the increasing concentration of chlorine with depth and, taking into consideration the depth where the archaeological material was found, this could be the cause of the bad state of conservation observed for the majority of metallic artifacts. The green compounds, well crystallized on their surface could possibly be chlorine-containing compounds and an investigation of powders sampled on their surface, will reveal their nature.

The presence of chlorine anions is particularly dangerous as it is the early step for the beginning of the *bronze disease*.

Bronze disease

At the end of XIX century, Marcellin Berthelot (1895) was the first who attempted an identification of the products of a reaction which brings to the instability to certain bronze objects [*Scott 2002*]. Nowadays, the bronze disease is a commonly observed phenomenon, but the mechanisms of its action are not yet clear enough.

Berthelot has identified the products of this reaction as a basic copper chloride, and also supposed the cyclic character of the reactions involved.

The currently accepted [*Scott 2002; Mazzeo 2004*] reaction which is believed to be at the basis of the phenomenon of bronze disease is the oxidation and subsequent hydrolysis of nantokite as:

$$2Cu_2Cl_2 + O_2 + 4H_2O \Leftrightarrow 2\underline{Cu_2(OH)_3Cl} + 2[H^+ + Cl^-]_{aq} \qquad \text{(IV.1)}$$
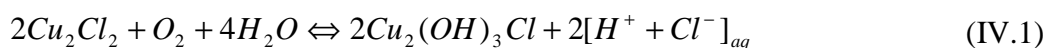
While in anoxic environments the reaction which takes place is the hydrolysis of nantokite (Eq. IV.2) with the formation of cuprite. The increase in acidity due to the reaction of hydrolysis, is supposed to accelerate the dissolution of bronze, or copper, (Eq. IV.3) and more Cu_2Cl_2 is then formed again: this explains the auto-catalytic character of the reaction.

$$Cu_2Cl_2 + H_2O \Leftrightarrow \underline{Cu_2O} + 2[H^+ + Cl^-]_{aq} \qquad \text{(IV.2)}$$

$$2Cu + 2[H^+ + Cl^-]_{aq} \Leftrightarrow Cu_2Cl_2 + H_2 \uparrow \qquad \text{(IV.3)}$$
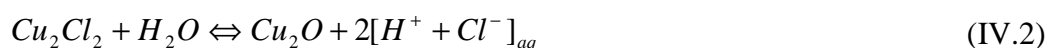
Anyway, this mechanism is not completely clear yet. In practice, when Cu_2Cl_2 is in contact with copper and a drop of water is added, cuprite formation does not occur and copper tri-hydroxyl-chlorides is the principal product [*Scott 1990*]. Also, the Gibbs free energy of formation is greater than 0 and the solubility of nantokite in water is very low (0.006g/100mL).

Pollard et al. [*1992*] has determined that the reaction (2) occurs under most oxidizing conditions. The authors has concluded that, despite the slightly positive value of Gibbs free energy of formation (ΔG_f = 13.5 Kcal/mol), this is the main reaction taking place in burial environments. However, when an object with presence of nantokite is exposed to air (as a consequence of excavation procedure), the cuprous chlorine tends to react to produce one of the copper hydroxochlorides.

Paratacamite (or clinoatacamite) results to be the most stable phase among the three polymorphs with the formula $Cu_2(OH)_3Cl$. Basing on the Ostwald principle [*Martens 2003*], which supposes that, when a chemical reaction result in several products, then the first phase to form is the one with the highest free energy of formation, the order of stability is clinoatacamite>atacamite>botallakite.

The role of cuprite has been elucidated by *Lucey* [*1972*]. He suggests that the cuprite layer, being an electrolytic conductor [*Stambolov 1985; Lucey 1972*] acts as a diffusion barrier, reducing the loss of copper (II) ions in solution and allowing the permeation of chlorine.

Moreover, cuprite acts as a bipolar electrode (Figure IV.4) with an anodic reaction taking place on the inner surface of cuprite and a cathodic reaction taking place on the outer surface.

Out	$O_2 + H_2O + 4e^- \rightarrow 4OH^-$
	$Cu^+ \rightarrow Cu^{2+} + e^-$
	Cu₂O, cuprite
In	$Cu + Cu^{2+} \rightarrow Cu^+$

Figure IV.4. Scheme showing the role of cuprite within a corrosion patina [Lucey, 1972]
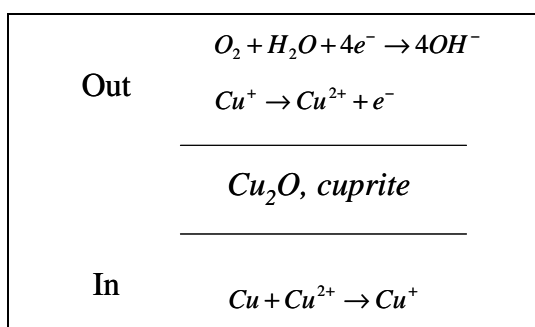
An interesting aspect has been pointed out by *Scott* [*1990*] the possible effect of the alloying

elements according to their redox potential, if a metal lower than copper in the electrochemical series is present, then the production of hydrogen is promoted thus representing a limiting factor for the reaction (IV.3) to occur. If it is so, it is clear the effect of zinc in the promotion of the hydrogen evolution.
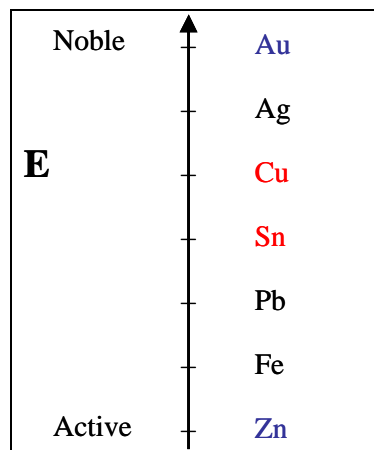
Figure IV.5. Electrochemical series of alloying elements and micro-elements commonly found in bronze alloys

However, observation on archaeological artefacts has shown the relative stability of nantokite, which lies in a dormant state until it comes in contact with oxygen and moisture again.

This situation is likely to occur during excavation procedures, as the stable state of a bronze artefact is "disturbed" and when it is brought back to light. [*Escalante 1989; Sandu 2006*].

FTIR characterization of corrosion products

FTIR spectroscopy represents a micro-destructive method which provides the molecular identification of corrosion products [*Stoch 2000*]. Its limit consists in the lost of spatial information as the powder is removed by scratching the object's surface. Nevertheless, it represents a fast and easy way to identify the nature of corrosion products.

Results are shown in the table (Table IV.2) and the spectra are reported in the Appendix I. Each object has been subjected to this analysis in order to characterize the nature of external layers of degradation.

The following observations have arisen:

- Soil components were identified for almost all the objects: namely aluminosilicates (montmorillonite), quartz (SiO_2) and calcite ($CaCO_3$); the source is, of course, the burial soil.

- Detection of cuprite (Cu_2O) was reported for few cases. This compound is usually located at the interface with the metal core and therefore it is unlikely sampled when the surface is scratched. This layer results much more evident when a sample is taken and a cross-section is realized.

- Hydroxochlorides are the main minerals identified for these objects, as corrosion products. The reason must be found in the location of the archaeological sites (see Chapter.III), which is along the coast of the Black Sea, close to the Danube Delta. This factor, together with the depth of finding, where concentration of chlorine is found to be higher due to its easy percolation, is the causes of the high amount of chlorine-containing minerals detected.

- Even tough malachite and azurite are the main corrosion products found on archaeological bronzes, the analysis have evidenced their presence only for few artifacts.

Table IV.2. FTIR spectroscopy results for the selected archaeological artifacts

No. crt.	Samples	Color	Quartz	Alumino-silicates	Calcite	Atacamite	Paratacamite	Cuprite	Malachite
1	Arg.00.1	light brown	+	+	+				
2	Arg.00.6	scratched	+	+	+	+	+	+	
	Arg.00.6	green	+	+	+	+			+ (?)
3	Ib.05.2	green/brown				+	+		
	Ib.05.2b	light green				+	+		
4	Ib.05.3a	light+dark green				+	+		
	Ib.05.3b	brown	+	+	+				
	Ib.05.3c	mixture	+	+	+	+	+	+	
5	Ib.05.5	scratched	+	+	+				
6	Ib.05.6	dark	+	+	+	+	+		
	Ib.05.6a	dark green		+	+	+	+		
	Ib.05.6b	light green				+	+		
7	Ib.05.8	mixture			+	+	+	+	
8	Ib.05.10a	light green				+	+		
	Ib.05.10b	brown	+	+	+				
9	Ib.05.12	brown	+	+					
10	Ib.05.13a	section	+	+	+	+	+	+	
	Ib.05.13b	mixture				+	+	+	
11	Ib.05.15	dark green				+	+		

No	Sample	Description	1	2	3	4	5	6	7
12	Ib.08.1	dark brown					+	+	+
13	Ib.08.3	red + green		+	+	+	+	+	+
14	Ib.08.4	mixture					+	+	+
15	Ib.08.5	green + brown		+	+		+	+	+
16	Ib.08.7	brown					+	+	+
17	Ib.08.12	mixture		+			+	+	+
18	Ib.08.15	mixture			+	+			
19	Ib.08.16	scratched					+	+	
20	Ib.08.17	ring-mix					+	+	+
21	Ib.06.01	mixture	+	+		+			
22	Ib.06.09	mixture	+	+		+			
23	Nuf00	mixture	+			+			

IV.1.3 Non-invasive identification of corrosion products

Analysis of archaeological and therefore unique artifacts poses the problem to identify the chemical nature of corrosion products using non-invasive method. Analysis by SEM-EDX is a choice as it requires no sample preparation, but it doesn't furnishes information about the molecular nature of the compounds, and measurements of carbon and oxygen signal are not reliable enough to base only on X-ray spectroscopy. It is therefore necessary to couple this technique with others, able to provide molecular information.

In our laboratory, we performed the investigation of corrosion products by means of a micro-FTIR spectroscopy using a normal FTIR bench coupled with an optical microscope. The possibility to focus both the visible and infrared light on a selected area of interest, allows to perform a molecular characterization and to couple the information to a microphotograph. This technique is particularly interesting as it is complementary to Raman Spectroscopy, which is also a technique providing molecular information based on the Raman scattering of an incident monochromatic radiation.

Measurements were performed in reflectance mode using a micro-FTIR spectrometer and its working principles are widely detailed in Chapter IV. Here we want to specify the working condition, which were used for the experiments. The aperture used was 250x250 μm, the spectral range 4000-600 cm^{-1}, 64 scans were recorded for each spectrum with a resolution of 4 cm^{-1}. As anticipated, no sample preparation is required and analysis can be performed directly on the object on a microscopic area. As background, we used a gold mirror which reflects nearly 100% of the incident infrared radiation.

The most interesting results have been obtained for green compounds on samples which are affected by the *bronze disease*.

As introduced before, the occurrence of *bronze disease* is very dangerous, as it can lead to the complete lost of the metal object. The possibility of a non-invasive detection of the compounds related to the occurrence of this degradation process is reported in this paragraph.

Among the investigated artifacts, several of them have shown a severe corrosion process which has occurred possibly after the excavation procedure.

Two samples were considered in detail: the *fibula* shown in the Figure IV.4 and the bronze bended sheet here illustrated, Figure IV.5. In both cases, two different green areas can be identified on their surfaces, one characterized by a light green colour and powdery nature and the other characterized by a dark vitreous green colour and crystalline nature.

a
b
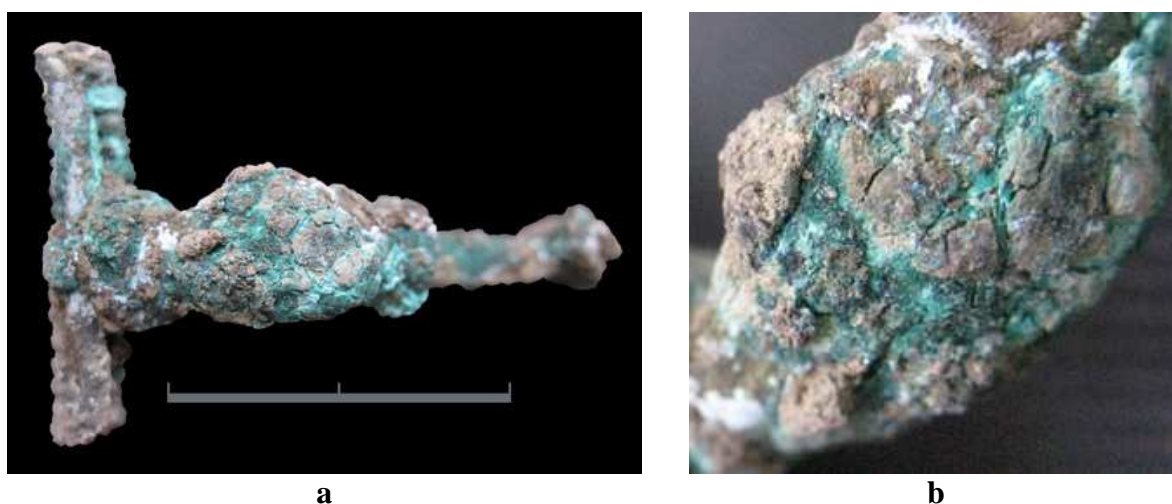
Fig. IV.6. The fibula (Ib.05.3) excavate in the site of Ibida in 2005. a-overview; b-surface detail.
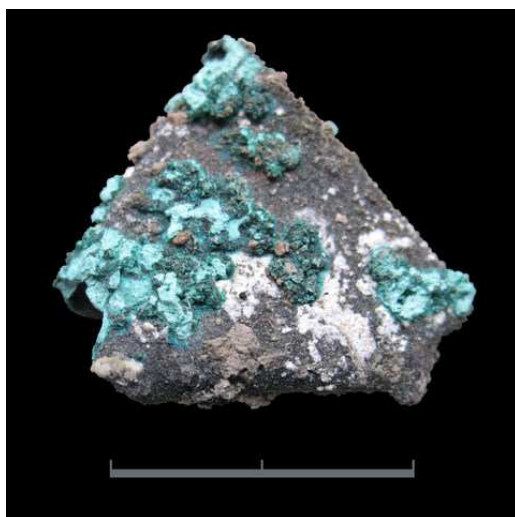
Figure IV.7. Object Ib.05.2: a bended bronze sheet.

Spectral features relative to each of these areas are reported in the following images. As introduced in the previous chapter, both diffuse and specular reflection phenomena can occur when the radiation interacts with the sample.

As a first approach, we selected all the artifacts for which the presence of these compounds was evidenced and we recorded the reflection spectra on these areas in order to evaluate the spectral features. Figure V.6 and V.7 show the spectra (uncorrected) collected directly on the external surface of a selection of objects for respectively the dark green and light green compounds.
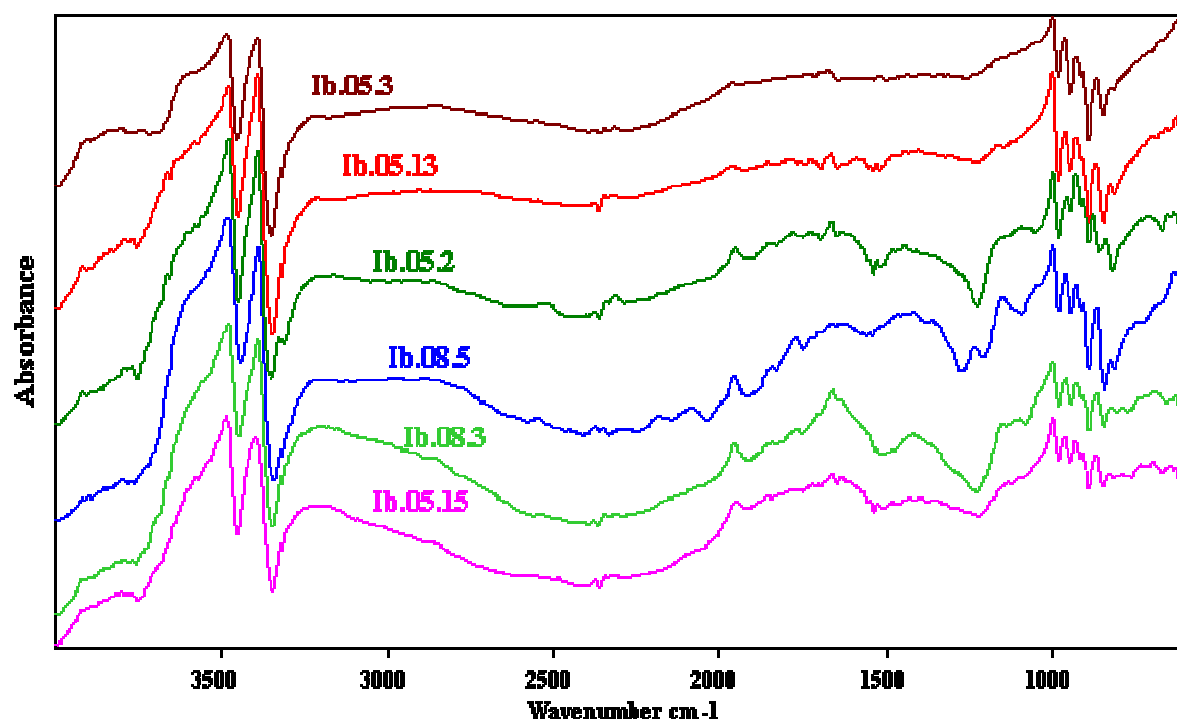
Figure IV.8: Spectra collected for the dark green corrosion compounds. It is worth noting the derivative-like shape of the peaks, particularly evident in the region of O-H stretching 3500-3300 cm^{-1} and below 1000 cm^{-1}.
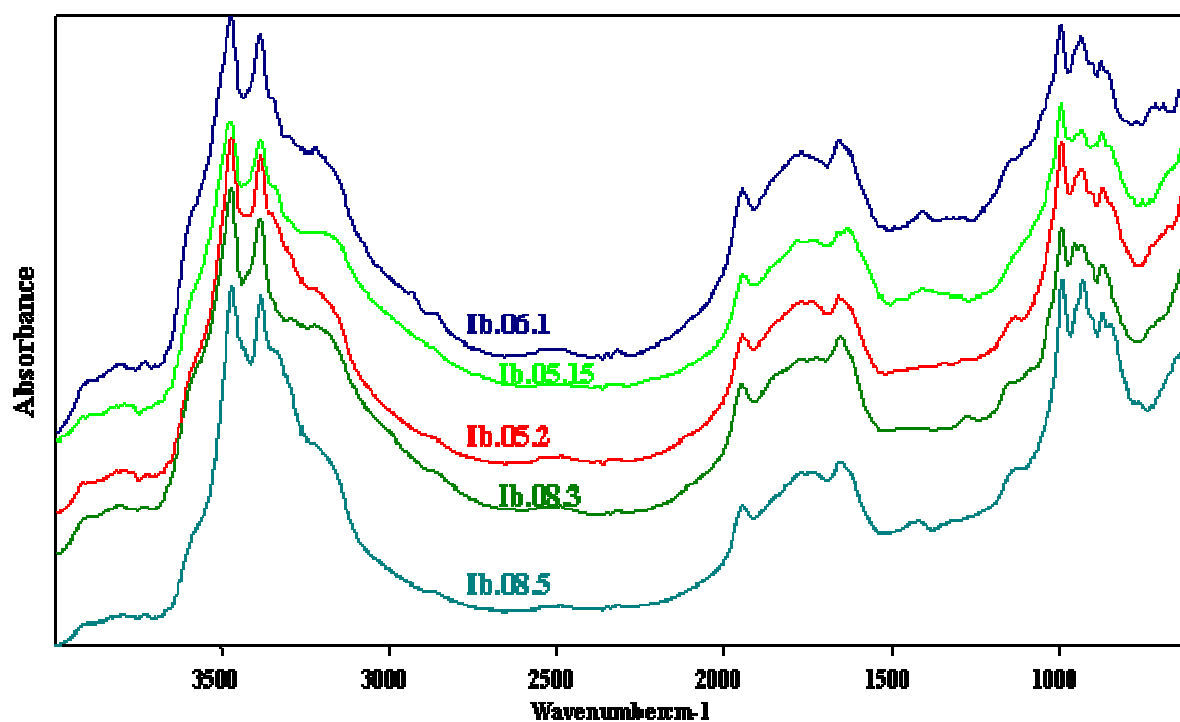
Figure IV.9. Spectra collected for the light green corrosion compounds. Absorbance peaks are again particularly intense in the region 3500-3000 cm^{-1} and below 1000 cm^{-1}.

It can be noticed that they present different shapes, and noticeable is the derivative-like shape of the spectra collected on the dark green areas.

The possibility to simultaneously take a photo and collect a spectrum over a selected area, allowed us to further investigate the phenomenon. Well crystallized dark green and powdery light green areas were selected on the artifacts and an infrared spectrum was collected in reflectance mode.
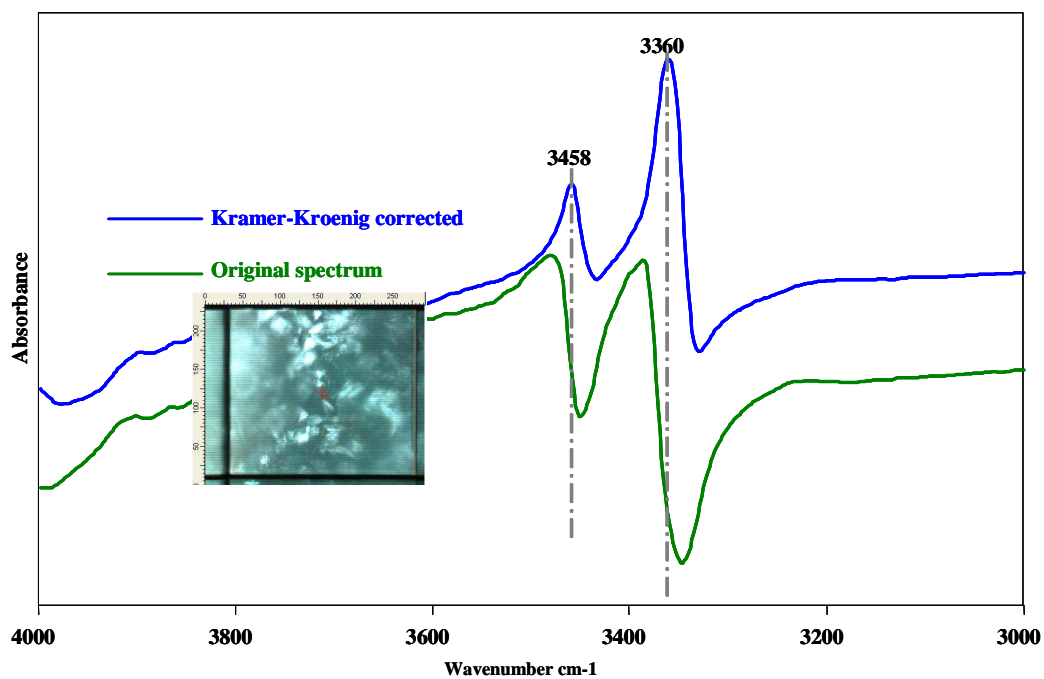
Figure IV.10. Spectral range 4000-3000 cm^{-1}: evidence of the shift and shape difference before and after the KKT.
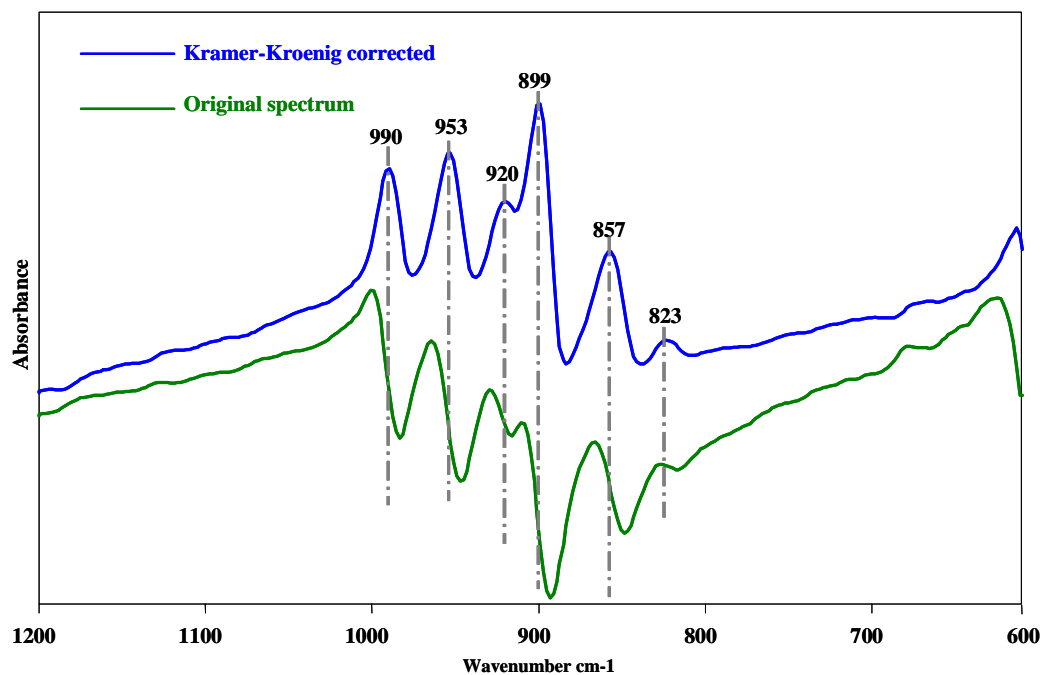
Figure IV.11. Spectral range 1200-600 cm^{-1}: evidence of the shift and shape difference before and after the KKT.

The results spectrum is affected by a strong distortion when the specular reflection occurs, while diffuse reflection spectra present only a variation in the relative intensities of peaks. Both these phenomena can be corrected using the Kramer-Kronig transformation (KKT) and the Kubelka-Munk correction (KM) using the OPUS software and the spectra compared with transmission spectra from databases.
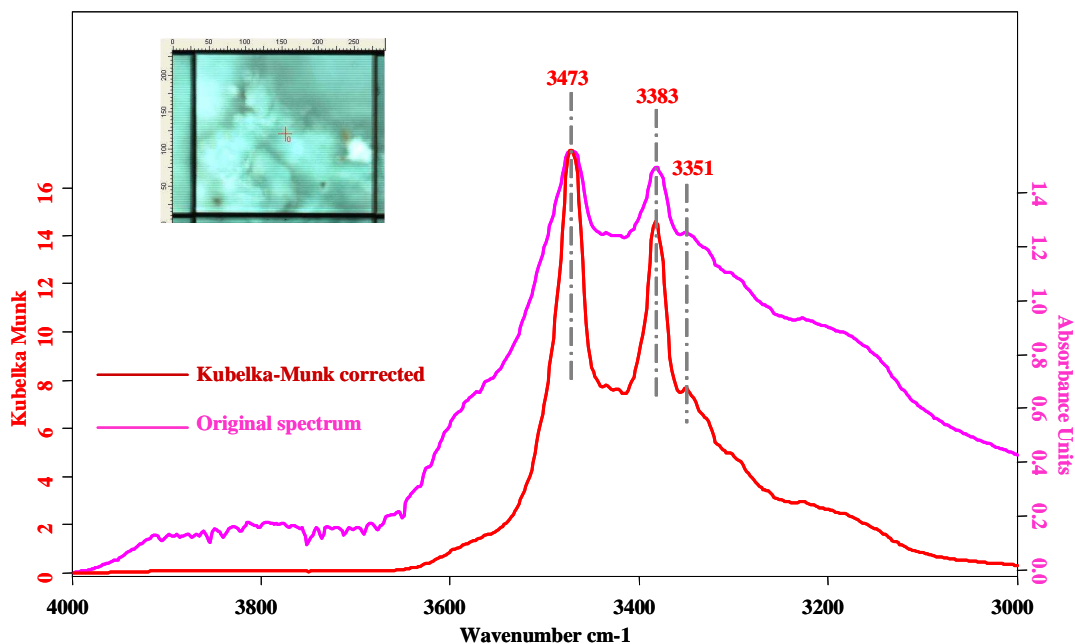
Figure IV.12. Spectral range 4000-3000 cm^{-1} of the spectrum recorded on light green area.
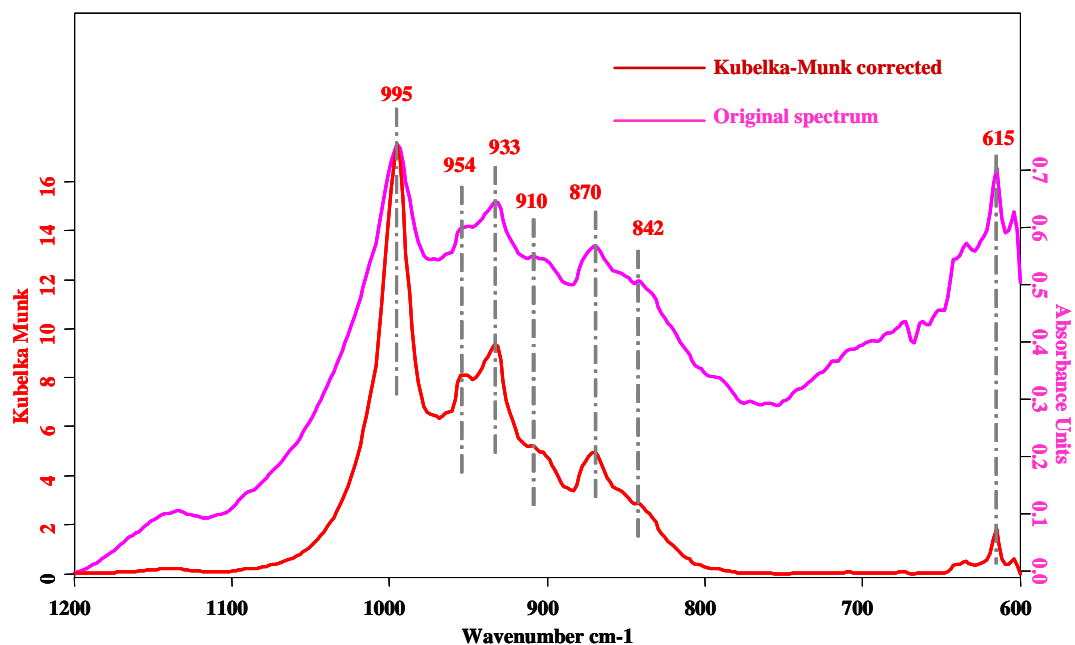
Figure IV.13. Spectral range 1200-600 cm^{-1} of the spectrum collected on the light green area.

It can be observed that, while for diffuse reflectance spectra the position of peaks doesn't change, the spectra collected on dark green areas, where the specular reflection is the main interaction, the use of the KKT correction allows to determine the exact position of peaks.

The following table (Table IV.3) provides a comparison between the peaks of experimental spectra compared to those of literature. A sensible difference exists between values of frequencies for the experimental data and those recorded for natural occurring minerals or synthesized ones and this is probably due to the effect of impurities and the different geographical origins of minerals.

Table IV.3. Infared wavenumbers (cm^{-1}): comparison between experimental (reflectance) and literature (transmission or attenuated total reflection) data.

Dark green	Atacamite	Atacamite	Light green	Paratacamite	Paratacamite	
Ib.05.3	*Ref. 1*	*Ref. 2*	Ib.05.3	*Ref. 2*	*Ref. 3*	Band Assignment
3458	3444	3457	3469	3420	3442	
3360	3337	3433	3386	3330	3358	
		3364	3342	3280	3307	Hydroxyl
		3349			3289	stretching
		3328				
		3208				
990	985	987	996	987	986	
953	949	974	954	926	921	
920	915	957	938	915	905	Hydroxyl
899	894	912	913	900	891	bending
857	849	864	873	865	862	
823	819		839		822	

Ref. 1: Omnic Library
Ref. 2: Frost. R. *et al.* Journal of Raman Spectroscopy, **33** 801-806 (2002)
Ref. 3: Martens, W. *et al.* N. Jb. Miner. Abh. **178** 2 197-215 (2003)

Around the identification of hydroxyl-chlorides many scientific efforts have been done in these last years [*Martens, 2003; Frost, 2002*]. The occurrence of bronze disease has always posed the problem to identify the chemical nature of the compounds formed by the interaction of cuprous chloride, nantokite, with moisture and oxygen. The minerals such as atacamite, clinoacamite and botallakite are polymorphous and they present minor spectral differences, being spectroscopically characterized by absorption peaks in the hydroxyl stretching (3500-3300 cm^{-1}) and deformation (1000-800 cm^{-1}) vibrations regions.

A draft identification of these compounds can be done based solely on optical microscope observations. As these corrosion products are minerals, their morphology and structure is well defined by mineralogists. Atacamite is found in form of orthorhombic crystals and vary in colour from emerald to blackish green. Paratacamite, or clinoatacamite, is more often found as a powdery, light green and present as spots on the patina surface or in pustules [*Scott, 2002*].

SEM-EDX observations of the external corrosion layers of the object Ib.05.3 has allowed to put in evidence the crystalline nature of the dark green mineral as it is reported in the Figure IV.14.
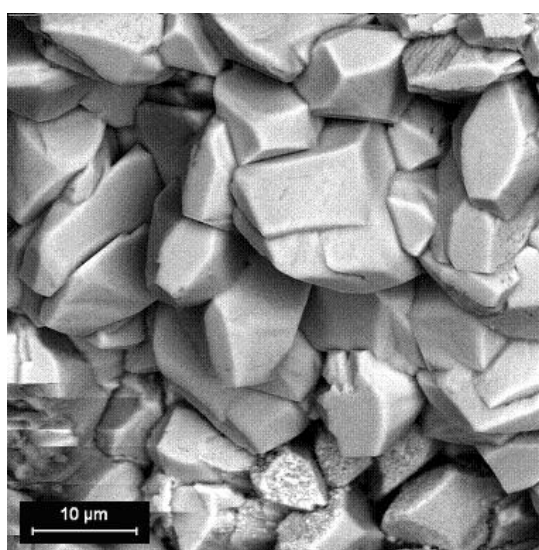
Figure IV.14. SE-BSE micro-photograph of the dark green spots on the object Ib.05.3

IV.1.4   Classification of corrosion structure

The following paragraphs report the results obtained for several case studies, at the end a summary of the corrosion typologies is provided.

Identification of corrosion or alteration products is challenging as it doesn't exist "the" analytical technique, which provides all the answers, but an integrated approach, based firstly on a careful visual examination, needs to be employed.

The usual methodology foresees a selective sampling in order to analyze the scratched powders by classical method, such as FTIR spectroscopy and XRD. When sampling is allowed, a representative fragment is withdrawn and, using the methodology detailed in the Chapter III, a transversal section is prepared and studied by means of optical and scanning electron microscope.

When more information is needed, other techniques, such as XRD, micro-XRD and Raman spectroscopy, have been used in order to provide the answers to the proposed questions.

IV.1.4.1   Striated corrosion patterns

Bronze objects recovered from burial condition often present periodic, rather than continuous, corrosion layers [*Graedel, 1987*]. This is the case of the objects reported here: possible pathways which brought to this behavior will be presented.

These objects, identified as fragments of an hairpin or hairstick, labelled Ib.06.09 and shown in Figure V.15, was discovered in 2006 in the archaeological site of Ibida, the village of Slava Rusa today. It has been discovered, during excavation procedures, at a depth of -3.30 m n the sector of Curtina G, close to the external city walls.

Figure IV.15. Photo-documentation of the object labelled Ib06_09: a bronze pin or hair-stick.

As anticipated, the main questions that arise when dealing with archaeological bronze, and an answer is due to the archaeologist and the restorer, is which possibly could be the original shape of the object? How did the object corrode?

As proposed already more than 30 years ago by *Jedrzejewska* [*1976*] corrosion layers, or patina, offer an opportunity to better understand degradation pathways which have taken

place over a long timescale, and excavated material that is excluded from the exposure in museums, can assume a significant scientific interest.

According to the experimental protocol, sampling of the corrosion layers has been performed and the powder has been analyzed by FTIR (Figure IV.16).
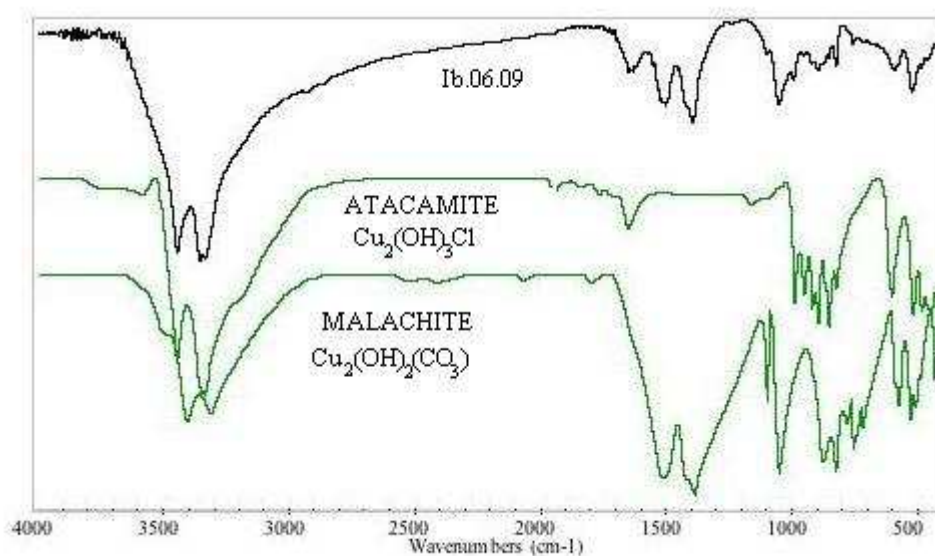
Figure IV.16. FTIR spectrum of the powder scratched from the sample Ib.06.09

Two common corrosion products were detected, typical of underground corrosion: malachite, a basic copper carbonate and atacamite, a basic copper chloride.

XRD patterns allow identifying the oxides (hardly detectable with infrared spectroscopy in the mid-IR region) such as cuprite (Cu_2O) and poorly crystallized cassiterite (SnO_2).

Optical microscope observations revealed the very particular sample's cross section and allowed appreciating the striated textured pattern (Figure V.17) surrounding a central solid metal core with a composition of Cu 90.2, Sn 9.8 (wt. %). Chemical etching with an alcoholic solution of $FeCl_3$ in HCl allowed studying the microstructure of the alloy (Figure V.18), which revealed to be a homogeneous recrystallized α-phase bronze showing very small twinned grains; this accounting for long and repeated working cycles.
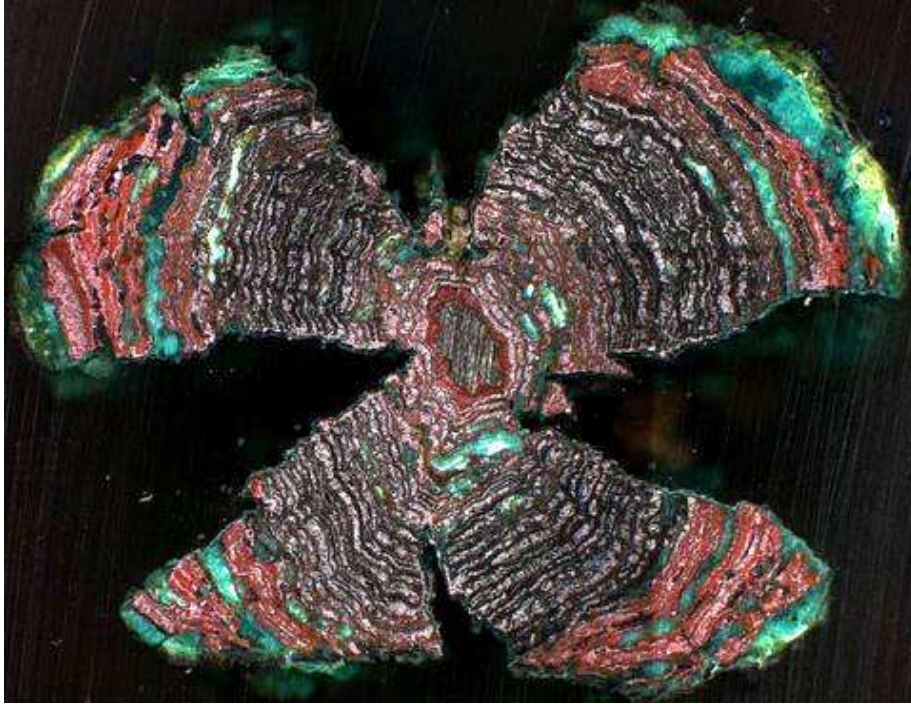
Figure IV.17. Micro-photography of sample's cross-section by OM, Dark Field: a. overview (50x).
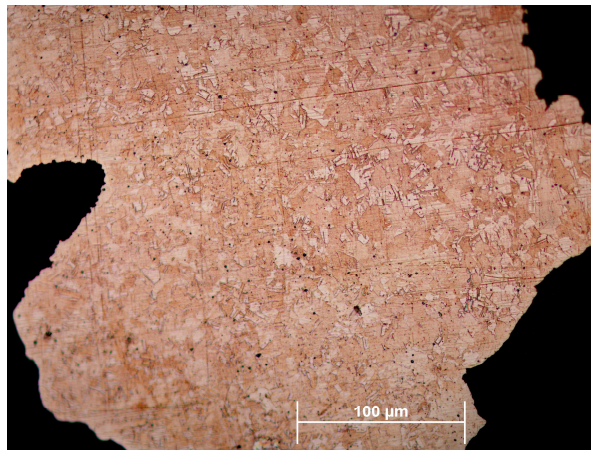
Figure IV.18. Metallographic section of the sample: small, re-crystallized grains.

An insight into the corrosion layer consisted in the investigation by SEM-EDX, characterizing the distribution of Cu, Sn, O, Cl in the cross-section. There is a segregation, around the central metal core (Figure V.19), of Cu-containing and Sn-containing compounds, possibly cuprite (as indicated also by the red-orange colour in the micrograph) and cassiterite.

The same segregation is observed also along the corrosion layers: subsequent layers of cuprite and cassiterite of variable thickness (few to hundred microns) are alternated, from time to time, with green layers, consisting of malachite and atacamite (as identified by FTIR spectroscopy), the latter being mainly located in the external area.
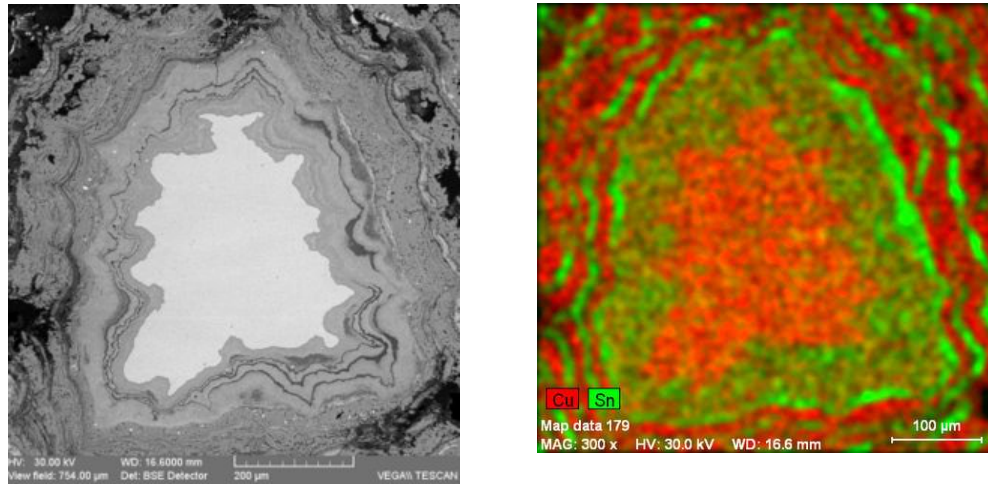
Figure IV.19. Comparison between BSE micrograph and image reporting the overlapping Cu-Sn showing the segregation of cuprite and cassiterite.

The fine structure of the striated textured pattern has been further investigated at higher magnification at the SEM-EDX. Results shown here have been obtained at the ICN, Amsterdam, with the researcher Ineke Joonsten.
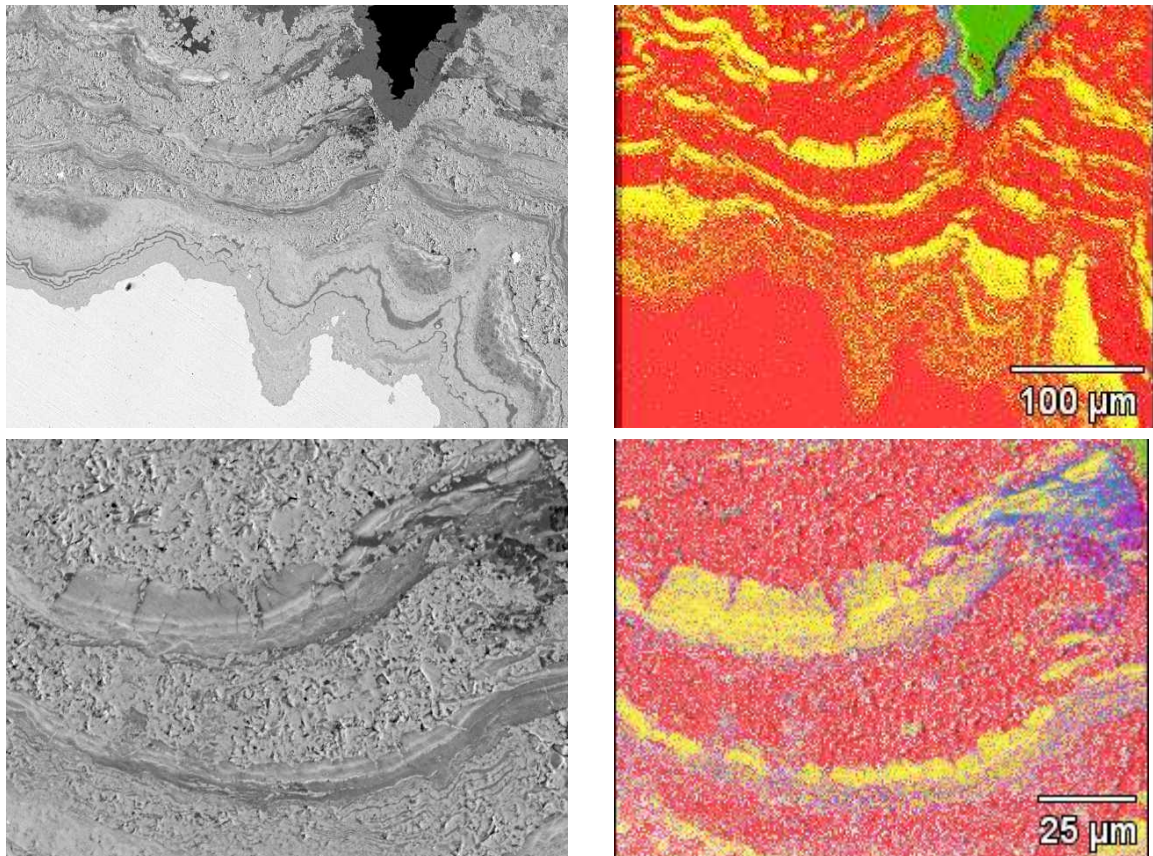
Figure IV.20. BSE images, and correspondig false colour picture, representing the Phases characterized by the spectra reported in Fig. 17 (the green colour in the right top image represent the embedding resin.

The advantage of this technique, compared to the EDX mapping performed in our laboratory, is the possibility to record a map where the different colours identify different phases,

characterized by a well defined spectrum (Figure IV.20).

In the following image (Figure IV.21) the three spectra characterizing the red, yellow and blue phases are reported.

According to these spectra, and correlating the results also with the FTIR and XRD results, it can be concluded that the red phase corresponds probably to a copper-rich phase, which is metallic copper in the alloy and cuprite in the corrosion layers. The spectrum relative to the yellow colour shows peaks of tin and oxygen, thus here cassiterite (SnO_2), or hydrated tin oxides are present. Peaks of copper, chlorine and oxygen identify the blue phase and can therefore be associated with the presence of an hydroxochloride, such as atacamite or paratacamite.

It is worth noting the porous nature of the cuprite layers if compared to those characterized by Sn-rich spectrum.
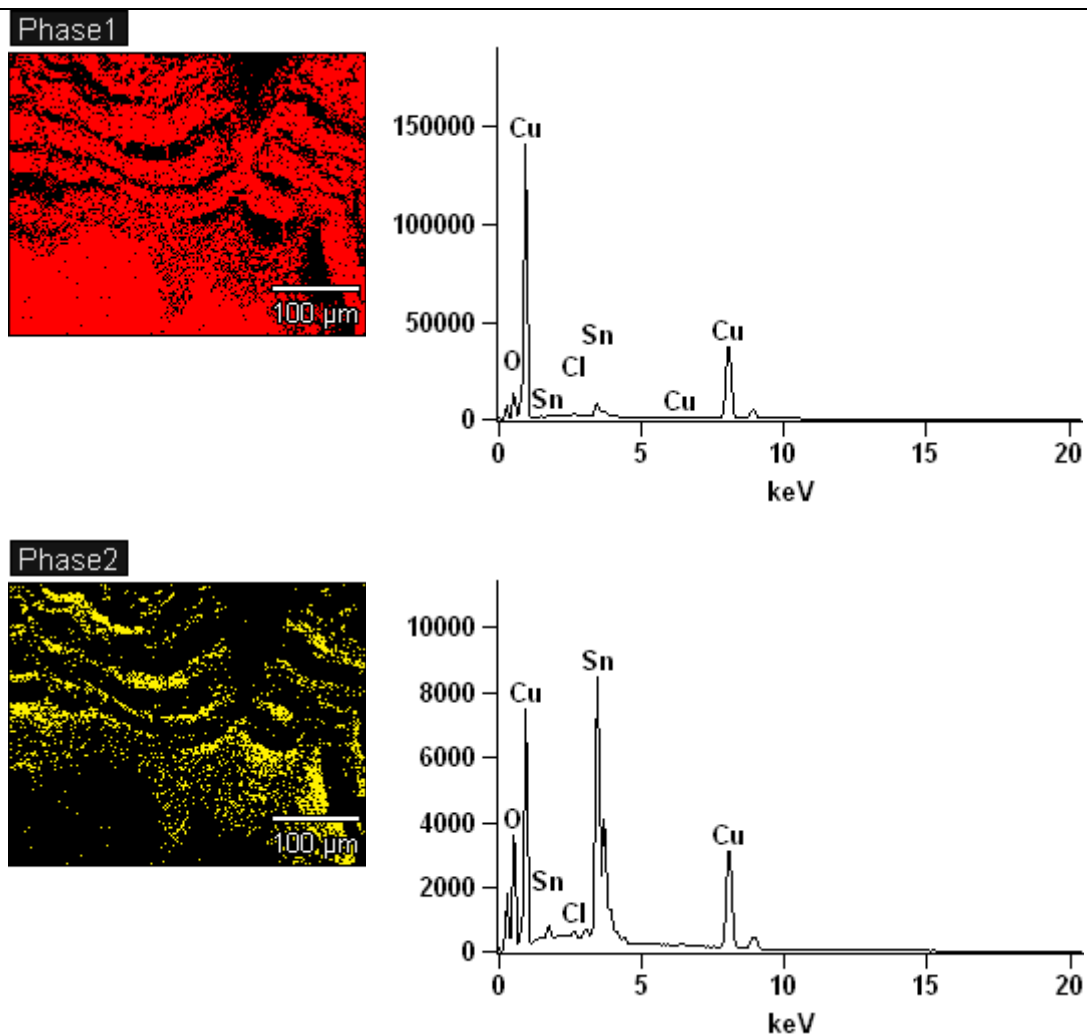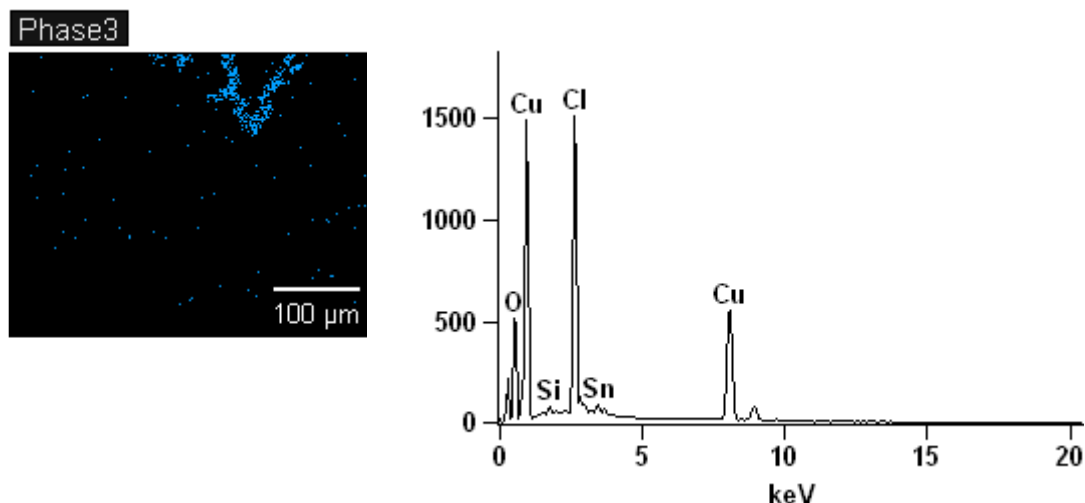
Figure IV.21. Phases and the relative EDX spectra. From top to bottom: <u>Phase 1</u> is characterized by copper-rich spectrum, <u>Phase 2</u> is characterized by Sn and O-rich spectrum and <u>Phase 3</u> contains Cu, Cl and O.

As demonstrated, the EDX mapping offers a useful tool to be coupled to the micro-destructive technique of FTIR spectroscopy, which however furnishes essential molecular information.

At the ICN, Amsterdam, we decided to confirm the chemical nature of these two phases by a technique able to give information about the crystalline structure, which is the X-ray diffraction XRD.

The main advantage of this technique is the possibility to collimate the X-ray beam on a selected area of 2x2 mm, visible through a webcam located in the chamber. The result is shown in Figure IV.22.
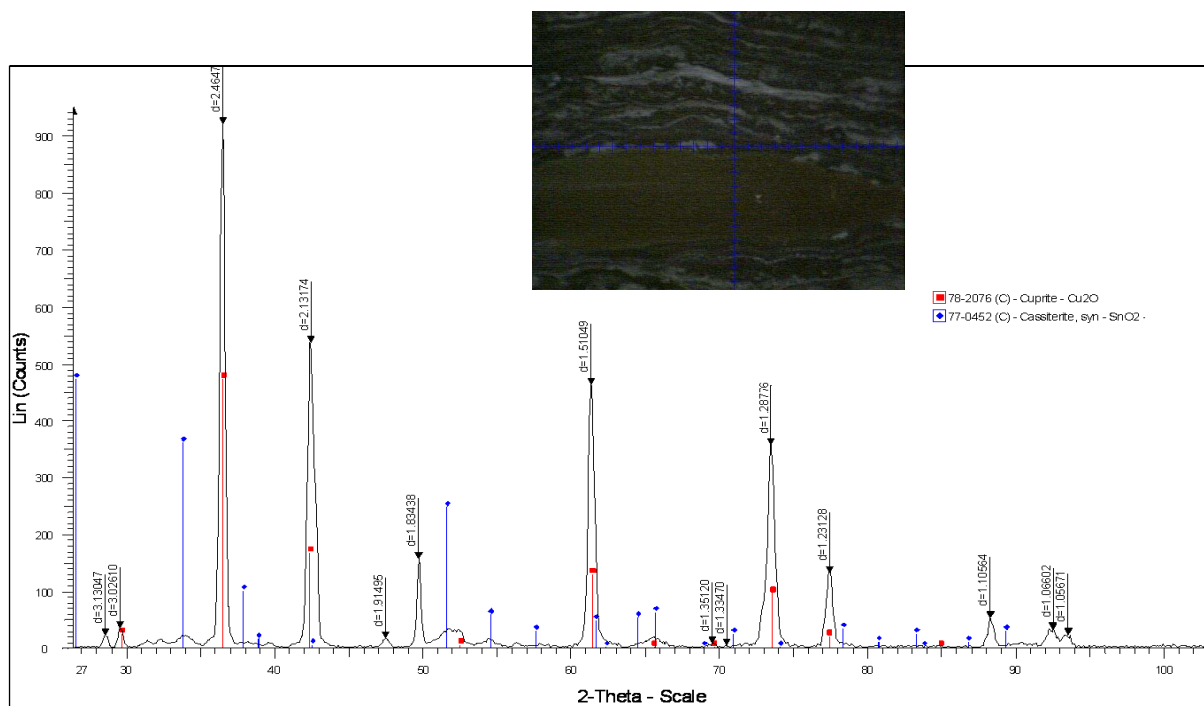
Figure IV.22. XRD pattern of the powder scratched from the sample Ib.06.09.

The nature of the compounds giving rise this striated structure was elucidated: a succession of cuprite, Cu_2O, and cassiterite, SnO_2, layers are the main components of this patterns, while on the outer layer tri-hydroxyl-chlorides are present. They were probably formed by the interaction of formerly present malachite with the chlorine in the environment.

Such a striated structure has been already observed by other authors [*Scott 2002; Brown, 1977, Stambolov 1985*], and attempts to relate it to the age of an object has been proposed. Even though these are fascinating theories, they have not been confirmed since underground corrosion is affected by many factors and the seasonal alternation of temperature, rainfall, moisture content or local content of carbon dioxide are only partly the cause of the phenomenon. As supposed by *Stambolov* [*1985*], if considered from the chromatographic point of view, this behaviour is more reasonable. Stannic oxide can act as a chromatographic adsorbent, such as silica gel, through which copper ions from the alloy are allowed to diffuse outwards, while soil components could move inwards [*Stambolov, 1985*]. When cuprite or malachite finds saturation condition, they precipitate, leading to this *striated textured structure*. Scott has considered such hypothesis in an article published in 1985, when he refers to periodic or oscillatory reactions, often called Liesegang phenomena [*Scott 1985; Müller 1982*]. These phenomena are observed in the laboratory using for example an agar gel solution in which a soluble electrolyte such as copper (II) acetate is used [*Keller, 1981; Mueller, 1982*]. A second medium is then allowed to slowly diffuse through he gel and a number of malachite layers are observed. Sometimes is possible to verify some mathematic relationship among the spacing and width of these layers according to experimental conditions and parameters such as pH.
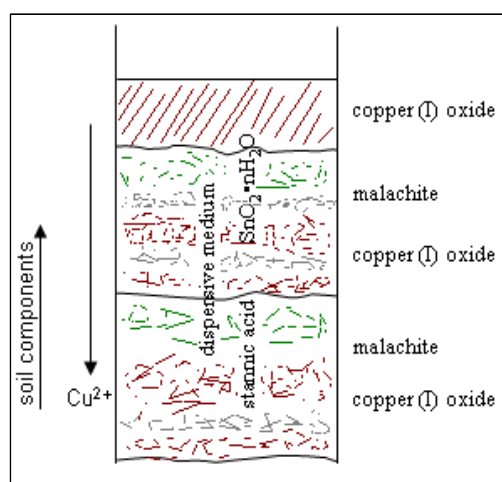
Figure IV.23. Scheme of the chromatographic behavior of stannic oxide layers [after Stambolov, 1985]

In burial condition, these phenomena could occur very slowly and factors such as seasonal variations in temperature, pH and amount of rainfall could led to the formation of these banding structures. It is proposed in the figure (Figure IV.23) a possible mechanism of formation of bending structure: tin oxide acting like a chromatographic adsorbent and copper ions diffusing through it.

However, it seems that these bandings are not explicable according to the initial microstructure of the alloy [*Scott, 1985*]. Even though an object

subject to cold working techniques, and presenting small grain size, would be more easily corroded along the grain boundaries.

Another interesting observation concerns the four fractures, which are observable in the cross section and also longitudinally along the height of the object (see Figure IV.15). An interpretation of this behaviour could be the original shape of the object, possibly realized using one of the illustrated techniques to realize metallic wires (Figure IV.24).
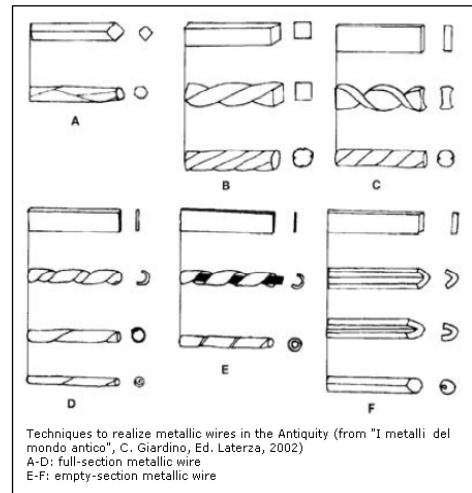
Figure IV.24. Illustration of the different techniques to realize metallic wires in the Antiquity (from "I metalli nel mondo antico", C.Giardino, Ed. Laterza, 2002).

As another example of striated corrosion patterns we report here the results obtained for another case study.

Figure IV.25. Ring fragment (labeled Ib.05.8) excavated at the archaeological site of Ibida in 2005 and subjected to scientific investigation

The object, made of bronze, is probably a fragment of a ring (Figure IV.25). It presents an inhomogeneous and incoherent corroded surface characterized by red, green, grey and brown corrosion products. It results, in few places, detached from the underneath layer but the minerals are strongly crystallized and the action to remove them with a scalpel results difficult.

FTIR spectroscopy has been used to characterize the powder sampled directly from the surface. The spectrum is reported in the appendix I. Copper oxide and copper hydroxyl-chlorides were detected, as well as soil component such as calcite, aluminosilicates and quartz. The discontinuity is due to the "spalling-off" effect as a consequence of formation of corrosion products of bigger relative volume with respect to the metal itself [*Mazzeo 2004*]. This phenomenon causes the lost of information and lost of sequence of corrosion layers.
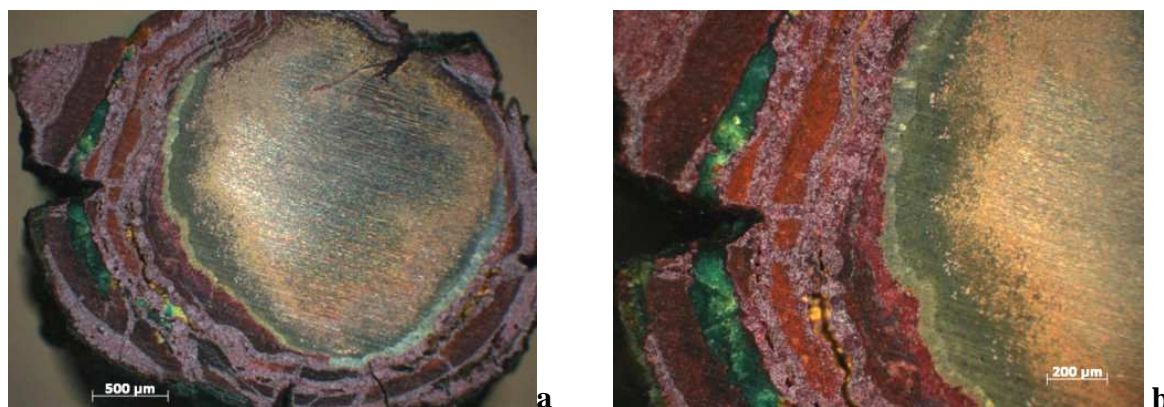
Figure IV.26. Micrograph (OM, DF) of the cross section (Ib.05.8). a- overview: 50x; b- detail of the layered structure: 100x.

A small fragment was sampled and a cross-section was prepared according to the standard methodology. Optical microscope observation of the stratigraphical section evidences the succession of corrosion layers, the whole sequence being preserved only on the left side.

A rough identification of the nature of corrosion compounds is conducted by simple optical microscope observation. Starting from the metal core, two green layers are present: the first one evidencing the crystalline microstructure of the alloy and the second one being more compact and slightly lighter.

Comparison between dark and bright field observation at the optical microscope, allows to better study the layers at the interface between the metal core and the first, red layer of cuprite. The compact layer, which results light green in the dark field image and translucent orange to blue in bright field, may be identified as nantokite, Cu_2Cl_2. Chlorides, and the electrolytic conductivity of the cuprite layer [*Lucey 1972; Stambolov 1985*], are responsible for its formation. As mentioned previously, this is the early stage of the so-called "bronze disease", the main harmful corrosion phenomenon, which, if not controlled, leads to the complete mineralization of the object.
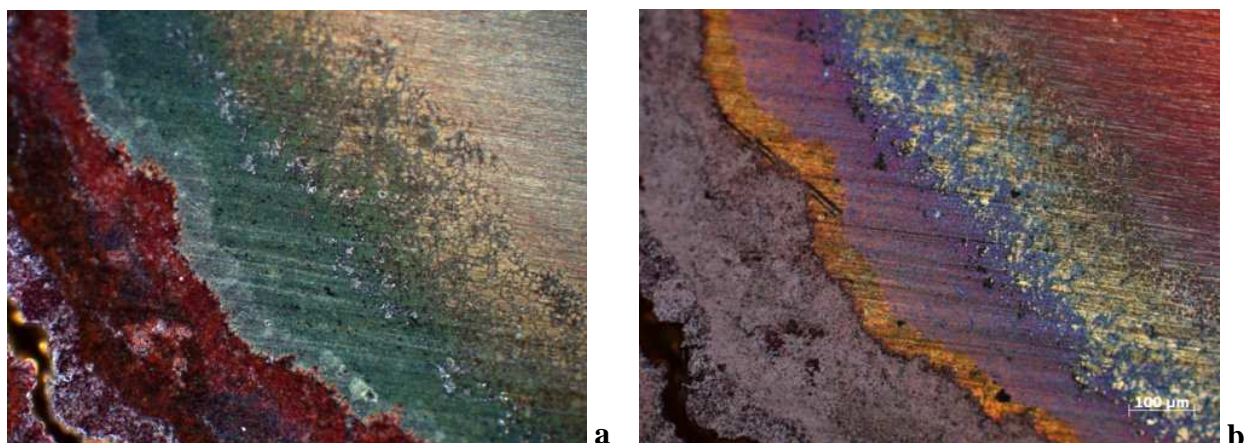
Figure IV.27. Micrograph (OM, DF) of the cross section (Ib05-8). a-overview: 50x; b-detail of the layered structure: 100x.

After these two, a sequence of red layers, alternated in the external part with a green layer possibly a copper hydroxyl-chlorides, are present. It is worth noting the different nuances of red layers, which it is sometimes alternated to slightly lighter layers: this is possible a consequence of the mixing of cuprous oxide (typically presenting an orange to red colour) and stannic oxide (characterized by a white colour).

The alloy composition was determined by Energy Dispersive Spectrometer (EDX) and it is given in the table (Table IV.4)

Table IV.4. Alloy composition by EDX.

	Copper	**Tin**	**Sulfur**	**Chlorine**	**Silicon**
wt. %	90.56	8.81	0.27	0.22	0.14

Metallography reveals the microstructure of the object. It presents very tiny, re-crystallized twinned grains, with the presence of straight twin lines (Figure IV.28). The object was probably obtained by annealing and hot-working, and eventually cold-worked to give the final shape. Darker areas in the section render the microstructure visible even without etching: is a sort of "natural" chemical attack due to the chlorine, which corrodes the alloy along the grain boundaries, thus revealing their structure.
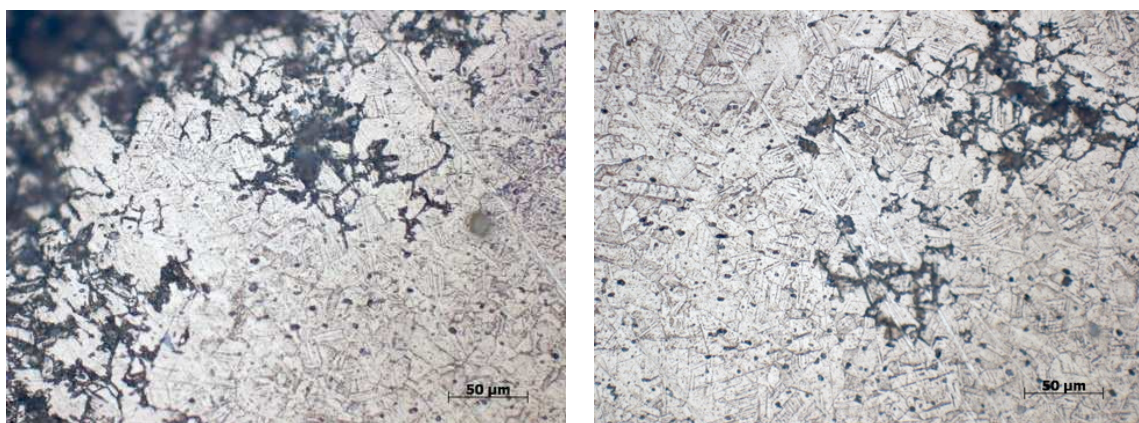
Figure IV.28. Metallography of the sample metal core showing the recrystallized structure and the intergranular corrosion due to chlorine

It is already pointed out here the danger of a corrosive attack driven by chlorine ions. As previously mentioned, their small dimension and the possibility to diffuse through the oxide layers forming the primary patina [*Lucey 1972; Stambolov 1985; Sandu 2006*] and directly react with the alloy's components.

We also want to mention here the similarity between the microstructure of this sample and the one previously presented. The corrosion layers in this case as well present a striated structure and the original surface is not easily detected anymore.

In order to better identify and characterize the corrosion layers, several EDX point analyses on the sample's cross section have been carried out, complementarily to the FTIR spectroscopy used on the powder scratched from the surface. Molecular spectroscopy identifies mainly cuprite (see spectrum in the Appendix I), as well as hydroxyl-chlorides.

An elemental line scan performed with the SEM-EDX is a powerful tool to put in evidence the distribution of the elements in order to make some hypothesis about the mechanisms of corrosion

It is reported in Figure IV.29 the line scan showing the elemental distribution of copper, tin and chlorine. It is evident the significant increase in the chlorine signal corresponding to the two green layers observed right next to the metal core and the corresponding decrease of the tin signal.

It can be therefore confirmed the presence of nantokite, or cuprous chloride, at the interface between the first layer of cuprite and the alloy.
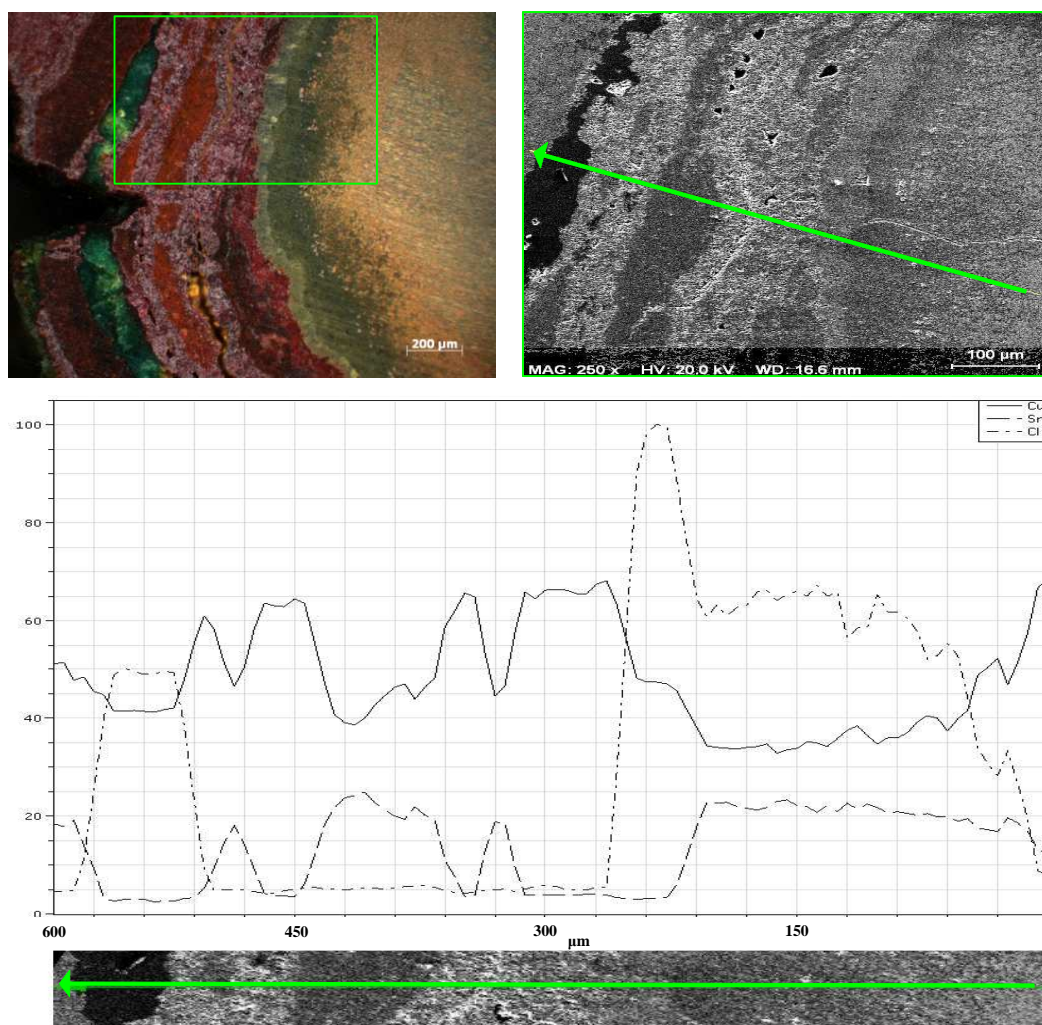
Figure IV.29. Element profile obtained by EDX-line scan: distribution of Cu, Sn and O.

The observations arising from the results of the EDX scan are the following:

- Decuprification occurs in the first 200 μm of the corrosion layers, corresponding to a increase in the chlorine;

- Tin mantains the same concentration for the first 180 μm: between 300 and 600 μm it is again present with relevant concentration. Tin forms the very insoluble stannic oxide, probably present as hydrated compound $SnO_2 \cdot nH_2O$. Its presence is detected even among the most external layers, in areas when copper concentration decreases, and when it is possibly present a mixture of tin and copper oxide;

- Low concentration of soil elements, or contaminants (Si, Al, …) even in the most external layer (not reported in the figure);

- Presence of chlorine: its concentration grows since the very internal layer demonstrating its diffusion until the sound metal (it was evidenced before the intercrystalline corrosion). Moreover, we observe an abrupt increasing around 200 μm: a depth which correspond to the light green layer identified as nantokite.

An experiment was carried out by exposing the sample's cross section to 100 % RH. The image below (Figure IV.30) shows the formation of complex hydroxo-chlorides (as confirmed by micro-FTIR spectroscopy) as a consequence of the reaction of nantokite with water.and oxygen (Eq. IV.1).
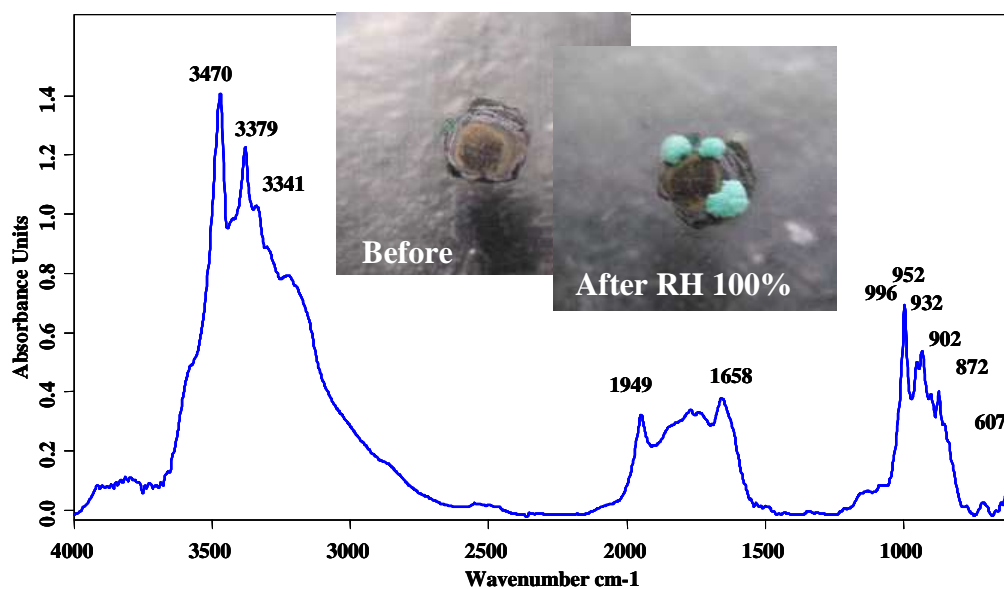
Figure IV.30. Photos before and after exposure of the specimen to condition of 100% RH: growth of hydroxyl-chlorides as verified by micro-FTIR

IV.1.4.2 Preferential-phase corrosion patterns

Interdendritic corrosion: cast objects

As stated, the corrosion patterns are different according to the microstructure of the alloy. An issue which is not yet clarified *[Scott, 1990; Taylor, MacLeod, 1984; Feipeng, 2009]* is the preferential corrosion of the Cu-rich rather than the Sn-rich phases in a cast object showing a dendritic microstructure. The experimental observation are reported here for two objects excavated in the archeological site of Argamum and simulation experiments are also aimed to a better understanding of the phenomenon.

Figure IV.31.

Bronze "pre-coin" excavated in Argamum in 2000. it is labeled Arg00_1

The object was described as a pre-coin by the archaeologists (from ICEM-Tulcea) and it is shown in Figure IV.31

Since the general conservation state is good and surface details are still evident, no sampling was allowed. It was therefore decided to polish only one side, along one of the edges, in order to study the metallography and the corrosion layer, by directly locating it in the SEM chamber. The images (Figure IV.32) illustrate the overall section of the coin and the alloy metal core, underling the presence of inclusions in the right-hand photo.
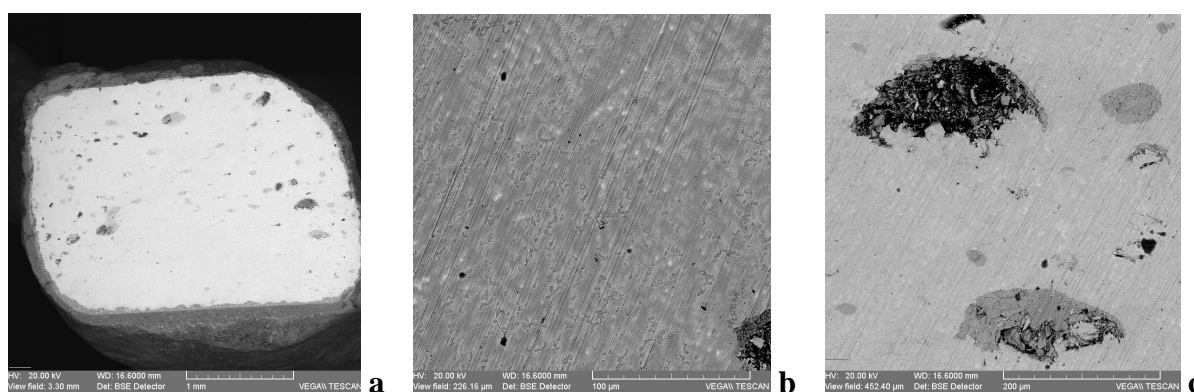
Figure IV.32. Micrographs obtained at the SEM: a_overview image; b_800x_solid metal core; c_500x_detail of the solid metal core, showing non-metallic inclusions

Backscattered electrons micrographs allow interpreting the structure according to the atomic number contrast, and higher molecular weight phases are recognizable by a lighter color. The lighter areas represent therefore Sn-rich phases, while darker ones the Cu-rich phases. Particularly interesting is to notice the presence of several non-metallic inclusions, mainly probably as cuprite or Si- and Cl- containing compounds, witness of the ancient metallurgical technology: the coin is dated back to the V-VI century B.C.

Table IV.5 . Elemental composition of the alloy. Mean value of three areas 400x400 μm.

	Copper	**Tin**	**Sulfur**	**Chlorine**	**Silicon**
wt.%	90.56	8.81	0.27	0.22	0.14

Metallography has been performed on one polished side of the coin. Micrographs are reported as Figure IV.33: it is observed the dendritic structure with locally distorted dendrite probably due to cold-working procedures after the casting.
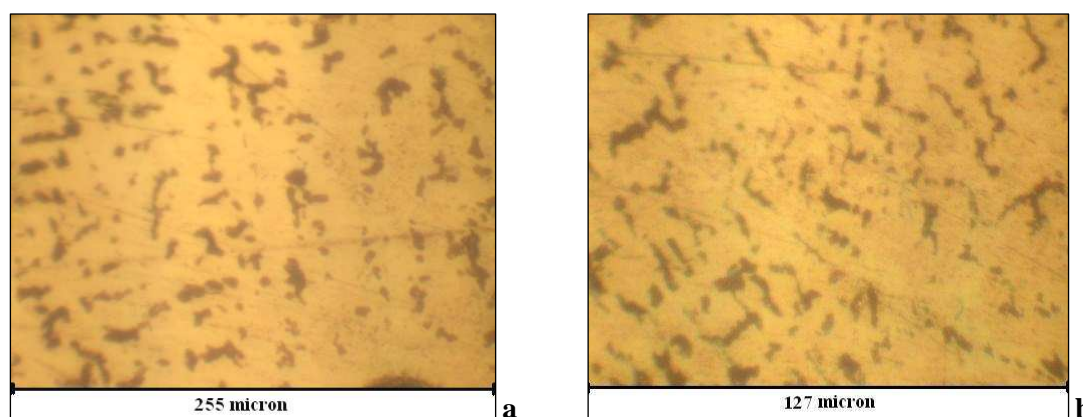
Figure IV.33. Metallography[1] of the edge surface of the coin: dendrites are observed; those in figure (b) are slightly distorted due probably to a cold working procedures after casting.

A further study of the corrosion layers has been undertaken by EDX mapping. This is a particularly useful tool allowing the location of element characterizing each layer. Results are shown in Figure IV.34. Again, the BSE image allows to appreciate the selective dissolution of copper in the internal layer, while the external one appears much darker, demonstrating the richness in low atomic weight elements such as silicon, aluminum and oxygen.

---

[1] Optical micrograph realized at the Material Science Department (SIM-UTI) by Prof. Romeo Chelariu.
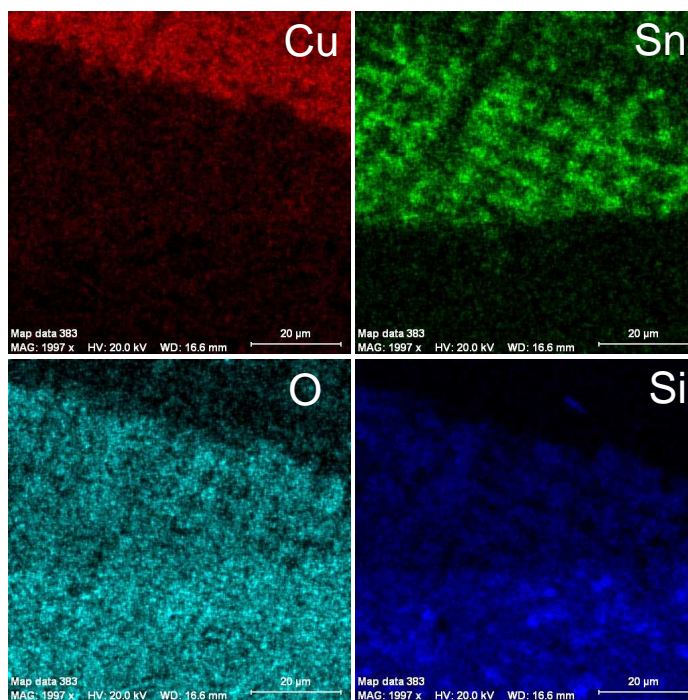
Figure IV.34. EDX mapping showing elemental distribution for Cu, Sn, O

The EDX maps allows to identify two layers above the original Cu-Sn alloy:

- an internal layer, between the original alloy and the external layer: richer in tin and oxygen (20-80 µm). Tin is probably present as tin oxide (SnO_2). This layer is found to very clearly delimit the *original surface* of the object;

- an external layer (100-200 µm), characterized by presence of oxygen and silicon, which could be defined as a contamination layer, where components from the soil are present (Si, O, in this case)

It is worth noting the total absence of copper in the external layers, being completely dissolved. This is confirmed also by the FTIR spectrum, reported in the Appendix I, where only soil components were identified.

It is important noticing that the replacement of the alloy with tin oxide occurs in a "pseudomorphic" fashion, without changing of volume and consequently, preserving the appearance of the surface. Analyzing the corrosion layers is still possible to deduce the dendritic structure of the alloy, typical of a cast object.

Tin oxide, being very insoluble, maintains the original shape of the object while copper ions are allowed to diffuse to this layer dissolving in the surroundings or re-precipitating as Cu(II) compounds in the external layers. It can also be argued that the corrosion proceeds from the original surface towards the internal layers.

A dissolution factor, f_{Cu}, can be calculated [*Robbiola 1998*] according to the following equation, assuming that the dissolution of Sn is neglected if compared to the one of copper.

$$f_{Cu} = 1 - \frac{\left(\dfrac{X_{Cu,p}}{X_{Sn,p}}\right)}{\left(\dfrac{X_{Cu,a}}{X_{Sn,a}}\right)} \quad \text{where: } X_{Cu,a} + X_{Sn,a} = 1 \quad X_{Cu} = \frac{Cu}{Cu + Sn}$$

X_{Cu} and X_{Sn} are the atomic fractions of copper and tin, while the pedicels *a* and *p* indicates, respectively, alloy and patina.

The results are shown in the following table. The dissolution factor assumes a value close to the unity for the middle layer, meaning that that copper has almost totally vanished from this layer. In the outer layer, the value approaches a value closer to 0, meaning that the ratio Cu/Sn ratio is preserved in this layer, like in the alloy. Probably, copper is present here as copper (II) compounds, mixed with soil contaminants.

Table IV.6. Values of Cu/Sn ratio and f_{Cu} calculated for each layer.

Layer	X_{Sn}	Cu/Sn (wt. %)	f_{Cu}
External layer		5.60	0.36
Internal layer		0.81	0.91
Alloy	0.06	8.80	-

This result is also in good accordance with *Robbiola* [*1998*], who found a value of approximately 0.94 for alloys where $X_{Sn} < 0.08$.

This kind of alteration layers recalls that "noble" patina to which Gettens was referring to in his work in 1975. This structure is also in good accordance with Robbiola's Type I patina that is passive-like layer, which preserves the alloy from further dissolution. In fact, in this case, it seems the alloy oxidation proceeds towards the core of the metal, while the external layer is relatively stable.

Taylor and MacLeod [*1985*] have observed that bronze corrosion in seawater is dependent on the oxygen level of the surrounding water. In well-oxygenated media, copper rich phase is preferentially attacked, whereas under less oxidizing condition, the tin rich ($\alpha+\delta$) eutectic is selectively corroded.

The case history of an arrow-head discovered in 2000 in the site of Argamum is reported in the following paragraph. Unfortunately, no information regarding depth and circumstances of finding were available. The object has been recovered in the archaeological site of Argamum and no information about the soil profile is available.

Figure IV.35: Photograph of the object named Arg.00.4.

The object presents a fairly good conservation state, with only few localized areas where green corrosion compounds, probably paratacamite (identifiable by its powdery nature and pale green color), is present.

However, the original shape of the object is still well recognizable, and it was therefore not allowed to sample a fragment for a metallographic study. However, it has been decided to polish the arrowhead on one side and to place it directly into the SEM chamber to study the stratification of corrosion layers. Also, no optical microscopy could be use to study the section as the object is too high and doesn't fit on the stage of the microscope.

Figure IV.36: BSE-SEM micrograph of the stratigraphical section of the arrowhead. Overview of corrosion layers: as it is commented in the text, the surfaces differ in the internal and in the external side of the section.

The object was probably obtained by casting using moulds as it is empty inside. The BSE micrographs show an overview of the corrosion layers on both the internal and the external surfaces (Figure IV.36). It can be observed the difference in the corrosion behavior of the external layer, where the surface appears disrupted, and the interior part, where the original surface is still well delimited.

Furthermore, it is worth noticing the non-metallic inclusions, which appears like black spots in the BSE micrograph. Higher SEM magnification of the metal core confirmed its dendritic microstructure (see Figure). The alloy composition is reported in the following table.

Table IV.7. Microstructure of the alloy (BSE, 1kx) and its composition (average over three analysis points)

	Copper	Tin	Zinc	Chlorine	Silicon	Sulfur
wt.%	86.50	11.07	0.84	0.22	0.14	0.27

Three different areas can be identified in the cross section of this object, each of them being characterized by a different distribution of copper and tin within the corrosion layers.

Internal side of the arrowhead
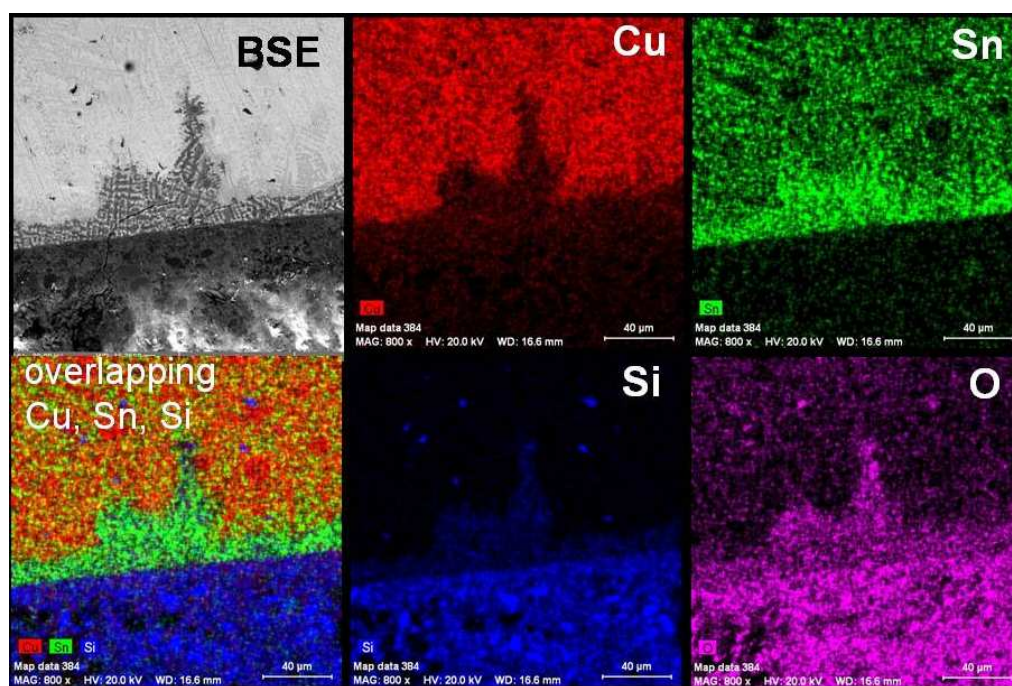
Figure IV.37. EDX mapping showing the elemental distribution of Cu, Sn, Si and O in the corrosion layers. (Magnification 800x)

The EDX elemental mapping (Figure IV.37) allows distinguishing three areas according to the elements characterizing each layer:

✓ Alloy: consists in the metal core and it is mainly characterized by the presence of Cu and Sn: original alloy. The local presence of Si or O or other elements coincides with the

presence of inclusions due to the metallurgical technique employed;

✓ Internal layer: as observed in the back-scattered image, this layer is characterized by lighter areas coinciding with the dendrites and a darker one, meaning that the atomic density is lower in those areas. The elemental map confirms this intuition and the main presence of oxygen suggests the presence of an oxidised phase, probably consisting of SnO_2;

✓ External layer is characterized by the absence of alloying elements, Cu and Sn, and by the only presence of Si and O: this is a contamination layer containing only elements of environmental origin (earth deposit: silica, clay,…).

This example, together with the "pre-coin", represents the case of interdendritic corrosion, particularly interesting because it is an evidence of the preservation of the original surface.

External side of the arrowhead
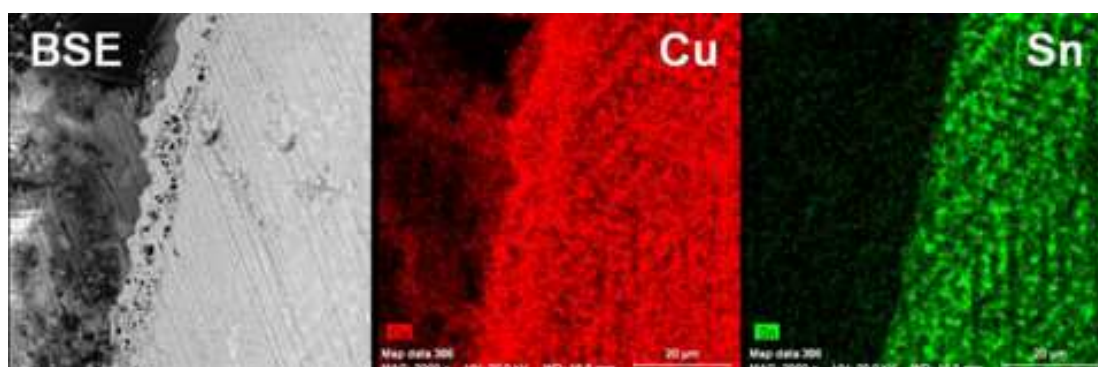
Figure IV.38. EDX mapping showing the distribution of copper and tin (magnification 800x).

The elemental mapping (Figure IV.38) reports the distribution of copper and tin over an external on the external side of the arrowhead. We observe an enrichment of copper in the outer layer which is in contrast with the generally observed phenomenon of decuprification.

The maps show that tin and copper well resemble the dendritic structure, indicating tin-rich and copper-rich phases. In this case is not straightforward affirming that the limit until where tin is present gives a clue for the localization of the original surface. Anyhow, a selective dissolution of tin is not likely to occur as it is normally assumed that its dissolution can be neglected with respect to its surface oxidation forming SnO_2 (ΔG_f^0 = -519 KJ/mol) or hydrated compounds [*Robbiola 1998*]. A possible explanation is the dissolution of copper and its re-precipitation as copper (I or II) compounds, in the outer layer, which is then covered by soil deposition/concretions.

Darker inclusions observed in the BSE image are probably quartz or other soil's mineral grains.

Localized corrosion

Some evidences of the disruption of the original surface are reported in the following pictures (Figure V.39). It is worth noting that these pictures refer to the external side of the object indicating that probably the alloy has suffered a different dissolution rate in the external side.
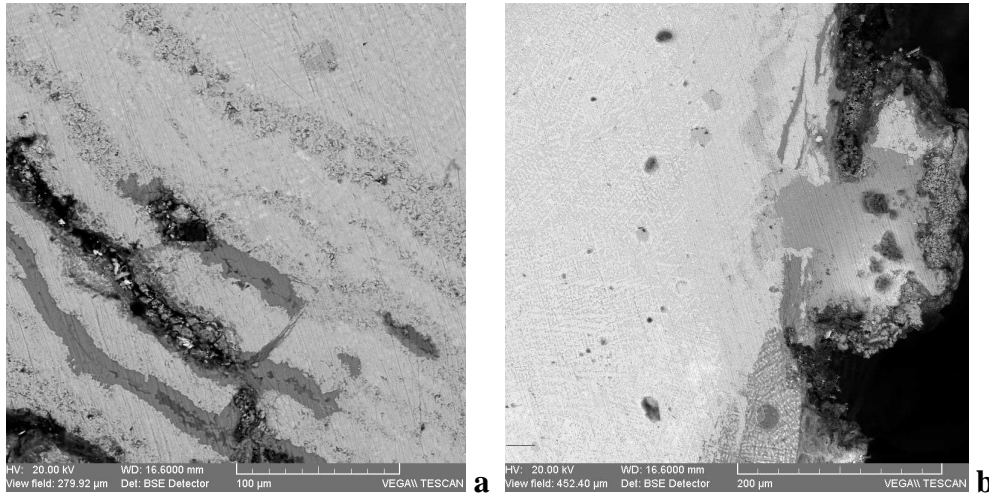
*Figure IV.39. BSE images of external corrosion layer evidencing the disruption of the original surface. The occurrence of bended structures (**a**) and localized corrosion due to chlorine (area correspondent to a green "pustola" (**b**).*

These structures, banded or sandwiched, are often observed on archaeological artifacts, but it is interesting to notice that different corrosion patterns could occur on the same object [*Robbiola,1998; this work*].

IV.1.4.3 Sulfiding reactions

Anaerobic conditions are likely to occur occasionally in soil, especially in peat or seawater sediments. In these environments, reduction of sulfate [*Scott 2002*] is possible by the action of anaerobic *sulfate-reducing bacteria* (SRB), which are able to produce sulfide ions by the reaction (Eq. IV 6):

$$2SO_4{}^{2-} = S^0 + S^{2+} + 4O_2 \qquad \text{(IV.6)}$$

Bacteria utilize the oxygen for their activity and the end product is hydrogen sulfide, H_2S.

It is thus not uncommon to discover bronze objects, excavated from this kind of environments, and covered with a black-bluish patina made up of copper sulfides.

A hoard of copper coins' fragments (Figure IV.40) were excavated in 2000 in the archaeological site of Nufarul. The archaeological site is situated in the beautiful context of the Danube Delta, being located on the bank of one of river's arm, "Sf. Gheorghe". Unfortunately, no information about circumstances of finding was available. An approximate dating of the hoard is to consider during the Byzantine times.
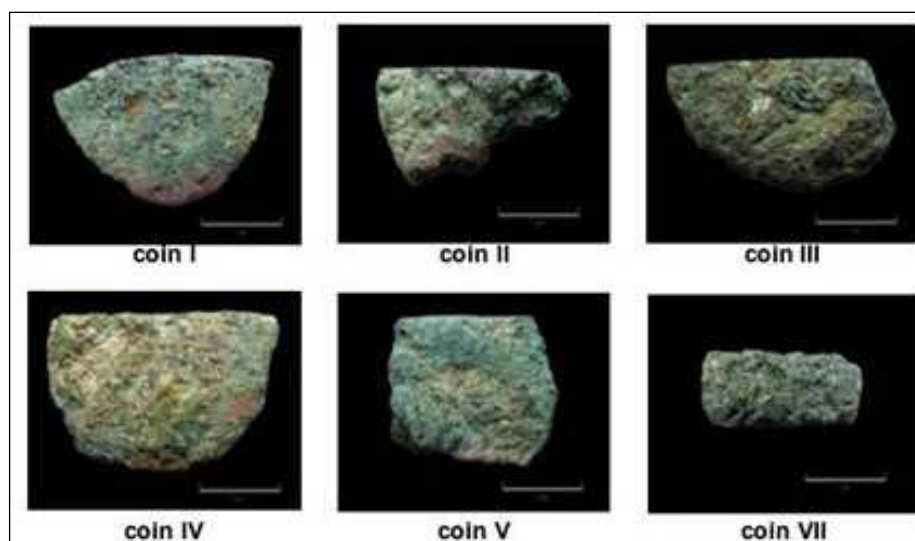
Figure IV.40. The hoard of copper coin excavated in Nufarul, Dobrogea, in 2000.

We faced here a case study where the corrosion has come to an end. The coins are completely (or almost completely) mineralized, their metal cores being replaced by corrosion products, as showed in the Figure IV.41.

Their conservation state is particularly bad and could be justified by the occurrence of some specific local conditions, which lead to a high dissolution rate of copper.

All the coins are characterized by the presence of a very thick external layer, black-bluish in color and lustrous in the aspect.

It is reasonable supposing that those anaerobic conditions could have occurred during the burial time of these coins and this could be the explication of the detection of copper sulfides. The interest and experimental efforts has been therefore driven to their identification. In the literature, there are few cases reported [*Oddy 1982*] and when their occurrence is reported, it is usually considered an *unusual* or *uncommon* phenomena.
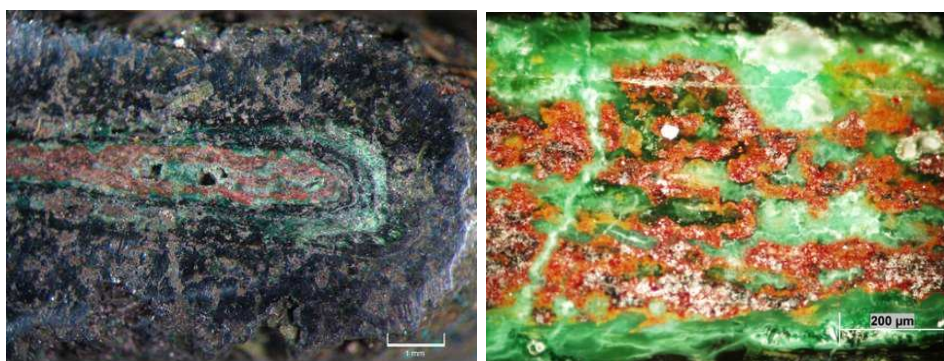
Figure IV.41. a-The transversal section of one of the coins excavated in Nufarul; b-Particular of the mineralized metal core.

The table below reports the description of the objects, their microstructure (where it is still observable) and the analytical technique employed for the characterization of corrosion layers.

Table IV.8. Summary of the results obtained by the scientific examination of the coin's hoard.

Label	Description	Alloy microstructure	Analytical technique	Identified Corrosion Products
I	coin fragment	Heavily corroded: Cu, Pb islands (Sb, As)	SEM-EDX ,XRD	Atacamite, Quartz
II	"	n.d.	SEM-EDX	-
III	"	Mineralized, Pb islands (Sb, As)	SEM-EDX ,XRD	Covellite, spionkopite, Anilite
IV	"	Copper α-phase, Pb islands (Sb, As)	SEM-EDX	-
V	"	Mineralized	SEM-EDX	-
VII	"	Mineralized, Pb islands (Sb, As)	SEM-EDX, FTIR	Atacamite, Malachite, Azurite, Covellite, Spionkopite, Anilite

All the coins have been investigated by optical (OM) and scanning electron microscope (SEM).

Microanalyses, performed by EDS on the cross section of coin I, revealed that high amount of chlorides (probably nantokite, Cu_2Cl_2, Figure V.42) are located below the red layer of copper (I) oxide, cuprite. This confirms the role of the copper (I) oxide discussed by Lucey [*Lucey*

1972]: it has been considered acting as an electrolytical membrane allowing the transport of anions such as Cl⁻ and O₂⁻ inward and cuprous ions outward.

Indeed, the presence of copper chlorides in the archaeological artefacts indicates a noticeable transportation of chloride ions from the soil through the permeable alteration product layers to the internal zone and remaining Cu matrix.

The very thick degradation layer appears to be partly detached from the corroded metal core, and looks very compact. A number of point measurements have been realized in order to characterize this layer. EDS measurements, together with Cu, have detected elements like Si, Al, Fe, Ca, Mg, and Cl, thus demonstrating the very strong relationship that exists between soil constituent and degradation products.
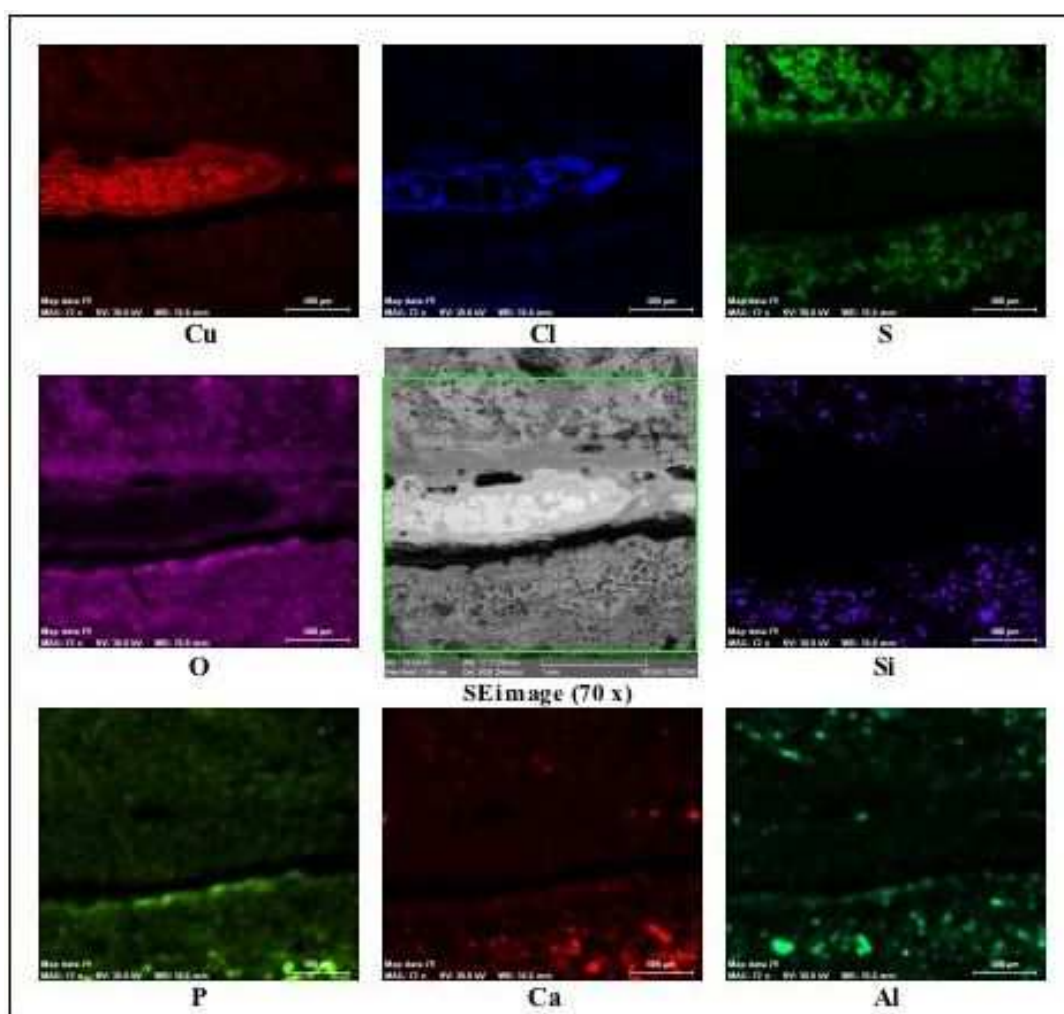
Figure IV.42. SEM-EDX mapping illustrating the distribution of Cu, Cl, S, O, Si, P. Ca, Al.

Elemental mapping, realized with the SEM-EDX, is a powerful tool to study the distribution of elements over a selected area. In this case, attention is given to the distribution of copper, sulfur, oxygen and silicon. The external thick and black layer of corrosion is characterized by areas, which appear light in the BSE micrograph (see Fig. 41, a) and black bluish with

metallic lustre in the OM image. It is worth noting the presence of sulfur associated with copper in the EDX maps: the black colour, with iridescent bluish reflections, of the thick external layer, suggests the presence of a copper sulfide such as CuS (covellite), Cu_2S (or more complex combination between these elements, including Iron as well.

Attempts to identify the crystalline form of the compound has been undertaken by means of Raman Spectroscopy[2] and Covellite (CuS) could be detected. Further XRD investigations were carried out at the ICN Instituut Collectie Netherland, Amsterdam, with Dr. Luc Megens, using an X-ray diffractometer equipped with a double detector.

We could identify the presence of three different phases: covellite (CuS), but also spionkopite ($Cu_{39}S_{28}$) and anilite (Cu_7S_4), Figure IV.43. These are the most stable phases as it was demonstrated also by McNeil and Little [*1992, 1999*].
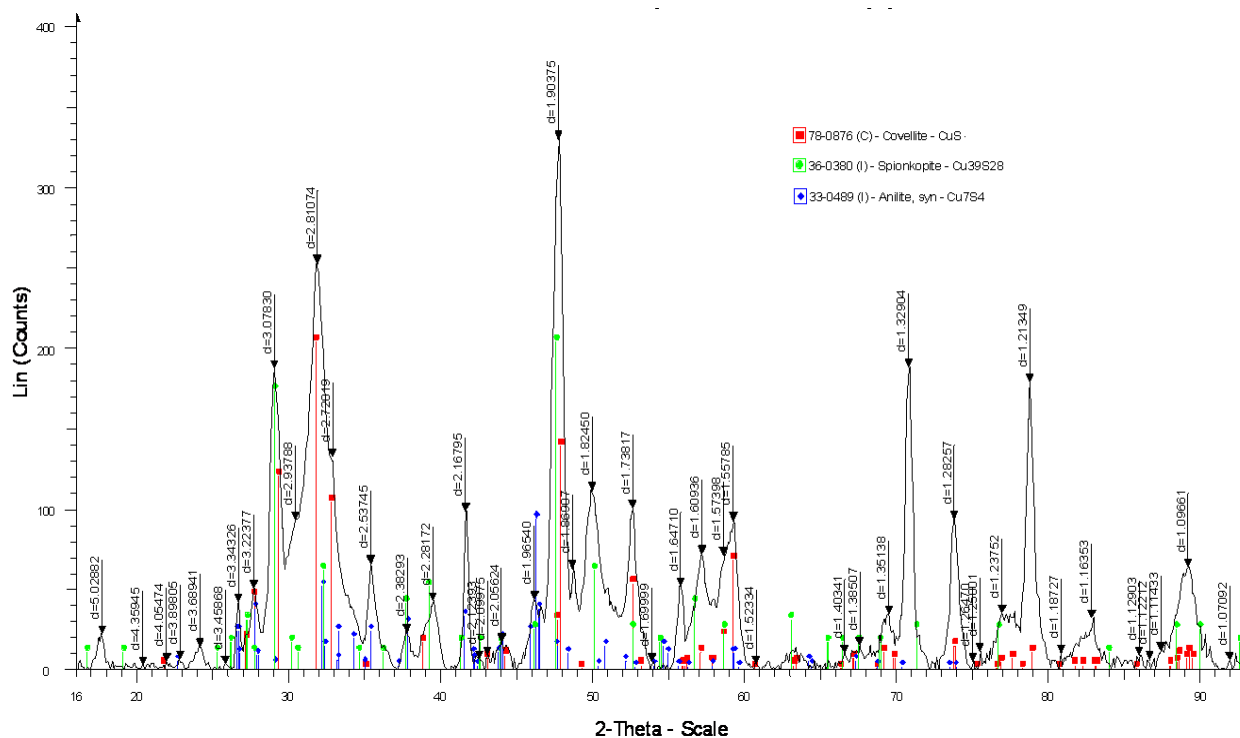
Figure IV.43 XRD pattern showing reflection identified as Covellite (CuS), spionkopite ($Cu_{39}S_{28}$) and anilite (Cu_7S_4)

.

IV.1.5   General corrosion features

The research took into consideration several case studies, and for some of them, a stratigraphical section was realized in order to thoroughly study the complex succession of corrosion layers. We observed the occurrence of few uncommon or atypical corrosion features, such as a complex striated or periodic structure and one characterized by the presence of a thick layer of copper sulphides.

The following table reports a comparison among the results obtained in this work and those found in the literature *[Robbiola 1992; Oddy 1982]*. The parameter chosen to classify them is the ration Cu/Sn, which was calculated both for the alloy and the corrosion layers.

It shall be pointed out here that the results presented from the reference [*Robbiola 1992*] were obtained by superficial analysis of corrosion layer, without any sample preparation. The data referring to reference 2 [*Oddy 1982*] and done in this work were obtained by analysis of the corrosion layers on a cross section of a fragment embedded in resin.

Table IV.9. Classification of bronze objects according to the value of Cu/Sn ratio in the corrosion layers.

Object	Corrosive medium	Cu/Sn corrosion (wt. %)	Sn (wt. %)	Cu/Sn alloy (wt. %)	Ref.
Sword (1000BC)	sandy soil	2.5	8.71	9.4	1
Droplet (100 BC)	soil	0.14 and 42.5	22.2	2.9	2
Stem (Iran, 2000 BC)	arid soil	0.8 and 0.12	9.6	9.4	1
Axe (Bronze Age)	temperate soil	0.55 and 0.64	10 to 15	6 to 9	1
Axe (Bronze Age)	temperate soil	0.55	11.4	7.8	1
Bronze buckle	marine	0.2	5.7 (Pb:0.6%)	16.4	1
Pre-coin (Arg.00.1)	arid soil, marine environment	0.91 and 5.60	10.1	8.9	This work
Ring (Ib.05.8)	arid soil, marine environment	2.60 to 86	8.6	10.6	This work
Bracelet (Ib.08.4)	arid soil, marine environment	2.95 to 6.48	1.28 (16.12 Zn; 2.11 Pb)	62.9	This work
Hairstick (Ib.06.9)	arid soil, marine environment	0.65 to 65.48	9.6	9.4	This work

(1) [Robbiola, 1992]
(2) [Oddy, Meeks, 1982]

According to the values of Cu/Sn in the corrosion layers, it is evident the general trend of corrosion which consist in the *decuprification* phenomenon.

It can be pointed out from the table the occurrence of very different values for the same object. This is due to the presence of copper-rich layers (probably cuprite), where the concentration of tin is very low. These samples are therefore characterized by two limit values of Cu/Sn ratio, the lower of which is always much lower than the same ratio evaluated in the bulk alloy, thus confirming the decuprification phenomenon.

In general, we observed different corrosion patterns according to the microstructure of the alloy: inter-granular corrosion is observed for an homogeneously recrystallized α–phase while, for dendritic structures, the α–phase corrodes first with respect to the (α+δ)–phase. According to the results obtained for the artifacts selected for this study, it seems that the microstructure has a role in the corrosion behavior of the alloy. Dendritic structures mostly showing the occurring of *Type I* patterns or *noble* patina with an easy identification of the original surface, kept by the presence of tin oxide.

Case study Arg.00.1: Interdendritic corrosion patterns

This object is characterized by a smooth and compact corrosion layer. Its stratigraphy presents a two-layered structure as it is evidenced in the BSE image (Figure IV.43).
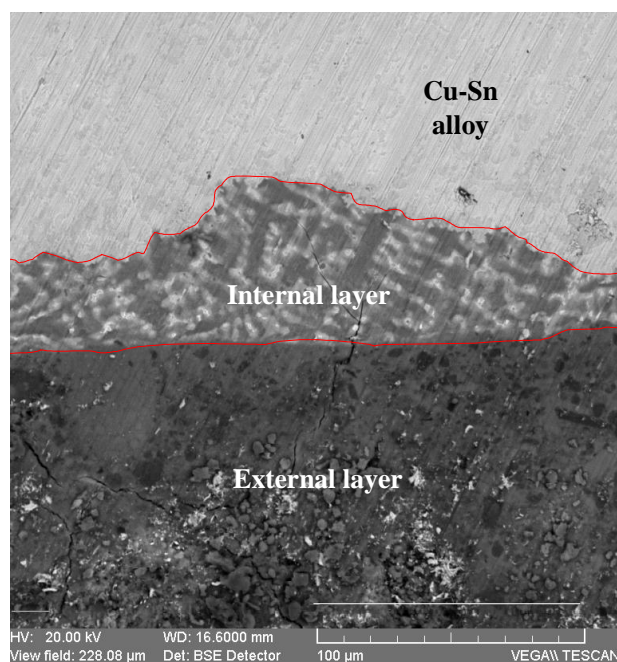
Figure IV.43. Backscattered electron image(1kx) of the corrosion layers for the precoin labeled Arg.00.1.

The internal layer shows the "ghost" structure of the dendrites characterizing the alloy microstructure. As already reported previously, the lighter areas in these regions are characterized by the presence of tin. This layer also clearly defines the original surface of the

object.

The graph (Figure IV.44) reports the concentration of Cu, Sn, O and Si in the corrosion three identified areas. This structure can be interpreted as the results of a two step corrosion mechanism, as proposed by *Robbiola* [*1998*]. In low aggressive media, it occur the formation of a passive layer, mainly composed by tin oxide (SnO_2). This fits well with the primary passive film defined by *MacDonald* [*1990*] for passive film formed under steady-state conditions. When a certain thickness is reached, the corrosion rate decreases and the migration through this layer becomes the rate-determining process.

A second step involves the growth of the corrosion through the previously formed passive film. This phase (according to MacDonald) is controlled by the mass transportation of cations from the bulk alloy outwards and the anions from the electrolyte in the opposite direction.

It is therefore concluded that this structure correspond to the Type I corrosion structure, according to the classification proposed by Robbiola. It is worth underlining that the corrosion patterns reveals the grain boundaries and this demonstrates that the patina grows into the alloy and the process is controlled by the inward transportation of oxygen anions.
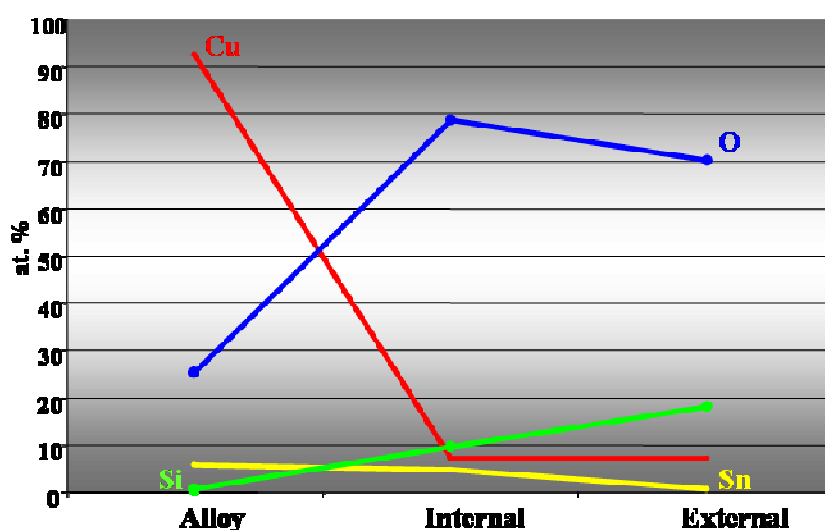
Figure IV.44 . Elemental distribution along the corrosion layers for the sample Arg.00.1

It is worth mentioning that in this case it hasn't been detected a layer of cuprite in the interface alloy-external layer. This is also mentioned by *Robbiola [1998]* as a feature by which Type I corrosion structures differ from Type II patterns.

Case study Ib.05.8: multilayered corrosion pattern

The case study here reported is a typical Type II structure, showing a complex, multilayered corrosion pattern. The BSE image shows a selected area of the striated textured corrosion, which is visible, complete, in the optical micrograph. Layer 1, 2 and 5 are characterized by a green colour, while the rest of the sequence shows different hues of red-orange colour and a porous texture. A fracture is also present within the corrosion layers, probably due to internal tensions due to the growing of corrosion products.
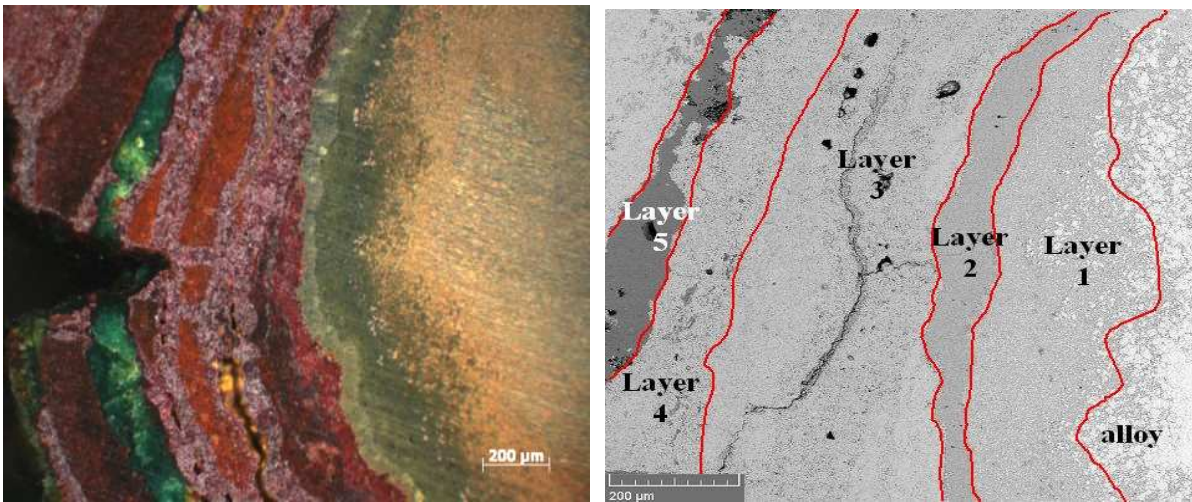
Figure IV.45. OM and BSE micrographs of the cross section (sample Ib.05.8) evidencing the layered textured structure.

The following graph (Table IV.46) reports the elemental distribution along the corrosion layers. It can be noticed that the decuprification occurs, but it is not as marked as in the former case. Also it shall be underlined the constant present of tin, which is comparable to its percentage in the original alloy, even in the corrosion layer. The red-orange layers which made up the corrosion pattern are made up of cuprous and stannic oxides. In fact, at a more careful sight, this layers show a white colour as well, mixed with the red cuprous oxide (cuprite, Cu_2O).
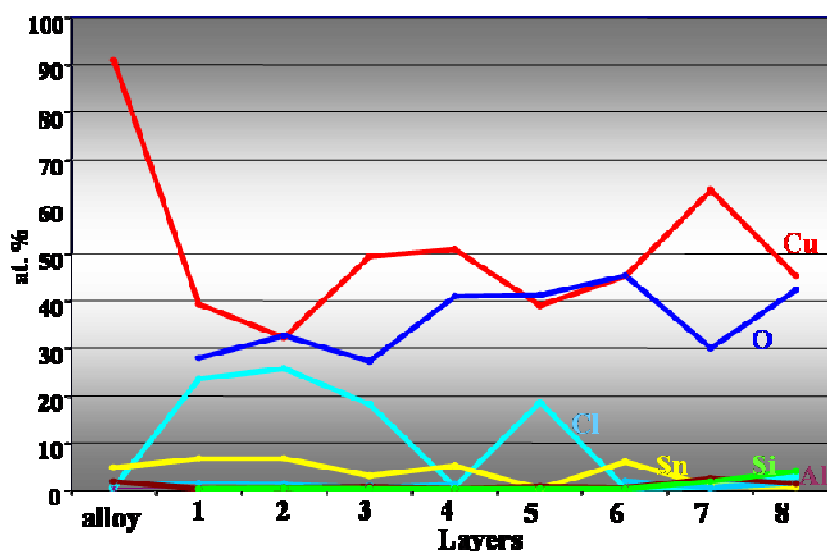
Figure IV.46. Elemental distribution along the corrosion layers for the sample Ib.05.8

In this case, possibly due to a high oxidation rate, tin and copper oxides are formed. The higher corrosion rate can be due either to an increased aggressiveness of the soil, but also to the alloy itself. The recrystallized microstructure, obtained as a consequence of intense working procedures, presents very small grains and therefore holds a higher strain energy, which could be the cause of an increased susceptibility to corrosion.

Afterwards, the growth of corrosion layers is under anionic diffusion control [*Robbiola 1998*] and it takes place though the porous oxide layer. The electrolytic conductivity of the cuprite layer, often mentioned in the text, is recalled here again as it explains the presence of chlorine in the internal layers. It then reacts with metallic copper to form the cuprous chlorine trough the reaction (3), already presented. In this way, the dissolution of alloy proceeds inward.

This layer lies dormant, as it is somehow protected by the oxide layers, until contact with air and humidity when it reacts to form the basic chlorides already introduced in the former paragraphs.

This structure well resembles the Type II corrosion structure leading to corrosion features which transfigure the original surface. In this case, the corrosion resumption could occur involving the formation of cracks which lead to the detachment of part of the corrosion layers.

Case study Ib.08.4: effect of other alloying elements

The third case is an object, probably a bracelet, made of brass alloy, which composition is given in the table. Lead globules are visible in the backscattered image as white spots. Figure IV.47 . reports the composition of the alloy.

Table IV.10. Elemental composition of the alloy (mean of three analysis points by EDX)

	Copper	Zinc	Lead	Tin	Iron	Aluminium
wt. %	80.04	16.12	2.11	1.28	0.17	0.27

As indicated in the backscattered image, a three layer structure is present. The first, internal layer is discontinuous and identifiable by the red colour, typical of cuprite, in the optical micrograph. Than, two different layers are present at the interface between the cuprite layers and the external layer, mainly a contamination one.
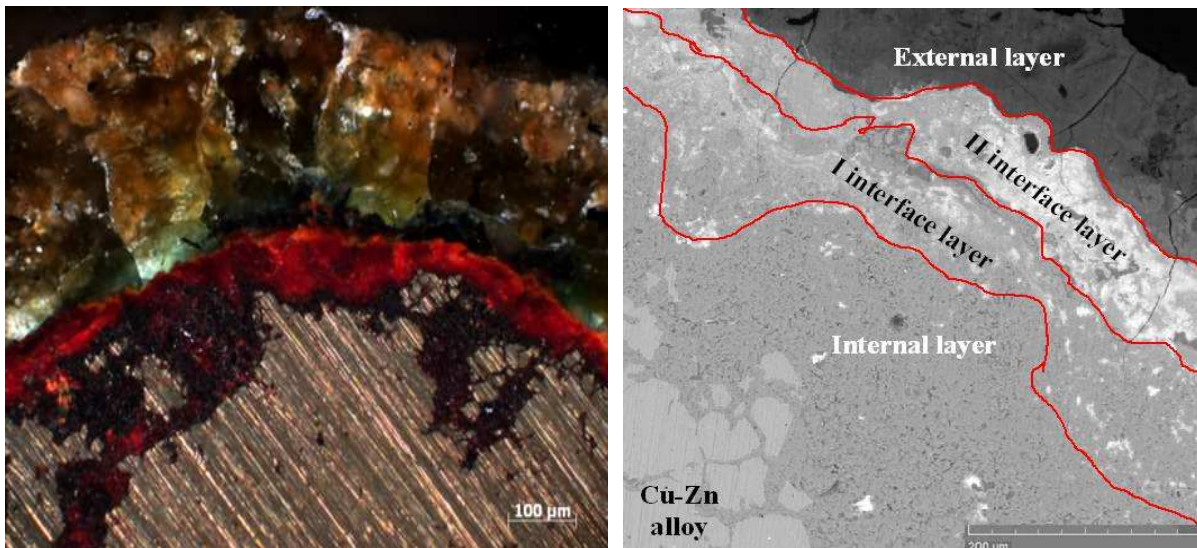
Figure IV.47. OM and BSE micrographs showing the three layered structure

In the same way, as for the other case studies, the following graph reports the elemental distribution along the corrosion layers. Since the amount of tin was very small we could ignore it in the presentation of results.

The graph shows a noticeable decuprification and dezincification. A wide literature exists [*Brown 1977, Jones 1996, Scott 1990*], about dezincification as, according to the electrochemical series of metals, it is much more active and it is selectively dissolved from the alloy.

It is worth noticing the increase in the concentration of lead, especially evident in the II interface layer, also visible in the BSE image as lighter areas.

Lead is insoluble in the bulk allow and it is found as globules or inclusions. Being

electrochemically more active than copper, it oxidise first probably forming some compounds such as $PbCO_3$ or lead oxides. Nevertheless, it is interesting notice its enrichment in the external corrosion layers.

The external layer is characterized by a decrease in the concentration of all other species excepting silicon and oxygen, thus revealing the contamination nature of the external layer.
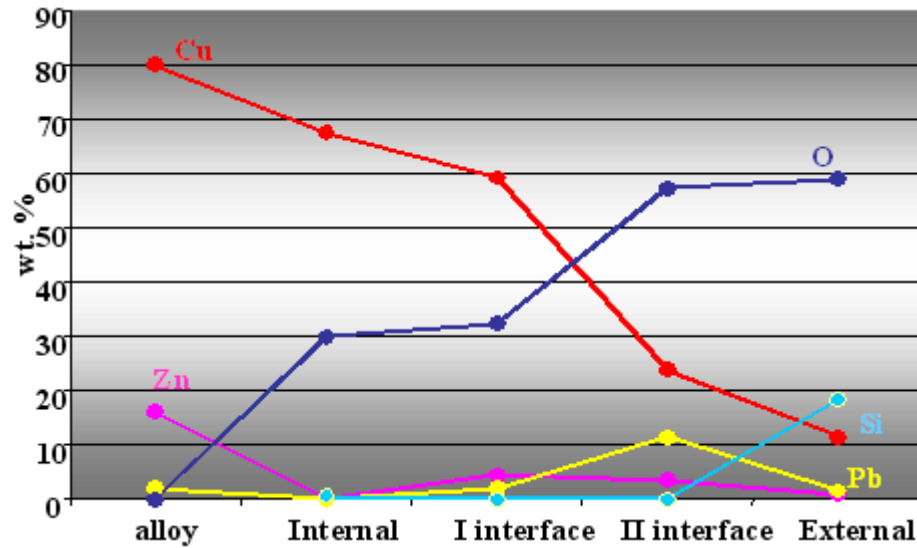
Figure IV 48. Elemental distribution along the corrosion layers: sample Ib.08.4

It seems, however, that the cuprite layer delimited by the first interface layer, could be ascribed to the original surface. According to the elemental distribution, this layer is also characterized by a still high copper concentration, which further decreases after that.

IV.2   Electrochemical behavior of bronze in natural environments

The results obtained studying the long-term behavior of bronze in burial condition has raised up the scientific interest to investigate the mechanisms through which these alloys corrode in natural environments.

We have therefore undertaken a research examining the electrochemical behavior of bronze (Cu-10Sn) in soil and soil simulated environments. We also took into consideration more aggressive media such as the sea water, as the archaeological objects which were studied often presented a degradation patterns involving chlorine. The sites where these artifacts were excavated are located next to the Black Sea and therefore an influence of chlorine is expected. The chosen alloy was considered representative for the majority of ancient alloys, as also demonstrated by the results obtained for case studies. The choice was also driven by the commercial availability.

IV.2.1   Evolution of Open Circuit Potential (OCP) in simulated and natural soil

The first approach for this investigation was the study of the evolution of OCP in soil-simulated environment. As reported in literature [*Van Der Schijff 1993, and references therein*], a simulation of soil can be obtained by using agar gel because its character provides a good aeration and the possibility to disperse an electrolyte in it.

Possibly due to the very low aggressiveness of the solution acting as electrolyte and to the variability in the room temperature, measurements of the OCP over a month time, were not satisfactory, and a general trend couldn't be identified. We've therefore decided to carry out the same experiment using the natural soil as corrosive medium.

Open circuit potential measurements were followed placing the bronze electrode in natural soil (sampled from area Bulding E1, see Chapter II), which was sampled in the archaeological site of Ibida during excavation procedures in the summer 2008.
OCP were recorded on a daily basis for a month and the results are reported in Figure IV.46. We observe a slight, linear decrease of the open circuit potential indicating a reduction of the corrosion resistance as the sample is kept in soil. The cause of this behavior could probably be related to the beginning of interdendritic corrosion which leads to the increasing of the active surface.
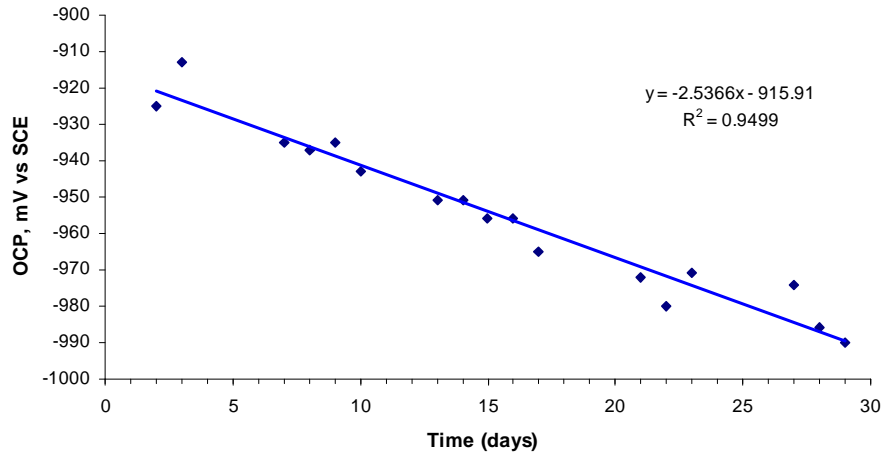
Figure IV.49. Evolution of OCP in natural soil over a period of 30 days.

It shall be underlined that OCP measurements depend on several environmental factors, such as temperature, relative humidity, etc., which are hardly kept under control.

Therefore, these measurements cannot be considered absolutely reliable if all these parameters are not known and carefully checked out.
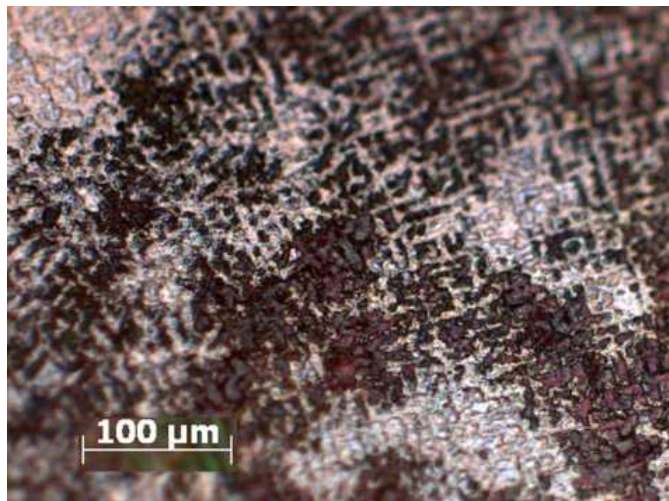
Figure IV.50. Micrograph of the electrode Bronze 2 after 30 days exposure to soil (200x, BF).

It is worth reporting the images obtained by OM of the electrode's surface after one-month exposure in the soil medium (Figure IV.50). The bright blue zones indicated the (α+δ)-phase which remains un-corroded, while the dark brown area indicates an oxidation of the α-phase. The same behavior is reported for Bronze 1 and 2.

This represents a first interesting result, as the phase-preferential corrosion is an issue which is not clear yet in the literature [*Scott 1990; MacLeod 1984; Feipeng 2009*]. As already observed for the case studies, the α-phase is the most likely to be corroded first. More evidences of this behavior will be pointed out in the following exposition of results.

IV.2.2 Comparison between pure copper and bronze behavior

As stated, the aim of the research is an investigation of bronze behavior in natural environments. In the literature [*Hamilton 2000; North 1987*], corrosion of bronze is often explained using the copper model because, in general, copper-containing compounds have been reported to the main constituents of bronze patina in many different environments.

The first approach was therefore to compare the copper and bronze behavior in soil solution and sea water, the two natural electrolytes chosen for this work, whose composition, pH and conductivity values are reported in Table IV.11.

Table IV.11. Composition of soil solution and Black Sea water used for the experiments.

	Cl^-	NO_3^-	PO_4^{3-}	SO_4^{2-}	pH	Conductivity
	mmol	mmol	mmol	mmol		mS
Soil Solution	1.128	0.726	1.053	1.145	8.86	0.32
Black Sea water	244.53			14.45	7.10	27.45

We performed linear potentiodynamic polarization using a sweeping rate of 10 mV/s and the results are reported in the following illustration (Figure IV.51 and IV.52).
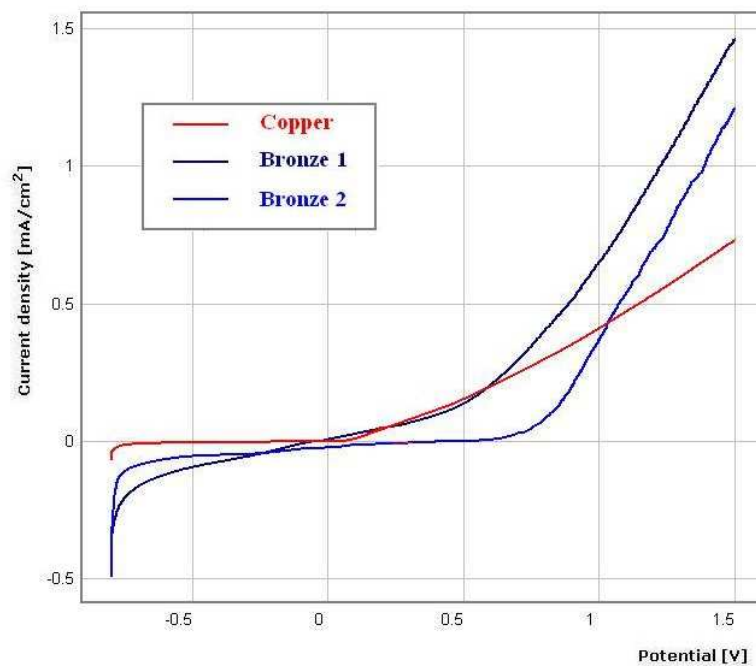
Figure IV.51. Linear polarization curves (sweeping rate 10 mV/s) registered in soil solution: comparison among pure copper, Bronze 1 and Bronze 2.
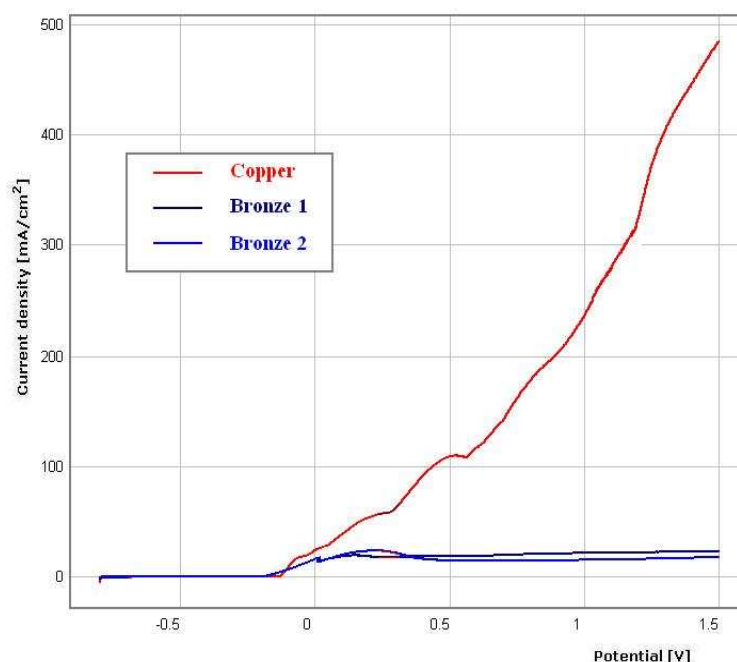
*Figure IV.52. Linear polarization curves (sweeping rate 10 mV/s)
registered in soil solution (a) and sea water (b): comparison among
pure copper, Bronze 1 and Bronze 2.*

At a glance, it can be observed that in the less aggressive medium of soil solution, the bronze specimens show a wider passive domain with respect to copper, for which on the contrary starts an active corrosion at the E_{corr}. Nevertheless, Bronze 1 behaves differently, its curve resembling that of pure copper. This inconsistence could be due to the low conductivity of the corrosive medium these curves may be more affected by errors due to ohmic (voltage) drop.

In the more aggressive medium of Black sea water, this behavior is enhanced and can be appreciated by the values of current density at higher potentials. The same behavior was reported in the literature [*Souissi, et al., 2007*] in aerated aqueous NaCl solutions.

The following table (Table IV.12) reports the value of corrosion potential and the correspondent instantaneous current density for copper and the two bronze specimens, respectively in soil solution and sea water.

In the case of sea water, both values of corrosion potential and current density indicate a much higher stability for the bronzes in comparison with copper.

*Table IV.12 Comparison of corrosion potentials and current density values
for linear polarization in soil solution and seawwater (Bronze 1).*

	Soil solution		Black sea water		
	$E_{(I=0)}$, (mV/SCE)	J_{corr} ($\mu A/cm^2$)	$E_{(I=0)}$, (mV/SCE)	J_{corr} (mA/cm^2)	J/J_{Cu}
Cu	33.5	3.067	-145	0.495	**1**
Bronze 1	-46.7	5.332	-226.4	0.118	**0.24**
Bronze 2	480	0.757	-206.8	0.169	**0.34**

- 122 -

IV.2.3 Influence of the potential scanning rate

It was investigated the influence of the potential sweep rate on the shape of the linear potentiodynamic polarization curve using the Black sea water as electrolyte (Table IV.11) , its composition). The graphs (Figure IV.53) reports a comparison, for the specimen Bronze 1, among the linear voltammograms registered over a range -800÷1500 mV using different potential scanning rate: 1-10-50-100 mV/s.

The results here presented related a comparison of linear potentiodynamic curves recorded for Bronze 1 and Bronze 2 in soil solution.
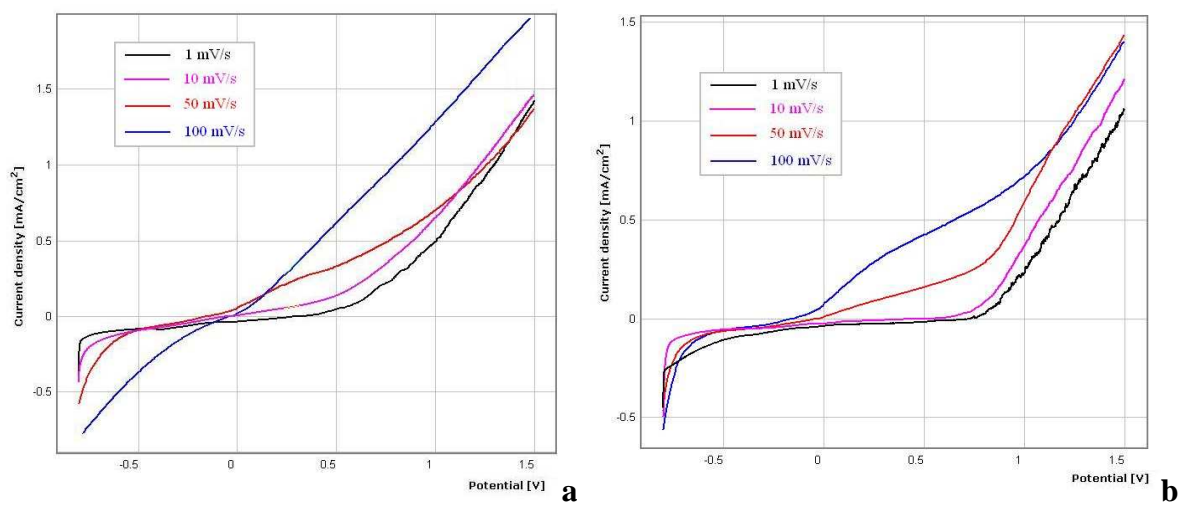
*Figure IV.53. Electrochemical behavior of Bronze 1 (**a**) and Bronze 2 (**b**) in soil solution.*

It can be observed that at high over-potentials the potential scanning rate doesn't appreciably influence the shape of linear polarization curve excepting for higher scanning rate (100mV/s). Moreover, in order to put in evidence the processes having place during the anodic polarization, in this study we have evaluate to perform cyclic Voltammetry using 10 mV/s as sweeping rate.

The curves registered in Black Sea water show a different shape (Figure IV.54). It is evidenced the loss of the differentiation of the two anodic peaks which are clearly distinguished for the black and red curves, respectively 1 and 10 mV/s. At this scan speeds the reaction has time to take place and the electrode reaction occur at equilibrium condition
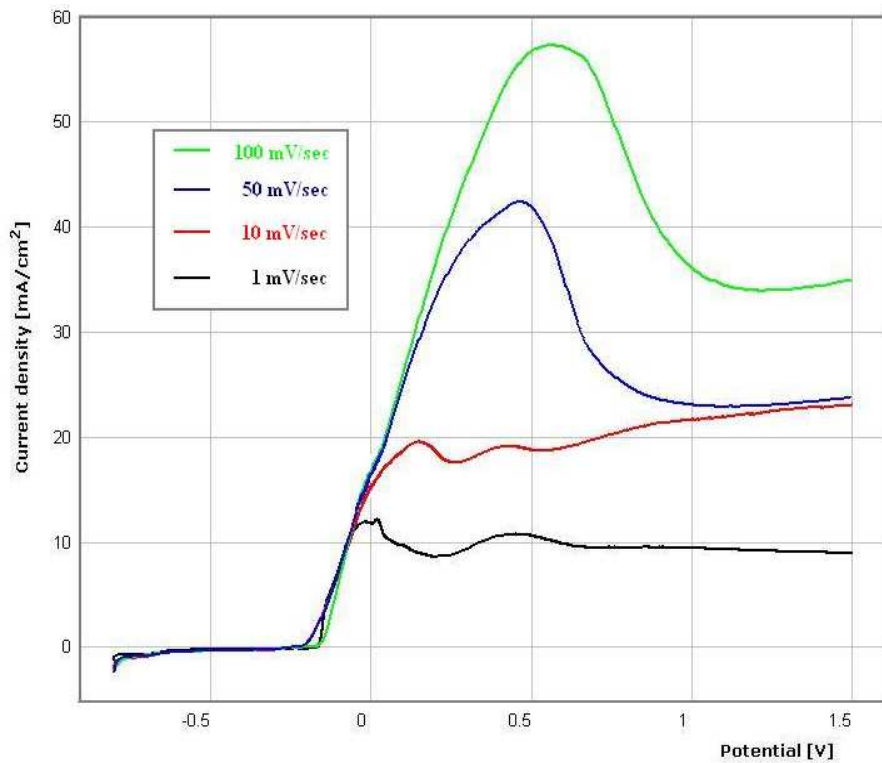
Figure IV.54. Specimen Bronze 1- comparison among polarization curves at different potential scanning rate, 1-10-50-100 mV/s.

This result was useful as in for future experiments of potentiodynamic polarization the chosen sweeping rate were respectively 1mV/s for linear voltammetry and 10 mV/s for cyclic Voltammetry, a value which has been judged appropriate for the investigation of electrode's processes.

It is evidenced and pointed out the effect of the potential sweep rate on the relative position of the peaks. Even though the shape of the curve resembles for the voltammetries at 1 and 10 mV/s, the position of anodic peaks (A_I and A_{II}) is shifted (Table IV.13).

Table IV.13. Influence of the potential scanning rate on the position of anodic peaks.

		1 mV/s	10 mV/s
A_I	E (mV)	-20.7	141
	J ($\mu A/cm^2$)	11.99	19.65
A_{II}	E (mV)	451	423
	J($\mu A/cm^2$)	10.79	19.25

IV.2.4 Potentiodynamic polarization in natural soil solution: a comparison between Bronze 1 and Bronze 2.

As a mean of distinction between bronze 1 and bronze 2, cyclic voltammograms were recorded in natural soil solution (E1; pH = 8.86 and conductivity = 316 μS) for the two specimens (Figure IV.55). The main parameters obtained from the curve are reported in the table (Table IV.14).
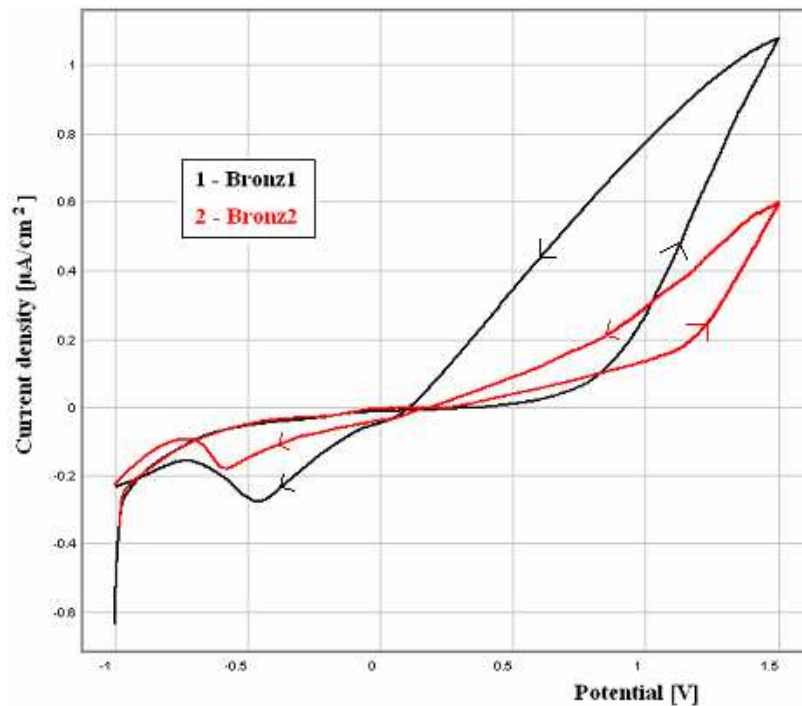
Figure IV.55. Comparison between cyclic polarization curves recorded in soil solution for Bronze 1 and Bronze 2.

Table IV.14. Parameters evaluated from the cyclic potentiodynamic curve

	Bronze 1	Bronze2
$E_{(I=0)}$, mV (SCE)	352	223
E_{BD}, mV(SCE)	730	-
E_{rp}, mV(SCE)	110	182
$J_{(E=1.5V)}$, mA/cm^2	1.08	1.13

It can be stated that they show similar behavior which is characterized by the presence of a hysteresis-like loop, typical for pitting behavior. As the potential is scanned towards higher values, we observe the occurrence of a passive domain until approximately 700 mV, where the breakdown of passivity occurs (the E_{BD} was taken in correspondence of the rapid and stable increase of the anodic current density). This is particularly evident for Bronze 1, while it cannot be well defined for Bronze 2. In this case, the pitting corrosion begins already at small potential, close to the corrosion potential and the pit growth occurs at slow rate until approximately 1100 mV, when it increases the growth speed with the current density.

After the loop, both curves move towards small values of current density, but they don't retrace the same path, thus demonstrating the pit's propagation [*Bellezze 2004*].

The repassivation potential are close for both bronzes, but the intensity of the pitting corrosion is much higher for Bronze 1, the area of the loop being proportional with the amount of pitting.

Surface characterization was performed by optical and scanning electron microscopy. The images show the pitting behavior for both Bronze 1 and 2, which confirms the result from the electrochemical experiments. The BSE micrographs (Figure IV.56) shows evidence better the preferential corrosion of the α-phase, the (α+δ)-phase being visible by the brighter color.

200x_BF   **1kx_BSE**

200x_BF   **1kx_BSE**
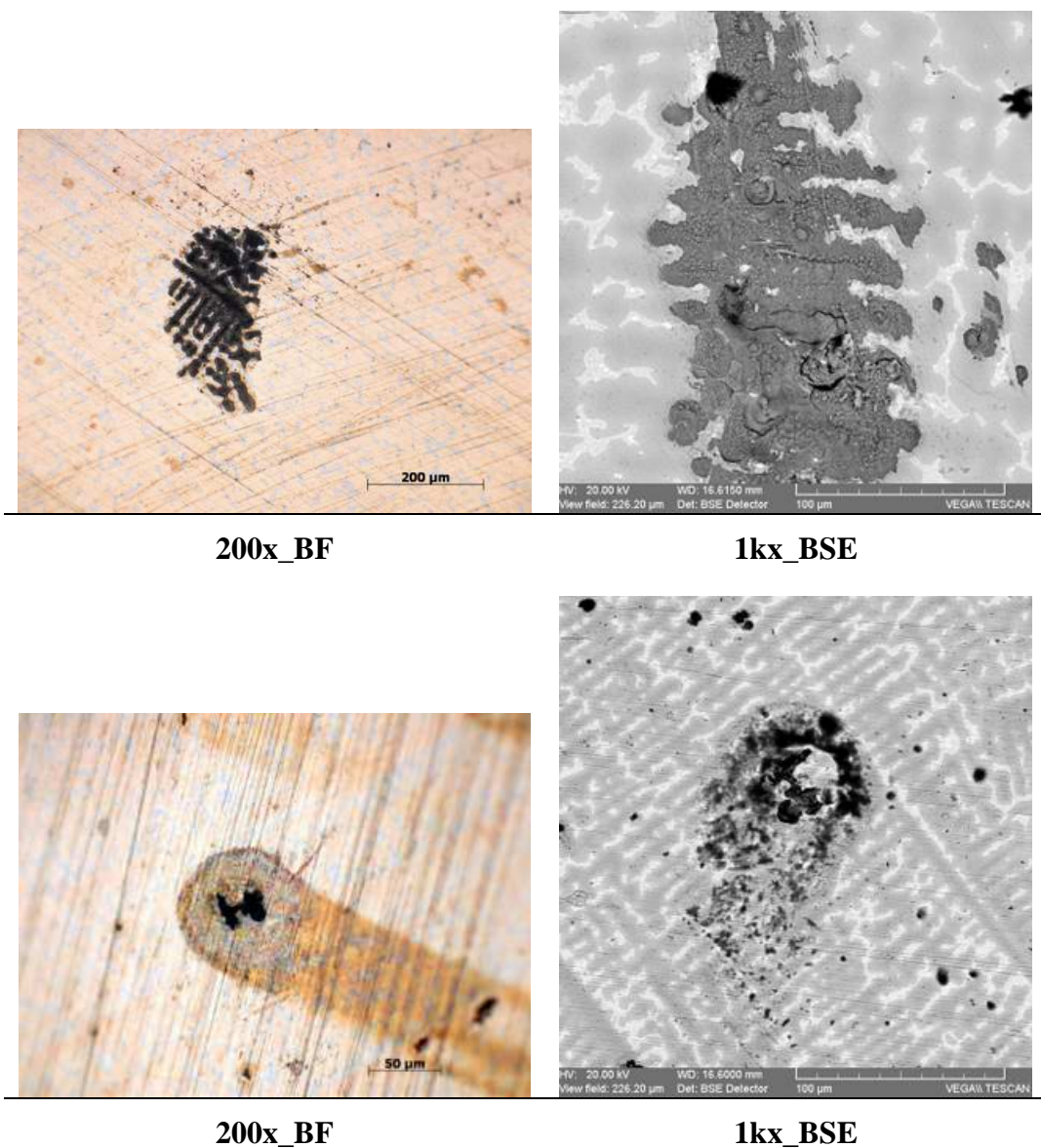
Figure IV.56. Comparison between Bronze 1 and Bronze 2. Optical and scanning electron characterization of the corroded surface. It is evidenced the localized corrosion

In the exposition of the next results, the most meaningful results, either obtained for Bronze 1 or Bronze 2 will be reported.

IV.2.5 Cyclic potentiodynamic polarization in natural and simulated soil solution

In order to have a term of comparison, two solutions, A and B, were prepared (Table IV.15) , for which the concentration of Chlorine, Nitrate, Phosphate and Sulphate anions are respectively doubled and increased 10 times with respect of the soil solution. These solutions can also provide a simulation of local increased concentration as a consequence, for example, of repeated events of water evaporation.

Table IV.15.Composition of electrolytes

	Cl^-	NO_3^-	PO_4^{3-}	SO_4^{2-}	pH	Conductivity
	mmol	mmol	mmol	mmol		mS
Soil Solution	1.128	0.726	1.053	1.145	8.86	0.32
Solution "A" (x 2)*	2.323	1.544	2.107	2.292	8.56	8.93
Solution "B" (x 10)*	11.273	7.256	10.529	11.581	8.95	13.03

Figure IV.57 reports the polarization curves recorded respectively in Soil Solution, Solution A and Solution B for the specimen Bronze 1. It can be observed that the corrosivity of these media is very different, the soil solution having a very low aggressiveness on bronze.
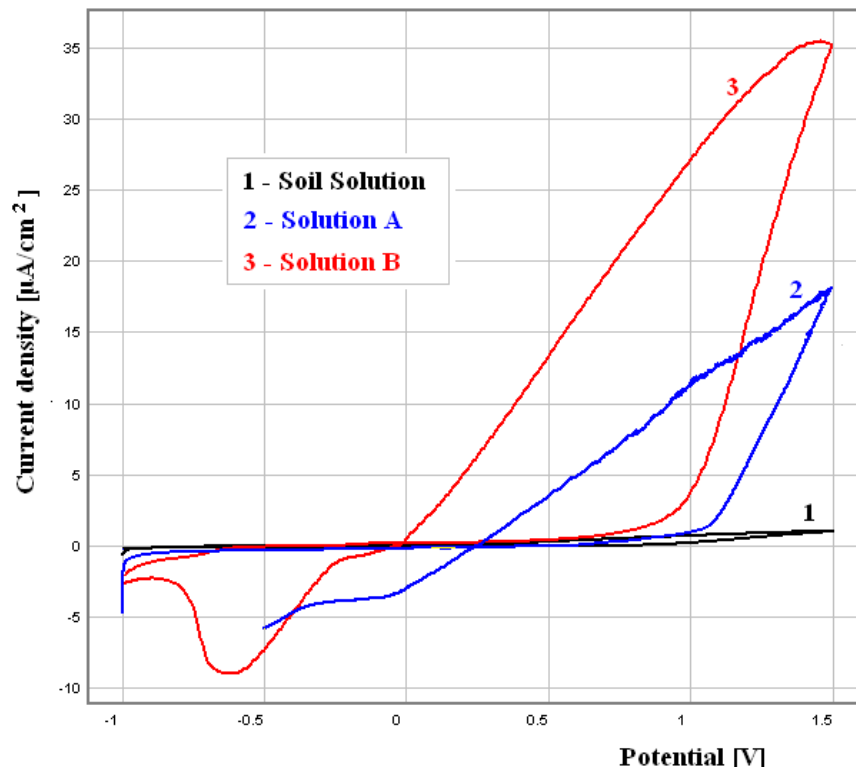
Figure IV.57. Cyclic potentiodyamic curves recorded respectively, in soil solution, solution A and solution B. results are shown for Bronze 1, but the same behavior was obtained for Bronze 2 as well.

The most concentrated solution, B, has been used also to simulate an "accelerated" corrosion of bronze and reaction products have been investigated by EDX spectrometer coupled with SEM.

The shape of the three voltammograms indicates that the alloy present a typical "pitting" corrosion behavior, as previously discussed. The parameters characterizing these processes are shown in the following table (Table IV.16):

Table IV.16.Composition of soil and simulated soil solution used as electrolytes

	E_{cor} (mV)	E_{BD} (mV)	E_{rp} (mV)	ΔE_{im} (mV)	J (E=1500mV) (mA/cm^2)	J/J$_{soil\ sol}$
Soil solution	350	230	109	121	1.17	1
Solution A	505	1035	247	788	18.23	15
Solution B	-293	834	-43	791	35.24	30

By comparing values of J (mA/cm^2) for E = 1500 mV it is possible to conclude that the sample is much more stable in soil solution than in solution A (15 times less stable) and solution B (30 times less stable).

It can be noticed that as concentration of salts increases, the passivity domain (represented by the value of ΔE_{im}) extends considerably.

It shall be underlined that the calculation of corrosion potential is affected by a considerable error because in these solutions at low potentials the specimen is practically passive and small fluctuations which could modify surface's quality (polishing grade, alloy's imperfections, but also local O_2 concentrations, temperature) lead to a considerable changing of the potential.

On the other side, it can be concluded that in absence of an external potential applied, the bronze sample is sufficiently stable.

The same behavior was observed for Bronze 2.

Optical and scanning electron microscopy (OM and SEM-EDX)

The surface morphology of the electrodes' surface has been investigated by optical methods after electrochemical experiments in order to fully characterize the corrosion process.

As expected from electrochemical results, optical observations have evidenced the pitting corrosion on bronze electrodes measured in soil and soil-simulated electrolytes. A general overview is provided by the BSE-image in the Figure IV.58, which reports the surface's morphology for Bronze electrode examined in solution B, the most concentrated (see Table IV.15)
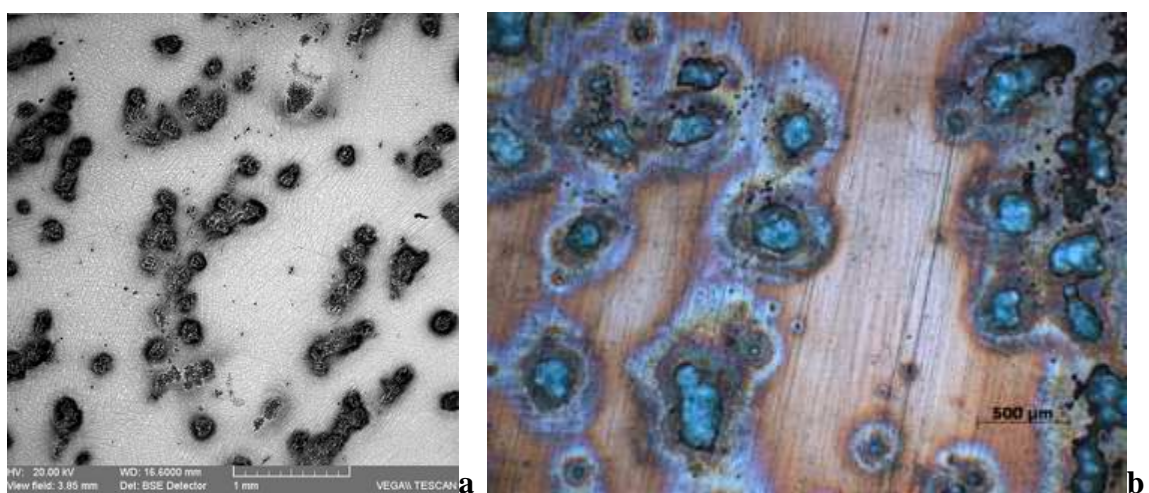
*Figure IV.58. Low magnification BSE image (**a**, 70x) and optical micrograph (**b**, BF, 50x) of the electrode surface after electrochemical experiments in solution B.*

A single pit was selected and an EDX line-scan was performed in order to characterize the elemental distribution across it.
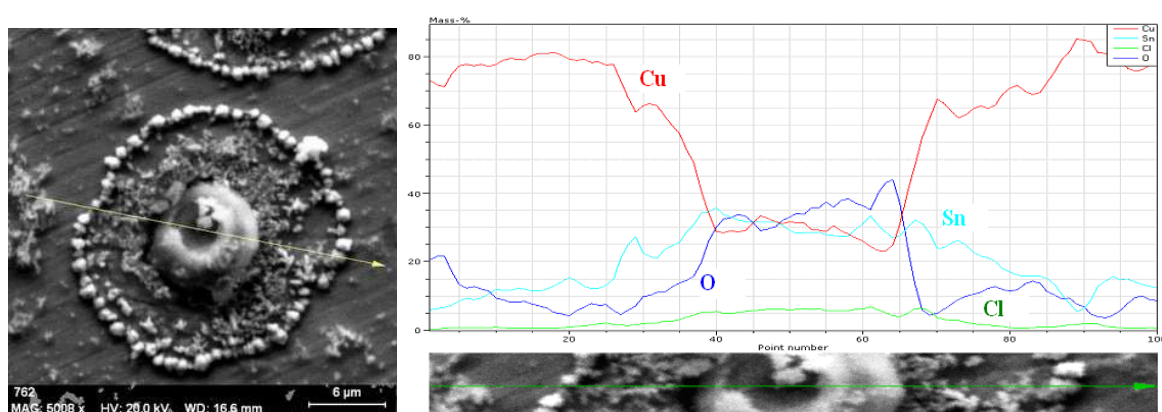
Figure IV.59. High magnification (BSE image, 5000x) of a pit and EDX line scan performed across it.

From result is provided in the Figure IV.59 it can be observed a significant decrease in copper, demonstrating its selective dissolution and the increasing of Sn and O content within the pit. A possible explanation is the formation of both copper and tin oxides, probably associated to an higher current density, locally.

Next to the pits some areas were identified and were characterized by the structure illustrated in the following images (Figure IV.60). It is evident, by examination of the BSE image, that corrosion selectively involves the dendritic phase, leaving uncorroded the (α+β)-phase (bright areas in the BSE image corresponding to the light blue phase in the OM).
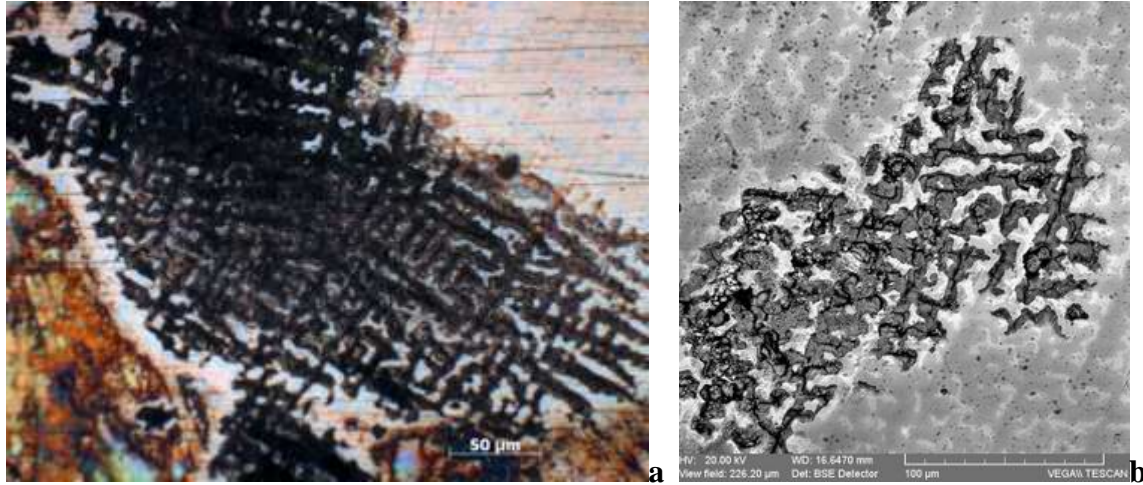
Figure IV.60. Evidences of selective corrosion involving the α-phase. (Bronze 2, after potentiodynamic polarization in solution "A"; **a**. *optical microscope, BF, 500x;* **b**. *BSE, 1kx)*

IV.2.6 Linear and cyclic potentiodynamic polarization in sea water

It is relevant for this study to investigate the bronze behavior in more aggressive environments. The interest is justified by the close vicinity of the archaeological sites in Dobrudja to the Black Sea and by the needing to study the particular effect of high concentration of chlorine as it is considered having a detrimental effect on bronze objects.

For this study, it was considered also the Mediterranean sea water as their composition have been found to be sensibly different by ion chromatography analysis (Table IV.17).

Table IV.17.Composition of the Black and Mediterranean Sea used as electrolytes

	Cl^-	SO_4^{2-}	pH	Conductivity
	mmol	mmol		mS
Black sea water	244.534	14.454	7.10	27.45
Mediterranean sea water	694.209	37.931	8.22	56.70

Figure IV.61 shows a comparison among the cyclic voltammograms recorded in soil solution, Black Sea water and Mediterranean Sea water. The reproducibility was verified performing three scan for each sample. Behavior of bronze in soil solution has already been discussed in former paragraph and it is reported in the image for sake of comparison.
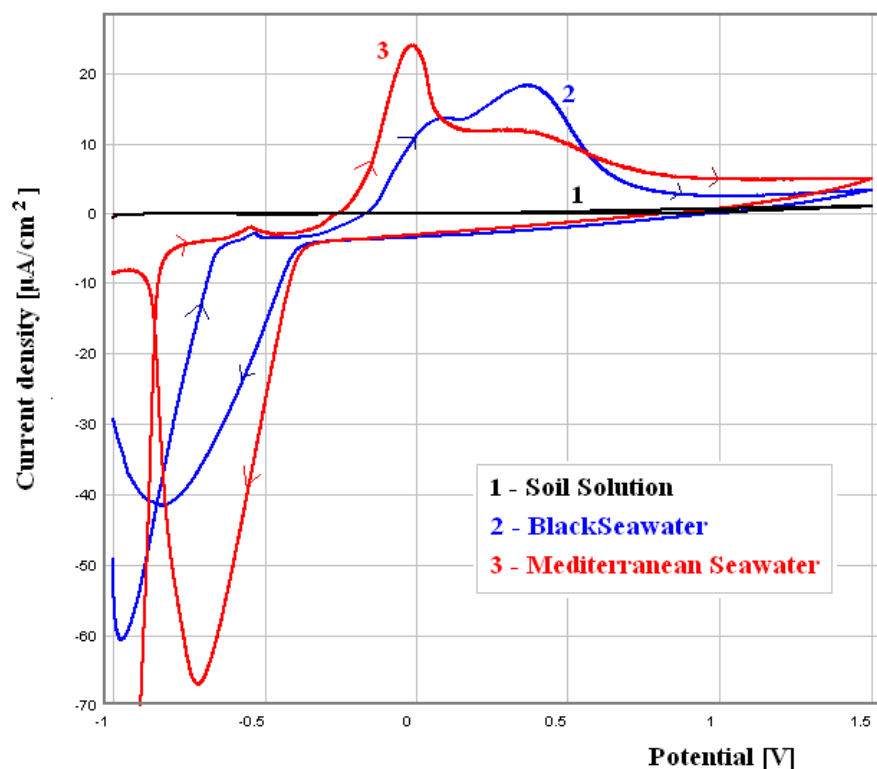
Figure IV.61. A comparison of cyclic potentiodynamic polarization curves for Bronze 1 in soil solution, Black and Mediterranean seawater.

In sea water corrosion is much more intense than in soil solution and this is demonstrated by both, the cyclic polarization curves and by the optical and scanning electron microscope observation of the electrode's surfaces.

On the anodic branch it is possible to identify three different peaks (Table IV.18), occurring for the two sea waters in different positions.

Table IV.18. Identification of anodic and cathodic peaks for Bronze 1 in seawaters

	A_I	A_{II}	A_{III}	C_I	
Black Sea	-524	98	340	-861	E (mV)
	-2.9	13.1	16.3	-408	J ($\mu A/cm^2$)
Mediterranean Sea	-548	-136	357	-718	E (mV)
	-198	24	11.9	-66.8	J ($\mu A/cm^2$)

The list of possible electrode reactions is presented, according to Pourbaix [*Babic 2001*].

$2\ Cu + H_2O \rightarrow Cu_2O + 4H^+ + 2e^-$

$Cu_2O + H_2O \rightarrow CuO + 2H^+ + 2e^-$

$Cu + 2H_2O \rightarrow Cu(OH)_2 + 2H^+ + 2e^-$

$Sn + 2H_2O \rightarrow SnO_2 + 4H^+ + 4e^-$
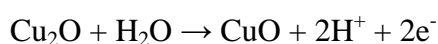
In the presence of chlorine anions, as we are in sea water, leads to the following reactions:

$Cu + Cl^- \rightarrow CuCl + e^-$

$Cu_2O + Cl^- + 2H_2O \rightarrow Cu_2(OH)_3Cl + H^+$

$CuCl + Cl^- \rightarrow CuCl_2^-$
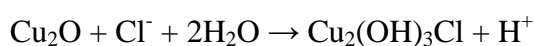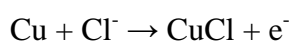
This last reaction, leading to the formation of complexes, takes place when an excess of chlorine anions is present [*Dos Santos 2007*].

The first small peak, at around -500 mV for both curves (Black and Mediterranean Sea) can be attributed to the beginning of Cu oxidation by formation of Cu(I) oxide, Cu_2O. The process goes on with increasing of the current density, proceeding to further corrosion by formation of $Cu(OH)_2$ or CuO; phenomena which occur with different speeds of formation in two different sea waters leading to the formation of a *duplex* structure [*Babic 2001*]. The formation of this duplex structure protects the bronze from further dissolution of the alloy and this can be demonstrated by the decreasing of the current density in the curves after the third peak. The presence of tin, forming the unsoluble tin (IV) oxide, SnO_2, is probably playing an important role in this behavior as it is insoluble over a wide range of pH.

In the cathodic branch, it is remarkable to observe the presence of a single peak, probably representing the reduction of cupric species to metallic Cu, cubic, as it also demonstrated by the BSE image showed in Figure V. and obtained after the electrochemical experiments.
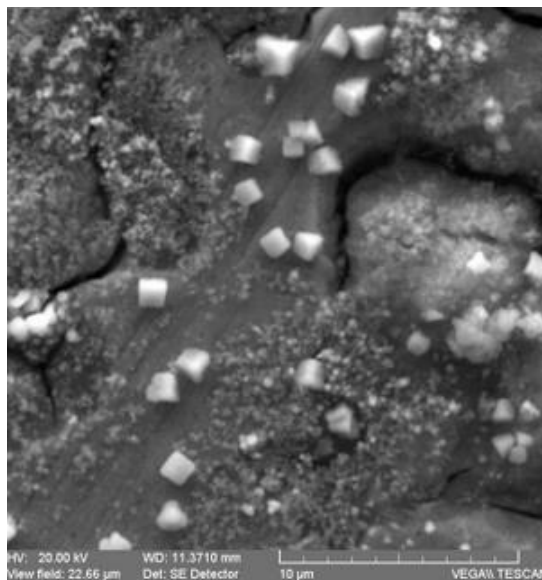
Figure IV.62. BSE image showing the formation of cubic Cu-crystals as a consequence of potential scan towards negative values.

Optical and scanning electron microscope characterization

In presence of chlorine and sulfate anions, the process doesn't stop at this stage: $Cu(OH)_2$ is unstable and subsequent reaction with chlorine lead to the formation of alkaline copper chlorides or sulphates. This is visible in the picture taken at the optical microscope and showing the formation of green-blue compounds.
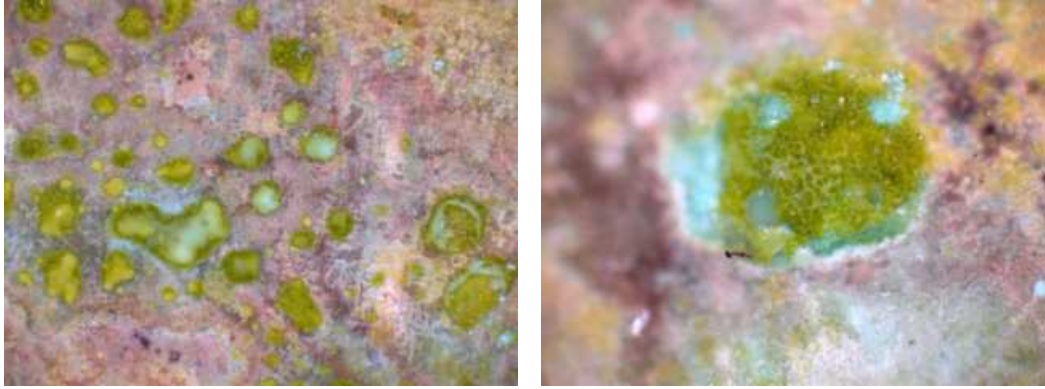
Figure IV.63.OM micrographs of Bronze 1 in Mediterranean Sea water after electrochemical experiments.
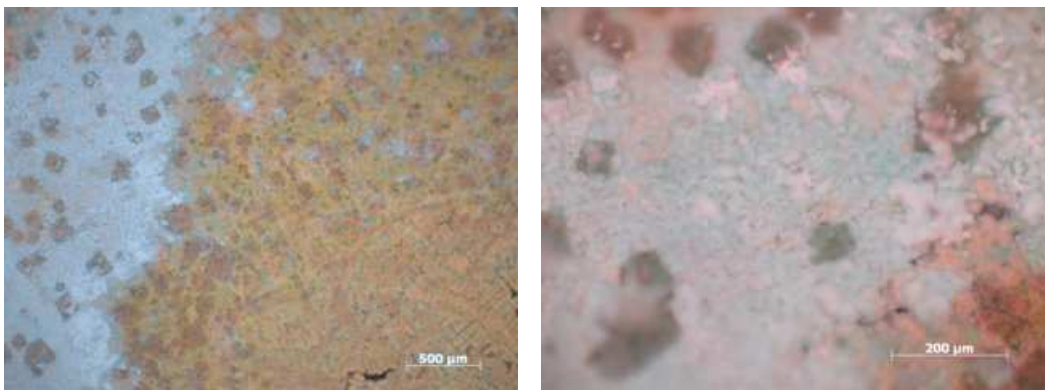
Figure IV.64.OM micrographs of Bronze 1 in Black Sea water after electrochemical experiments.

SEM-EDX allows performing point and area elemental analysis of the surface, on selected areas. The bronze specimen withdrawn from the Mediterranean Sea exposure was subjected to such an investigation in order to identify the elements characterizing the corrosion structure.

Figure V. reports the BSE image, magnified 1000 times, and the correspondent spectrum recorded on the selected area, for the electrode after electrochemical experiments in Mediterranean Sea. Two different zones are identified: one correspondent to these blue/green deposition and another one, characterized by a compact layer, which presents cracks. The EDX spectrum registered on the deposit confirm its supposed nature, being identified by Cu, Cl and O, the elements characterizing the hydroxyl-chlorides, such as Atacamite or Paratacamite. The compact area results to be composed by Cu, Sn, Cl, and O, the exact nature

of this compounds being not clarified, and micro-XRD or similar advanced methods are required for its identification. It can be supposed that a complex layer, formed by a mixture of tin (IV) oxide, Cu(I) oxide and Cu(I) chlorides or other compounds involving Cu(II) species such as hydroxyl-chlorides is there.
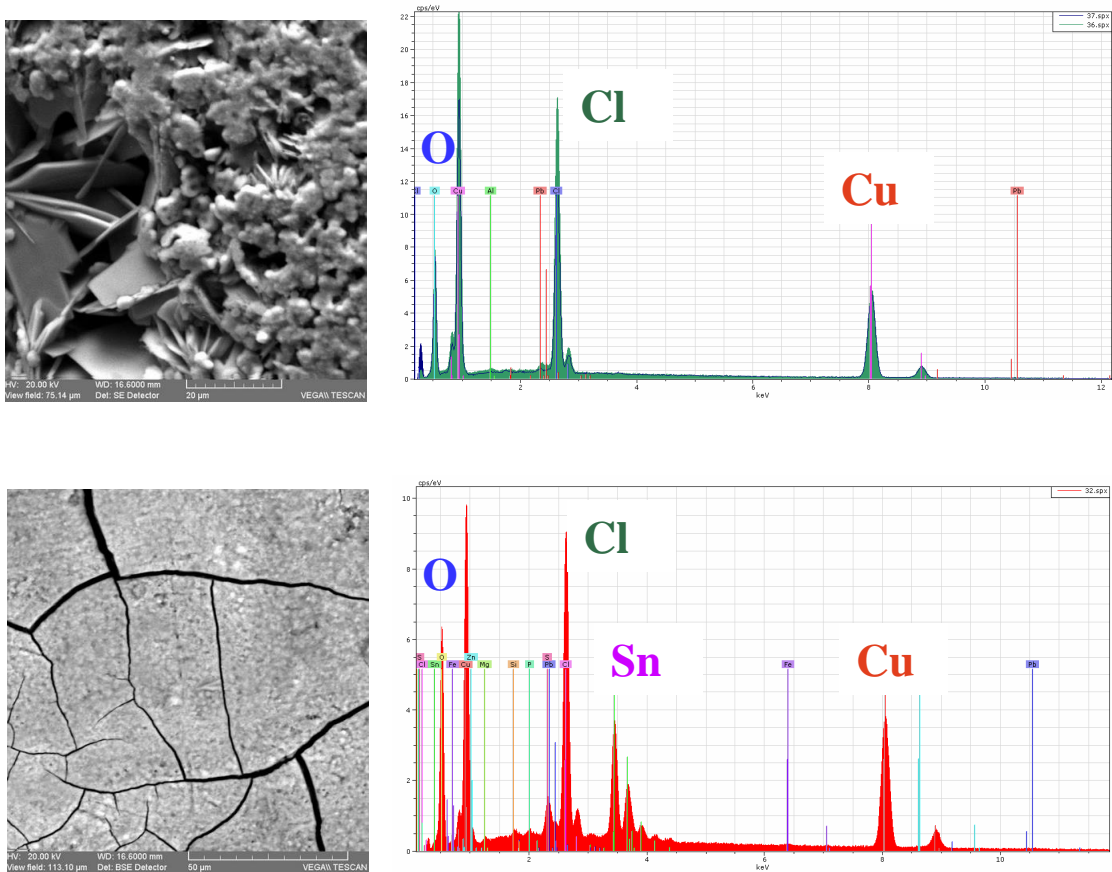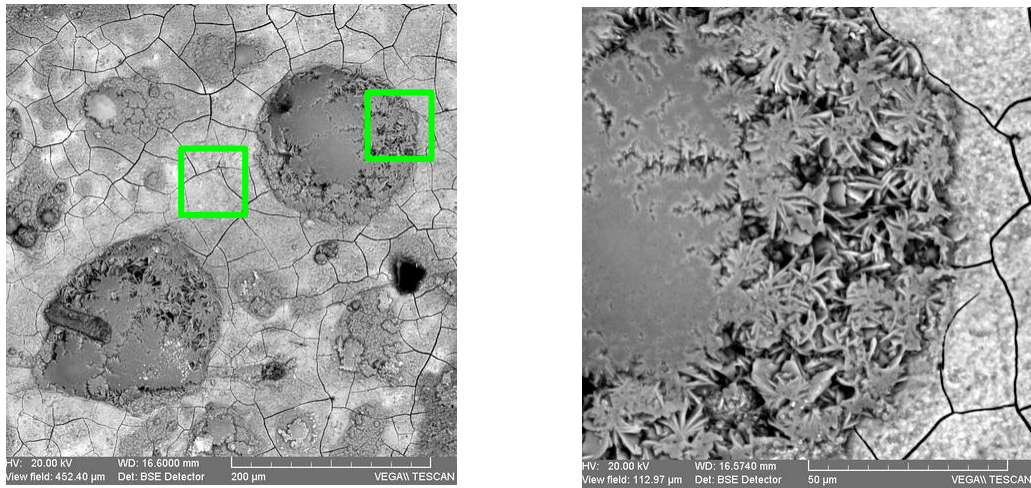
Figure IV.65. BSE images of the corroded surface. The selected area were analyzed by EDX and chlorine has been found to be the main corrosive agent.

IV.2.7 Comparison between soil-simulated solution and sea water

The comparison between the polarization curve in sea water and soil solution previously presented, doesn't allow appreciating the difference. It is proposed here a comparison among curves registered in Black sea water and the solution B, which, I remind, was prepared by ten times increasing the concentration of Cl^-, NO_3^-, SO_4^{2-}, SO_4^{2-}.
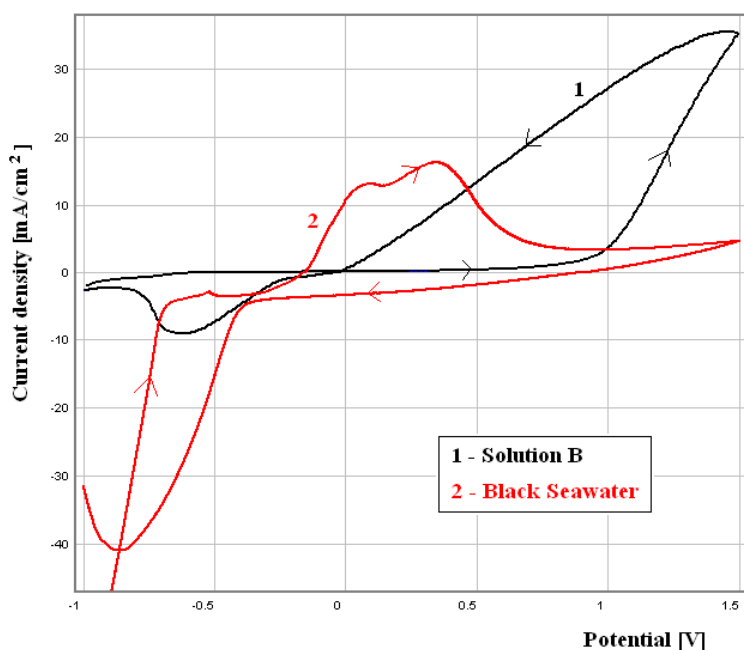
Figure IV.66. Cyclic polarization curves for Bronze 1 recorded in Black seawater and solution B.

The behavior of bronze in sea water is different from that of bronze in soil and soil simulated media, in which case the potentiodynamic curve shows a wide passive domain. A protective passive layer is likely to be formed, even though the breakdown of passivity, occurring at higher potential, leads to a pitting phenomenon which is observed already at naked eyes (Figure IV.67).
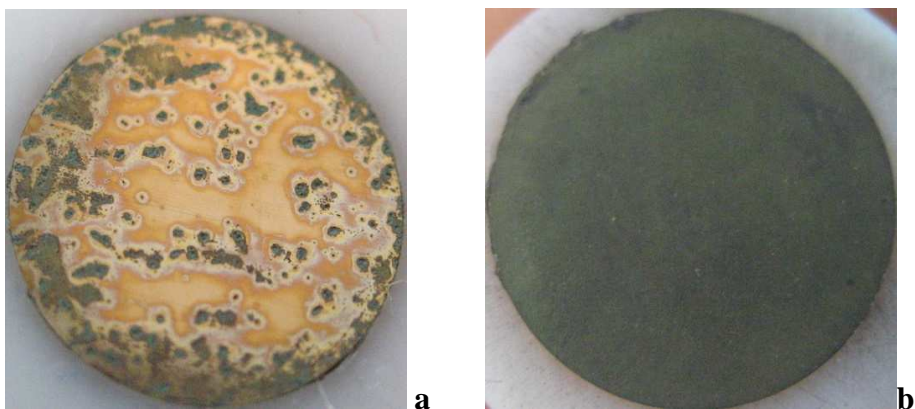
Figure IV.67. Photographs of bronze 1 electrodes after electrochemical experiments (a-in sol B; b-in Black Sea)

IV.2.8 Surface characterization of bronze electrodes kept in soil by optical and potentiodynamic polarization methods

Bronze electrodes were kept in soil for a total period of two months. Each month, one electrode was removed from the container and its surface investigated by optical and scanning microscopy before the electrochemical measurements.
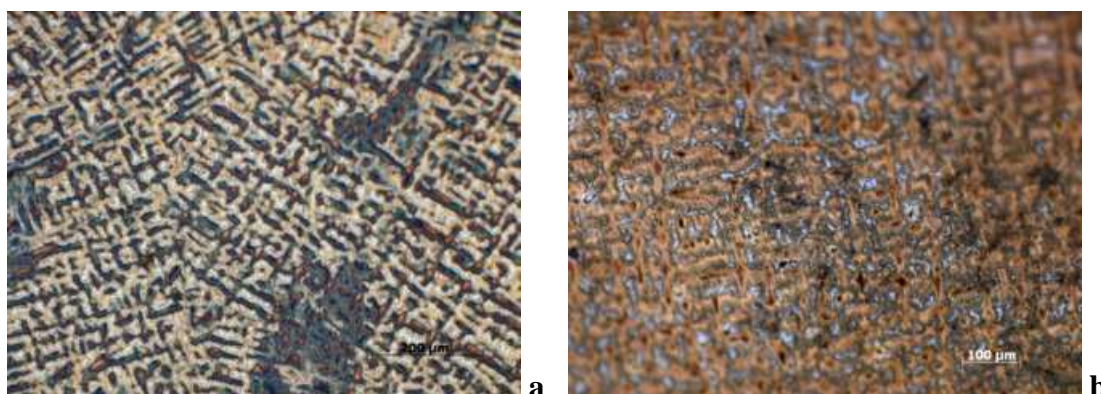
*Figure IV.68. Optical micrographs (200x, BF) showing the bronze electrodes surface after, respectively, 30 (**a**), 60 (**b**).*

It can be observed from the images (Figure IV.68) that also for sample buried in soil, the oxidation starts from the copper-rich phase, while the tin-rich remains uncorroded and it is visible by the light blue colour.

We believe that the corrosion process involves the formation of a very thin layer of tin and copper oxides, few nanometers thick only, which act as a passive layer. Tin (IV) oxide is a very stable species, being insoluble over a wide range of pH [*Pourbaix 1977*].

Afterwards, linear and cyclic potentiodynamic polarization curves were recorded using the natural soil solution as electrolyte. The results for the linear voltammetry are reported in the following table (Table IV.19) and compared with the behavior of a freshly polished electrode.

Table IV.19. Parameters characterizing linear voltammetry: a comparison among freshly polished electrode and kept in soil for 30 and 60 days.

Parameters	freshly polished	Bronz1, **in soil 1 month,** soil sol.	Bronz1, **in soil 2 months,** soil sol.
surface (mm^2)	0.55	0.5027	0.5281
OCP (mV/SCE)	-76	-60	-55
E (J=0) (mV/SCE)	29.00	-0.40	-121.10
J_{corr} $(\mu A/cm^2)$	**1.01**	**1.13**	**2.16**
R_p (kohm x cm²)	40.74	25.07	12.61
b_a (mV)	242.2	202.6	152.6

b_c (mV)	-259.2	-149.6	-197.0
v_{corr} (µm/year)	11.86	13.17	24.55

Particularly relevant for a critical comparison are values of the corrosion potential ($E_{J=0}$) instantaneous current density (J_{corr}) and the resulting corrosion rate (v_{corr}) calculated using the Tafel method.

Polarization curves, for a freshly polished surface and for samples maintained in soil one and two months respectively, measured in soil solution, reveals that for these last two specimens the tendency to corrode becomes higher as it is evident from values of E_{cor} calculated from the linear polarization curves. [-0.4 ÷ -121.0 mV] and from the instantaneous values of the corrosion current, which becomes higher [$1.13 ÷ 2.16$ µA/cm^2].

Moreover, the stability plateau (or the passive domain), is much more pronounced for the polished sample, while it is not present for the other two samples, for which the corrosion begins already at the corrosion potential but with relatively low rate (values of current density ~0.1 mA/cm^2), as the corrosion process has already began by electrochemical and chemical processes in soil.
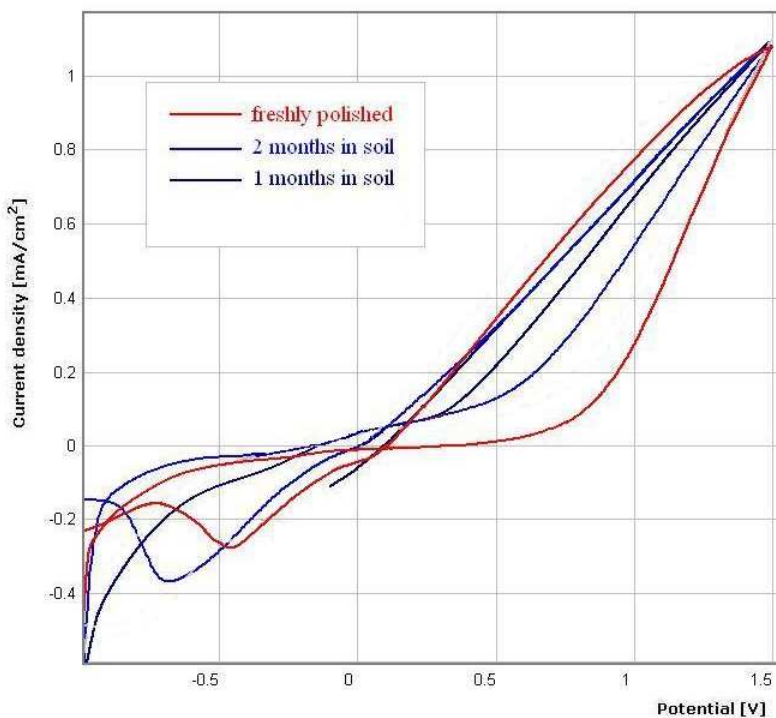
Figure IV.69. Cyclic polarization curves relative to Bronze 1, freshly polished and after 30, 60, 90 days kept in soil, registered in soil solution.

It can be notices that, once with time, the shape of the curve tends to resemble the one of the polished sample, indicating an increase in the passive behavior of the surface especially at over-potentials higher than ~300 mV.

IV.2.9 Surface characterization of bronze corrosion products after exposure in sea water by optical methods

Bronze electrodes were kept in a closed container in sea water, both Black Sea and Mediterranean Sea. Their surfaces have been investigated after 40 days by optical and scanning electron microscope as well as by electrochemical impedance spectroscopy (EIS).

Bronze 1 in Mediterranean Sea water

50x_DF   **100x_DF**
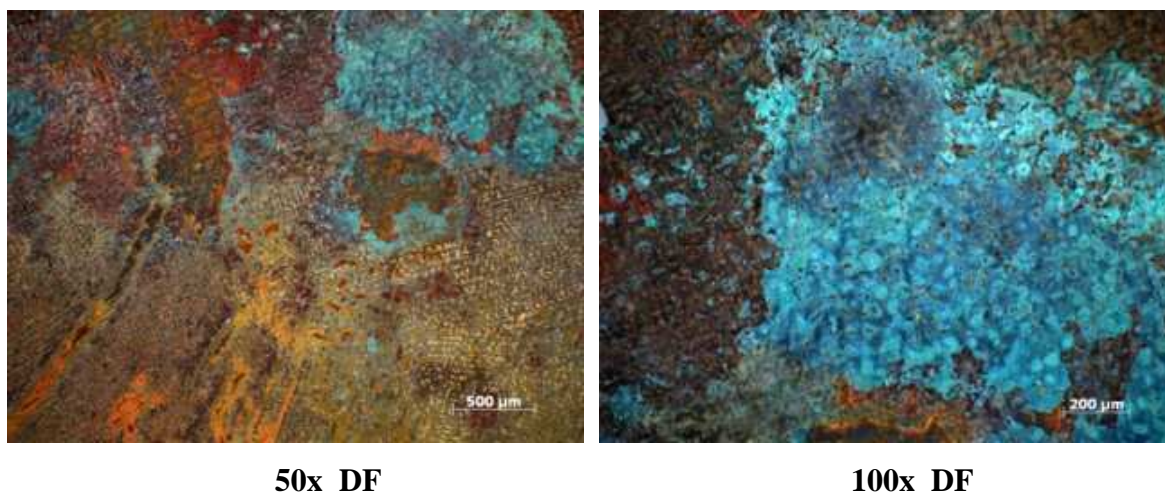
Figure IV.70. Dark field observation at the OM reveals the colorful corrosion products which have formed on the electrode's surface after exposure to Mediterranean Sea water for 40 days.

200x_BF   **200x_DF**
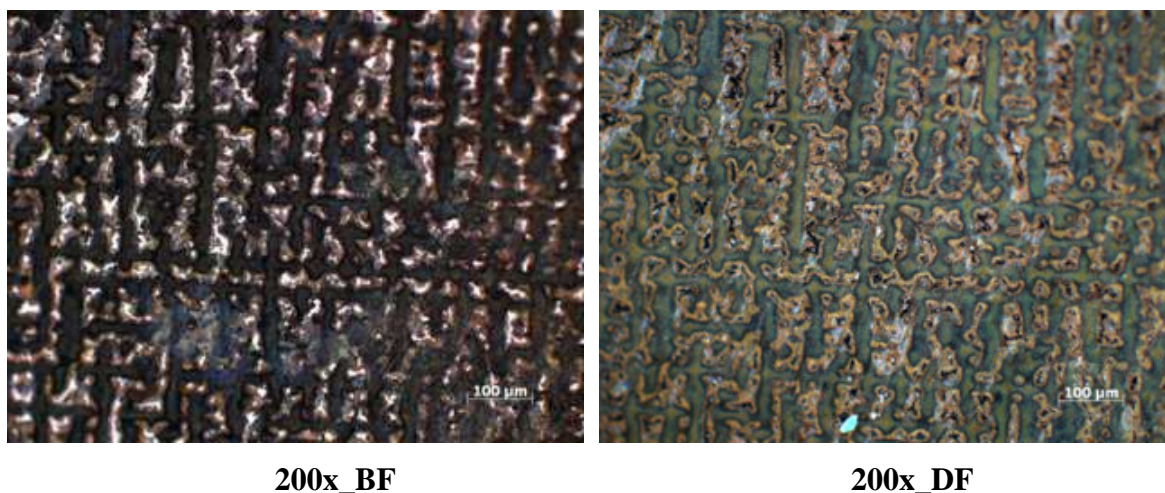
Figure IV.71. .A comparison between dark and bright field allows evidencing the un-corroded phase, α+δ in this case, which appears brighter under bright field conditions; the dark field observation allows appreciating the colour of corrosion product: the green colour can be attributed most probably to basic copper chlorides.

One month exposure to the Mediterranean seawater produces a variety of colorful corrosion products, as we can observe in the pictures above (Figure IV.70). Orange to red compounds are possibly ascribed to copper(I) oxide, while green to blue compounds can be identified as copper (II) hydroxide or basic copper chlorides and sulphates. It is worth noticing once again,

the preferential attack of the α-phase, clearly visible in the left image in Figure V.71. The brighter areas represent the (α+δ)-phase which is still uncorroded. This result demonstrates that even in more aggressive environments, always aerated, the preferential dissolution of the copper-rich phase occurs.

The following BSE images (Figure IV.72) show at higher magnifications the electrode's surface. The image on the left-hand side shows again the tin-rich interdendritic phase and the presence of an inhomogeneous corrosion layer affecting the dendritic α–structure. These areas are characterized by copper and an high tin content, beside elements such as O, Na and Mg finding their origin in the corrosion medium (i.e. the seawater).

The image on the right shows the presence of tetrahedral crystals, few μm big, whose EDX spectrum is presented in the below the image.
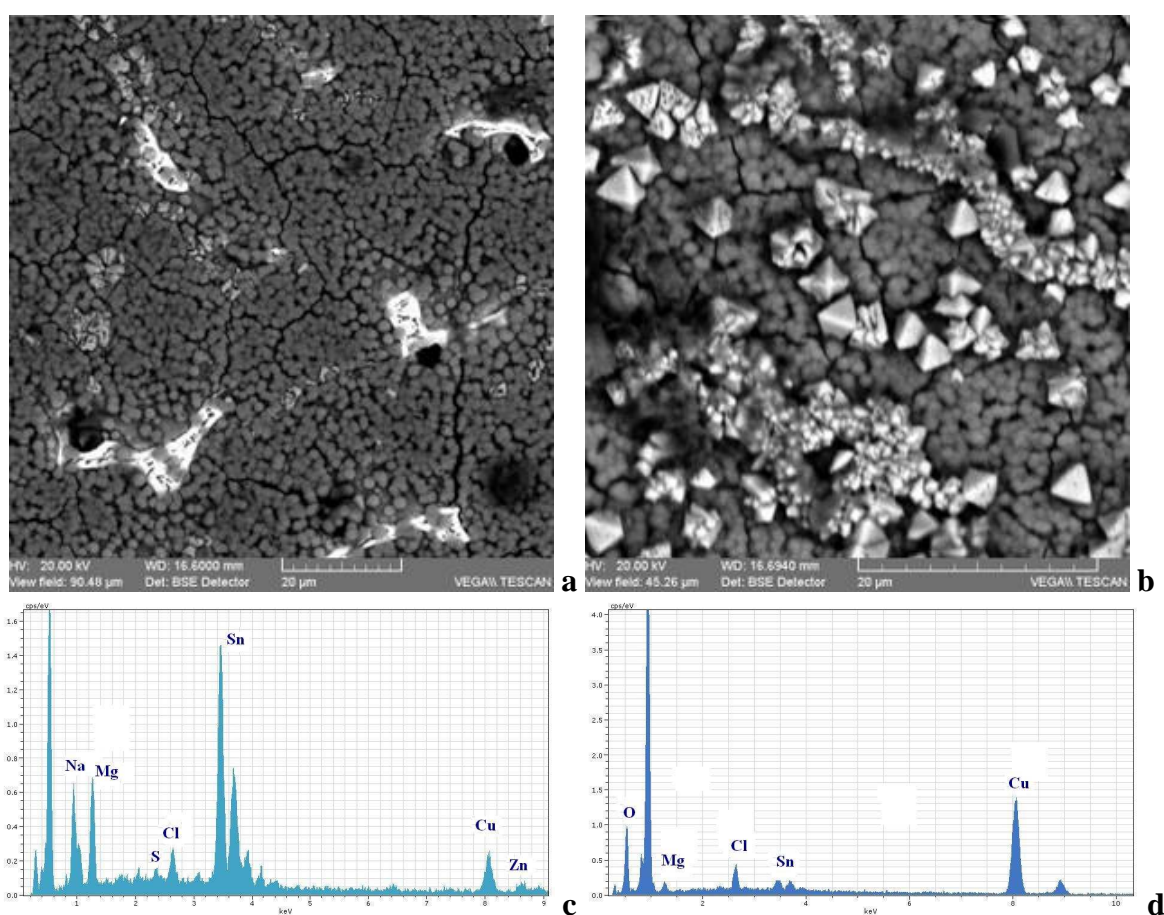
*Figure IV.72. BSE micrographs of the bronze electrode exposed to Mediterranean sea water. The brighter zone in the left-hand image (**a**) are the uncorroded (α+δ)-phase, while in the right-hand image (**b**) tetrahedral crystals are observed.*

Bronze 1 in Black Sea water

Visual examination of the electrode's surface after one month exposure to Black Sea water let us appreciate the occurrence of a more or less homogeneous surface, covered by green/blue compounds. Optical micrographs provide an insight into the surface.

50x_DF	**100x_DF**
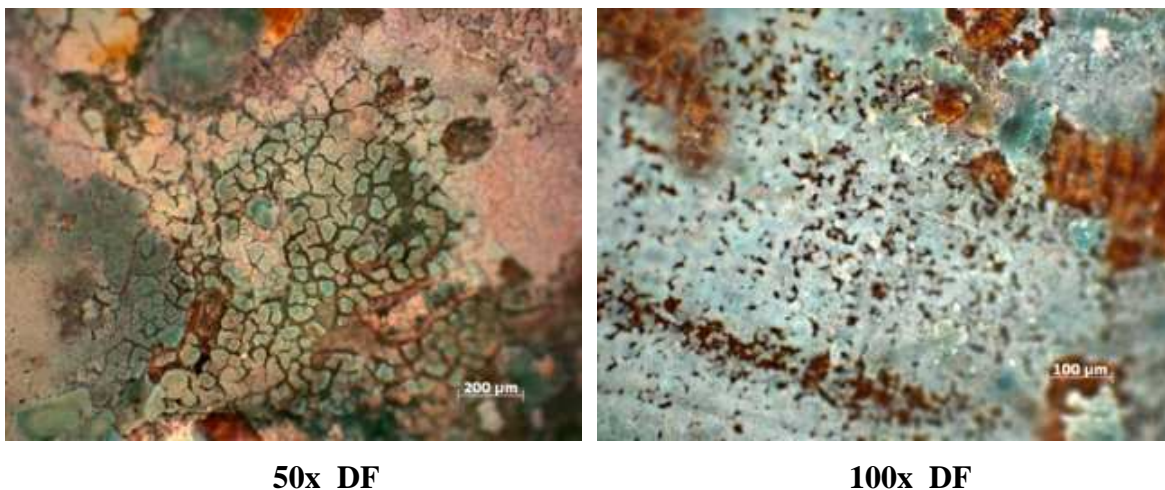
Figure IV.73. Dark field observation at the OM reveals the colorful corrosion products which have formed on the electrode's surface after exposure to Mediterranean sea water for 40 days.

BSE images, showed in Figure V.74, illustrate the morphology of corrosion structure. It is evidenced the occurrence of two typologies of corrosion products, their exact nature remaining unidentified.

The EDX-spectra provide a source of information as regards the qualitative information about the element present. In both cases, copper and oxygen are present as major component, while tin, chlorine, sulphur and aluminium are present as minor elements. It can be supposed that copper is present as cuprous oxide or basic chlorides, while tin is present as tin oxide, even though signal from the original alloy is expected. The source of aluminum would likely be the Sea.

This is in accordance with the literature [*dos Santos 2007, Wang 2006*], as the main corrosion compounds detected on bronze alloy are copper basic chlorides and a mixture of copper and tin oxides.
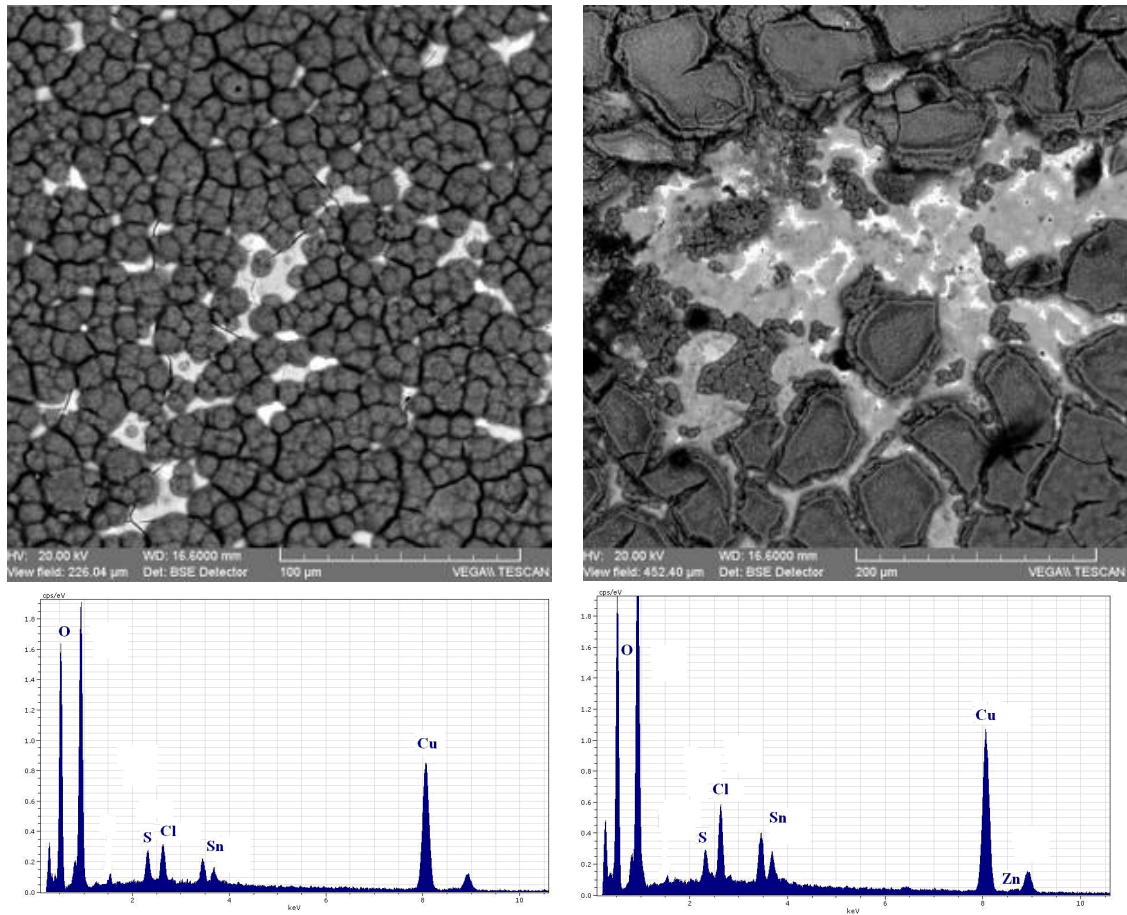
Figure IV.74. BSE micrographs of the bronze electrode exposed to Black sea water.

IV.2.10 Electrochemical impedance spectroscopy: comparison between the behaviors of corrosion layers formed in soil and seawater.

In the last part of the work, scientific efforts were aimed to characterize the corrosion layers formed on bronze specimen both in soil and seawaters. The following represent preliminary results, which disclose possible further developments for the research.

Electrochemical Impedance Spectroscopy is maybe the most spread technique for the characterization of surface structure of a corroded metal [*Cano 2008*]. It is a powerful method which allows the estimation of corrosion resistance of electrochemical and corrosion system. EIS is essentially a steady state technique that is capable to access relaxation phenomena, whose relaxation times vary over orders of magnitudes and permits single averaging within a single experiment to obtain high precision levels.

The EIS spectra recorded in natural soil solution for Bronze 1 after burial in soil after 30, 60 and 90 days are shown in Bode plots (Figure V.75) of the logarithm of impedance magnitude and of the phase angle as a function of the frequency's logarithm. The impedance spectrum indicates the formation of an oxide with two layers, i.e. a porous outer layer and a compact inner layer [*Pan et al. 1996*]. Those can be divided in two distinct frequency regions: the high-frequency part, which arises from the uncompensated ohmic resistance due to the electrolytic solution and the impedance characteristics resulting from the penetration of the electrolyte through a porous film, and the low-frequency part accounting for the processes taking place at the substrate/electrolyte interface [*Souto et al. 2003*].
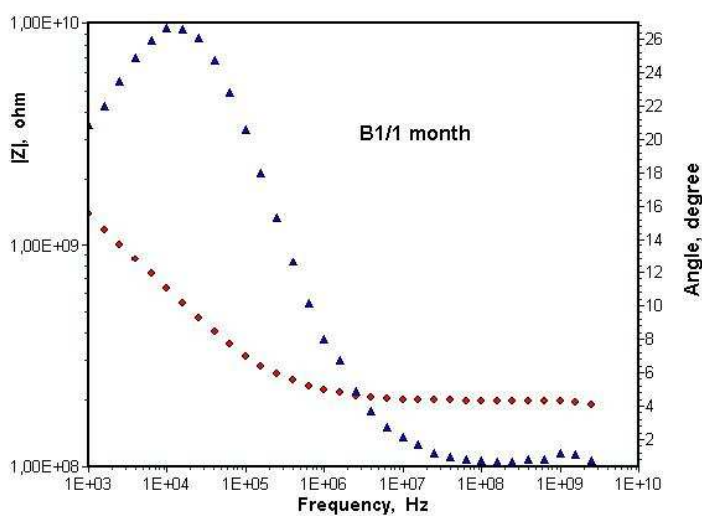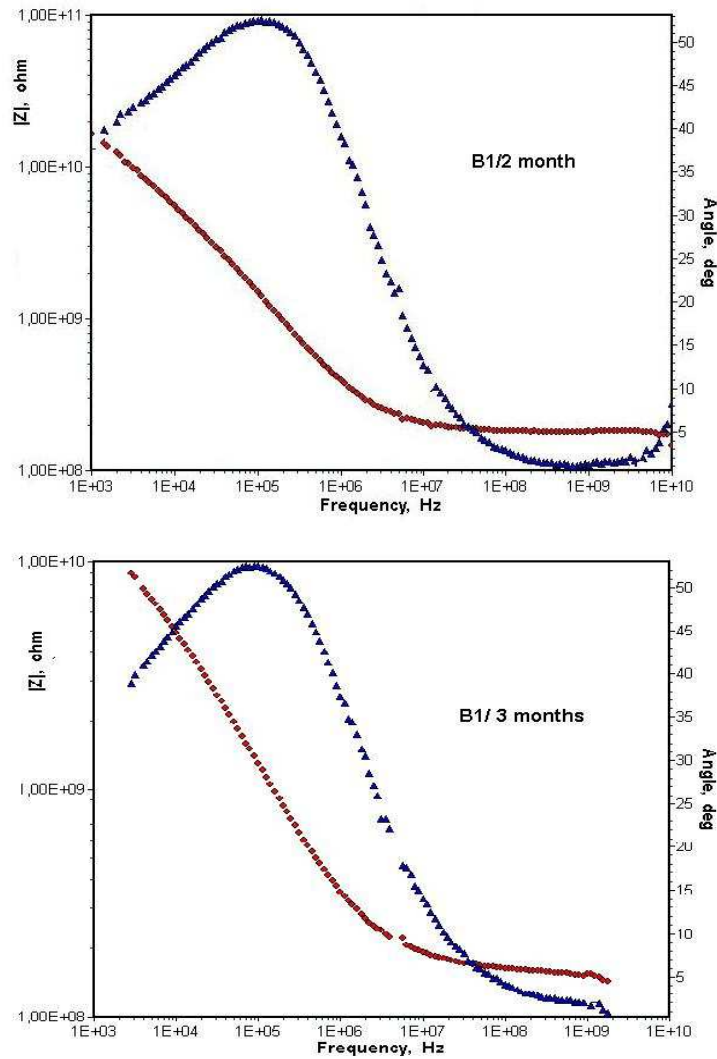
Figure IV.75. Bode plots for Bronze 1 after one, two, three months exposure in soil.

For the interpretation of the electrochemical behavior of a system from EIS spectra, an appropriate physical model of the electrochemical reactions occurring on the electrodes is necessary. The electrochemical cell, because it presents impedance to a small sinusoidal excitation, may be represented by an equivalent circuit (EC). An EC consists of various arrangements of resistances, capacitors and other circuit elements, and provides the most relevant corrosion parameters applicable to the substrate/electrolyte system. The usual guidelines for the selection of the best-fit EC are the following.

- The employment of a minimum number of circuit elements;
- The χ^2 (chi-squared) error was suitably low ($\chi^2 < 10^{-4}$), and the error associated with each element were up to 5%.

Instead of pure capacitors, constant phase elements (CPE) were introduced in the fitting procedure to obtain good agreement between the simulated and experimental data.

The impedance of CPE is defined (Eq. IV.4) as

$$Z_{CPE} = \frac{1}{Q(j\omega)^n} \qquad \text{(IV.4)}$$

where Q is the combination of properties related to both the surfaces and electroactive species independent of frequency; n is related to a slope of the lg|Z| vs lg(f Bode)–plots; ω is the angular frequency and j is imaginary number ($j^2 = -1$). Q is an adjustable parameter used in the fitting routine**:** the exponent *n* is $-1 \le n \le 1$. When *n* is 0, the CPE is equivalent to a pure resistor, when *n* = 1, the CPE is equivalent to a capacitors and when *n* = -1 the CPE is equivalent to an inductor. Finally if *n* is 0.5, the CPE is equivalent to the Warburg impedance. Warburg impedance is an element that model the impedance associated to diffusion (i.e. mass transfer) processes and is commonly used when the diffusion of the species through the pores of corrosion products controls the corrosion rate [*Cano et al. 2009*].

After testing a number of different electrical circuit models in the analysis of the impedance spectra obtained at the open circuit potential, it was found that the whole set of data for all the samples could be satisfactory fitted with the EC given in Figure IV.76. This is based on the consideration of a two-layer model for the surface film. The table reports the relative impedance parameters (Table IV.20).
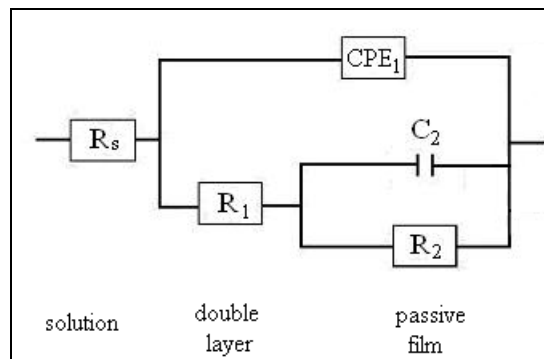
Figure IV.76. Equivalent electric circuit for corrosion layers formed in soil.

Table IV.20. Impedance parameters reported for Bronze 1 after one two and three months' exposure to soil.

Sample	R_s ($k\Omega \times cm^2$)	CPE$_1$			C		χ^2
		Q_1 ($S \cdot s^n cm^2$)	n_1	R_1 ($k\Omega \times cm^2$)	C_2 (F)	R_2 ($k\Omega \times cm^2$)	
Bronze 1- 1 month in soil	19.54	1.94E-08	**0.60**	1.29E+02	1.22E-09	4.39E+01	4.76 10^{-4}
Bronze 1- 2 month in soil	17.84	5.16E-10	**0.71**	1.40E+03	6.27E-15	1.67E+03	6.37 10^{-4}
Bronze 1- 3 month in soil	15.68	8.95E-10	**0.68**	1.58E+03	1.17E-10	7.87E+02	6.74 10^{-4}

The components of the EC are:

> R_s – ohmic resistance of the electrolyte;
>
> CPE_1 – constant phase element of the outer porous layer;
>
> R_1 – resistance of the outer porous layer;
>
> R_2 – resistance of the compact inner layer;
>
> C_2 – capacity of the compact inner layer

The EIS results allow to qualitatively estimate the nature of corrosion layers formed on the bronze specimen after exposure to a soil environment. According to the proposed model, the film consists of two layers, a compact inner layer (passive film in Figure IV.77, right-hand) characterized by pure condenser behavior, and an external one, which is described by the CPE_1 and is identified by values of the exponent n_1 less than unity, thus indicating an imperfect condenser.

These results indicate than the protection provided by the passive layer is predominantly due to the compact inner layer, while the outer layer is characterized by an higher defectiveness, heterogeneity and roughness of the surface [*Souto et al. 2000*].
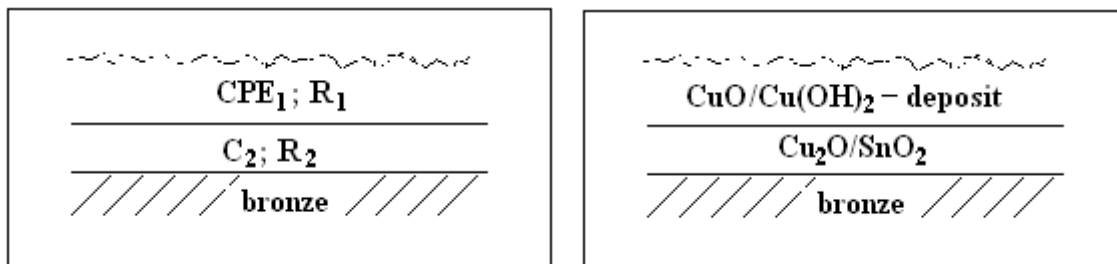
Figure IV.77. Qualitative model for the film formed on bronze after exposure to soil: on the right, the proposed structure of the film.

Comparison among the impedance parameters for the Bronze specimen after 30, 60 and 90 days do not show significant differences, meaning that probably the structure of the corrosion layers is stable and doesn't change within 3 months time.

As a conclusion, EIS measurements contributed to propose a qualitative model which is consistent with the results previously obtained by potentiodynamic polarization methods. In fact, the equivalent circuit used for the interpretation of results, is analogous to a double-structured layer, consisting in a passive film covered by a porous and defectiveness layer. the structure can be proposed is illustrate in Figure VI.77 (left-hand).

The EIS spectra for Bronze specimen (Bronze 1) exposed to Black Sea water and Mediterranean Sea water are reported in Figure IV.78, their shape being significantly different than those recorded in soil solution.
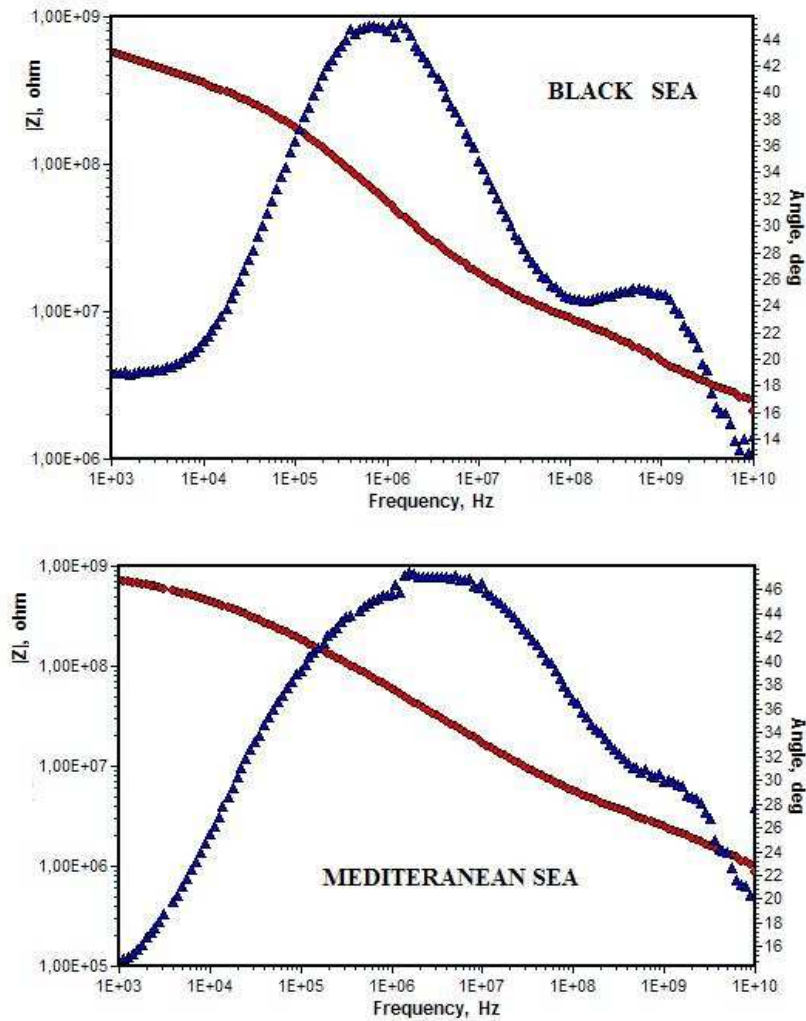
Figure IV.78. Bode plots for Bronze 1 after 35 days-exposure to Mediterranean and Black seawaters.

The impedance spectra exhibit two time constants, well distinguishable for the Black Sea, and related to the presence of a double layer. The presence of the second time constant allow to advance the hypothesis that, in this case, the passive layer fails in its protective behavior, allowing processes of mass transfer to occur within it.

We found that the set of data for EIS curve recorded in Black Sea and Mediterranean Sea well satisfy the requisites of the equivalent electric circuit shown in the Figure IV.79, as it can be evaluated by the impedance parameters reported in the Table IV.21.

The components of the EC are:

R_s – ohmic resistance of the electrolyte;

CPE_1 – constant phase element of the passive film;

R_1 – resistance of the passive film;

W_1 – Warburg element for the passive film;

R_2 –   resistance of the outer porous layer;

CPE_2 –   constant phase element for the outer porous layer.
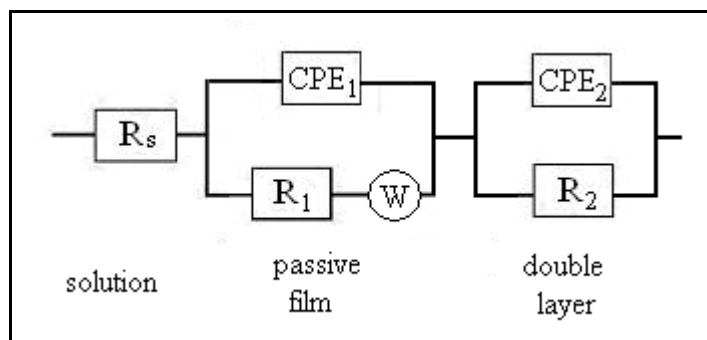
Figure IV.79. Equivalent electric circuit for corrosion layers formed in seawaters.

Table IV.21. Impedance parameters reported for Bronze 1 after one two and three months' exposure to seawaters.

| Sample | R_s ($\Omega \times cm^2$) | CPE$_1$ | | | W | CPE$_2$ | | | χ^2 |
		Q_1 ($S \times s^n \times cm^2$)	n_1	R_1 ($k\Omega \times cm^2$)		Q_2 ($S \times s^n \times cm^2$)	n_2	R_2 ($k\Omega \times cm^2$)	
Bronze 1-35 days in Mediterranean seawater	81.46	1.11E-08	0.57	38.15	5.15E-07	6.19E-12	0.90	0.05	1.22E-03
Bronze 1-35 days in Black seawater	223.00	2.07E-10	0.71	0.29	2.43E-07	4.27E-09	0.65	17.3	7.52E-04

The model is described by two, phase constant elements, connected in-series. It can be observed that the values of the exponent, n, varies in the two cases. For the Mediterranean seawater, n_2 is close to 1 and therefore ascribed to a condenser, or a passive film, showing protective properties. The constant phase element 1 is characterized by a value of n_1 which approaches 0.5, in which case the element can be considered as working as a Warburg element, which accounts for the diffusion process through the layers.

In case of Black seawater, the n value does not approach the unity meaning that both the constant-phase elements don't behave as perfect condenser, but rather as a porous and inhomogeneous layer, through which the electrolyte can diffuse. In fact, the value is close to the Warburg impedance which, as stated, accounts for a mass transport through the pores of corrosion layers. This mechanism would determine the corrosion rate.

As a remarkable behavior, which distinguishes the nature of the layers formed in seawater with those formed in soil, it is worth underlining the appearance of the Warburg element in the circuit, which is correlated to the breakdown of the protective properties of the passive layer. This can be imagined as a compact layer where, perhaps due to the more aggressive

conditions, some pitting appears, leading to the breakdown of passivity. In marine environments, other compounds, such as atacamite $[Cu_2(OH)_3Cl]$ or copper sulphates can form and partially fill the pores, but still allows the mass transfer trough them. The figure (Figure IV.80) reports the qualitative model proposed.
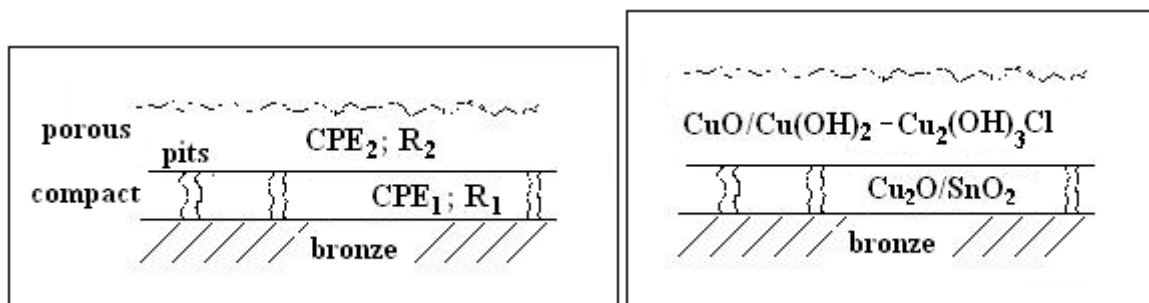
Figure IV.80. Qualitative model for the film formed on bronze after exposure to seawaters: on the right, the proposed structure of the film. In the case of Mediterranean seawater, due to the high presence of sulphates, the formation of copper sulphates (brochantite) is also likely to occur.

Chapter V

Conclusions

This thesis is mainly composed of two parts: one aimed to characterize degradation layers of archaeological bronzes and their burial context, and the second one, carried out on the basis of the results obtained in the first part, aimed to investigate the behavior of commercial bronze alloys in natural corrosion media. The commercial bronze alloys were chosen so that their composition resembled the one of ancient bronzes.

The project started from the scientific interest and the research question to study the long-term corrosion behavior of bronze alloys and it developed with the comparison with their short-term behavior in order to clarify the mechanisms of corrosion.

These points will be touched upon in the following general conclusions of the research work.

Archaeological context and physical-chemical characterization of soil

In this study, the collaboration with archaeologist from the Research Institute ICEM located in Tulcea, Dobrudja, Romania, has allowed to undertake an investigation of bronzes excavated from three different locations in the region, namely (L)Ibida, Argamum and Nufarul. A detailed description of the archaeological site, in terms of characterization of soil profiles, have been conducted and allowed to assess some general features of corrosion mechanisms.

As regards soil aggressiveness it can be stated that, even tough from a chemical point of view it is not corrosive, its texture shows a high porosity which implies an easy access to water and air. The main cause of a high dissolution rate of bronze alloys is therefore the alternate water saturation and instauration of the soil, for example on a seasonal scale.

Furthermore, ion chromatographic analysis carried out within a soil profile allowed to appreciate the increasing in chlorine concentration with depth.

Conservation state of archaeological findings and correlation with burial environments

Visual observation of the objects was the first mean of classification of archaeological bronzes according to the appearance of their corroded structures. Information regarding the colour, aesthetical appearance, hardness of external layers was reported, as well as details about the conservation of the original surface.

These observations let us classify these corrosion structures as mainly owning to the Type II corrosion patterns, even if few exceptions were observed. Anyway, a stratigraphic study of the patina helped to understand how the succession of corrosion layers has developed.

The spectroscopic investigation of corrosion products scratched from the objects' surface revealed their chemical nature and allowed achieving a general correlation about conservation state and burial environment.

As a general conclusion it can be observed that the main corrosion products are copper basic chlorides. This is in accordance with the visual observation of their state of conservation: most of them present coarse and uneven surfaces, characterized by concretions of green minerals. These are the ultimate results of the occurrence of *bronze disease*, an autocatalytic reaction induced by chlorine anions, leading to the formation of tri-hydroxo-chlorides. In few cases this has brought to the loss of the metal core, which is completely mineralized.

This result is understandable as the depth at which most of the object was found was below 2 m. At this profundity, the concentration of chlorine increase very much due mainly to the percolation rate, but also due to the presence of the Black Sea in the vicinity of the site.

Non-invasive identification of corrosion products

A certain attention in the present work has been given to the non-invasive methodologies for the detection of corrosion compounds. We have analyzed the external corrosion concretions by specular and diffuse reflection techniques using a micro-FTIR spectrometer.

Few objects presented two different green spots: one light green in colour and amorphous in nature, while the other one well crystallized in a dark green mineral.

It has been possible to clearly recognize the spectral features of copper tri-hydroxo-chlorides using the two mathematical corrections, Kramer Kroning Transformation (KKT) for the crystalline sample surface and Kubelka Munk (KM) for the amorphous one.

Classification of corrosion features

A significant number of archaeological bronzes were investigated for this study. The variability of ancient alloys, in terms of nature and amount of alloying elements and microstructures, render it difficult to establish absolute and commonly valid mechanisms of degradation. Even though the results obtained shall be considered as case studies and not valid in general, some features can be generalized.

Optical methods, such as optical microscope (OM) and Scanning electron microscope coupled with energy dispersive spectrometer (SEM-EDX), have allowed conducting an ample study of the cross section of selected corroded samples. On this basis, it is possible to point out three main corrosion features according to the elements characterizing the cross-section, starting from the metal core, towards the external layers.

- *Decuprification.* This phenomenon can be verified by the evaluation of Cu/Sn ratio in the corrosion layers, which have much lower values (0.65-2.95) if compared to the same ration in the metal core (9.4-62.9).

  A distinction shall be done here between Type I („even" surfaces) and Type II structures („coarse" surfaces). In the first case, this feature is much more pronounced and corrosion layers do not contain a cuprite layer at the interface between the sound alloy and the external corrosion layers. On the contrary, for coarse surfaces and corroded structures characterized by striated textures, several layers of cuprite are detected, well identifiable by the orange/red hues simply by optical microscope observation. These layers are characterized by a very low amount of tin and, therefore, this account for the high values (up to 65) of the Cu/Sn ratio reported.

- *Correlation microstructure-corrosion behavior.* Different corrosion patterns occur according to the microstructure of the alloy: *intergranular corrosion* is observed for homogeneously recrystallized α-phase, while for *dendritic microstructures*, the copper-rich, α-phase is selectively dissolved with respect to the tin-rich phase.

  The main corroding agent, as previously mentioned, is chlorine. Its mechanisms of action are based on its ability to diffuse through the porous and electrolytic conductor layer of cuprite, to react directly with the alloy forming cuprous chloride (Cu_2Cl_2). Its presence was very clearly put in evidence on one of the analyzed case studies (Ib.05.8). In this case the original surface of the object could not be identified among the corrosion deposit and a complex succession of layers makes up the *patina*.

  It was particularly interesting to observe the conservation state of the original surface for an ancient cast Greek pre-coin. The corrosion has mainly involved the α-phase, and the ghost structure of the tin-rich phase is still visible due to the oxidation of tin to the highly insoluble tin oxide (SnO_2, cassiterite) or its hydrated compounds.

  The issue of preferential corrosion in dendritic structure is still contradictory in the literature. It was advanced the hypothesis of the role of oxygen: it seems that in aerated environments it is the (α+δ)-phase corroding first, while in anaerobic media the α-phase is preferentially attacked. The result obtained can represent a confirmation of this hypothesis as the characterization of archaeological contexts has revealed the porous nature of soils and the facility of water and air movements within the soil profile.

- *Effect of the alloying elements.* Most of the case studies were comprised of pure copper-tin alloys, in few cases the minor presence of other elements were detected.

Only one case study presented a typical brass composition with a Zn content of ~ 16 wt. %.

It is worth pointing out here the effect on Sn, which is not always associated with the presence of a protective, passive-like layer, as objects with comparable amount of tin in their sound alloy showed different corrosion behavior. Probably this is due to the environmental parameters and their influence of the corrosion rate of the alloy. In most aggressive condition it is unlikely to form a compact and protective layer, and mass transport of anions inward could take place easily.

The behavior of zinc is widely documented in the literature and the results obtained confirmed the dezincification process which leads to the selective dissolution of zinc from the alloy, which forms soluble compounds and, therefore, is not detected among the corrosion layers.

Lead is insoluble in the Cu-Sn alloy at every concentration, therefore it is found as globules dispersed in the alloy matrix. It was found an enrichment of lead compounds (probably cerussite, $PbCO_3$) within the corrosion layers.

Uncommon degradation patterns were also encountered and pointed out. These were mainly related to the presence of unusual corrosion products, such as copper sulphides (mainly spionkopite and covellite), which have been detected on a copper coin hoard excavated next to the Danube river. These compounds are usually found where microbial consortia, under anaerobic conditions, are able to produce sulphidric acid, which could react with the alloy elements.

Furthermore, it was reported the case of a finely striated textured structure, whose interpretation was challenging, and most likely understood using the model of oscillatory reactions, due to fluctuating environmental conditions, perhaps on a seasonal scale.

Electrochemical behavior of bronze in natural environments

Electrochemical measurements allowed evaluating the corrosiveness of soil and investigating the corrosion behavior of bronze in different electrolytes. The comparison of these results with data obtained for more aggressive solutions allows a better understanding of the phenomena, which occurs based on the kind of medium that serve as electrolyte (the aggressiveness of the solution was obtained by increasing (x2 and x10) the concentration of Chlorine, Nitrate, Phosphate and Sulphate, in respect to the one measured for soil extracts, respectively A and B; and also Black Sea and Mediterranean seawaters),. The optical, structural and elemental characterization has allowed to conduct an ample study of the

electrodes' surface after electrochemical experiments and represented an important tool to confirm the advanced hypothesis.

Commercially available bronzes (Cu11Sn) were chosen on the basis of tin content, which had to be comparable to that encountered in the case studies. Results have shown that the presence of tin significantly influences the electrochemical behavior of bronze, which, in the aggressive, chlorine-containing medium, such as seawater, present a higher corrosion resistance if compared to pure copper.

- Electrochemical experiments carried out in soil solution evidenced its non-aggressiveness, which is demonstrated by the very low value of current densities recorded for the cyclic voltammetry. The shape of potentiodynamic curves presents the "*hysteresis-like loop*", typical of pitting corrosion. Optical characterization of surface electrodes confirmed it.

- The employment of more concentrated solutions, aimed to simulate specific condition which could occur in soil, has allowed to further study the phenomenon of localized corrosion by optical and elemental techniques. These have evidenced the selective dissolution of copper within the pit, and the enrichment in tin, possibly due to the formation of SnO_2. Moreover, the optical characterization of some corroded areas have evidenced a selective attack of the α-phase, instead of the (α+δ)-phase. This is a particularly interesting result as it is comparable with those observed for ancient bronze alloys, encountered as case studies. Nonetheless, this topic remains a controversial issue, as there are evidences in the literature of preferential corrosion at expenses of the tin-rich phase. Further experiments would be necessary to clarify this phenomenon.

- The electrochemical experiments carried out for bronze in seawaters (Black Sea and Mediterranean Sea) showed a very different behavior. The anodic region of the current density-potential curves presents three peaks, occurring with different current densities and potentials for the two seawaters. These can be related to the formation of different species, which can be identified as copper and tin oxides and hydroxides, even though, the presence of chlorine, would lead to the formation of species such as CuCl or coordinative compounds $[CuCl_2]^-$. Anyhow, in these media the main corroding agent is found to be chloride, in spite of the presence of significant amount of sulphate as well.

- A better understanding of the nature of corrosion layers formed on bronze electrodes exposed to different environments was obtained by electrochemical impedance spectroscopy. The results obtained allowed us proposing a qualitative model for their surface structures. The surface of the electrodes kept in soil for a period of 30, 60 and 90 days exhibit the formation of a double-structured layer consisting of a passive film, covered by a porous and defectiveness layer. The passive film may be due to the formation of a compact tin oxide layer. In case of electrodes exposed to seawater, the surface structure was also found to be characterized by a double-structured layer. The appearance of a Warburg element in the equivalent circuit (EC) is correlated in this case with the breakdown of the passive layer and the presence of pits partially filled with salts, and thus can be identified as an inhomogeneous and uneven porous layer.

Final remarks

A concluding observation, as final outcome of the research, is driven by the author's desire to propose some general conservation guidelines in order to better preserve excavated archaeological artifacts.

During the present work, the detrimental effect of chlorine anions on degradation of bronze object recovered from the archaeological site of Dobrudja (Romania), was pointed out. The occurrence of *bronze disease* was mostly detected for artifacts excavated in 2005 and thus probably stored under unsafe environmental conditions.

The investigation has evidenced the occurrence of cuprous chlorine within the corrosion layers, beneath several cuprite layers and therefore protected from the interaction with moisture and oxygen, which would cause the formation of hydroxyo-chlorides, having a higher relative volume and therefore leading to the disruption of the original surface.

In this condition, excavated bronzes shall be preserved either under wet conditions or under dry condition, in this last case it very important to avoid any oxygen contamination.

Critics to the present work and proposals for future developments

A general limitation, when dealing with scientific investigation on works of art, is the limited availability of samples or sampling opportunities. Moreover, in case of the present work, the choice of samples could not be based only to scientific requirements, but more likely, to the accessibility of the objects excavated which were carefully chosen with archaeologists.

A useful study would consider objects similar in shape, dimensions, composition and microstructure, possibly originating from different archaeological sites, and thus exposed to different environments. This opportunity would be given by the proposals and implementation of projects involving different Institutions and, perhaps, Countries, leading to an interchange of results.

As far as electrochemical experiments are concerned, it is surely worth mentioning that the present work gave an interesting insight into the behavior of bronze alloys in natural environments. An opportunity for future developments would be based on the choice of material as its microstructure was found to have an important influence of corrosion behavior. Perhaps the collaboration with artistic foundries, if available to experiment ancient metallurgical techniques, would be a choice to carry out further experimentation. Also, the chance to sacrifice ancient artifacts themselves would be a possibility to further investigate the nature of natural corrosion layers produced over a long timescale, surely nor comparable with the laboratory's time constrictions.

Furthermore, even thought coupling optical and elemental methods to the electrochemical investigation has allowed an ample characterization of corrosion structures, more powerful analytical techniques, such as synchrotron-based FTIR spectroscopy or X-rays diffraction could be used to determine the molecular nature of corrosion compounds.

References

Ammelot, F. *et al.*, (1999) Characterization of the Oxide Layers on a Cu-13Sn Alloy in a NaCl Aqueous Solution Without and With 0.1 M Benzotriazole. Electrochemical and Photoelectrochemical Contributions, *Electrochimica Acta* **44** 2549-2558;

Angelini, E. *et.al.*, (1998) Effect of Burial in Different Soils on the Decay of Iron Artefacts. Laboratory investigation. METAL98 *Proceedings* 106-110;

Atkins, P. (1997). *Chimica Fisica.*, IIIrd Ed. Zanichelli, Bologna, Italia;

Babic, R. *et al.,* (2001) A study of Copper Passivity by Electrochemical Impedance Spectroscopy, *Journal of the Electrochemical Society* **148 4** B146-B151;

Bard A.D. and R. Faulkner, (1980) *Electrochemical Methods*, Wiley, New York, p.316,;

Beljoudi, T. *et.al.,* (2001) Surface Modification Processes on European Union Bronze Reference Materials for Analytical Studies of Cultural Artefacts, *La revue de metallurgie*;

Bernard, M.C., Joiret, S. (2009) Understanding corrosion of ancient metals for the conservation of cultural heritage, *Electrochimica Acta* **54** 5199-5205;

Bellezze, T., *et al.* (2004), Electrochemical characterization of three corrosion-resistant alloys after processing for heating-element sheating, *Electrochimica Acta* **49** 3005-3014;

Bernardi, E., Chiavari, C., Lenza, B., Martini, C., Morselli, L., Ospitali, F., Robbiola, L., (2009) The atmospheric corrosion of quaternary bronzes: the leaching action of acid rain. *Corrosion Science* **51** 159-170;

Bertholon, R., (2001) The Original Surface of Corroded Metallic Archaeological Objects: Characterization and Location, *La Revue de Metallurgie*;

Brown, B.E *et al.* (Ed.) (1977), Corrosion and Metal Artefacts: A dialogue between Conservators and Corrosion Scientists. National Bureau of Standards Special Publication 479, Washington D.C.;

Calliari, I., Dabalà, M. Brunoro, Ingo, G.M., (2000) Advanced Surface Techniques for Characterization of Cu-based artefacts, *Journal of Radioanalytical and Nuclear Chemistry,* **247, 3** 601-608;

Callister, W.D. Jr., (2003) Materials Science and Engineering: An Introduction, Ed. VI, Wiley Interscience;

Cano, E. *et al.* (2009) Use of EIS for the evaluation of the protective properties of coating for metallic cultural heritage: a review. *Journal of Solid State Electrochemistry* **on line version**;

Casaletto, M.P. *et.al.* (2006) Production of Reference "Ancient" Cu-based Alloys and their Accelerated Degradation Methods, *Appl.Phys. A* **83** 617-622;

Chaker, V. and Palmer, D. (1987) Effects of soil characteristics on corrosion, Proceedings of the symposium helded in Cincinnati, Ohio, 12 May 1987. ASTM Committe G-1-Corrosion on metal- ISBN 0-8031-1189-4;

Chase, W.T., (1995) Chinese Bronzes: Casting, Finishing, Patination and Corrosion, METAL95 *Proceedings*, 85-118;

Chiavari, C., Rahmouni, K., Takenouti, H., Joiret, S., Vermaut, P., Robbiola, L., (2007) Composition and electrochemical properties of natural patinas of outdoor bronze monuments, *Electrochemical Acta* **52** 7760-7769;

Constantinides, I. *et.al.*, (2002) Surface Characterization of Artificial Corrosion Layers on Copper Alloy Reference Materials, *Applied Surface Science* **189** 90-101;

Dayal, H.M., *et al.*, (1988) Underground Corrosion by Microorganisms. Part-1: Analytical Studies of Some Indian Soils, *Def.Sci.J.* **38 2**;

Debiemme-Chouvy, C. *et al.*, (2001) X-ray photoemission investigation of the corrosion film formed on a polished Cu-13Sn alloy in aerated NaCl solution, *Applied Surface Science*, **174** 55-61;

Derrick, M.R., Stulik, D. C. *et al.* (1999) Infrared spectroscopy in conservation science. Los Angeles, The Getty Conservation Institute;

DIN Standard 50929 (1997) "Soil Archives classification in terms of impacts of conservability of archaeological heritage" Technical Report;

Dorigo, A., Fiaud, C., Labbè, J-P., Robbiola, L., Brunella, P., Bocking, H., (1998) Characterization of the corrosion structures of Roman copper alloys by SEM and EDSX.

IMMACO: Improvements of Means of Measurements on Archaeological Copper Alloys for Characterization and Conservation, *METAL 98,* James &James Publishers, 145-151;

Dos Santos, L.M.M., Lemos Salta M.M., Fonseca, I.T.E., (2007) The electrochemical behavior of bronze in synthetic seawater, *Journal of Solid State Electrochemistry* **11** 259-266;

Efestus Project Report 2007, INCO-MED CONTRACT No. ICA3-CT-2002-10030; coordinated by G.M. Ingo (ISMN-CNR) www.efestus.just.edu.jo/index.jsp ;

Escalante, E. (1989) Concepts of underground corrosion, *Effects of Soil Characteristics on Corrosion*, ASTM, STP 1013, V. Chaker and J.D. Palmer, Eds., American Society for Testing and Material, Philadelphia, pp. 81-94;

Evans, H.T., *et al.*, (1976) Crystal Structure Refinement of Covellite, *American Mineralogist,* **61** 996-1000;

Feipeng, Sun (2009) *private communication*;

Fjaestad, M. *et al.*, (1996) Environmental Threats to Archaeological Artefacts, *ICOM Committee for Conservation*;

Fjaestad, M. *et al.*, (1997) The Decay of Archaeological Copper-Alloy Artefacts in Soil, *METAL95 Proceedings*;

Franceschi, E. *et.al.,* (1998) The Corrosion of Metallic Artefacts within Different Environments. Archaeological objects and laboratory simulation. METAL98 *Proceedings* 92-93;

Franquelo, M.L. *et al.* (2009) Comparison between micro-Raman and micro-FTIR spectroscopy techniques for the characterization of pigments from Southern Spain Cultural Heritage, *Journal of molecular structure*, **924-926** 404-412;

Frost,R.L., *et al.* (2002) Raman spectroscopy of the basic copper chloride minerals atacamite and paratacamite: implications for the study of copper, brass and bronze objects of archaeological significance, *Journal of Raman Spectroscopy*, **33** 801-806;

Frost, R.L. (2003), Raman spectroscopy of selected minerals of significance in corrosion, *Spectrochimica Acta Part A*, **59** 1195-1204;

Galliano, F. *et.al.,* (1998) Monitoring Metal Corrosion and Soil Solution at Two Excavation Sites and in the Laboratory, METAL98 *Proceedings* 87-91;

Garagnani, G. and Martini C. (2004) Indagini microstrutturali dei manufatti metallici di interesse archeological ed artistico, in *Studio e Conservazione di manufatti metallici*-Nardini Editore-Firenze 2004;

Gerwin, W. and Baumhauer, R., (2000) Effect of Soil Parameters on the Corrosion of Archaeological Metal Finds, *Geoderma* **96** 63-80;

Gettens, R.J. (1975) Patina: Noble and Vile, *Art and Technology: A symposium on classical bronzes*, The MIT Press;

Garagnani, G.L., Martini, C., (2004) Indagini Microstrutturali dei Manufatti Metallici di Interesse Archeologico ed Artistico, in *Studio e Conservazione di Manufatti Archeologici –* Nardini Editore – Firenze;

Glazov, N.N. *et al.,* (2006) Soil Corrosion of Differential Aeration Cells and Condition of Their Operation, *Protection of Metals*, **42 3** 238-243;

Goldstein, J. *et al.*, (2003) Scanning Electron Microscopy and X-Rays Microanalysis, III Ed. Springer Science+Business Media, Inc.;

Graedel, T.E., *et al.* (1987) Copper patinas formed in the atmosphere-I. Introduction, *Corrosion Science*, **27 7** 639-657;

Graedel, T.E., *et al.* (1987) Copper patinas formed in the atmosphere-II. A qualitative assessment of mechanisms, *Corrosion Science*, **27 7** 721-740;

Hamilton D.L. (1998) *Methods of Conserving Underwater Archaeological Material Culture*, Conservation files: Antropology 605, Conservation of Cultural Resources I, Nautical Archaeology Program, Texas A&M University. Downloaded from: http://nautarch.tamu.edu/class/anth605/File0.htm ;

Ingo, G.M. *et.al.*, (1995) Chemical and Metallurgical Aspects in Bronze Punic Coins, Proceedings of the 1st Congress on "Science and Technology for the Safeguard of Cultural Heritage in the Mediterranean Basin", vol.1, Catania, Siracusa, Italia;

Ingo, G.M., *et al.,* (2004) Combined Use of Surface and Micro-Analytical Techniques for The Study of Ancient Coins, *Appl.Phys. A* **79** 171-176;

Ingo, G.M, *et al.*, (2006) Uncommon corrosion phenomena of archaeological bronze alloys, *Applied Physics, A* **83** 581-588;

Jedrzejewska, H., (1976) "A corroded Egyptian bronze: Cleaning and discoveries", Studies in Conservation, 21 101–114;

Jones, D. (1996) Principles and Prevention of Corrosion, Prentice Hall;

Leoni, M., (1984) Elementi di Metallurgia Applicata al Restauro delle Opere d'Arte, *Corrosione e conservazione dei manufatti metallici*, OpusLibri, Firenze;

Letardi, P., *et al.*, (1998) Application of electrochemical impedance measurements as a tool for the characterization of the conservation and protection state of the bronze works of art, *Metal 95*, James and James (Science Publishers) Ltd., pp 303-308;

Leyssens. Karen (2006) Monitoring the conservation treatment of corroded cupreous artefacts: The use of electrochemistry and synchrotron radiation based spectroelectrochemistry. PhD Thesis, Ghent University

Lins, A. and Power, T., (1995) The Corrosion of Bronze Monuments in Polluted Urban Sites: A Report of the Stability of Copper Mineral Species at Different pH Levels*,* METAL95 *Proceedings*, 119-151;

Lucey, V.F., (1972) Developments Leading to The Present Understanding of the Mechanism of Pitting Corrosion of Copper, *British Corrosion Journal* **7** 36-41;

Kaihara, M. and Sato, Y., (2000) Extraction of Diffuse Reflection Spectrum on Reflectance Spectroscopy for Solid or Powder Surfaces, *Spectrochimica Acta Part A***, 56** 897-900;

Kear, G., *et al.*, (2004) Electrochemical corrosion of unalloyed copper in chloride media-a critical review, *Corrosion Science* **46** 109-135;

Kars, H., (1998) Preserving our in situ archaeological heritage: a challenge to the geochemical engineer. *Journal of Geochemical Exploration* **92** 139-147;

MacDonald, D. and Urquidi-MacDonald M., (1990) Theory of Steady State Passive Films, *Journal of Electrochemical Society* **137 8** 2395;

MacDonald, D., (1992) The Point Defect Model for the Passive State, *Journal of Electrochemical Society* **139 12** 3434-;

Malvault, J.Y. *et al.* (1995) Cathodic reduction and infrared reflectance spectroscopy of basic copper (II) salts on copper substrate, *Journal of applied electrochemistry* **25** 841-845;

Mansfeld, F., (2007) The Interaction of Bacteria and Metal Surfaces, *Electrochimica Acta* **52** 7670-7680;

Marcus, P. (2002) Corrosion Mechanisms in Theory and Practice, II Ed. Marcel Dekker, Inc.;

Martens, W., Frost, R.L., Williams, P.A. (2003), Raman and infrared spectroscopy study of the basic copper chloride minerals – Implication in the study of the copper and brass corrosion and "bronze disease", *Neues Jahrbuch für Mineralogie* **175 2** 197-215;

Mattson, E. *et.al.,* Deterioration of Archaeological Material in Soil. Results on Bronze Artefacts. *Central Board of National Antiquities, National Historical Museum, Conservation Institute.* Riksantikvarieambetet, 1996.

Mazzeo, R., (2004) Patine Su Manufatti Metallici, LE PATINE:Genesi, Significato e Conservazione. *Proceedings of the conference,* Firenze, Nardini Editore. Kermes quaderni: 29-43;

McNeil, M.B. and Little, B., (1992) The Use of Mineralogical Data in Interpretation of Long-Term Microbiological Corrosion Processes: Sulfiding Reactions, *JAIC*, **38, 2,** art.6;

McNeil, M. and Little, B. (1999) Corrosion Mechanisms for Copper and Silver Objects in Near-Surface Environments, *JAIC*, 31, 3, art.7;

North N.A., MacLeod I.D. (1987) Corrosion of Metals, in: Pearson C., *Conservation of Marine Archaeological Objects*, Butterworths, London, 68-98;

Mourey, W. (1987) *La conservation des antiquités métalliques,* Draguignan;

Nord, A.G., Mattson, E., Tronner, K., (2005) Factors Influencing the Long-Term Behavior of Bronze Artefacts in Soil, *Protection of Metals* **41** 339-346;

Oddy, W.A. and Meeks, N.D., (1982) Unusual phenomena in the corrosion of ancient bronzes, *Science and Technology,* IIC Washington Congress, Brommelle&Thomas Ed. pp 119-124;

Ostroumov M., Lasnier B., Lefrant S. (1995). Infrared reflection spectrometry of gem materials *Analysis* 23, 39-45.

Ostroumov M., Lasnier B., Lefrant S., Fritsch E. (2000). Infrared reflection spectrometry of minerals and gemological materials, Available at: http://mineral.virtualave.net ;

J.Pan, D.Thierry, C.Leygraf (1996) *Electrochimica Acta*, **41** 1143-;

Pîrnău, R. (2009) – *Cercetări pedologice în situl arheologic Slava Rusă (judeţul Tulcea). Contribuţii la studierea interdisciplinară a sitului*, capitol în Simina Stanc (ed.), Arheozoologia primului mileniu d.Hr. pentru teritoriul cuprins între Dunăre şi Marea Neagră, Editura Universităţii „Alexandru Ioan Cuza", Iaşi, ISBN 978-973-703-448-9;

Plenderleith, H.J. and Werner, A.E.A. (1971) The conservation of antiquities and works of art. Treatments, Repair and Restoration, II edition, Oxford University Press;

Pourbaix, M. ( ) Atlas of electrochemical equilibria in aqueous solutions, Pergamon Press Cebelcor;

Rahmouni, K., *et al.*, (2005) Corrosion of Copper in 3% NaCl Solution polluted by Sulphide Ions, *Corrosion Science* **47** 3249-3266;

Rocchini, G., (1993) Corrosion Rate Monitoring by the Linear Polarization Method, *Corrosion Science* **34 12** 2031-2044;

Robbiola, L., Queixalos, I., Hurtel, L.-P., Pernot, M., Volfovsky, C., (1988) Etude de la Corrosion de Bronzes Archaeologiques du Fort-Harrouard : Alteration Externe et Mecanisme d'Alteration Stratifiee, *Studies in Conservation* 33 205-215 ;

Robbiola, L., Fiaud, C., (1992) Apport de l'analyse statistique des produits de corrosion a la comprehesion de processus de degradation des bronzes archeologiques, *Revue d'Archéometrie,* **16** 109-119 ;

Robbiola, L, Fiaud, C., (1993) Corrosion structures of long-term burial Cu-Sn alloys-influence of the selective dissolution of copper, *Editions de la Revue de Métallurgie,* n.6, 157-162 ;

Robbiola, L., Fiaud, C., (1994)Basic structure of passive layers of Cu-Sn alloys applied to patinas of archaeological bronzes, *Electron microscopy, Les Editions dePhysique*;

Robbiola, L., Blengino, J.-M., Fiaud, C., (1998) Morphology and Mechanisms of Formation of Natural Patinas on Archaeological Cu-Sn alloys, *Corrosion Science,* **40, 12** 2083-2111;

Robbiola, L., Pereira, N., Thaury, K., Fiaud, C., Labbè, J-P, (1998) Decuprification phenomenon of Cu-Sn alloys in acqueous solution in nearly neutral pH conditions, *METAL 98*, James&James Publishers, 136-144;

Robbiola, L., *et al.*, (2001) A New Data for Improving Authentication of Bronze Artefacts, *Proceeding of the ICOM Committee for Conservation of Metals Working Groups, METAL2001* 117-122;

Robbiola, L. and Portier, R., (2006) A Global Approach to the Authentication of the Alloy-Patina-Environment System, *Journal of Cultural Heritage* **7** 1-12;

Robbiola, L. *et al.*, (2008) Characterization of Anodic Layers on Cu-10Sn Bronze (RDE) in Aerated NaCl Solution, *Corrosion Science* **50 8**2205-2215;

Romanoff, M., (1957) Underground Corrosion, National Bureau of Standards;

Sandu, I., Ursulescu, N., Sandu, I.G., Bounegru, O., Sandu, I.C.A., Alexandru, A., (2008) Pedological Stratification Effect of Corrosion and Contamination Products on Byzantine Bronze Artefacts, *Corrosion Engineering, Science and Technology* **43 3** 256-266;

Sandu, I.G., Stoleriu, S., Brebu, M., Sandu, A.V., (2005), Autentificarea monedelor antice din bronz prin studiul patinei arheologice: I. Compositie si structura, *Revista de chimie,* (Bucuresti), **56 10;**

Satovic, D. Valek Zulj, L., Desnica, V., Fazinic, S., Martinez, S. (2009) Corrosion evaluation and surface characterization of the corrosion product layer formed on Cu-6Sn bronze in aqueous Na_2SO_4 solution, *Corrosion Science* **available on line;**

Schweizer, F., (1995) Bronze Objects From Lake Sites: From Patina to Biography, METAL95 *Proceedings*, 32-50;

Scott, D.A., (1985) *Periodic* corrosion phenomena in bronze antiquities, *Studies in Conservation,* 30 49-57;

Scott, D.A., (1990) Bronze Disease: A Review of Some Chemical Problems and the Role of Relative Humidity, *JAIC*, 29, 2, 193-206;

Scott, D., (1991) Metallography and microstructure of Ancient and Historic Metals, GCI,;

Scott, D.A., (1994) An examination of the patina and corrosion morphology of some Roman bronzes, *JAIC* **33 1 1** pp. 1-23;

Scott, D., (2002) Copper and Bronze in Art: corrosion colorants, conservation. Los Angeles, The Getty Conservation Institute;

Sidot, E., Berthelin, S., Kahn-Harari, A., Robbiola, L., (2001) Structural characterization of copper-tin based alloys: Evolution of the unit cell constant of alpha bronze with tin content, *METAL 2001, Proceedings of the ICOM Committee for Conservation Metals Working Group*, 123-130;

Sidot, E. *et al.*, (2005) The Lattice Parameter of α-bronzes as a function of solute content: application to archaeological materials, *Materials Science and Engineering A* **393** 147-156;

Sidot, E., *et al.*, (2006) Study of the Corrosion Behavior of Cu-10Sn Bronze in Aerated Na_2SO_4 Aqueous Solution, *Corrosion Science* **48** 2241-2257;

Souissi, N., *et al.* (2007) Corrosion Behavior of Cu-10Sn Bronze in Aerated NaCl Aqueous Media – Electrochemical Investigation, *Corrosion Science* **49** 3333-3347;

R.M.Souto, M.Alanjali (2000) *Corrosion Science*, , **42**, 2201-;

R.M.Souto, M.M.Laz, R.L.Reis (2003) *Biomaterials*, *24*, 4213-;

Stambolov, T., (1985) The Corrosion and Conservation of Metallic Antiquities and Works of Art, CL Publication, Central Research Laboratory for Objects of Art and Science, Amsterdam,;

Stoch, A., (2001) FTIR Studies of Copper Patinas in The Urban Atmosphere, *Journal of Molecular Structure* **596** 201-206;

Taylor, R.J. and MacLeod, I.D., (1985) Corrosion of bronzes on shipwrecks. A comparison of corrosion rates deduced from shipwreck material and from electrochemical methods. *Corrosion-NACE* **41 2**;

Tylecote, R.F., (1979) The Effect of Soil Conditions on the Long-Term Corrosion of Buried Tin-bronzes and Copper, *Journal of Archaeological Science* 6 345-368;

Uhlig's Corrosion Handbook (2000) ed. R. Winston Revie, 2nd Ed. Electrochemical Society Series,;

Van der Schijff, O.J., *et al.*, (1993) AC-Induced Pitting of Tin-Coated Copper Utility Cables, *Corrosion Engineering Section-Corrosion*. 310-314 www.nace.org;

Vione, D. *et al.* (2006) *Environmental Science Technology* **40** 3775-.

Wadsak, M., *et al.*, (2000) Multianalytical Study of Patina Formed on Archaeological Metal Objects from Bliesbruck-Reinheim, *Mikrochimica Acta* **133** 159-164;

Wagner, D., *et.al.*, (1995) "Soil Archive" Classification in Terms of Impacts of Conservability of Archaeological Heritage. METAL95 *Proceedings* 21-26;

Wagner, D.H.J., *et.al.,* (1998) A Systematic Approach to the Evaluation of the Corrosion Load of Archaeological Metal Objects, METAL98 *Proceedings* 80-86;

Wang, J., Xu, C., Lv, G. (2006) Formation processes of CuCl and regenerated Cu crystals on bronze surfaces in neutral and acidic media *Applied Surface Science* **252** 6294-6303;

Wang, N., He J.-q., Sun, S.-y., Xiao, (2007) L., Bronze Samples in Various Typical Electrolytes, *Science of Conservation and Archaeology,* **19 4** 45-49;

Wayman, M.L., (2004) Metallography of Archaeological Alloys, in *Metallography and Microstructure*, Vol.9, *ASM Handbook*, ASM International, , p.468-477.

http://integratio.univeur.org/dobrogea_de_nord/default_en.asp?id=245;

Appendix I

FTIR-spectra

Appendix I –FTIR spectra-

Argamum
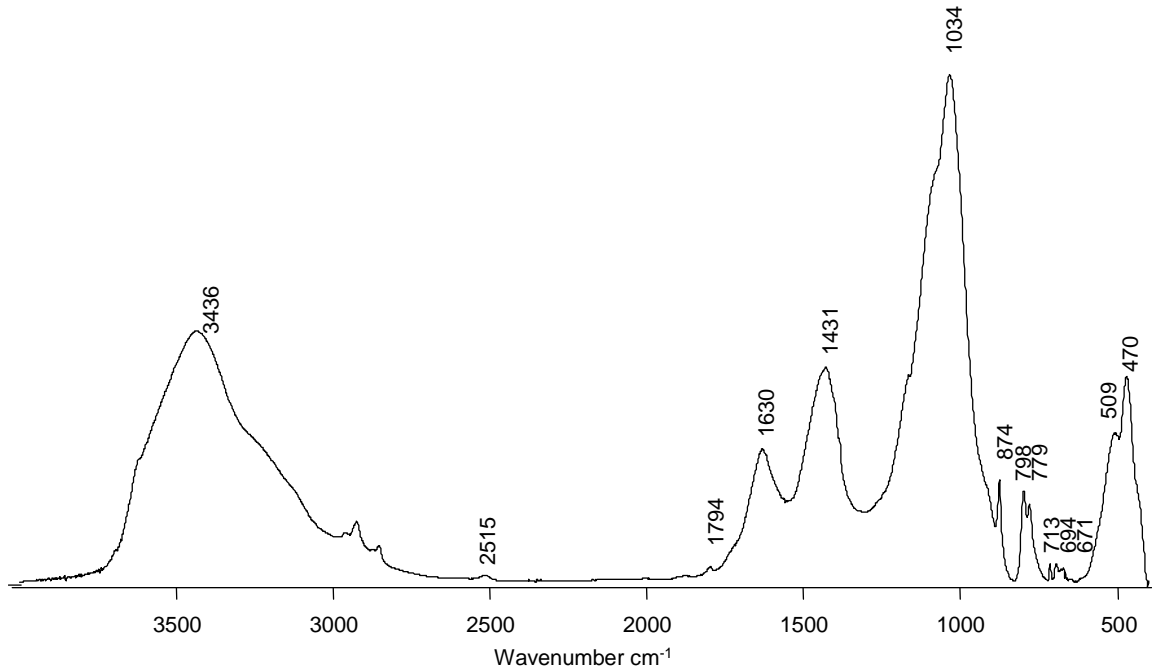
Figure.A.1. Arg.00.1: Quartz ,Aluminosilicates and Calcite were identified.
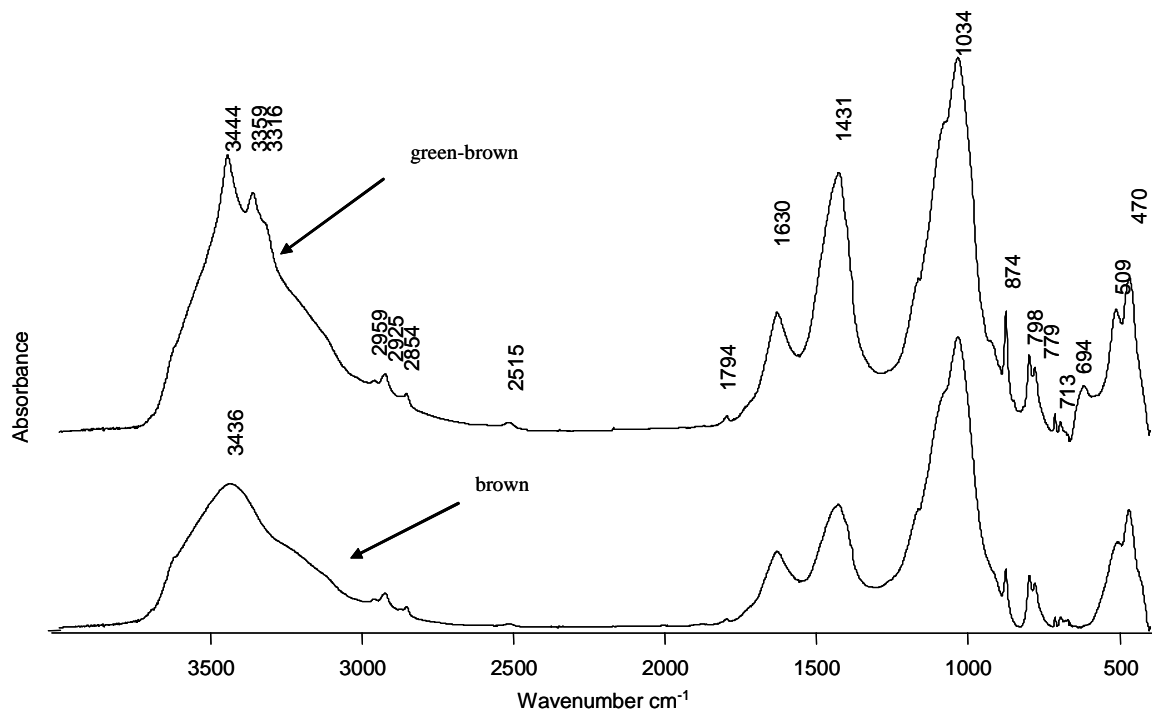
Figure A.2. Arg.00.6: Quartz, Aluminosilicates, Calcite were identified, while Atacamite is present as well in the green powder.

Ibida
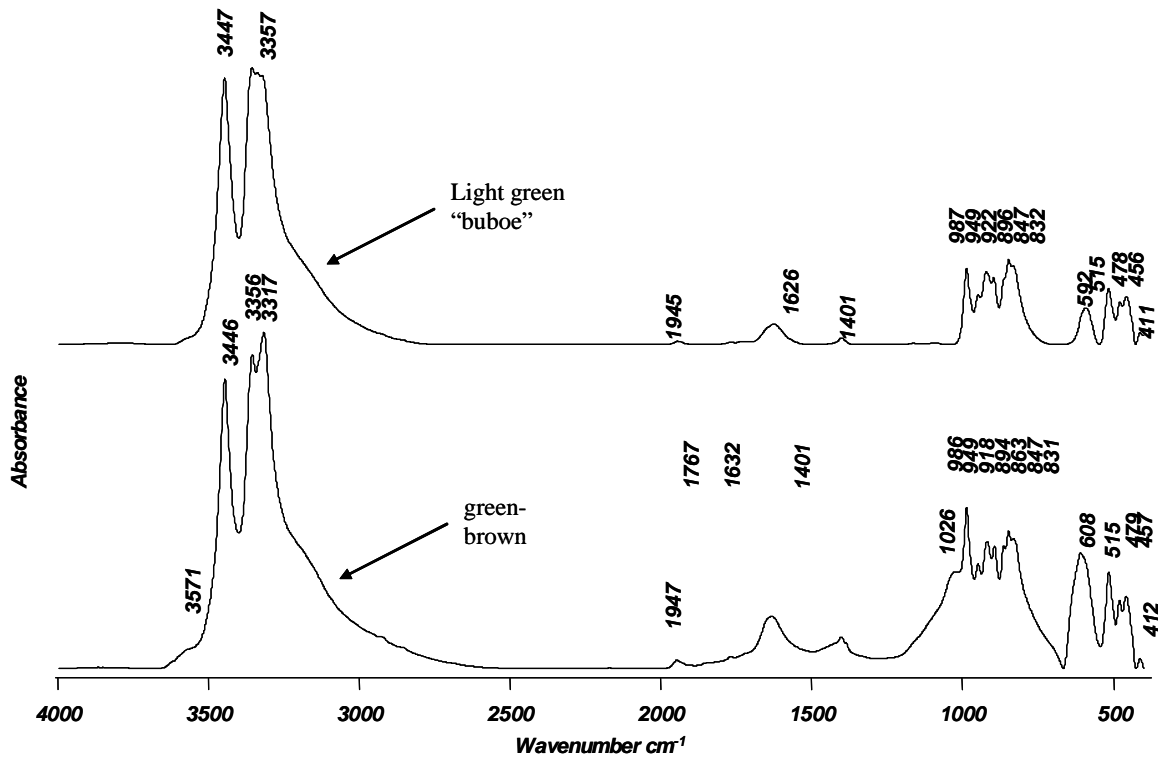
Figure A.2. Ib.05.2: Paratacamite was identified in both spectra.
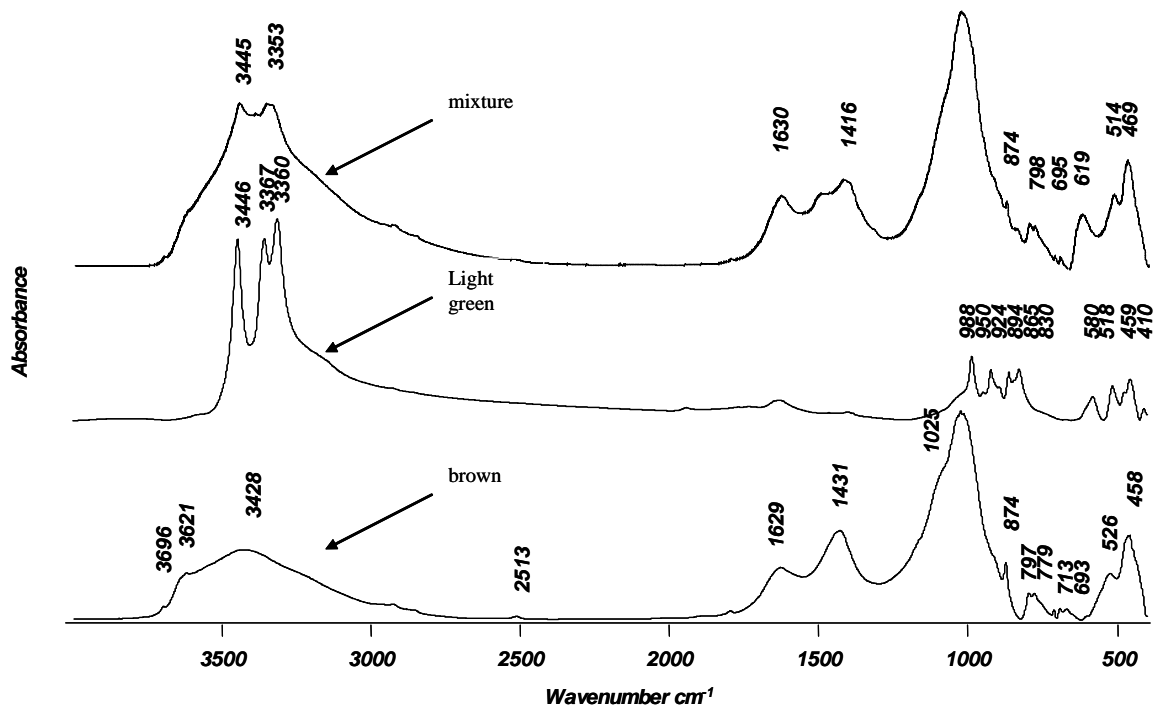
Figure A.3. Ib.05.03: the light green spectrum is identified as Paraatacamite, while the other two a mixture of Aluminosilicates, Calcite and Quartz.
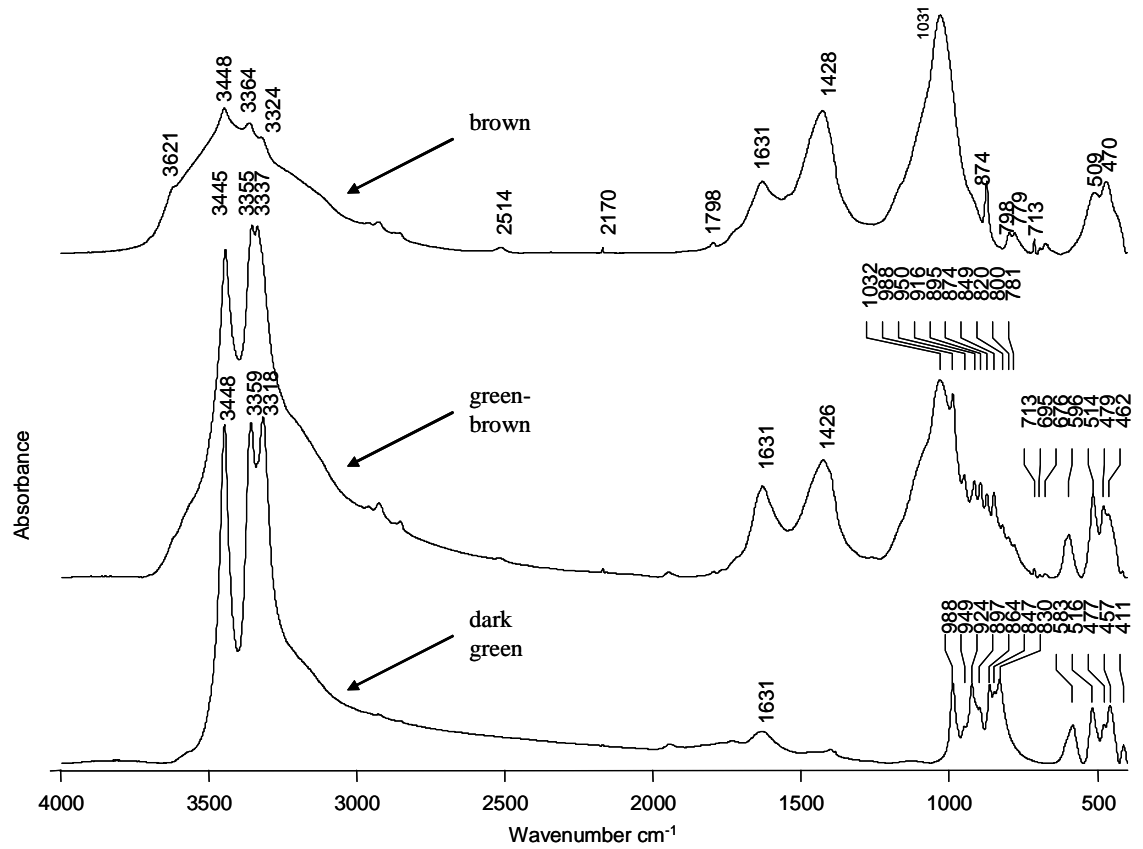
Figure A.4: Ib.05.6: Calcite, Aluminosilicates and Quartz were identified for the brown powder, while a mixture of Atacamite and Paratacamite and only Paratacamite for the green ones.
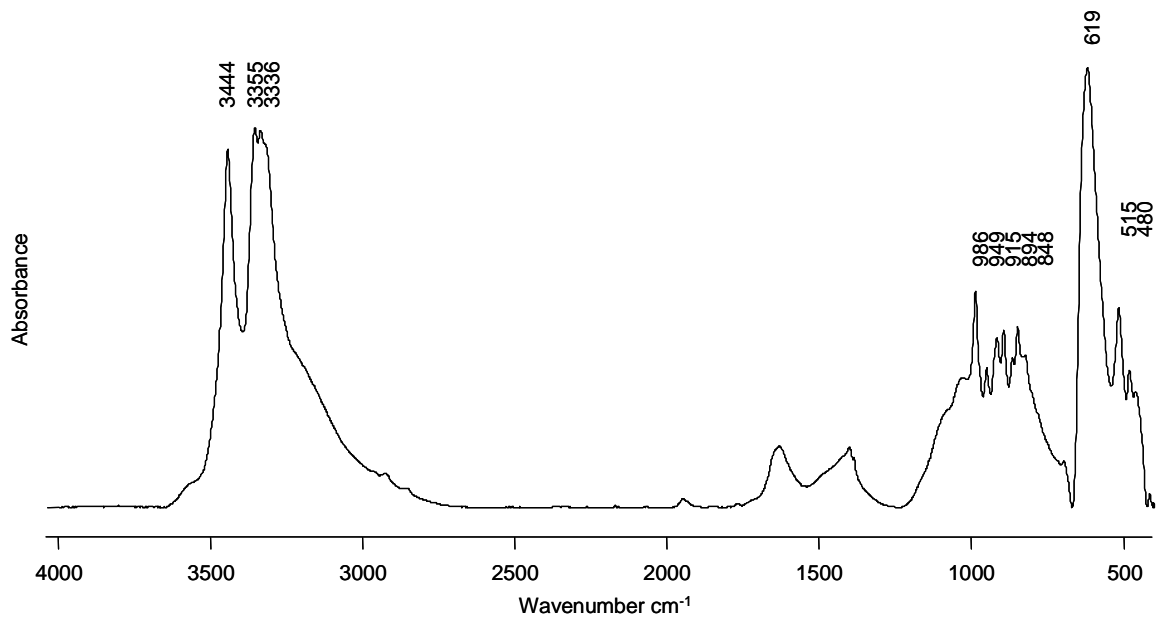
Figure A.5: Ib.05.8: a mixture of Paratacamite and Atacamite and Cuprite were identified, also basing on the red colour of the sample.
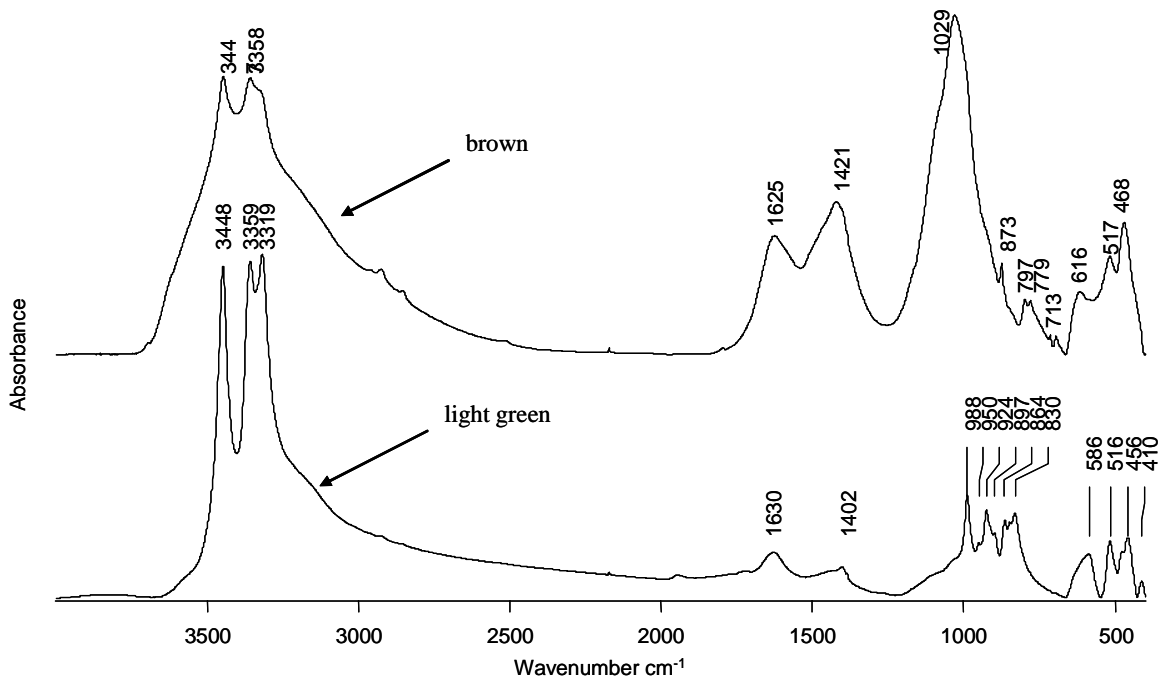
Figure A.6: Ib.05.10: Respectively, a mixture of Aluminosilicates, Calcite, Quartz and Paratacamite were detected for the brown sample, while Paratacamite was identified for the green one.
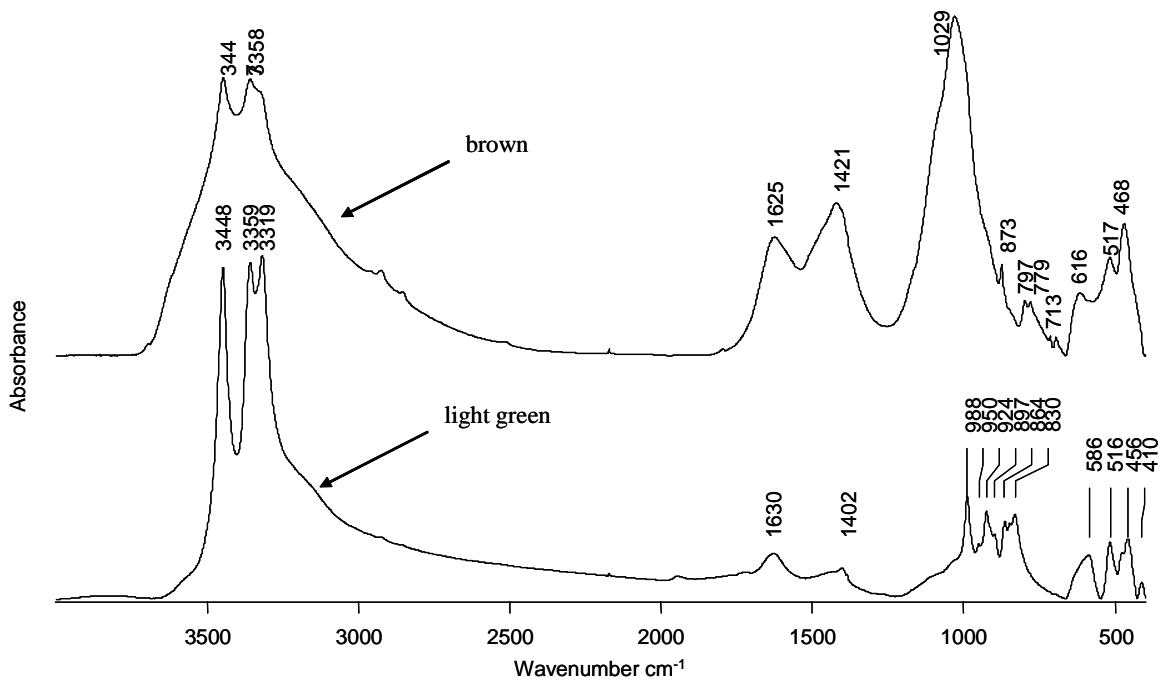
Figure A.7: Ib.05.12: Respectively, a mixture of Aluminosilicates, Calcite, Quartz and Paratacamite were detected for the brown sample, while Paratacamite was identified for the green one.
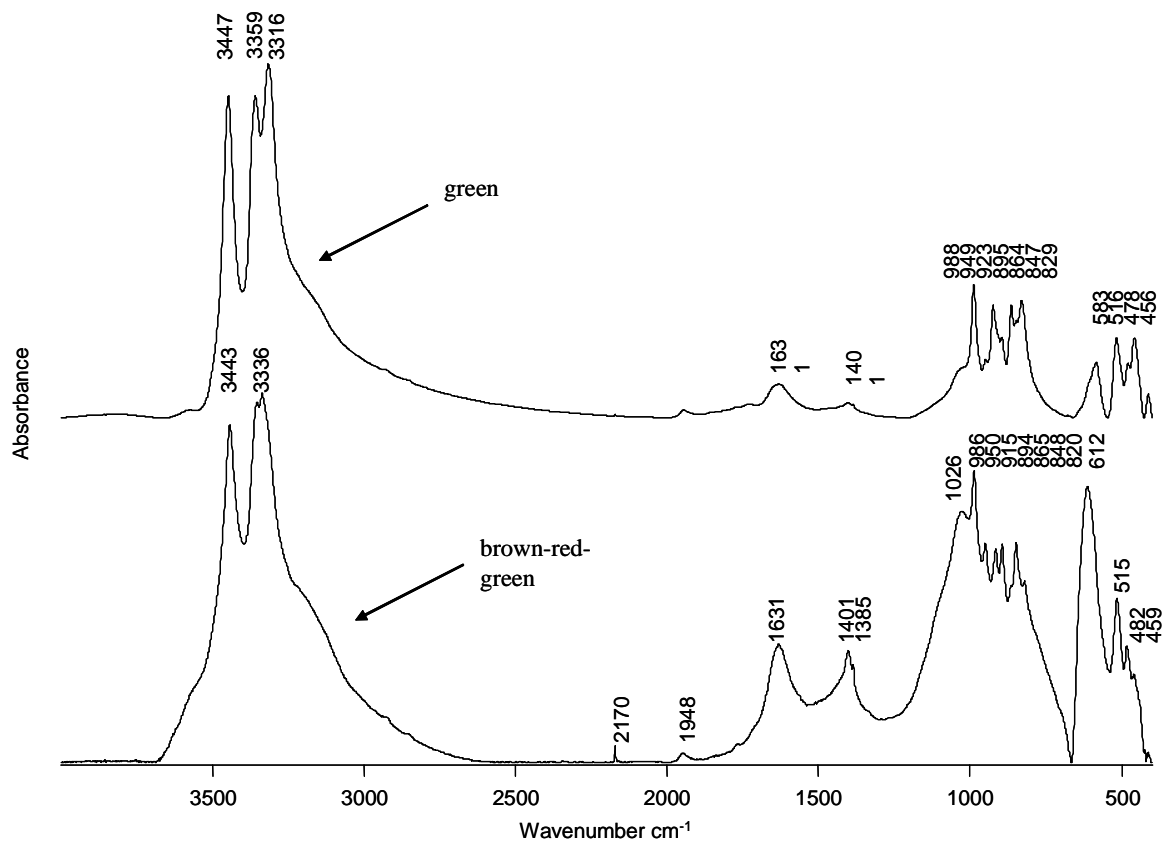
Figure A.8: Ib.05.13: a mixture of Paracatamite and Atacamite was identified for both samples, while Cuprite was also detected for the brown-red sample.
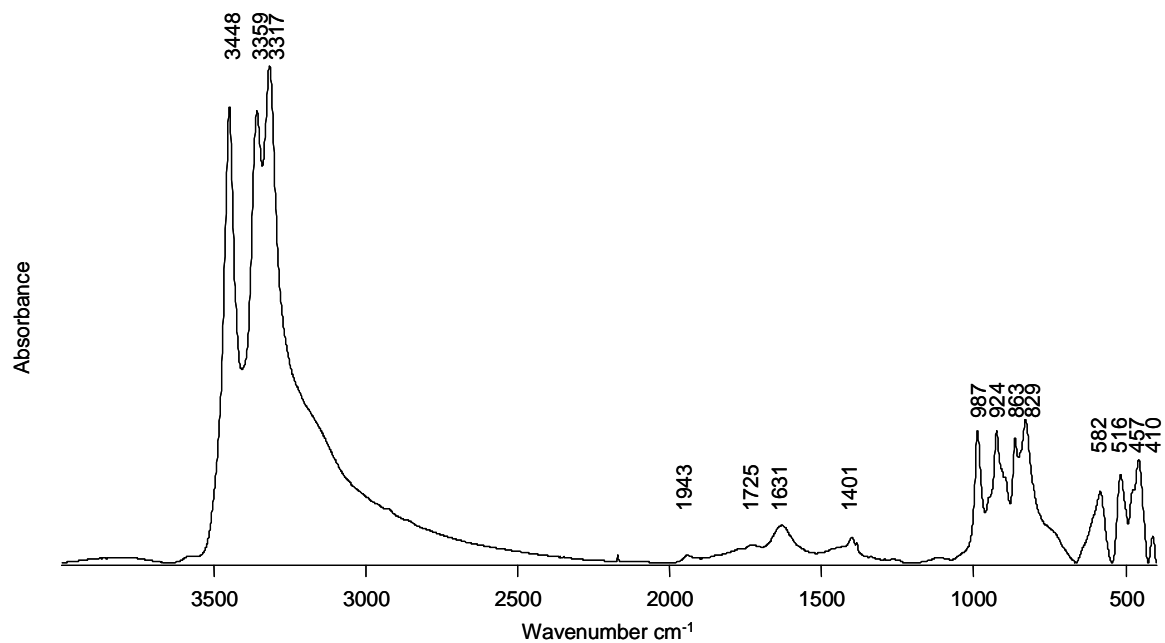
Figure A.9: Ib.05.15: Paratacamite was detected.
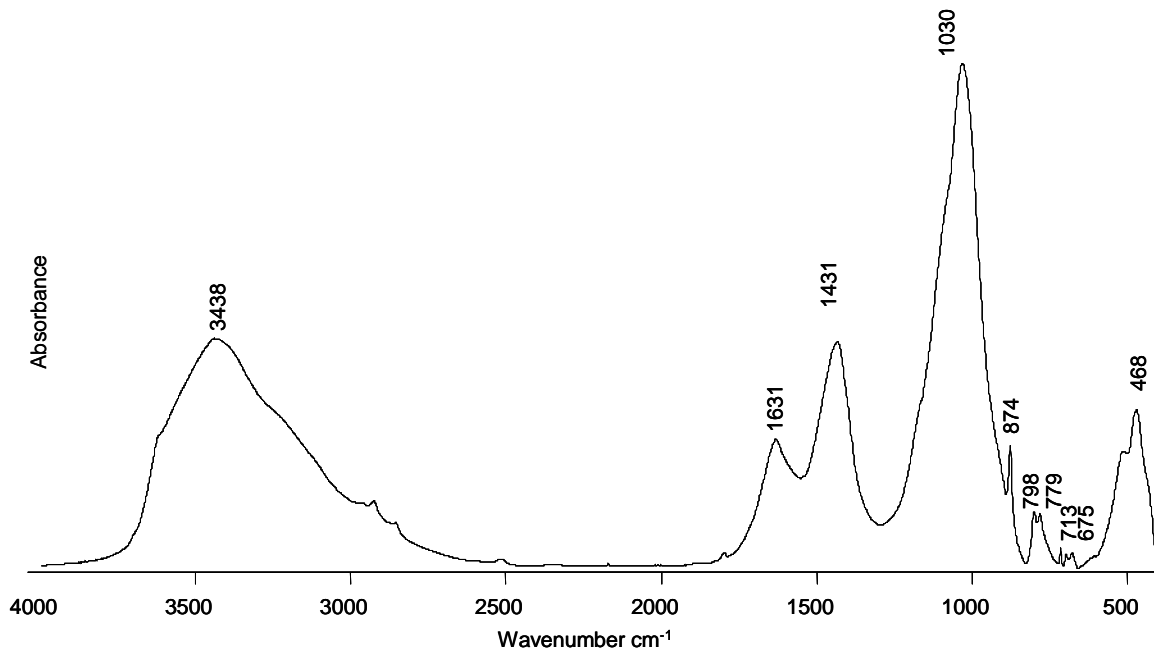
Figure A.10. Ib.08.1: Aluminosilicates, Calcite and Quartz were detected.
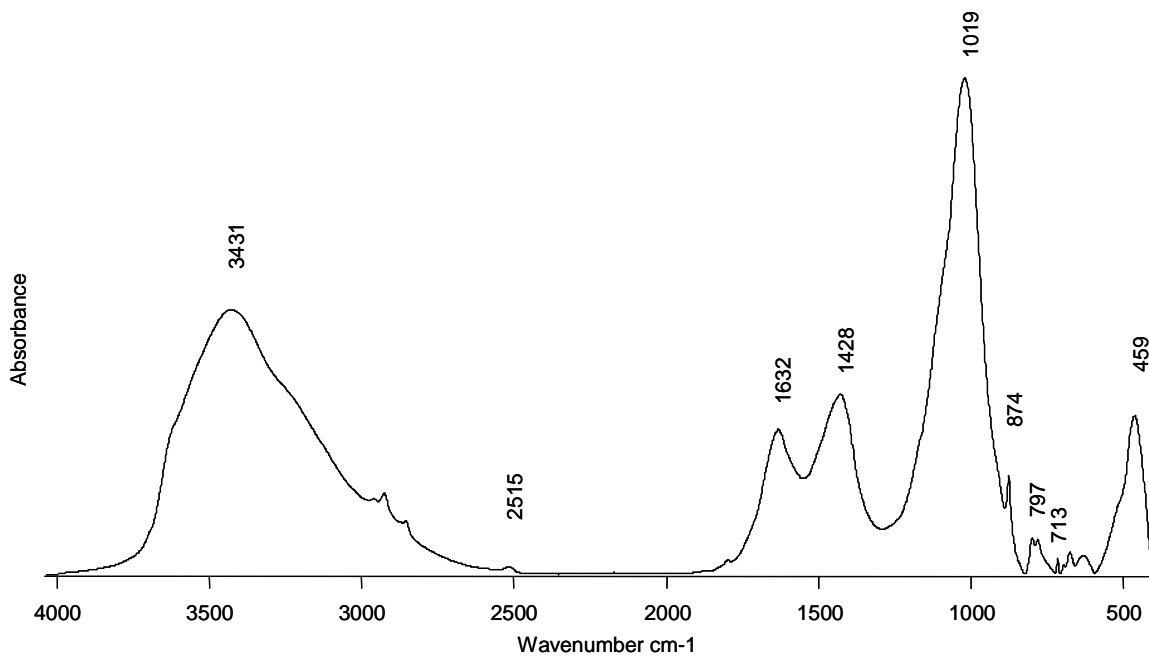
Figure A.11. Ib.08.4: Qluminosilicates, Calcite and Quartz were detected.
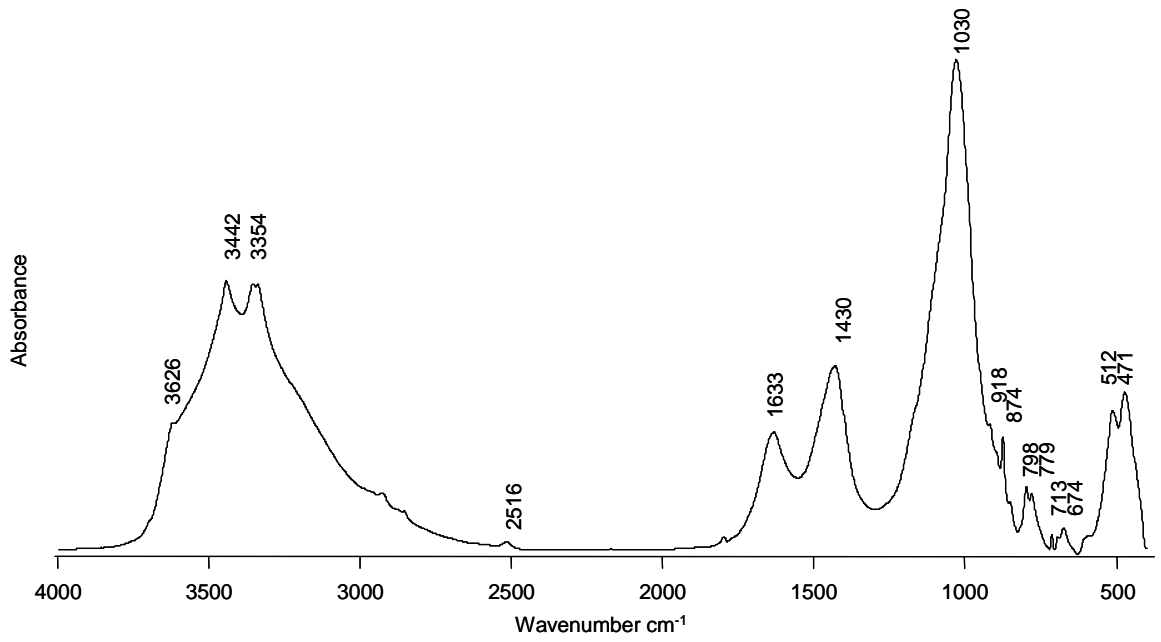
Figure A.11: Ib.08.5: Aluminosilicates, Calcite, Quartz and Paratacamite were detected
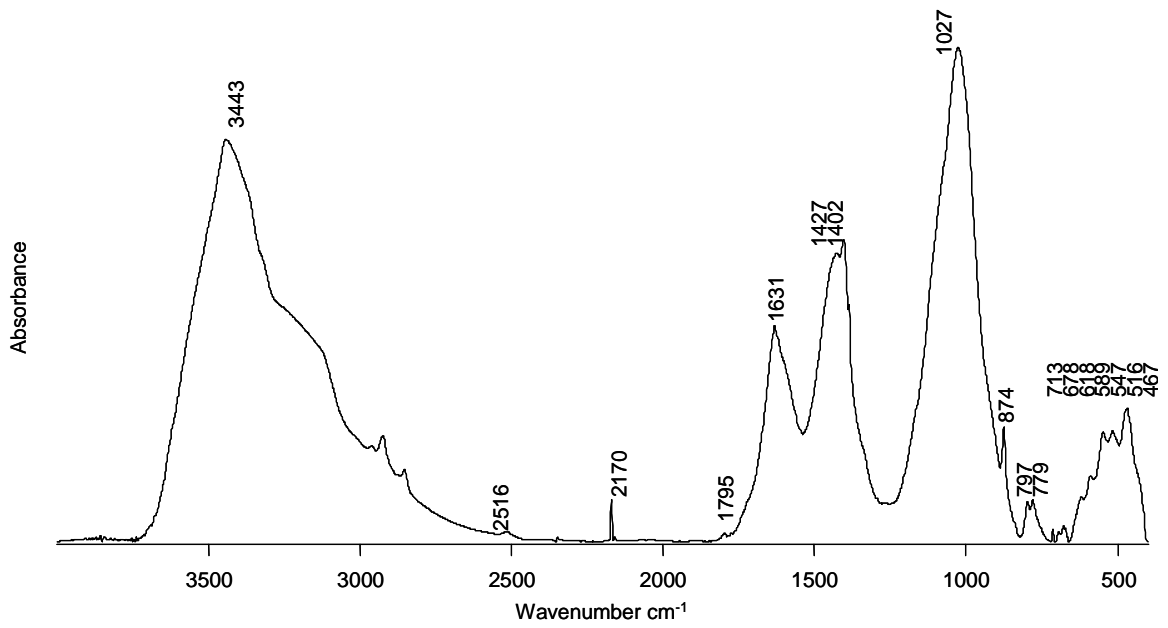
Figure A.11. Ib.08.7: Aluminosilicates, Calcite and Quartz were identified.
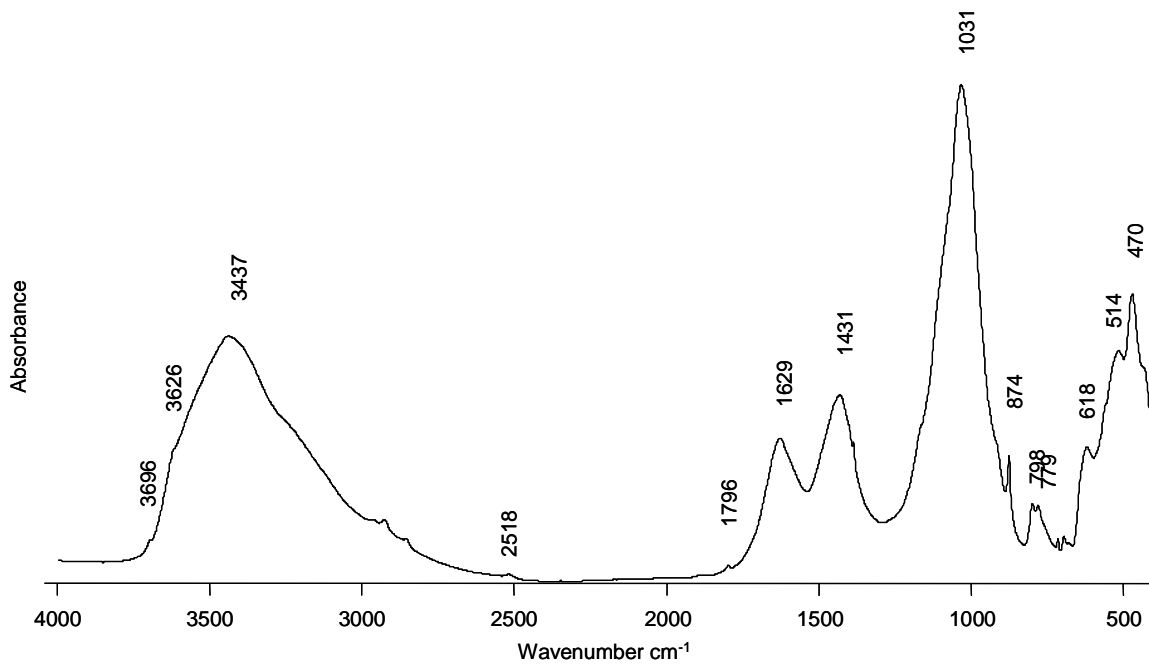
Figure A.12. Ib.08.12: Aluminosilicates, Calcite and Quartz were identified.
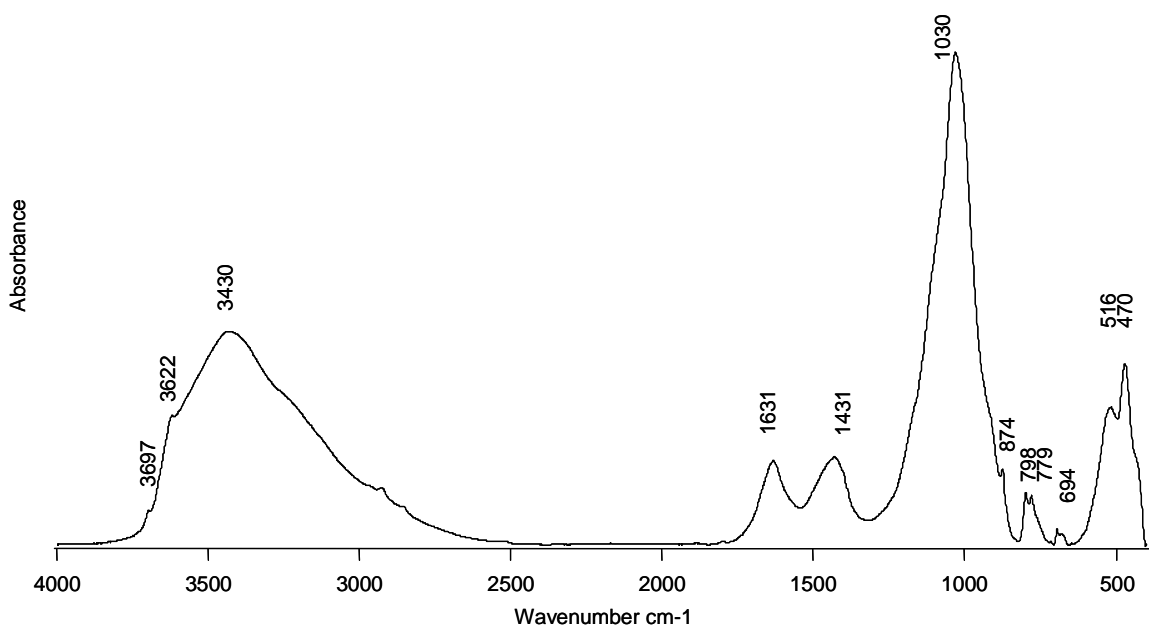
Figure A.13. Ib.08.15: Aluminosilicates, Calcite and Quartz were identified.
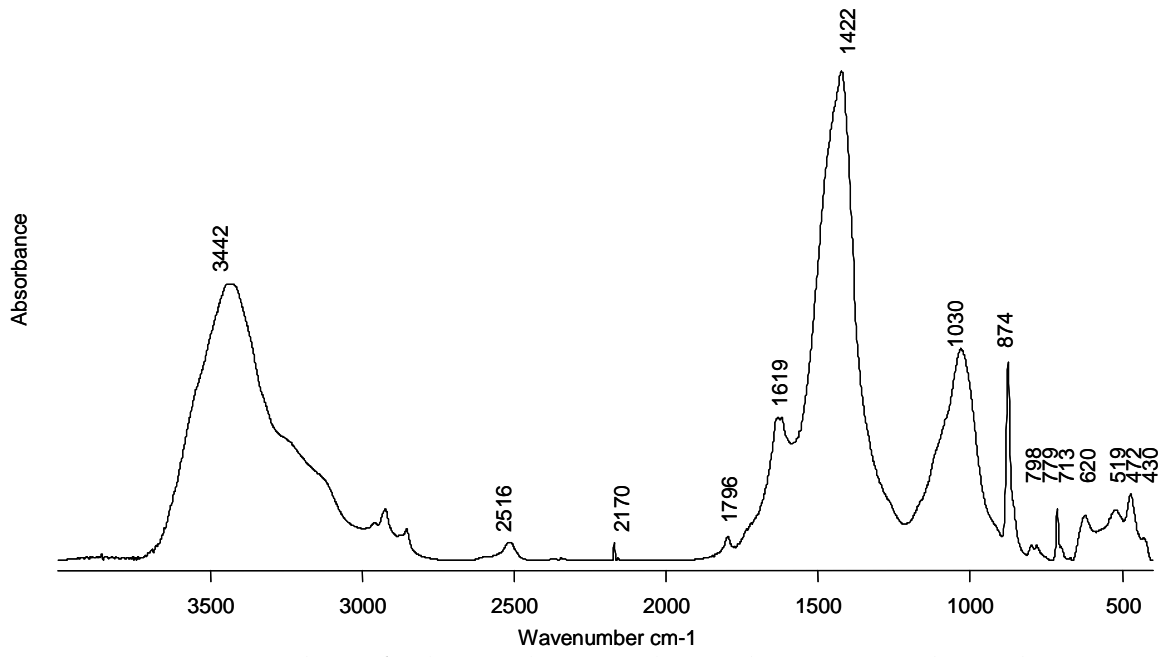
Figure A.14. Ib.08.16: Aluminosilicates, Calcite and Quartz were identified.
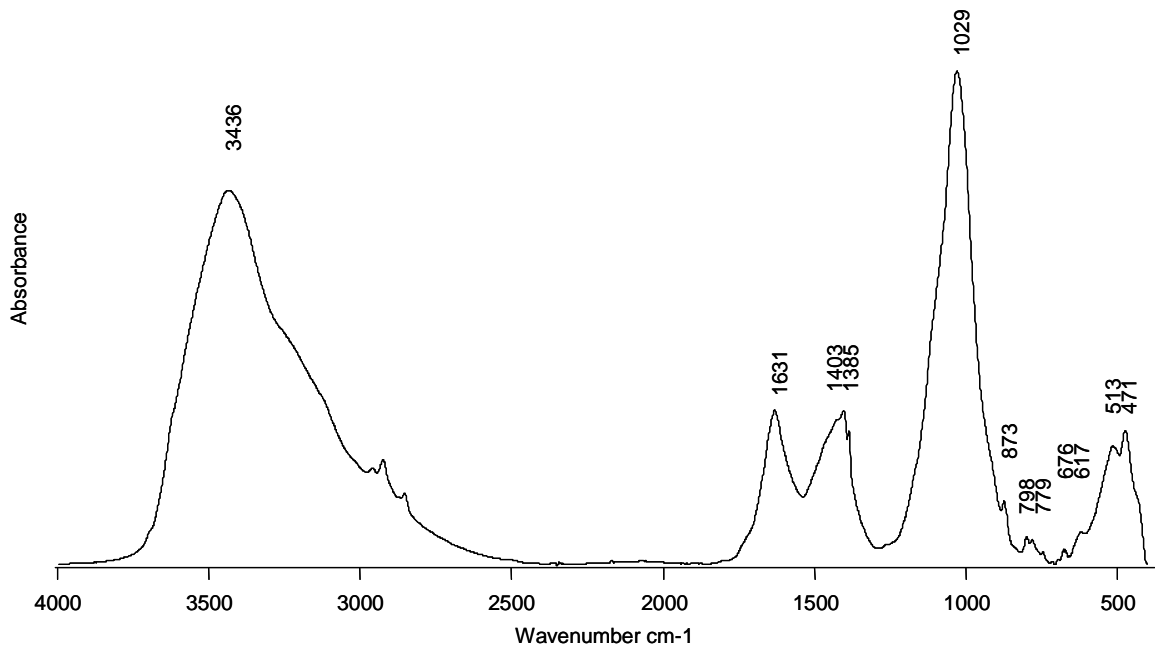
Figure A.15. Ib.08.17: Aluminosilicates, Calcite and Quartz were identified.
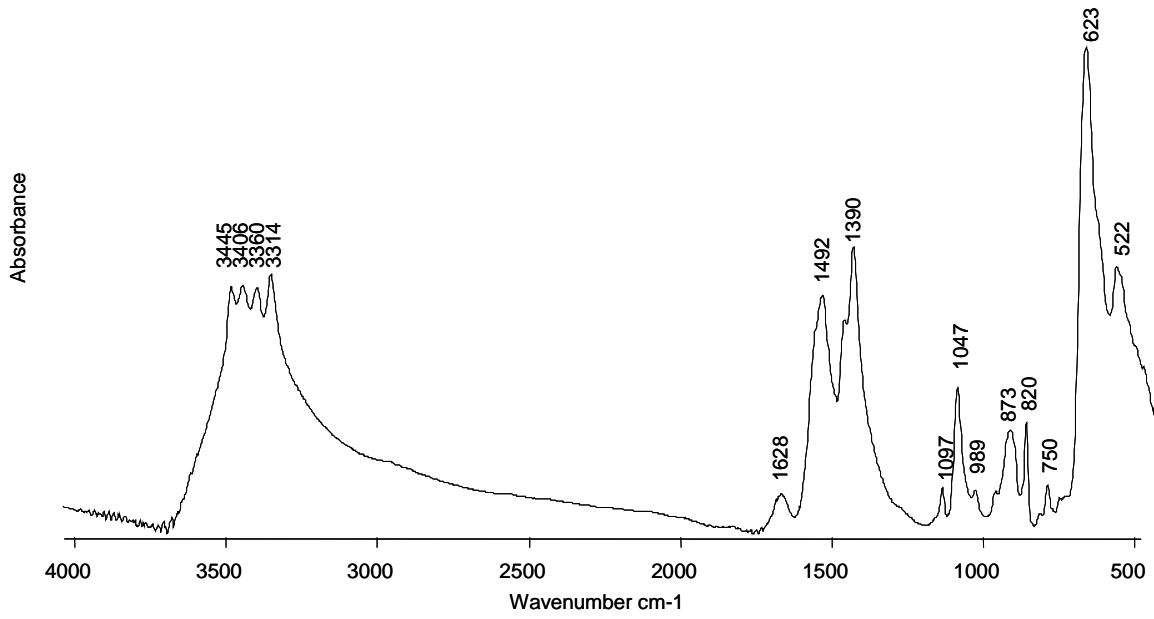
Figure A.16. Ib.06.9: Both Paratacamite and Malachite were detected, along with Cuprite.
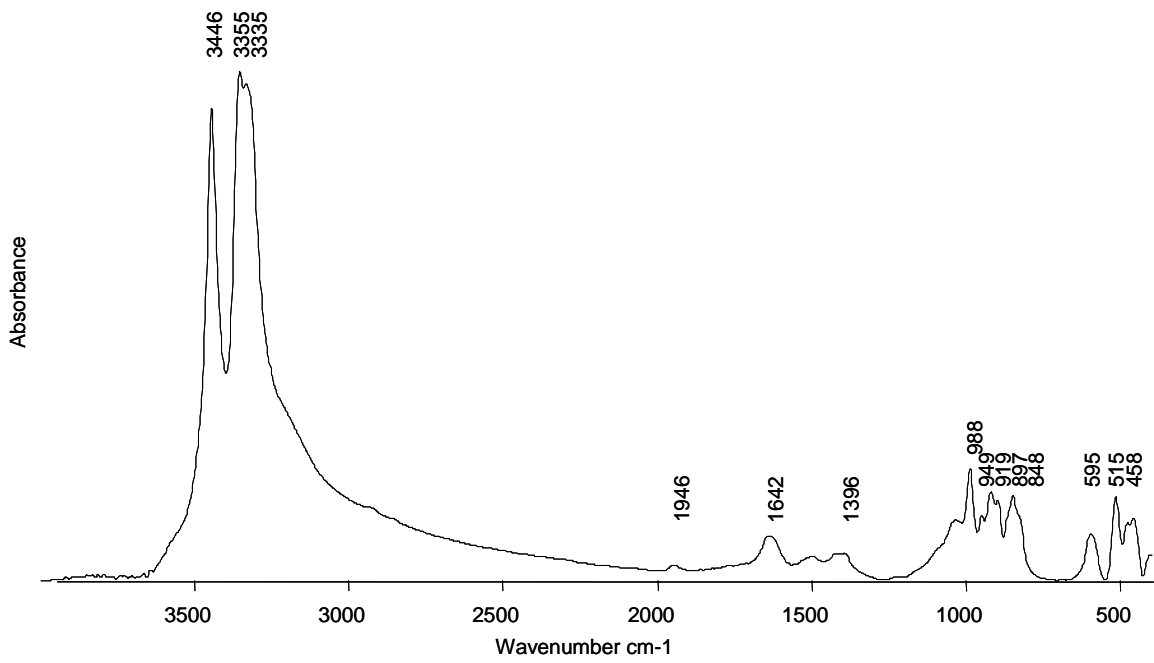
Figure A.17. Ib.06.1: Paratacamite was identified.

Nufarul
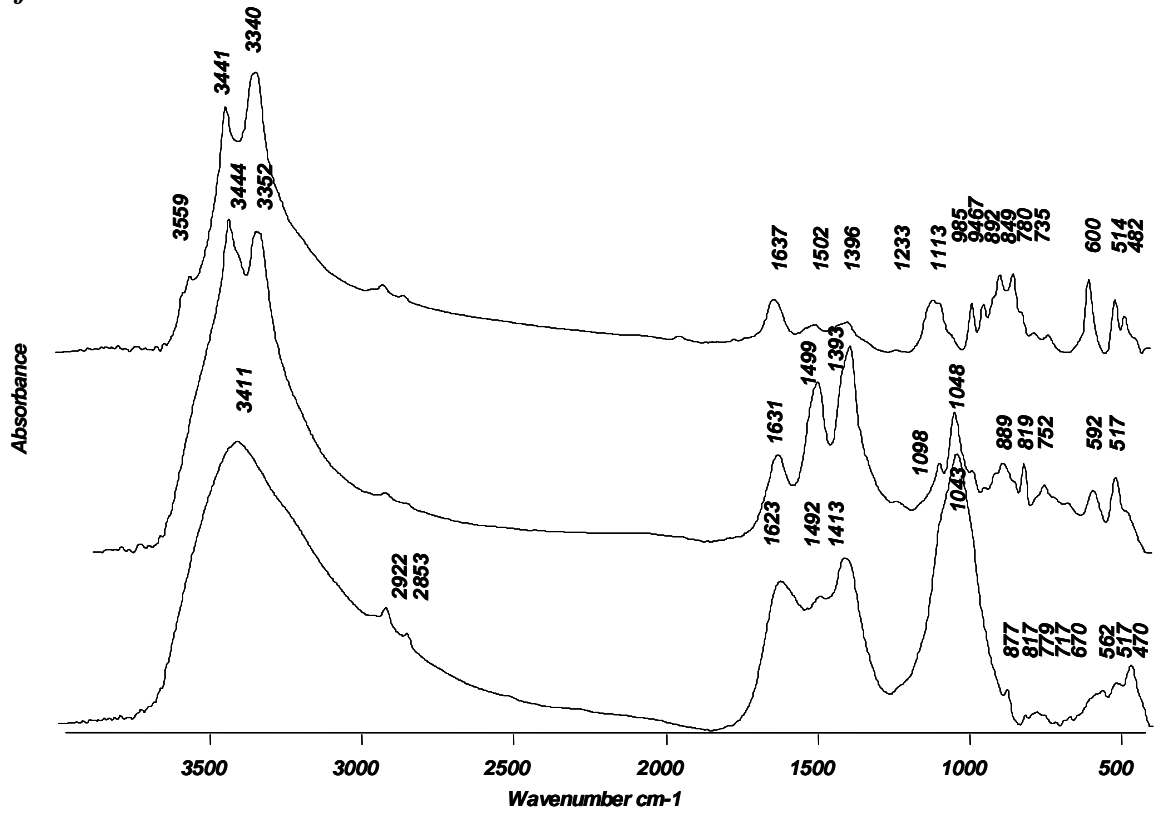
Figure A.19. Nuf.00.VII: in this case Malachite was also detected among the corrosion layers (spectrum in the middle), while Atacamite and soil components (Calcite, Aluminosilicates and Quartz) were identified as well.

Acknowledgements

EPISCON is the first PhD in Science for Conservation. I am proud of being part of the fulfillment of what, most likely, was a dream for people involved since the very beginning.

First of all, I would like to thank Prof. Rocco Mazzeo, coordinator of the project, for his guidance throughout these years, since the times of my master degree, and for his strength in the management of the project.

I would like to thank Prof. Ion Sandu, supervisor and "initiator" of my Romanian experience. I bear in mind his warm welcoming in this Country, and the first winter tour visiting the famous Romanian monasteries!

This project couldn't be carried out without the essential support of the whole University "Al. I. Cuza", the Arheoinvest Platform and the collaboration with other institution in Iasi, such as the Technical University "Gheorghe Asachi" and the Institute for Macromolecular Chemistry, "Petru Poni", directed Prof. Bogdan Simionescu.

I sincerely acknowledge Prof. Florin Brinza, Prof. Romeo Chelariu and Prof. Sergiu Stanciu for conducting me through the first steps in the characterization of corroded bronzes.

The archaeologists Lucretiu Birliba, Mihaela Iacob and Dorel Paraschiv are kindly thanked for providing the "material" and for letting me try a taste of the life *in situ*. I won't ever forget the week spent at Slava Rusa during August 2008.

Back in Iasi, I would like to thank Prof. Ioan Carcea for providing the bronze specimen for the simulation experiments, Prof. Daniel Timpu and Dr. Drobota Mioara for the XRD and FTIR analysis ("Petru Poni" Institute) and Prof. Nicolae Buzgar for Raman investigations (UAIC).

Dr. Radu Pirnau and Prof. Iuliana Breaban are kindly thanked for helping me in performing part of the experiments aimed to characterization of soils.

Prof. Romeo Olariu and Prof. Cecilia Arsene are gratefully acknowledged for their substantial help in the characterization of soils by Ion Chromatography and Atomic Absorption Spectroscopy, and for their precious advices.

The present work couldn't be successful without the presence of Prof. Neculae Aelenei, guide in the interesting domain of electrochemistry and essential support in practical aspects of experimental planning.

Last, but absolutely not least, I would like to thank Adeline Camelia Ciocan, for her patience and fundamental help with micro-FTIR measurements in reflectance mode.